Alma Mater Studiorum - Università di Bologna

DOTTORATO DI RICERCA IN

SCIENZE BIOTECNOLOGICHE, BIOCOMPUTAZIONALI, FARMACEUTICHE E FARMACOLOGICHE

Ciclo 35

Settore Concorsuale: 05/D1 - FISIOLOGIA
Settore Scientifico Disciplinare: BIO/09 - FISIOLOGIA

PATHOGENETIC MECHANISMS OF GASTROINTESTINAL SYMPTOMS IN A MOUSE MODEL OF FABRY DISEASE: INSIGHTS ON THE MICROBIOTA-GUT-BRAIN AXIS

Presentata da: Cecilia Delprete

Coordinatore Dottorato   **Supervisore**

Chiar.ma Prof.ssa Maria Laura Bolognesi   Prof. Marco Caprini

Esame finale anno 2023

INDEX

LIST OF ABBREVIATIONS

5-HT, 5-hydroxytryptamine, serotonin

Ach, acetylcholine

AITC, allyl isothiocyanate

ANOVA, analysis of variance

ANS, autonomic nervous system

ASIC, acid-sensing ion channel

AUC, area under the curve

AWR, abdominal withdrawal reflex

CaCCs, Ca^{2+}-activated Cl^- channels

CALB, calbindin

CCh, carbachol

Cer, ceramide

CFTR, cystic fibrosis transmembrane conductance regulator

CGRP, calcitonin gene-related peptide

ChAT, choline acetyltransferase

CNS, central nervous system

CRD, colorectal distension

CTCF, corrected total cell fluorescence

DBS, dried blood spot

DIV, day in vitro

DRA, downregulated in adenoma (anion exchanger)

DRG, dorsal root ganglia

EGCs, enteric glial cells

EMG, electromyographic

ENaC, epithelial Na^+ channels

ENS, enteric nervous system

EPANs, extrinsic primary afferent neurons

EQ-5D, EuroQoL five-dimension

ER, endoplasmic reticulum

ERT, enzyme replacement therapy

FD, Fabry disease

FSK, forskolin

GABA, gamma-aminobutyric acid

Gb3, globotriaosylceramide 3

GC-MS, gas chromatography-mass spectrometry

GFAP, glial fibrillary acidic protein

GI, gastrointestinal

GLA, alpha-Galactosidase A gene

GPCRs, G-protein-coupled receptors

HPA, hypothalamic-pituitary axis

IBD, inflammatory bowel disease

IBS, irritable bowel syndrome

IFANs, intestinofugal neurons

IPANs, intrinsic primary afferent neurons

I$_{sc}$, short circuit current

KO, knock-out

LC-MS, liquid chromatography-mass spectrometry

LM, longitudinal muscle

lyso-Gb3, globotriaosylsphingosine

MP, myenteric plexus

M6PR, mannose-6-phosphate receptor

NBS, newborn screening

NeuN, neuronal nuclei

NHE, Na$^+$/H$^+$ exchanger

NKCC, Na$^+$/K$^+$/Cl$^-$ cotransporter

NO, nitric oxide

NOS, nitric oxide synthases

PAG, periaqueductal gray region

PAR2, protease-activated receptor 2

PAT1, putative anion transporter

PCT, pharmacological chaperone therapy

PGP9.5, protein gene product 9.5

PKA, protein kinase A

PPQ, pyrimido-pyrrolo-quinoxalinedione

RT, room temperature

S100β, S100 calcium-binding protein beta

SCFAs, short chain fatty acids

SD, standard deviation

SEM, standard error of the mean

SGLT, sodium-glucose linked transporter

SMP, submucosal plexus

Sox10, SRY-related HMG-box 10 transcription factor

SP, substance P

TEER, transepithelial electric resistance

TLR2, Toll-like receptor 2

TRPA, transient receptor potential ankyrin

TRPs, transient receptor potential channels

TRPV, transient receptor potential vanilloid

TTX, tetrodotoxin

VER, veratridine

VGSCs, voltage-gated sodium channel

VHS, visceral hypersensitivity

VIP, vasoactive intestinal peptide

VMR, visceromotor response

WT, wild-type

α-Gal A -/0, hemizygous male mouse for α-Gal A gene deletion, knock-out mouse

α-Gal A +/0, hemizygous male mouse for α-Gal A gene, wild-type mouse

α-Gal A, alpha-Galactosidase A enzyme

ABSTRACT

Background: Fabry disease (FD) is an X-linked metabolic disorder caused by a deficiency in α-galactosidase A (α-gal A) activity. This causes the accumulation of glycosphingolipids, mainly globotriaosylceramide (Gb3) and globotriaosylsphingosine (lyso-Gb3), in several organs. Gastrointestinal (GI) symptoms - abdominal pain, nausea, diarrhea, constipation and early satiety - are among the earliest and most common. Frequent episodes of diarrhea (up to 12 or more times a day) severely impact patients' quality of life. However, the origin of these symptoms is complex and multifactorial and the exact mechanisms of pathogenesis are still poorly understood, thus the pressing need to improve their knowledge.

Aims: In view of our previous work on a FD murine model α-gal A -/0 showing GI structural and morphological alterations, here we aimed I) to evaluate whether these animals also capture the functional GI issues experienced by Fabry patients and can be considered valuable model for their investigation. Then, we meant to explore the potential mechanisms involved in the development and maintenance of GI symptoms, also looking at the gut-brain axis involvement.

Moreover, given the growing body of evidence on the potential causal role of lyso-Gb3 in FD pathogenesis, II) we sought to examine the effects of lyso-Gb3 on colonic contractility and on the intestinal epithelium and the enteric nervous system, which together play important roles in regulating intestinal ion transport and fluid and electrolyte homeostasis.

Methods: I) Visceral sensitivity was assessed using the colorectal distention (CRD) technique, measuring the visceral motor and abdominal withdrawal responses. Gut motility was evaluated by analyzing stool amount and water content. Open Field and Elevated Plus Maze Tests were used for anxiety-like behavior and locomotor activity assessment. Microbial profile (taxonomic and functional) and SCFAs analysis were performed from fecal samples via 16S rRNA sequencing and coupled GC-MS, respectively. Ion channels expression was measured by immunofluorescence. II) Lyso-Gb3 effects on fluid and electrolytes transport and its mechanisms of action were studied in mucosa-submucosa preparations by Ussing chamber. Short circuit current (I_{sc}) and transepithelial resistance (TEER) after serosal administration of lyso-Gb3 at increasing concentrations were measured. To investigate the nature of the currents, different secretagogues were applied.

Results: α-Gal A -/0 mice revealed visceral hypersensitivity and a diarrhea-like phenotype accompanied by anxious-like behavior and reduced locomotor activity, reasonably related to pain. In addition, Fabry animals reported an imbalance of SCFAs with increased propionic and butyric acid

and an early compositional and functional dysbiosis of the gut microbiota, which partly persisted with advancing age. Of note, most of the dysbiotic features suggest altered gut homeostasis and altered communication along the gut-brain axis. In addition, overexpression of TRPV1 was found in affected mice, and at specific ages partial alteration of TRPV4 and TRPA1 as well. This suggests an involvement of these channels in the generation and maintenance of visceral hypersensitivity, identifying them as possible therapeutic targets. Finally, the results of the Ussing chamber regarding lyso-Gb3 accumulation showed an increase in I_{sc} at 3 μM, perhaps mediated by the movement of HCO_3^- ions, which significantly affects neuron-mediated secretion, especially capsaicin and partly veratridine-mediated.

Conclusions: This first characterization of gut-brain axis dysfunction in the α-Gal A -/0 mouse model of FD through the study of visceral sensitivity, intestinal motility, fecal microbiota and SCFAs, as well as anxiety behavior, locomotor activity and ion channel alteration, provides functional validation of the model, suggesting new targets and possible therapeutic approaches. Furthermore, we can state that lyso-Gb3 is not only a valuable marker for diagnosis and follow-up of FD but significantly influences the colonic ion transport process which may play a crucial role in the dysregulation of intestinal function in FD in patients.

BACKGROUND

Healthy

Gb3

Fabry

PSYCHOLOGICAL — OCULAR

NERVOUS SYSTEM — CARDIAC

— RENAL

GASTROINTESTINAL

— SKIN

AIM 1 (Chapter 2-3)

α-Gal A +/0 (WT)

α-Gal A -/0 (KO)

8-10 weeks   16-20 weeks   12 months

↑ anxiety-like behaviour
↓ locomotor activity

↑ TRPV1
↑ TRPV4
↑ TRPA1

(SCFA) Propionic Acid ↑

↑ Visceral hypersensitivity

↑ *Porphyromonadaceae, Rikenellaceae, Prevotellaceae*
↑ Tryptophan degradation, GABA synthesis

AIM 2 (Chapter 4)

Healthy adult male

lyso-Gb3

VER   Caps
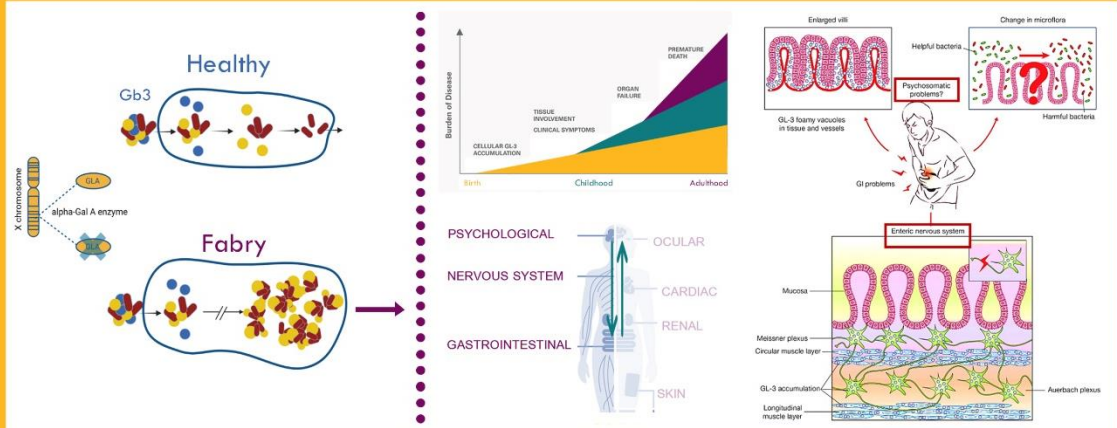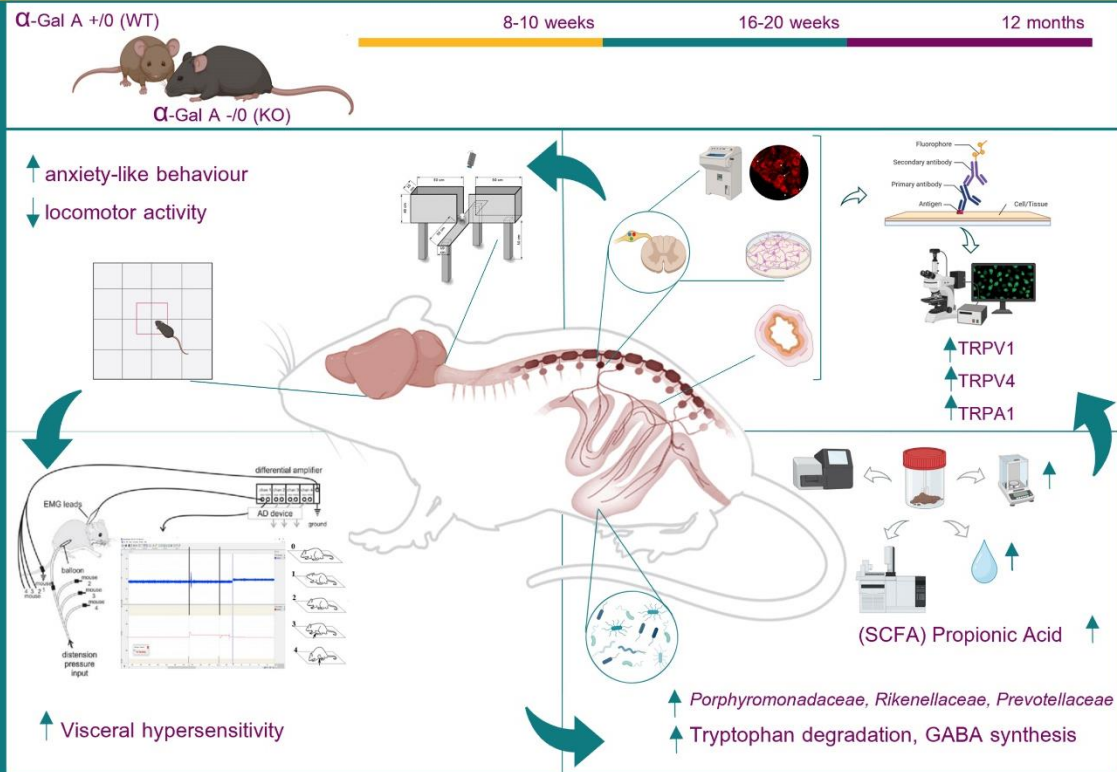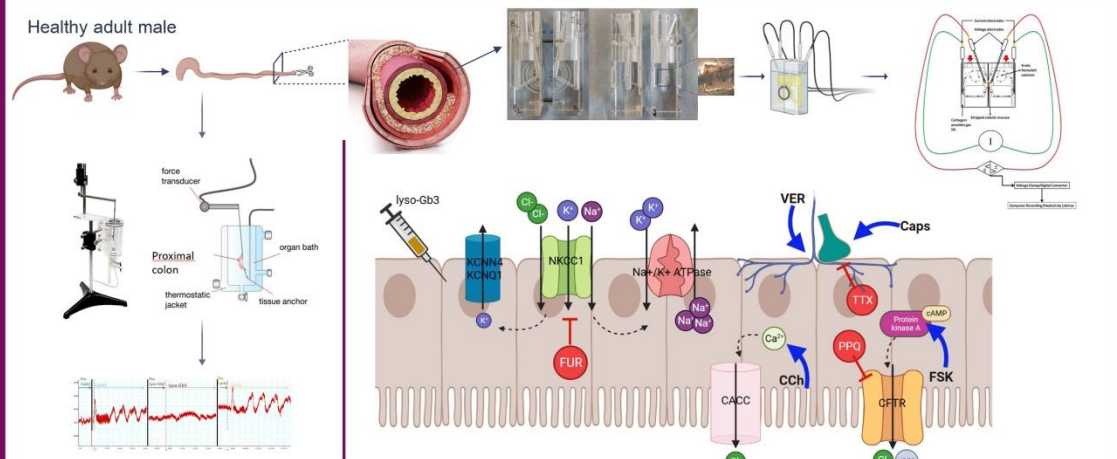
- lyso-Gb3 induces an acute **increase** in baseline **I$_{sc}$ Potentiated** by NKCC1 inhibition **NOT** mediated by the enteric nervous system or Cl-

- lyso-Gb3 **increases** secretagogue-induced secretion **neuronal-, especially capsaicin-mediated**, **NOT** epithelial-mediated

7

INTRODUCTION

1. Fabry Disease

1.1 An overview: etiology, lifespan, and inheritance

Fabry disease (FD, OMIM #301500) is a rare inherited X-linked disorder ranked among the lysosomal storage diseases, of which it represents the second most common after Gaucher disease. FD is caused by mutations in the GLA gene (gene mutation, OMIM #300644; HGNC: 4296), leading to a reduced or absent α-galactosidase A (α-Gal A) enzymatic activity[1–3]. This mutation-dependent deficiency or absence of activity results in a progressive accumulation of glycolipids, mainly globotriaosylceramide (Gb3) and its deacetylated and soluble derivative globotriaosylsphingosine (lyso-Gb3) within the lysosomes of several cell types, including endothelial cells, vascular smooth muscle cells, podocytes, cardiomyocytes, fibroblasts, and nerve cells[4–6]. Therefore, patients suffer from a progressive life-threatening pleiotropic disorder in which the number of affected organs and the burden increase with age, leading to organ failure and reduced life expectancy[5,7].

In FD patients the lifespan is reduced by about 10-20 years: in male patients, the median survival is 57 years, while in heterozygous females is 72 years, although with the introduction of dialysis and enzyme replacement treatment there have been improvements[8]. In this regard, it must be said that though FD follows an X-linked inheritance, it is neither recessive nor dominant, and it is no longer considered appropriate to define heterozygous females as "carriers"[5,9,10]. While in males one altered copy of the gene in each cell is sufficient for the disease to occur, in females this is not always true. Heterozygous females show high penetrance, with at least 70% of patients showing symptoms of the disease that can be as severe as hemizygous males ones[11,12]. This can be attributed to the process of lyonization, the skewing of X inactivation, which leads females to exhibit a mosaic of cells expressing genes of maternal or paternal origin[13].

1.2 Epidemiology

FD is reported to be pan-ethnic but owing to its rarity and the variety of clinical manifestations an accurate determination of prevalence remains a challenge and its incidence is most likely still underestimated[14,15]. Recent data report a frequency in male patients at 1:40000 to 1:117000, nevertheless, targeted new-born screening (NBS) programs revealed a higher frequency[2]. In Italy,

Spada and colleagues in three pivotal trials based on enzymatic analysis of dried blood spots described an incidence of 1:3100 in male[16]; however, according to the latest data recorded in the north of the country, it seems to be even higher, amounting to 1:7879[17]. For Hungary, Austria, and Spain NBS programs registered 1:3000-1:4000[18–20]. The United States reported 1:5495 and 1:8454 in Washington and Illinois respectively, while in Taiwan, an incidence at 1:1250 was found[21–23].

1.3 GLA gene, Fabry-related mutations, and genotype-phenotype correlations

α-Gal A enzyme is coded by the GLA gene, which has been entirely sequenced and characterized and is located on the long arm of the X-chromosome in the region 22.1 (Xq22.1)[24,25]. GLA comprises 7 exons between 92 to 291 bp and 6 introns from 0.2 to 3.8 kb. The complete sequence of 1437-bp cDNA codes a precursor peptide of 429 amino acids, containing a 31-residue signal peptide. The mature 398 amino acid subunit contains 4 N-glycosylation consensus sequences[26,27].

Currently, there are more than 1000 GLA mutations reported in the Human Gene Mutation Database (HGMD, at the Institute of Medical Genetics in Cardiff, Public database, GLA gene http://www.hgmd.org) causing FD. Missense and nonsense modifications are the most common followed by small deletions, splicing defects, and insertions. Furthermore, the vast majority of the reported mutations are private, restricted to one or a few families[28].

Nonsense mutations and most frameshift mutations result in little or no α-Gal A enzymatic activity and are associated with the classic phenotype. In contrast, missense mutations and rare splicing mutations may encode enzymes with reduced but present activity, and thus potentially associated with a late-onset[29]. Specifically, missense mutations include (I) mutations that modify the active site of the enzyme by altering its three-dimensional structure; (II) mutations that interfere with the proper folding and stability of the protein; and (III) mutations that while not falling into the previous categories negatively impact catabolic function. In this regard, it has been reported that replacement of cysteine 56 with glycine, phenylalanine, or tyrosine disrupts a major disulphide bond, leading to a lack of enzymatic activity[30].

Information about the genotype-phenotype association is available on the database at http://www.dbfgp.org, however, it should be considered that since the same mutation can lead to different clinical manifestations, this correlation is still complex[31]. Environmental factors and blood groups may also play a relevant role. Indeed, patients with blood group AB or B may manifest more severe symptomatology given by a greater accumulation of glycosphingolipids in the membrane of B-type erythrocytes[32,33]. Anyway, among late-onset patients, it has been shown that those with

mutations encoding p.F113L and p.N215S are more predisposed to cardiac manifestations[34,35]. Also of interest is the acting of a mutation occurring in 10% of Caucasians, in the 5' untranslated region of the GLA gene (c.-10C>T), which can decrease normal α-Gal A activity by 25% and if present in a patient with late-onset, can strongly aggravate the symptoms[36].

Regarding the area of genotype-phenotype association, although not directly related to mutations in the GLA gene, variants potentially associated with gastrointestinal symptoms identified in a study on 49 Fabry patients are worth mentioning. These are 9 single nucleotide polymorphisms within four genes: ABCB11, SLCO1B1, NR1I3, and ABCC5. These operate in the export, detoxification, and absorption of bile acids in the liver, and are associated with an increased susceptibility to develop gastrointestinal symptoms in FD[37,38].

1.4 α-galactosidase A enzyme function and protein structure

α-galactosidase A is a glycoside hydrolase enzyme that cleaves the terminal α-d-galactosyl residues from glycolipids and glycoproteins. Among these Gb3 is mainly included, but glycosphingolipids are also present in galabiosylceramide and group B blood antigens[39,40]. In FD patients, loss of functional enzyme leads to the accumulation of substrates[41]. In general, sphingolipids or glucosylceramides are lipids having a set of aliphatic amino alcohols that comprises sphingosine, which forms the backbone of these lipids. In sphingolipids, the amine group of sphingosine is linked to the acyl group of fatty acid, and this combination leads to the formation of the ceramide unit (Cer), which is contained by all sphingolipids[42]. The sphingosine-bound head group then differentiates them from each other[43]. Cer can be brought from the endoplasmic reticulum (ER) membranes through the ceramide-transfer protein (CERT) and transferred to the trans-Golgi (TGN), where it is mostly used for sphingomyelin synthesis, or it can move to cis-Golgi where produce glucosylceramide (GlcCer) via glycosylation. GlcCer is translocated to the luminal Golgi leaflet and to TNS membranes, where it is galactosylated to produce lactosylceramide (LacCer), a metabolic step for the development of different complex glycosphingolipids[44–47].

As mentioned earlier, α-Gal A is synthesized as a 429-amino acid pre-protein, and only after several post-translational modifications turn up to its mature form of 2 identical 49-kDa subunits[25,26,48]. Specifically, the pre-protein moves into the phospholipid bilayer of the rough ER, where it loses the signal peptide and transforms into a pro-protein, then proceeds to the smooth ER. Here a group of different chaperones determines its proper folding[49].

The crystal structure of α-Gal A (Fig. 1) was solved in 2004 by Scott Garman's group[30]. The mature protein is a homodimeric glycoprotein in which each monomer is composed of two domains: the first, a N-terminal (β/α)8 domain containing the active site; the second, a C-terminal β domain with 8 antiparallel filaments assembled into two layers making a β sandwich[41]. Human α-Gal A contains three glycosylation sites: N139, which is generally associated with complex carbohydrates, N192 and N215[27]. Because oligomannosyl carbohydrates contain mannose-6-phosphate, the lysosomal targeting signal, N-linked carbohydrates at N192 and N215 are responsible for targeting the glycoprotein to lysosomes[50]. Indeed, mutation of N215 to serine eliminates the carbohydrate attachment site, leading to unsuccessful trafficking of the enzyme to lysosomes[27].
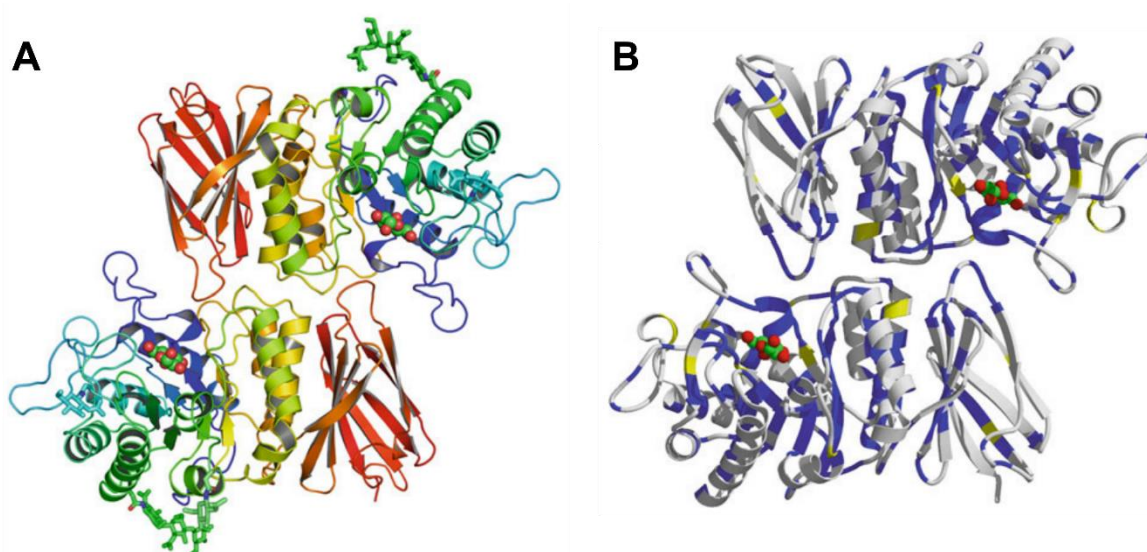
Figure 1 α-galactosidase A dimer structure and Fabry-related sites. (A) α-galactosidase A (α-Gal A) polypeptide rainbow-trace from *blue* at the N-terminus to *red* at the C-terminus. N-linked carbohydrates are shown as bonds, and the galactose ligand is shown as spheres, marking the active site in the first domain. (B) α-Gal A dimer in ribbon form with residues affected in severe (*blue*) and the atypical (*yellow*) variants of FD. Modified from Guce et al. (2010).

1.4.1 Biological significance of Gb3

Gb3 (also known as CD77) comes under the glycosphingolipids class. Although glycosphingolipids are not considered essential for cell life, as they modulate the function of membrane proteins and contribute to cell-cell communication, they are nevertheless necessary for the development of multicellular organisms[51,52]. Moreover, their involvement in "sensing" the environment and creating/maintaining cell identity has been validated through the identification of modulatory effects on specific plasma membrane receptors[53].

In the specific case of Gb3, once synthesized, it lies on the surface of the plasma membrane, assembled between lipid rafts, with its glycan portion facing the extracellular environment and the two hydrocarbon chains of ceramide embedded in the plasma. When endocytosis and transfer to lysosomes occur, the glycan portion faces the lysosomal lumen, which also contains α-Gal A, essential for the turnover of this glycosphingolipid[54].

In addition, cell surface Gb3 is involved in infectious processes, being the cell surface receptor that the Shiga toxin family uses for entry into cells[55]. Shiga toxins include Shiga toxin itself, produced by *Shigella Dysenteriae*, and verotoxins, produced by *Enterohemorrhagic Escherichia Coli*. Basically, Shiga toxins bind Gb3 molecules present on the plasma membrane and, following endocytosis, are transported to the ER, where they inhibit ribosomal protein synthesis leading likely to the hemolytic uremic syndrome[14].

Finally, Gb3 has also been observed on the surface of some cancer cells, for example in colorectal adenoma, Burkitt's lymphoma, or breast and testicular carcinomas[56–60]. Remarkable is the correlation between Gb3 and metastasis in colorectal adenoma. In fact, healthy colonic epithelial cells do not express Gb3, while colon cancer cells overexpress it[57].

1.4.2 From the role of Gb3 to that of lyso-Gb3 in Fabry disease

Since Gb3 consists of a sugar chain linked to a ceramide portion of sphingosine and various fatty acids (Fig. 2A), it is inferred that different isoforms exist in organs and tissues due to their respective metabolic pathways[43]. In fact, as a result of increasingly sensitive analytical methods such as liquid chromatography-mass spectrometry (LC-MS) and nano-liquid chromatography-tandem mass spectrometry (nano-LC-MS/ MS), it has been possible to detect the different isoforms of Gb3 and measure small amounts of lyso-Gb3 (Fig. 2B) (which is more water-soluble and not trapped in lipoproteins)[61,62]. Although Gb3 is itself a cellular component, its excessive accumulation has been shown to cause endothelial dysfunction and nephropathy[63–65]. In fact, it has been supposed that lysosomal accumulation and cellular dysfunction trigger a cascade of events that can lead to cell death, impact energy metabolism, impact small vessels and endothelial cells, induce oxidative stress, and cause tissue ischemia till irreversible fibrosis of cardiac and renal tissue[66]. Therefore, it is now well accepted that Gb3 deposits are deeply associated with the pathogenesis of FD and have long been recognized as a diagnostic and predictive marker[67]. It must be considered, however, that a large proportion of late-onset patients (males and females) shows no Gb3 accumulation in plasma, thus making quantification of plasma Gb3 limiting[68]. Furthermore, since replacement therapy does

not lead to remission and Gb3 levels do not always correlate with the intensity of symptomatology, recent studies have hypothesized the existence of other factors besides Gb3[69,70].

The measurement of circulating lyso-Gb3 levels, augmented in both patients and animal models by 100- to 500-fold compared to controls, has been indicated as a promising target, not only for diagnosis but also for the evaluation of therapeutic efficacy[68,71–73]. Recently, the fact that lyso-Gb3 reflects the disease severity has been also demonstrated by Nowak and colleagues, who reported that lyso-Gb3 levels in serum correspond to Gb3 load in organs. Since lyso-Gb3 results from the de-acylation of Gb3 deposits or consequent glycosylation of accumulating sphingolipid precursors, the authors speculate that the effects of lyso-Gb3 may play a direct toxic effect[71,74]. To support this, it has also been shown that lyso-Gb3 appears to support the Notch1-mediated inflammatory response in podocytes[75]. In addition, an *in vitro* study on lyso-Gb3-treated sensory neurons found that it markedly enhances voltage-dependent calcium channels leading to increased intracellular levels[70]. As well at the tissue level, a remarkable lyso-Gb3 concentration was found in the liver and intestine of FD mice, significantly exceeding plasma levels[71]. Lastly, in a recent work by Aguilera-Correa and colleagues, it has been demonstrated that lyso-Gb3 alters the gut microbiota by impacting the biofilm-forming capacity[76].
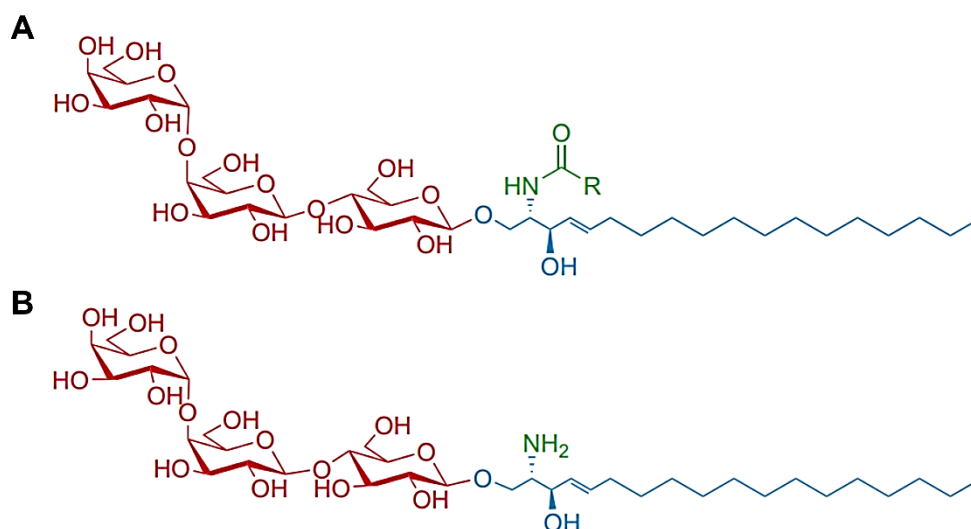
Figure 2 Globotriaosylceramide (Gb3) and globotriaosylsphingosine (lyso-Gb3). (A) Gb3 structure consisting of the sugar chain (*red*) and the ceramide portion of sphingosine (*blue*) and various fatty acids (*green*); (B) lyso-Gb3 structure consisting of the sugar chain (*red*) and the sphingosine (*blue*). Modified from www.matreya.com

1.5 Fabry patient's clinical picture

Although FD presents a progressive and extremely heterogeneous clinical picture both as regards involved organs and severity (as it usually happens with lysosomal storage diseases), many patients

remain asymptomatic in the first few years of their life. However, the primary process may even begin during fetal development[77,78]. Based on the age of onset of the first symptoms and their features, FD is commonly classified into two variants: the classic (or Type 1) and the late-onset (or atypical or Type 2). The first occurs mainly in males, in childhood or adolescence, affects patients with less than 1-3 % enzyme activity, and involves many organs[31,79]. The second appears with higher enzyme activity and the manifestations can also be restricted to a single organ. In fact, we talk about specific variants such as "cardiac" or "renal"[80,81].

1.5.1 Signs and symptoms in the classic phenotype

In the classic phenotype, generally between 3 and 10 years in males and a few years later in females, the first symptoms impact the child's well-being and performance. With advancing age, progressive damage to vital organs develops in both sexes, leading to organ failure (Table 1)[82,83]. Ultimately, renal damage and life-threatening cardiovascular or cerebrovascular complications limit the life span[7,66].

Among the earliest and most frequent symptoms affecting about 70% of children is pain, for both sexes (albeit with generally later onset in female)[82,84]. FD patients report pain as evoked pain (allodynia or hyperalgesia), pain attacks, permanent pain, and pain crises[85]. To simplify we could divide the Fabry pain into two categories: chronic pain and "Fabry crisis". The former is characterized by burning and tingling acroparesthesias that may occur daily, and the latter, which consists of episodes of excruciating, aching pain that originates in the hands and feet and radiates to other parts of the body[86]. This type can last from several days to weeks and is often associated with mild febrile states and elevated erythrocyte sedimentation rate, while it may be preceded by fever, exercise, fatigue, stress, and rapid temperature changes[85,87]. Recurrent painful acroparesthesias and crises may become progressively more frequent and severe, even though they generally occur less frequently during the second and third decades of life. Because of pain, patients with FD have a significantly reduced quality of life[88,89]. Numerous pieces of evidence, including the identification of Gb3 deposits in dorsal root ganglion (DRG) neurons, describe Fabry's pain as principally neuropathic[90]. In addition, a reduction in small Aδ nerve fibers and C nerve fibers, which mediate pricking pain and cold perception, and "slow" pain and heat perception, respectively, have been reported[91–93]. This is matched by experimental studies, such as that of Choi and colleagues (2015), in which pain is associated with hyperexcitability of peripheral nociceptive neurons mediated by increased Ca^{2+} lyso-Gb3-dependent influx, or that of Lakomá et al. (2016) in which the role of sodium

ion channel Nav1.8 and transient receptor potential cation channel subfamily V member 1 (TRPV1) ion channels is reported[70,94,95].

Another early clinical evidence of FD is angiokeratoma. It generally appears in childhood and may progressively increase in size and number. This consists of clusters of small, purplish-red skin angiomas caused by accumulation damage in vascular endothelial cells leading to dilatation of vessels in the dermis. They are typically located on the buttocks, groin, around the umbilicus, and thighs, sometimes also on mucosal areas, such as the mouth[31,96–98]. An additional aspect associated with the skin is hypo-hidrosis, or even anhidrosis, which can be a cause of heat and exercise intolerance[99,100].

In almost all Type 1 affected males and 90% of heterozygous females from families with classic variant ophthalmologic changes are also found. These constitute a characteristic FD feature known as "cornea verticillata," but this rarely has visual significance[31,101].

A further common manifestation of adolescence, but one that may persist into adulthood and worsen, is that of gastrointestinal (GI) symptoms, which are reported by over 70% of males with the classic phenotype[84]. These symptoms include abdominal pain, severe diarrhea, bloating, constipation, nausea, and vomiting[102–105]. They can worsen after meals and cause anorexia[84]. Since these features can also be found in other common disorders patients are often misdiagnosed thus contributing to the delay of FD diagnosis[37]. A more detailed examination of GI symptoms will be provided in the paragraph 1.5.3..

Even though major organ dysfunction is not present during childhood and adolescence, the symptoms listed so far contribute to significant morbidity severely limiting children in their normal social habits. Indeed, psychiatric studies have revealed a high incidence of severe, which correlates with the degree of interfering symptoms with normal life[88,106,107]. A recent study by Polistena and colleagues (2021) on 106 Italian Fabry patients revealed that the poor average quality of life may be even lower than those of other inflammatory chronic disorders (i.e. Crohn's disease, chronic hepatitis, cirrhosis, multiple sclerosis). Social choices are the first to be impacted: the sensitivity of refusal and the perception of people's judgments are the main reported feelings. The awareness of an impossible recovery can also lead to mood disorders that might further worsen the clinical picture[108].

After the third decade, the most significant complications appear: renal, cardiac, and/or cerebrovascular manifestations, which are the most frequent cause of death for Fabry patients, reducing life expectancy by about 20 years compared to the healthy population[109]. These symptoms

are the consequence of the progressive accumulation of Gb3 in renal podocytes, cardiomyocytes, and microvascular system, respectively. At the kidney level between 20- and 30 years, microalbuminuria and proteinuria are principally found. As in diabetic nephropathy, it seems to contribute directly to the progression of FD nephropathy. Progressively, proteinuria worsens as renal function, until azotemia is reached between 40 and 50 years of age[110]. Death most often results from uremia, unless chronic hemodialysis or renal transplantation is undertaken[7]. Cardiac symptoms, including left ventricular hypertrophy, arrhythmia, angina, and dyspnea, are reported in about 40-60% of patients with FD[7,31,111]. Cerebrovascular manifestations can lead to wide-ranging symptoms, extending from headache and dizziness to transient ischemic attacks and ischemic stroke and more rarely vascular dementia[112–114].

Age	Organ system and related symptoms
Childhood and adolescence (< 16 years)	- *Peripheral nervous system*: neuropathic pain, «Fabry crisis», chronic or episodic pain triggered by thermal changes, physical or emotional stress, intercurrent diseases or alcohol consumption; impaired sweat function (hypoidrosis). - *Intestine*: abdominal pain, diarrhea, constipation, bloating, nausea, vomiting. - *Skin*: angiokeratomas. - *Eyes:* cornea verticillata; conjunctival and retinal vasculopathy. - *Ears*: tinnitus; progressive sensorineural hearing loss. - *Musculoskeletal*: deformation of the fingers interphalangeal joints, in some cases drum flail fingers and toes. - *Kidney*: microalbuminuria, proteinuria. - *Heart*: abnormal heart rate variability. - *Others:* reduced body growth, delayed puberty, fertility disorder, impotence, characteristic facial features, anomaly in the oral and dental area such as cysts and pseudocysts of the maxillary sinus.
Early adulthood (17-30 years)	In addition to the above-mentioned manifestations: - *Renal*: Fabry nephropathy, proteinuria and progressive organ insufficiency, often renal cysts, renal hypertension. - *Cardiac*: cardiomyopathy, left ventricular hypertrophy, conduction issues (atrial fibrillation, supraventricular and ventricular tachycardia), valve dysfunction, angina pectoris, intramyocardial fibrosis. - *Cerebral*: transient ischemic attack, ischemic insult, rare intracerebral hemorrhage, ectasia of the basilar artery and white matter lesions, disturbed cerebral blood flow, lymphedema of the lower extremity, depression, psychoses, limited quality of life.
Later adulthood (> 30 years)	Progression of the above-listed manifestations: Renal insufficiency (dialysis, renal transplantation), heart failure, malignant arrhythmia, recurrent TIAs and insults, vascular dementia

Table 1 Classical manifestation in Fabry Disease according to age. Modified from Ortiz et al. (2018) and Lenders et al. (2021).

1.5.2 Fabry Disease atypical variants

Since late-onset patients do not have microvascular Gb3 accumulation, they do not manifest the classic early symptoms described above, including pain, angiokeratoma, hypo-hidrosis, or GI complications. These patients are generally diagnosed in the fourth to eighth decade of life by screening patients in hemodialysis, transplantation, cardiology, and stroke clinics[31,115]. As mentioned earlier, based on the organ primarily involved, a distinction tends to be made between cardiac and renal variants. In the former, symptoms are limited to the heart and manifest in the sixth or seventh decade of life with hypertrophy of the left ventricle. In this case, patients do not have significant impairment of renal function although they may have proteinuria[80]. In the renal one, patients while not showing any manifestations of Type 1, appear at the same age with advanced-stage renal disease, often at first diagnosed as chronic glomerulonephritis[116].

1.5.3 Focus on gastrointestinal symptoms in Fabry Disease

As mentioned before, amongst the clinical manifestations GI symptoms (Table 2) are counted as the earliest and most frequent, as well as disabling for Fabry patients. However, it frequently happens that they are underestimated or misinterpreted, identified as signs of other more common GI disorders such as irritable bowel syndrome (IBS) or inflammatory bowel disease (IBD), or even Chron's disease and celiac disease[84,103,117]. Thus, this contributes to the delay in correct diagnosis, which can come as late as 10 to 15 years[5,66,118]. Added to this is the proven negative impact on the quality of life of adults and children as reported in surveys EuroQoL five-dimension (EQ-5D)[84,119]. Although treatments with enzyme replacement therapy (ERT) seem to have an ameliorative effect on GI symptoms, about 50% of patients complain of discomfort even during treatment or develop new ones[120–122]. In this case, despite the help of drug treatments, they do not eradicate the problem[37]. Therefore, there is a pressing need to boost the level of clinical suspicion in order to recognize and treat patients[123].

Going into the incidence of GI symptoms, data show that these interest more than 50% of females and about 60% of untreated children enrolled in the Fabry Outcome Survey[84,105,124]. Cohort studies state that these would affect about 70% of patients[125].

Diarrhea and abdominal pain are the two main symptoms, however, the incidence varies by gender and age[82]. Abdominal pain described as burning or colic-like pain may involve the entire abdomen or only the lower part and is reported by between 43% and 56% of patients[126,127]. It may worsen as a result of food intake or dietary changes. Additionally, it is reported more in children and less in

adults, in 49% and 38% according to Hoffman et al. (2007), respectively. Regardless of the age-related differences, it is interesting to note that in this large court surveyed by the authors no gender differences emerged[124]. In this context, a recent study by Hopkin and colleagues (2020) that examined 171 male Fabry patients before treatment showed a prevalence of abdominal pain of 56%[127].

The other widely complained GI symptom is diarrhea, present in 40-45% of cases[126,128]. In the same 2020 study, 57% of subjects complained of diarrhea, showing an age-dependent correlation[127]. In this case, there also seems to be a sex dependence, in fact, it occurs more in males than in females, ranging from 25.9% to 57% of male patients with variant 1[124,129]. Constipation, on the other hand, is found more in female patients and can be severely disabling[124]. Constipation-diarrhea alternation has also been recorded[109]. On laboratory analysis, stools show no blood, and endoscopic examination reveals no findings. Nausea and vomiting are reported infrequently, in 12.3% and 6.7%, respectively. Overall GI symptoms lead Fabry patients to reduce food intake resulting in weight loss, albeit recent data do not seem to support these findings[7,124].

Main GI manifestations	References
• Abdominal discomfort (42.9-56 %) • Diarrhea (41.8-57 %) • Constipation (13.5 %) • Nausea (12.3 %) • Vomiting (6.7 %)	Martins et al. 2019; Hopkin et al. 2020; Nampoothiri et al. 2020; Hoffman et al. 2007
Other GI manifestations	
• Gastritis, peptic ulcer • Hemorrhoids • Pancreatitis • Diverticular bowel disease • Gastroesophageal reflux • Achalasia • Appendicitis • Chronic bowel pseudo-obstruction • Post-prandial fullness • Delayed gastric emptying • Autoimmune diseases (celiac disease, Crohn's disease) • Chest pain, belching, excessive flatulence	Thomas et al. 2014; Hopkin et al. 2020; Nampoothiri et al. 2020; Germain et al. 2019; Tümer et al. 2004; MacDermot et al. 2001; Deegan et al. 2006; Roberts et al. 1984

Table 2 Gastrointestinal symptoms in Fabry Disease. Modified from Radulescu et al. 2022.

1.5.4 Hypothesis on the gastrointestinal disorders' pathogenesis in Fabry disease

As regards the origin of GI symptoms in FD, given the complex and multifactorial nature, countless hypotheses have been made[37]. Gb3 deposits in ganglion cells of enteric plexuses have long been seen and have been associated with GI disorders like altered motility and pain[102,130]. Studies on autopsies and biopsies exhibited myenteric and submucosal plexuses affected with inclusions, and histopathological investigation revealed vacuolization of ganglion cells and surrounding axons with intracellular Gb3 accumulation[102]. According to these findings recently it has also been demonstrated in the first morphological and molecular study on the colon of a murine model of FD, the thickening of the muscle layer with alteration of ganglionic areas, the presence of Gb3 deposits in nerve fibers entering mucosa and their numerical reduction and morphological damage[131]. These deposits in enteric neurons might contribute to abdominal pain, like it has been supposed to be in patients[102,105,119,132]. The small fiber neuropathy might provoke GI tract ischemia, causing abdominal pain[37]. Furthermore, neuronal damage, by impacting peristalsis, may play a key role in bacterial growth and consequently diarrheal phenomena[133]. This involvement of enteric neurons and vessels would also impair the autonomic nervous system (ANS) causing uncoordinated contractions and inflammation, which are contributing factors to diarrhea. Moreover, it was supposed that Gb3 accumulation may also cause modifications in invariant natural killer T cells, leading to an amplified inflammatory response[134]. Additionally, it was reported that Gb3 deposits impact nitric oxide (NO) pathways inducing a prothrombotic environment[135]. These alterations might be transferred to GI symptoms. It was suggested that abdominal pain is due to inadequate blood flow to the GI tract. Overall, it seems that the neuropathy of FD patients and that of diabetics have many similarities suggesting a similar mechanism[136].

To date, from a clinical-diagnostic point of view, there are no guidelines or tools specifically created for investigating the GI tract of Fabry patients[123]. However, two types of questionnaires, not yet validated, have recently been developed to allow a proper evaluation of FD patients: on the one hand, the FD Patient-Reported Outcome-Gastrointestinal (FABRO-GI), on the other that consisting of a series of questions in combination with the Gastrointestinal Symptom Rating Scale[4,105].

Though there are no diets specifically designed for FD, it is essential to adopt specific eating habits[137]. The same recommendations for the management of IBS are those most recommended for Fabry patients[138,139]. Along these lines, in FD a diet low in short-chain fermentable carbohydrates, foods that attract water and increase gas production, is suggested to ameliorate GI disorders[140]. In IBS it has indeed been shown that a diet low in FODMAPS (fermentable carbohydrates or

fermentable oligosaccharides, disaccharides, monosaccharides, and polyols) improves symptoms of bloating, flatulence, and diarrhea[141].

1.6 Fabry Disease diagnosis

The onset of typical manifestations or family history may lead to the suspicion of FD. Measurement of enzyme activity and genetic testing are the two most commonly used procedures for the diagnosis. In males, the gold standard is the quantification of α-Gal A activity either on dried blood spot (DBS), which is more practical and cost-effective, or in leukocytes[142]. In contrast, for heterozygous females, in whom values within normal ranges can be found, this is not always a reliable method. In fact, in this case only genetic testing, which allows the identification of the genetic mutation, can confirm the diagnosis[4,143]. Genetic testing is also useful for males to identify the specific mutation and then administer the most appropriate therapy. Initially, it was used to measure Gb3 in urine or plasma, however, to date, the measurement of lyso-Gb3 is preferred given its higher sensitivity and specificity[144]. Finally, in cases of controversial mutations and/or ambiguous enzyme activity and lyso-Gb3 values, tissue biopsy can be performed. Indeed, in the latter, it is possible to detect the presence of so-called "zebrafish bodies," i.e., multilamellar myelin bodies[145]. α-Gal A activity can also be measured in chorionic villi or amniotic cells cultured during prenatal diagnosis in the case of a known mutation in the family[2,104].

1.7 Available therapies for Fabry disease treatment

There is no definitive cure for FD, but a lifelong treatment to slow the symptomatic progression. Typically, two levels are simultaneously intervened: on the one hand, the metabolic defect is addressed through enzyme replacement therapy (ERT) or chaperone drug therapy (PCT), and on the other hand, the symptoms as such are addressed with supportive treatments. Currently, in addition, there are promising therapeutic avenues: a) substrate reduction therapy, b) gene therapy, and c) alternative enzyme therapy[79,146].

Nowadays, ERT represents the first-line treatment. This is based on the exogenous administration of the deficient enzyme to slow the progression of the disease[5]. The recombinant enzyme, which expresses the mannose-6-phosphate receptor (M6PR), is collected and transported to lysosomes endocytically[147]. There are currently two preparations available on the market: agalsidase alpha (Replagal®, Shire HGT, Inc., Cambridge, MA, USA; 0.2 mg/kg every 2 weeks) and agalsidase beta (Fabrazyme®, Sanofi Genzyme, Cambridge, MA, USA; 1 mg/kg every 2 weeks). Both were approved

in 2001 by the European Agency for the Evaluation of Medical Products, whilst only Fabrazyme® was approved by the FDA for use in the United States[79].

Data report that Replagal®, which is safe even in children, can improve life expectancy in both males and females[148–150]. In people with advanced kidney disease, a slowing of the loss of function has been shown[151,152]. Patients with abnormal renal function or cardiac hypertrophy before treatment showed modest progression of symptoms, while those with normal renal or cardiac function under 10-year treatment showed no significant advancement[153].

Regarding Fabrazyme®, increased Gb3 clearance has been demonstrated in kidney, heart, and skin treated patients[154]. In addition, male patients, five years after treatment, reported improvement in GI disorders[155]. About renal and cardiac disorders, in other cohorts, cardiac hypertrophy has not advanced and the renal decline has returned parameters[156,157].

PCT migalastat (Galafold™; Amicus Therapeutics, Cranbury, NJ, USA) employs small molecules designed to increase residual enzyme activity, preventing misfolding of the mutated enzyme or its degradation in the cell[158]. The advantageous aspects of PCT are several: increased compliance, given by oral administration; good tolerability, being immunogenic; and the fact that it can diffuse across membranes and reach therapeutic concentrations in different organs, (including the brain) due to its small size. However, PCT also has a major limitation, namely that it can only be used for chaperone-responsive mutations, called "amenable mutations"[159]. In 2016 it was approved in the European Union; in 2018 it was approved in the United States[79].

Therapies under investigation:

a) Substrate reduction therapy

This therapy is designed to decrease pathological substrate production by inhibiting glucosylceramide synthase. To date, *in vitro* and *in vivo* studies are available and clinical trials are ongoing (NIH, ClinicalTrials.gov, Interventional Studies Fabry disease, 2019)[160–162].

b) Gene therapy

This has been validated in the mouse model of Fabry disease[163,164]. To date, experiments of *in vivo* gene therapy using adeno-associated virus vectors and *ex vivo* through autologous stem cell transplantation are being investigated; also the systemic mRNA therapy has been proposed[165–167].

c) Alternative enzyme therapy

This is a PEGylated version of the recombinant enzyme with a longer circulating half-life, as demonstrated in a Phase II study. It also appears to promote a reduction in Gb3 inclusions in peritubular capillaries and stable renal function[168].

1.8 α-Gal A knockout mouse: a reliable model for Fabry Disease study

In FD research the α-Gal A knockout (KO) mouse model is commonly used. This model was developed through a constitutive ablation of the GLA gene as detailed described in Ohshima et al. (1997)[169]. Even though the α-Gal A deficient mouse has some limitations due to lack of some symptoms that occur in human patients (as reported in Table 3)[170], over the years many papers have reported the validity of the model for mood/sensory behavioral and small-fiber neuropathy investigations, as well as for studies on novel drug therapies[94,95,171–175].

Indeed, similar to FD patients, in whom heat hyposensitivity and pain evoked with mechanical hypersensitivity are frequently reported, α-Gal A KO mice show mechanical and heat hypersensitivity associated with cold hyposensitivity[94,172,176]. However, it should be noted that pain studies conducted in KO mice are not always uniform likely cause of mixed genetics background, which makes it difficult to obtain healthy strain-matched controls[177].

Although much remains to be known, at the GI level, studies on the GLA KO mouse have so far shown some evidence that makes it also a reliable model for the study of Fabry-associated GI disorders. In fact, in cross sections of murine ileum and colon, by analysis with high-resolution light microscopy and transmission electron microscopy, Bangari and colleagues (2015) found features that well reflected those of Fabry patients. They identified pathological deposits of Gb3 in smooth muscle cells and ganglia, with enlargement and vacuolization of neurons in the myenteric and submucosal plexuses. In addition, by mass spectrometry, they measured Gb3 levels in ileum and colon samples of KO mice finding significantly higher levels than in wild type (WT)[178]. Therefore, these results already indicated the potential of the α-Gal A KO model for studying neuropathy and enteropathy in FD. Recently, these results have also been corroborated and extended by Masotti et al. (2019)[131]. The authors reported the thickening of the muscle layer with alteration of ganglionic areas, the presence of Gb3 deposits in nerve fibers entering mucosa, and their numerical reduction and morphological damage[131]. Moreover, in this study, as well as in the one proposed in this thesis, the problem of genetic background described above has been overcome. Specifically, the authors separated homozygous α-Gal KO and WT mice after at least 4 generations and performed all

experiments after more than 10 generations, thus eliminating any strain variability in the two genotypes[177].

Signs or symptom in Fabry patient	Presence in mouse model	References
Gb3 deposits	yes	Rodrigues et al. 2009
Ion channel abnormalities	yes	Lakomà et al. 2014; Üçeyler et al. 2016
Abnormal small fiber conduction	yes	Namer et al. 2017
Pain	yes (neuropathic); uncertain (chronic)	Formaggio et al. 2022; Hofmann et al. 2018; Rullo et al. 2021; Üçeyler et al. 2016
Abdominal pain/Visceral Hypersensitivity	yes	The present work
Acroparesthesia	yes	Bangari et al. 2015; Hofmann et al. 2018
Thermal sensitivity	yes	Lakomà et al. 2016; Spitzel et al. 2022
Mechanical sensitivity	yes	Rullo et al. 2021; Spitzel et al. 2022
Sweating abnormalities	no (roditors do not sewat)	Miller et al. 2020
Corneal and lenticular opacities	unknown	
Hearing loss	no	Noben-Trauth et al. 2007; Sakurai et al. 2010
Gastrointestinal distress	yes	Masotti et al.2019; The present work
Renal insufficiency	no (but presence of accumulates)	Rodrigues et al. 2009
Cerebrovascular disease	unknown (but presence of accumulates)	Rodrigues et al. 2009
Vascular/Cardiac disease	yes (partially)	Nguyen et al. 2012; Park et al. 2008
Mood disorsers	yes	Hofmann et al. 2017; The present work

Table 3 Correlations between the signs and symptoms of Fabry disease and the alpha-Gal A KO mouse model

2. Gastrointestinal tract: structures and functional organization

2.1 Anatomy and Histology of the gastrointestinal tract

Anatomically, the GI system is divided into the following parts: oral cavity and salivary glands, esophagus, stomach, small intestine or upper GI tract (divided into duodenum, jejunum, and ileum), and large intestine or lower GI tract (consisting of cecum, colon, and rectum). The upper tract is involved in the transport of the food bolus, enzymatic digestion, and absorption of nutrients, as well as protection against the external environment; while the lower tract in dehydration, storage of fecal material, and reabsorption of water and solutes.

From a histological point of view, we observe an organization into four concentric layers distributed as follows: mucosa, submucosa, tunica muscularis, and serosa (Fig. 3). The mucosa is characterized by adjusting morphology and architecture of the epithelium along the different levels of the GI tract according to the function of the specific segment (digestion, absorption, secretion). The mucosa is made up of 3 components: the epithelium, consisting of a single layer of specialized cells (enterocytes) in columnar arrangement, held together by tight junctions; the lamina propria, consisting mainly of loose connective tissue containing collagen fibrils and elastin; and the muscolaris mucosae, a thin layer of smooth muscle involved in local movements of the GI mucosa.

The submucosa consists mainly of loose connective tissue and collagen and elastin fibrils. Here are mucus-secreting glands, blood and lymph vessels, and one of the two enteric nervous system (ENS) plexuses: the Meissner plexus or submucosal plexus (see paragraph 2.3.1).

The tunica muscularis (or muscolaris propria) is a layer of smooth muscle consisting of an inner layer, where the fibers are organized circularly, and an outer layer, where they are instead longitudinal. This is responsible for peristaltic movement and is the site of the second nerve plexus: the Auerbach's (or myenteric) plexus, located between the two muscle layers mentioned above.

Finally, the serosa is composed of a secretory epithelial layer (mesothelium), which produces a mucus-like lubricating serous fluid to reduce the friction of muscle movement, and an underlying connective tissue layer that provides blood vessels and nerve fibers to the mesothelium as well as adhesion to the intestine. On the other hand, the retroperitoneal parts are covered by adventitia, consisting of collagenous tissue for the passage of the large blood vessels and nerves that support and modulate the entire GI tract.
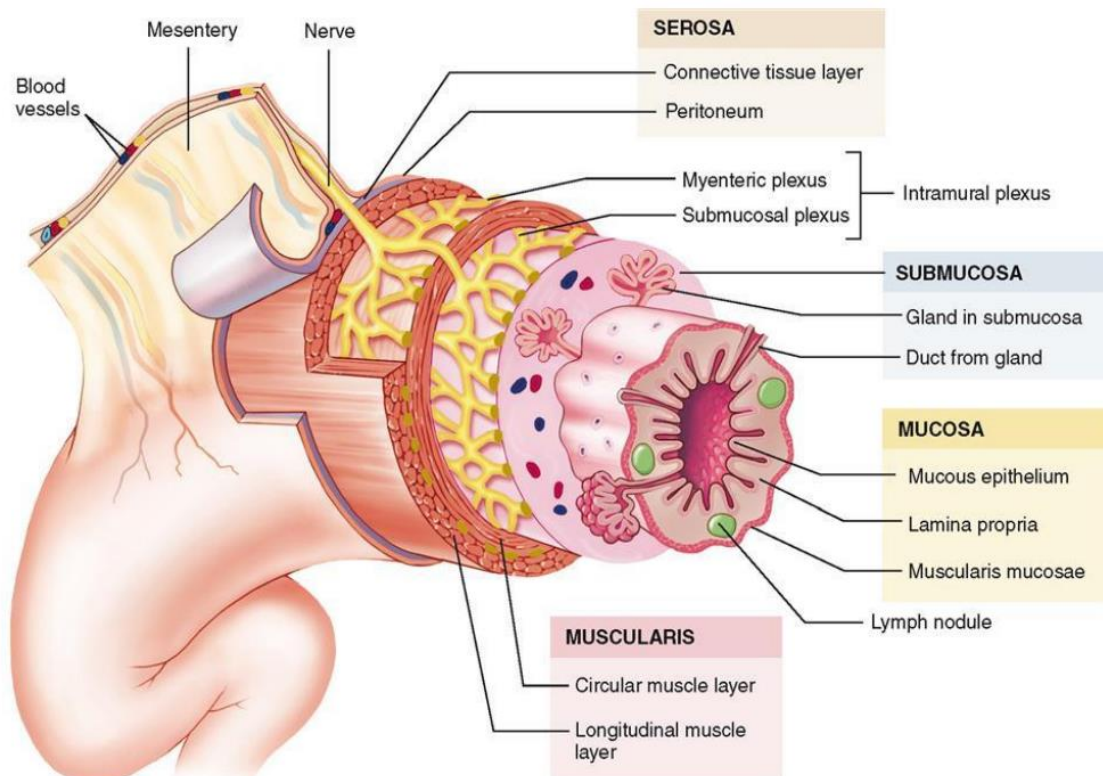
Figure 3 Representation of the gastrointestinal layers. The image illustrates the four layers of GI wall: mucosa, submucosa, muscularis and serosa and the relative sub-layers (*boxes*). The localization of glands, lymph glands, nerves, myenteric and submucosal plexuses and blood vessels are also represented. From Gastrointestinal Tract Histology.

2.2 Human and murine gastrointestinal tract comparison

The GI tract of humans and mice consists of anatomically similar organs and exhibits similar physiological mechanisms. This makes the mouse a valuable and commonly used model in the research field. However, different diets, body sizes, and metabolic requirements mean that there are also significant differences[179–181].

As with the human intestine, the mouse one is divided into upper and lower tracts (Fig 4). In an adult mouse, the small intestine measures about 35 cm. Whilst the large intestine is shorter and is 14 cm approximately[182]. Macroscopically, despite the average ratio "intestinal surface area: body surface area" is similar between the two species, it considerably varies in different segments. For instance, the small intestine: colon length ratio is 2.5 in mice and around 7 in humans[183,184]. Again, the human cecum is quite small, conversely, the mouse one is particularly developed, nearly one-third of the total length of the large intestine, and serves as a fermentation container. Indeed, in mice, this is essential for the fermentation of plant materials and the production of vitamins K and B, which they reabsorb through coprophagy[181,184]. An appendix is also present in humans, whereas it is absent in mice[185]. Another relevant difference is about intestinal villi, which are bigger in mice than in humans

so that the available surface area is expanded. Regarding the colon, of particular relevance to this study, in the mouse, this is rather smooth and lacks the typical sacs (haustra) found in human (Fig. 4). Such differences between murine and human GI tracts, especially regarding the greater fermentation capacity of mice, are to be considered for their impact on the diversity and composition of microbial communities in the colon. Indeed, these bacterial populations are crucial as they are involved in the production of essential host complements such as vitamins K and B and short-chain fatty acids (SCFAs) as well as in the fermentation of indigestible food components[179].
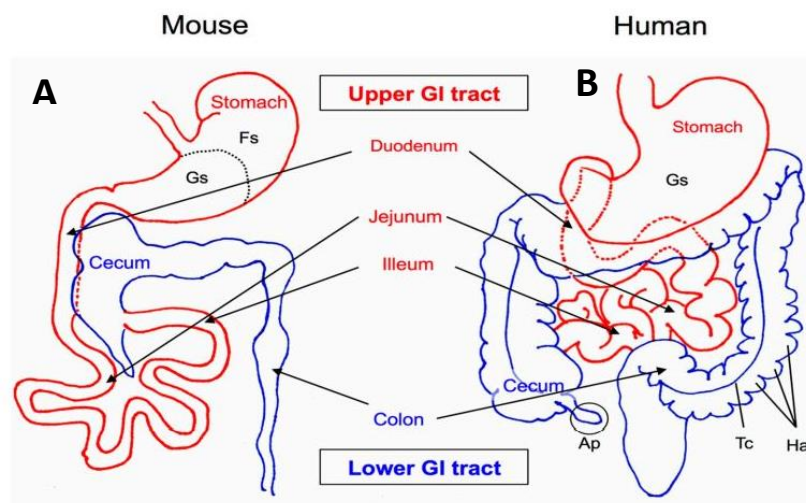
Figure 4 Murine and human gastrointestinal tract comparison. The upper (*red*) and the lower (*blue*) GI tract of mouse (A) and (B) human are shown. Fs, forestomach; Gs, glandular stomach; Ap, appendix; Tc, taenia coli; Ha, haustra. Modified from Nishiyama et al. 2016.

At the microscopic level, some relevant differences can also be found: the murine colon has a thin muscularis mucosae in which the submucosa cannot be distinguished, whereas the human colon is covered by a thicker mucosal wall. The presence of transverse strips along the length of the colonic mucosa in humans, and the presence of these only in the cecum and proximal colon, is another important difference[184,186].

At the cellular level, differences include those of Goblet and Paneth cells. The former, which produce mucin, in humans are almost evenly distributed from the cecum to the colon, whereas in mice they are very abundant along the surface of intestinal crypts in the proximal colon but diminish in the distal and rectum; the latter, which secrete antimicrobial compounds into the lumen of the small intestine, are rare but present in the cecum and proximal colon of humans, but completely absent in the mucosa of the murine colon, where they are found exclusively in the cecum. The different localization of the above cells also implies differences in local immune responses, which could shape the composition of the intestinal microbiota[179,181,182,187].

2.3 Enteric Nervous System (ENS)

The GI tract is the only internal organ with its own intrinsic innervation system, known as the enteric nervous system (ENS), which can function independently of input from the central nervous system (CNS)[188,189]. Indeed, for years it has been demonstrated that *ex vivo* the gut can continue to generate propulsive neurogenic motor patterns even after extrinsic nerves removal[189–192]. However, despite the ENS can function autonomously, is considered to be quasi-autonomous[193]. The control of GI functions is based on a complex system of interaction/integration between local enteric reflexes, reflexes that pass through the sympathetic ganglia, and reflexes that pass from the gut to the CNS[194]. Indeed, innervation includes intrinsic sensory neurons completely contained in the GI wall, intestinofugal fibers that project to prevertebral ganglia, and vagal and spinal afferents that project into the CNS (Fig. 5)[195,196]. The ENS regulates and coordinates several intestinal functions from motility, fluid and electrolyte transport, and mucin secretion to cytokine production and GI barrier maintenance[194,197,198]. All of these functions represent essential aspects of GI physiology. In fact, impairment of one or more of these functions is found in various GI diseases such as IBD and IBS, as well as in various neuropathies, whether congenital, sporadic or associated with other diseases[194]. Therefore, it is not surprising that there is a growing scientific interest in understanding what role ENS might play in GI disorders[199].
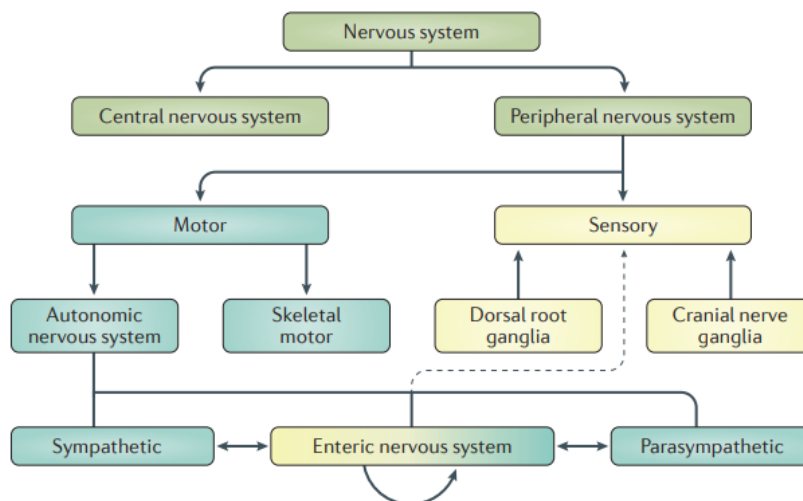
Figure 5 Schematic representation of the two-way communication between the ENS and CNS. From the periphery to the CNS the afferent information travel via neurons in dorsal root or cranial nerve ganglia ("sensory" portion; *yellow*). Thanks to CNS integration, the efferent output moves through the "motor" division (*green*). From the CNS, the efferent projections reach either skeletal muscle or the ANS, which consists of sympathetic, parasympathetic and ENS. The ENS neurons are organized in an integrated circuit that contains intrinsic primary afferent neurons (IPANs) able to respond intrinsically to local stimuli and to combine information and organize motor responses. The exceptional ENS sensory and motor properties are indicated (*dotted line*). From Rao and Gershon 2016.

2.3.1 Organization of ENS: myenteric plexus, submucosal plexus, and muscle innervation

In humans, the ENS consists of about 400 to 600 million neurons and even more supporting cells (enteric glia) outnumbering from 3 to 5 times enteric neurons[197]. These are grouped into ganglia in neuronal continuity with each other to form two ganglionic plexuses: the myenteric plexus (MP) or Auerbach's and the submucosal plexus (SMP) or Meissner's (Fig. 3)[197]. Within each of the two plexuses are different neuronal populations distinguishable by neurochemical coding, projections, and function[188]. Both consist of the axons of neurons located there, a mix of afferent neurons, interneurons, and secretomotor neurons. There are also extrinsic afferent fibers from the nodose or jugular ganglia (vagal afferents), and the dorsal root ganglia (DRG) (spinal afferents)[195,197,200]. Thus, a communication network is established between the GI tract and the brain for coordination between gut reflexes and behavioral responses CNS specific, as well as for pain perception (Fig.6)[201–
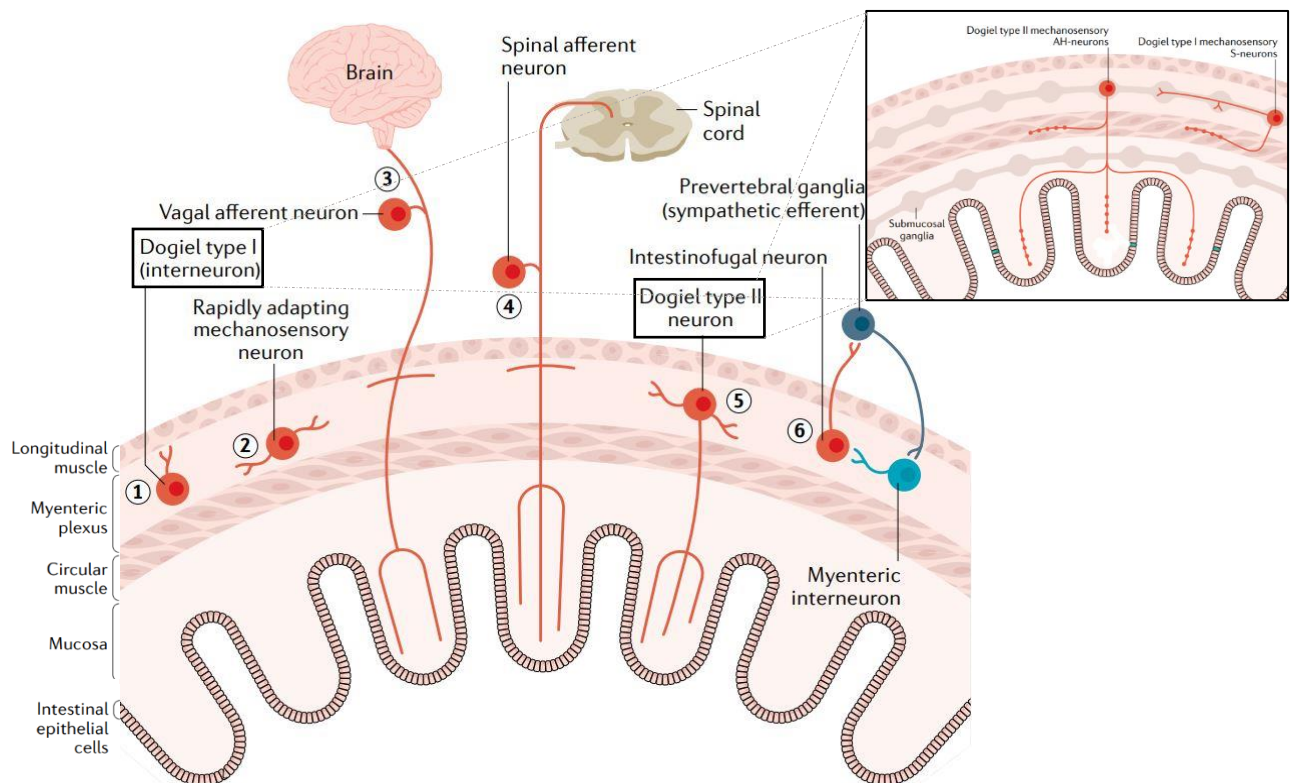
Figure 6 ENS organization with different types of intrinsic and extrinsic sensory neurons. Myenteric and submucosal plexuses are represented. (1) Dogiel type I neurons (*zoom in the box*) are myenteric mechanosensory that functionally act as interneurons and are largely length sensitive and tension insensitive. (2) Rapidly adapting myenteric mechanosensory neurons (cholinergic and nitrergic). (3) Extrinsic vagal afferent neurons innervating mostly the upper gut and acting as slowly adapting tension receptors. (4) Spinal afferents providing a rich sensory innervation of the lower tract, strongly activated by stretch and muscle tension. (5) Dogiel type II neurons (*zoom in the box*) are myenteric chemo- and mechanosensory with projection into the mucosa. They receive fast and slow synaptic inputs from other enteric neurons. (6) Intestinofugal neurons, generally thought as second order neurons, but can be also directly mechanosensitive and respond to mechanical compression stimuli. Modified from Spencer and Hu 2020.

[203]. The MP is a network located between the two layers of longitudinal and circular musculature and forms a continuum around the entire GI tract. Its main function is motor innervation of the musculature for peristaltic movements[197].

The SMP lies between the muscolaris mucosae and the circular musculature. It generally has smaller ganglia than MP and a finer inter-ganglionic connection[188,200,204]. In large mammals it is possible to distinguish two layers, sometimes separated by an additional intermediate layer[205,206]. Instead, in small mammals, as in the guinea pig and mouse, there is a single layer containing secretomotor neurons[207,208]. The nerve fibers of the SMP innervate the smooth muscularis mucosae and establish a functional interaction with epithelial cells (enterocytes, caliciform cells, enteroendocrine cells, Paneth cells, microfold cells, cup cells, and tuft cells) in the mucosa[197].

The motor innervation of longitudinal and circular muscles is basically from neurons that have their neuronal bodies in the MP. In particular, the innervation of longitudinal muscles depends on their thickness: for thick muscle layers, a longitudinal muscle plexus consisting of bundles of nerve fibers parallel to the muscle can be found[209]. In contrast, for thinner layers, there are bundles of MP axons adjacent to the inner wall of the muscle. Circular muscles have innervation consisting of thin bundles of nerves parallel to the muscle. Largely these are motor neurons with the cell body in MP, but they can also originate from the SMP[197].

2.3.2 Morphological and electrophysiological classification of enteric neurons

Despite many similarities with the CNS, the morphology, function, and neurochemistry of GI neurons differ significantly from those of the sympathetic and parasympathetic autonomic divisions. In fact, the enteric ganglia are interconnected and can integrate and process information similarly to the brain and spinal cord (hence the term "mini-brain in the gut"). However, the sympathetic and parasympathetic ganglia act more as intermediaries between the brain and spinal cord, and the periphery[190].

Morphologically, ENS neurons can be classified, based on the descriptions provided by Alexander S. Dogiel, into Dogiel Type I and Dogiel Type II (Fig. 6)[210]. They have discoidal, flattened cell bodies from which multiple neurites unravel, adapting to the intestinal wall during contraction and relaxation processes/filling and emptying of the organ; Dogiel Type I account for approximately 80-90% of the neurons present in the MP and SMP[211,212]. They project in the circumferential and longitudinal plane and are flat; they have many short processes (dendrites), that receive synaptic input, and a single long process (axon) that projects long distances through many layers of ganglia.

Depending on their direction of projection, they express specific neurotransmitters. Dogiel Type II neurons exhibit different configurations, smooth surfaces, and both long and short processes that can cross inter-ganglionic fiber tracts and several layers of ganglia in circumferential, oral or aboral directions. All Dogiel Type II neurons in the MP develop towards the submucosa/mucosa[190]. In addition, in the murine colon MP, they have been seen to project both to other myenteric ganglia and the SMP, suggesting a key role in regulating the coordination of enteric reflexes[213,214].

Also from the point of view of electrical behavior, two subtypes can be distinguished: S-type and AH-type neurons. S-type neurons are characterized by monophasic potentials, the presence of fast excitatory postsynaptic potentials, and the absence of long-lasting hyperpolarizing after potentials[211]. Studies have revealed that S-type neurons are repetitively activated during intraneuronal injection of long-duration depolarizing current via microelectrode recording. The frequency of the repetitive discharge increases in proportion to the amplitude of depolarization produced by the injected pulses[190,215]. In contrast, this repetitive discharge of the potential generally does not occur in AH-type neurons. These are characterized by lower membrane excitability, produce biphasic responses, contain a hump on the repolarizing phase of the action potential, generally contain slow after-hyperpolarization and do not produce fast excitatory postsynaptic potentials. S-type behavior is mainly found in Dogiel Type I neurons, AH-type one in Dogiel Type II morphology[190,215,216].

2.3.3 Functional classification and chemical coding of enteric neurons

From a functional point of view, ENS neurons can be classified into: a) intrinsic primary afferent neurons (IPANs); b) motor neurons; c) interneurons; d) intestinofugal neurons (IFANs) (Fig. 7)[214,217].

a) Intrinsic primary afferent neurons.

IPANs, primary neurons of the intestinal reflex pathways, have cell bodies, processes, and synaptic connections embedded in the intestinal wall (Fig.7, *blue*). They respond to stimuli such as distension, luminal chemistry and mechanical stimulation of the mucosa, conveying information to local integrative reflexes[197,204,218–220]. Indeed, they are involved in the control of motility, secretion, and blood flow[221]. Their targets are mainly at the mucosal level but can also be other MP and SMP neurons[205,212,222]. Of note, IPANs can also act as nociceptors, triggering protective responses through the spinal pathway[197].

Morphologically, IPANs are multi-axonal (Dogiel Type II) and make up 10-30% of neurons in the SMP and MP ganglia of the small and large intestines. Electrophysiologically, they have broad action potentials Na$^+$- and Ca^{2+}-mediated followed by early and slow hyperpolarizing potentials.[221] Studies in guinea pig ileum report that more than 80% of MP IPANs express calbindin (CALB), a calcium-binding protein, against 30% of SMP[223–225]. Instead, the majority express cytoplasmic NeuN and Choline acetyltransferase (ChAT)[226–230]. In the mouse colon, CALB also emerged as not being a good marker of IPANs; in fact, anti-calcitonin-gene-related-peptide (CGRP) antibody emerged as the most specific marker of these cells[231,232].

b) Motor neurons

Motor neurons refer to all neurons that innervate the longitudinal and circular muscularis propria and muscolaris mucosae. Excitatory and inhibitory neurons are included in this category (Fig. 7, *light blue and dark green*)[214]. Generally, the neuronal bodies of neurons innervating the muscularis propria are located in the MP[197,214,233]. In this case, the neurochemical code is well defined: the primary excitatory transmitter is acetylcholine (Ach), although tachykinins (especially substance P, (SP)) colocalize with ACh; conversely, the inhibitory one is nitric oxide (NO), although again there is the involvement of other neurotransmitters such as adenine triphosphate (ATP) and vasoactive intestinal peptide (VIP)[197,216,233–236]. Another important subclass is represented by secretomotor and vasomotor neurons. These neurons have their cell bodies in the SMP and mucosal projections[214,237,238]. The neurochemical code for these cells also seems well defined: in all species studied, small VIP-positive neurons have mucosal projections and are probably involved in secretory processes[239–241].

c) Interneurons

Interneurons, located mainly in the MP, are responsible for the formation of local circuits (ascending and descending) and have the longest projections[241,242]. Sometimes, they can also act as mechanoreceptors[188,243,244]. Ascending interneurons (Fig. 7, *yellow*) are Dogiel Type I, cholinergic, and may also contain calretinin and SP, while those descending (Fig. 7, *light green*) are cholinergic but can also be distinguished by their positivity to NOS/VIP, and 5-hydroxytryptamine (5-HT)[214,245–247]. A study by Porter and colleagues (2002) showed that in the human colon, 90% of the oral projection interneurons contains only ChAT, whereas other neurons are ChAT- and nNOS-negative; among the anal projection interneurons, it is possible to distinguish between neurons expressing

ChAT and NOS, neurons only NOS-positive, and neurons only ChAT-positive[248]. Moreover, in humans, descending-projection NOS-positive interneurons can co-express VIP[249].
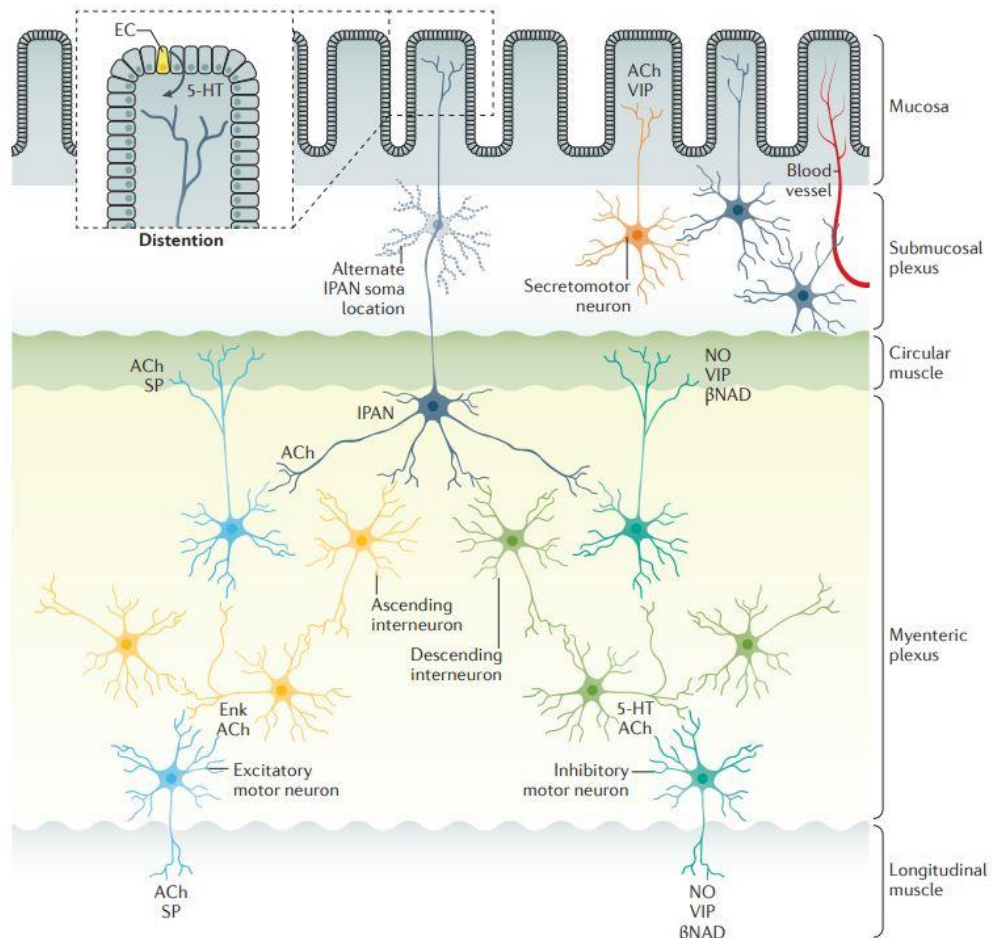
Figure 7 Localization and chemical coding of ENS neurons. Mechanoreceptive endings of intrinsic primary afferent neurons (IPANs) are displayed (*blue*). They are directly activated by luminal distension/distortion or indirectly by serotonin (5-HT) release from enterochromaffin cells (ECs) in the epithelium. IPANs activate ascending (*yellow*) and descending (*light green*) interneurons, which stimulate excitatory (*light blue*) and inhibitory (*green*) motor neurons, respectively. Ach, acetylcholine; SP, substance P. Enk, encephalin. NO, nitric oxide; VIP, vasoactive intestinal peptide; βNAD, β-nicotinamide adenine dinucleotide. Modified from Rao and Gershon 2016.

d) intestinofugal neurons

IFANs display mainly Dogiel Type l morphology and sometimes Type II. They have the cell body in MP and project outward from the intestinal wall[250]. Their function is to detect changes in volume and respond to muscle stretching, as mechanoreceptors[251,252]. Once activated, they release Ach to sympathetic neurons by evoking fast postsynaptic potentials. Some IFANs, following colonic distension, may also release gamma-aminobutyric acid (GABA) into the prevertebral ganglion promoting Ach release. This would cause norepinephrine release in the GI wall, and thus muscle contractions or control of myenteric neurons[253–255].

2.3.4 Extrinsic innervation

As previously mentioned, though the ENS is capable of acting autonomously, its connection with the CNS cannot be ignored[193]. In fact, the ENS and CNS cooperate in bidirectional communication. The connections between them can be classified into *vagal* and *spinal*; the latter in turn divided into *thoracolumbar* and *lumbosacral*. Each of these has sensory (afferent innervation) and motor (efferent innervation) functions[194,256]. Sensory afferent fibers originate in the intestinal wall and project to the CNS through the vagus nerve and the spinal pathway[256]. Most of these are thinly myelinated Aδ or unmyelinated C fibers with free endings directly in the target organ[257]. They are distinguished into intraganglionic MP ganglia laminar, mucosal, intramuscular, muscularis mucosae (close to the muscularis mucosae) and vascular[258,259]. Efferent fibers come from the CNS and project into the enteric ganglia by controlling and/or modifying their activity. The sympathetic pathway is specific to the thoracolumbar connections, while the parasympathetic to the craniosacral connections[256].

2.3.4.1 Vagal innervation

The vagus nerve mainly innervates the upper GI tract (esophagus, stomach, proximal small intestine, liver, pancreas) whil in the caudal small intestine and proximal colon, it is less present[256]. In fact, there are enteroendocrine cells that detect information and release hormones such as cholecystokinin (CCK) and serotonin (5-HT). These create a chemoreception mechanism of vagal afferent endings for reaction to luminal stimuli[260–262]. Appetite, satiety, esophageal propulsion, gastric volume, contractile activity, acid secretion, gallbladder contraction, and pancreatic enzyme secretion are some of the functions regulated by these afferents neurons[256]. In addition, the vagus nerve is involved in the perception of adverse sensations such as bloating, nausea, apnea, and unpleasantness associated with visceral pain[257].

2.3.4.2 Spinal innervation - Thoracolumbar region

The sympathetic innervation of the GI tract originates from the thoracolumbar (T5-L2) region of the spinal cord. The afferent section arises in the DRGs and the axons are predominantly unmyelinated C-fibers[256]. Endings are found around the arterioles of the intestinal wall, in musculature, in the MP and SMP ganglia, and the lamina propria; fibers have also been identified in the serosa[259,263,264].
A large number of these neurons appear CGRP- and VIP-positive, markers commonly used for sensory fibers[265,266]. In addition, they express the Transient Receptor Potential Vanilloid 1 (TRPV1)

channel, known to be involved in visceral nociception[267,268]. In contrast, the sympathetic efferent section predominantly involves the two plexuses, blood vessels, and sphincter muscle[256].

The sympathetic pathway comprises preganglionic and postganglionic neurons. Preganglionic neurons have their cell bodies in the intermediate columns of the spinal cord; postganglionic ones in the paravertebral ganglia (mainly vasoconstrictor neurons) and prevertebral ganglia (vasoconstrictor neurons, neurons controlling motility and secretion)[197].

2.3.4.3 Spinal innervation – Lumbosacral region

The lumbosacral region of the spinal cord provides afferent and efferent innervation to the distal colon and rectum from the sacral and lumbar roots[256]. Pelvic afferents are characterized by the presence of nociceptive fibers[269]. In the case of mild touches of the colonic or small intestine mucosa, the fibers carry information as low-threshold mechanoreceptors[270]. In contrast, in the rectum, mucosal mechanoreceptors act in response to stretching and distension of the wall, up to the level of pain[271]. As for the efferent pelvic pathways, these innervate the enteric ganglia of the distal colon and rectum[272]. It should be mentioned that in the lumbosacral L5-S3 region of the spinal cord is located also the defecation center. Distention or irritation, through this center, can trigger the different reflexes involved in defecation control[273].

2.3.5 Enteric glia: structure and functions

Enteric glial cells (EGCs) represent a large and unique population of peripheral neuroglia first described by Gabella (1972)[274]. EGCs lack myelin coating and are found associated with the cell bodies and processes of enteric neurons throughout the GI tract[275]. Their number exceeds that of enteric neurons. In the guinea pig ileum's MP ganglia, glial cells are twice as abundant as the neuronal population. Moreover, their structure and morphology have been shown to be more similar to astrocytes than to Schwann cells[276]. In the GI tract, it is possible to distinguish between different types of EGCs based on their anatomical settings: glia associated with the cell bodies of MP and SMP neurons, glia within the bundles of nerve fibers connecting the MP ganglia, extra-ganglionic glia, associated with nerve fibers of either plexus or mucosa, and glia associated with nerve fibers of the smooth muscle layers[275].

From an immunohistochemical point of view, several markers can be used to identify EGCs. Among them, the transcription factor Sox10 (SRY-related HMG-box 10), glial fibrillary acidic protein (GFAP), and calcium-binding protein beta S100 (S100β) are the most widely used[277–282]. Sox10 is expressed

by enteric neural crest progenitors, thus it is used as an early and general marker; GFAP and S100β, meanwhile, are expressed only in specific subpopulations[283]. EGCs broadly serve functions in controlling ENS homeostasis. More recent advances have begun to define more precisely what these functions are and the mechanisms involved. Published data revealed that enteric glia has a marked dynamicity in signaling, renewing the idea of glial cells as merely support cells[275]. Whether there is a correlation between functional heterogeneity and different localization remains to be clarified[284]. However, it is known that glia in MP and SMP support and modulate neuronal signaling in mice, while in mucosa influences enterocyte development and immune responses in cell culture[285–291]. Enteric glia has also a neuroprotective action which is expressed in several ways: by increasing neuronal survival and reducing oxidative stress-induced cell death, by secreting glial mediators with neuroprotective effects and substrates for neuronal enzymes involved in the neuro-mediators synthesis, by regulating the neuro-mediators expression, regenerating enteric neurons, and participating in postnatal ENS development via Toll-like receptor 2 (TLR2) expression[292–295]. Furthermore, the role in controlling GI non-neuronal functions: regulation of motility and homeostasis of the intestinal epithelial barrier[287,289,296]. In 2019, Morales-Soto and Gulbransen highlighted that there is abundant evidence suggesting a crosstalk between EGCs and nociceptors. This might lead to link mechanisms of visceral hypersensitivity and enteric glia, emphasizing the role of EGCs in pain perception[297]. In addition, TRPV1 and TRPV4 ion channels, notoriously associated with pain, are expressed in EGCs and may play a role in glial maturation in mice and inflammation in colitis patients, respectively[298,299]. Since GI neuropathologies are roughly the failure of homeostasis maintained by the ENS, it is critical to consider the role of glia in any study[300,301]. In this context, in Parkinson's disease, GI inflammation has been associated with glial dysregulation[302]. Impairments were also observed in slow transit constipation and megacolon, two severe disorders of GI motility[281]. Additionally, in IBD, the proliferation of EGCs has been found to be altered in GFAP and S100β expressions[282]. Finally, in a mouse model of mucopolysaccharidosis IIIB increased expression of GFAP in MP and SMP was interpreted as enteric glial activation secondary to lysosomal deposits[303].

2.4 Gut-brain axis

The bidirectional neuronal pathway connecting CNS and ENS has prompted researchers to develop the "gut–brain axis" concept. The concept arises with the intent to elucidate the mechanisms underlying the linking between cognitive, emotional, and autonomic centers and the ENS, and

neuroendocrine-immune system. In the early '90, the first observation regarding this two-way biochemical communication was by Pavlov, with his work about classic conditioning in the cephalic phase of digestion, where there was stimulation of gastric and pancreatic secretions in response to sensory signals[304]. The complex network includes the vagus nerve way, with its sympathetic and parasympathetic signals, and the hormonal and immune pathways[305–308].

Vagal afferents with cell bodies in the nodose ganglion project to the solitary nucleus in the brainstem. Visceral afferents converging at the spinal level terminate in the dorsal horn with second-order neurons projecting to higher centers via the dorsal column pathway, the parabrachial pathway, and the spinothalamic tract, as described in the previous paragraph[309]. Studies in which dorsal column lesions have been executed displayed suppression of pain stimulation-induced inhibition of exploratory behavior and visceromotor reflexes elicited by colon-rectal distension[310]. To the vagal afferents of the nucleus solitarius, spino-parabrachial projections reach higher limbic and cognitive centers, including the amygdala, hypothalamus, and periaqueductal gray, namely areas involved in affect[309,311]. Thus, the afferents are involved in activating and regulating the Hypothalamic Pituitary Adrenal (HPA) axis. Electrical stimulation of afferent vagal fibers leads to the production of IL-1 beta in the brain, which in turn is implicated in HPA axis functions[307]. In this context, the clinical measurement of vagal tone is found to be reduced in conditions of anxiety and dysbiosis as is the case of IBD and IBS.

In contrast, vagus nerve stimulation would help restore homeostasis in the microbiota-gut-brain axis[312]. Regarding the latter, several pieces of evidence suggest that the connection between gut and brain should be extended to the gut microbiota (see paragraph 2.4.1). Hence, the comprehensive name microbiota-gut-brain axis (Fig. 8). The hypothesis that bacterial populations in the GI tract may participate in CNS development and maintenance is now confirmed[313]. Germ-free mouse models have shown altered neurogenesis and morphology of the hippocampus and amygdala, as well as of the microglia morphology[314–316]. These findings established a connection between pathological alterations in the gut microbiota and neurological diseases. Interestingly, studies on germ-free mice and rats transplanted with microbiota from patients also revealed a "microbiota-anxiety behavior" and "microbiota-depression" association, respectively[317,318].
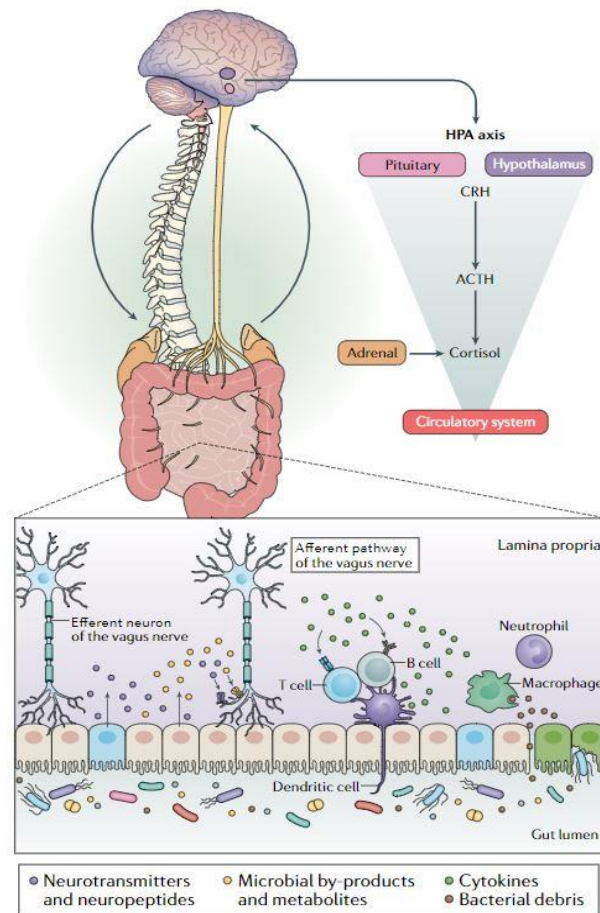
Figure 8 Microbiota-Gut-brain axis This bidirectional communication between the GI system and CNS is mediated by direct and indirect ways of the gut-brain axis. The communication pathways involve the ANS (e.g., ENS and vagus nerve), neuroendocrine system, hypothalamic-pituitary-adrenal (HPA) axis, immune system, and metabolic routes. Within the gut, the microbiota can produce neuroactive compounds such as neurotransmitters (GABA, norepinephrine, dopamine, and serotonin, amino acids (e.g., tyramine and tryptophan), and microbial metabolites (e.g., SCFAs). These metabolites move through the portal circulation and interact with the host immune system, affecting the metabolism and/or local CNS neuronal cells and vagus nerve afferent paths that signal directly to the brain. The microbiota may also act on the integrity of the gut barrier, which in some neuropsychiatric disorders, such as anxiety, autism spectrum disorder, and depression may be compromised. Stress can activate the HPA axis response, involving neurons in the hypothalamus that secrete hormones such as corticotropin-receptor hormone, triggering the release of adrenocorticotrophic hormone, which causes the synthesis and release of cortisol. The latter regulates neuroimmune signalling responses that, in turn, affect the integrity of the intestinal barrier. Stress hormones, immune mediators, and neurotransmitters can activate CNS neuronal cells and vagus nerve afferent pathways, altering the gut environment and changing the microbiota composition. From Morais et al. 2021

2.4.1 Gut microbiota

"Gut microbiota" refers to a collection of microorganisms, mainly bacteria, that colonize the GI tract. The number of these bacteria has been estimated to be around 10^{14}, weighing approximately 2 kg, more than the cells of the entire human body[319]. Based on variation in 16S rRNA genes, between

500 and 1000 different species belonging to more than 70 genera have been estimated. Suffice it to say that the human gut microbiome contains 100 times as many genes as the human genome[320]. Each individual has a unique and specific microbiota, the composition of which is the result of many factors such as genotype, host pathophysiology, mode of first colonization, and not least environmental factors, diet, and medication use. However, as revealed by a metabolic reconstruction based on data from the Human Microbiome Consortium, metabolic function among the individuals examined does not vary that considerably due to the redundancy of biochemical pathways among alternative members of the microbiota[321].

The fetus does not have its own microbiota but acquires it from its mother by vertical transmission at the time of birth and from contact with the external environment. Its composition stabilizes about 3-4 years. In this regard, recent studies revealed that there is variability between children born of natural birth or cesarean delivery, as well as between breastfeeding or artificial feeding[322–324]. Then, over the course of life, the microbiota changes and diversifies[325].

The human gut microbiota most abundantly includes two major gram-negative anaerobic phyla, the *Bacteroidetes* and *Firmicutes*, and one gram-positive phylum, *Actinobacteria*[326–328]. Other identified types are present in small numbers and include some species of the *Proteobacteria*, *Cyanobacteria*, *Verrucomicrobia*, and *Actinobacteria* phyla[329].

Bacterial colonization brings with it two main advantages. The first is to educate the immune system and increase tolerance to microbial immune determinants; the second is to metabolize, degrade otherwise indigestible substances, potentially toxic food compounds (e.g. oxalate), and synthesize some vitamins and amino acids[330]. During these processes, the microbiota releases a wide range of metabolites and small molecules that affect the body. The main site of fermentation is the proximal colon, where substrate availability is higher. The latter along the distal colon decreases, and with it the microbial production. Specifically, saccharolytic primary fermenters such as *Bacteroidetes* ferment nondigestible carbohydrates in the proximal colon and produce short-chain fatty acids (SCFAs), along with CO_2 and H_2 gases[331]. At the most distal part of the colon, however, fermentation of bacterial proteins and amino acids derived from primary fermenters occurs by secondary fermenters, proteolytic bacteria. The degradation of proteins and amino acids results in branched-chain fatty acids, accompanied by potentially toxic metabolites such as amines, phenolic compounds, and volatile sulfuric compounds[332].

In addition, the gut microbiota, under healthy conditions, can stimulate the immune system and induce the release of proinflammatory cytokines such as IL-1β, IL-6, or TNF-α, thus considerably

affecting the immune response and protection of the host from pathogens[333]. As a result, any alteration in gut microbial composition, diversity, or function may pose a risk[334]. A good balance between microbiota and mucosal immunity ensures intestinal homeostasis, whose imbalance can lead to adverse conditions such as IBD, Crohn's disease, and ulcerative colitis[326].

Experiments in germ-free mice have shown the importance of the microbiota also in relation to several essential CNS processes. These include the metabolism of serotonin (of which tryptophan is a precursor), a neurotransmitter responsible for mood and appetite, produced mainly by enterochromaffin cells of the GI tract[335]. In addition, germ-free animals also showed cognitive impairment, sociability problems, and depressive and anxious behaviours[336].

2.4.2 Short Chain Fatty Acids (SCFAs)

SCFAs are saturated aliphatic organic acids composed of one to six carbons. Acetate (C2), propionate (C3), and butyrate (C4) account for 95%[337]. These are present in an approximate 30:10:10 molar ratio in colon and feces[338–340]. Their total concentration can vary from 70 to 140 mM in the proximal colon to 20-70 mM in the distal colon, depending on diet[331].

Most GI bacteria get acetate as their net fermentation product. In contrast, propionate and butyrate are produced by more specific bacterial species. Butyrate can be produced via glycolysis from acetate, lactate, amino acids and various carbohydrates by two different pathways: the butyryl-CoA: acetate CoA-transferase or the phosphotransbutyrylase and butyrate kinase pathway. For example, some families from the order *Clostridiales* (*Firmicutes*) such as *Lachnospiraceae* (*Coprococcus, Eubacterium, Anaerostipes*, and *Roseburia*), and *Ruminococcaceae* (*Faecalibacterium)* are able to produce butyrate[341–343]. Propionate is produced from various substrates, including amino acids, carbohydrates, lactate, and 1,2-propanediol, via succinate substrate, its precursor. The succinate pathway is specific to *Bacteroidetes* and some *Firmicutes*. An alternative way used by some *Firmicutes*, belonging to the *Lachnospiraceae* and *Ruminococcaceae*, is the acrylate pathway, where the substrate for propionate production is given by lactate. The commensal bacterium *Akkermansia muciniphila* (phylum *Verrucomicrobia*) produces propionate from the propanediol pathway from deoxy sugars[344]. For the microbial community, SCFAs are a necessary waste product to balance the production of redox equivalents in the anaerobic environment of the gut[345]. However, SCFAs are responsible for much more. In fact, they are involved in the regulation of gut motility and brain, secretion, and signaling. To do this, they act through receptors for free fatty acids on epithelial, enteroendocrine, immune cells, and both intrinsic and extrinsic neurons of the GI tract[346–348]. There

are several mechanisms by which SCFAs can affect the host. These include regulation of acetylation and methylation of histones and G-protein-coupled receptors (GPCRs), secretion of various hormones and neurochemicals (e.g., serotonin), and induction of vagus nerve signaling[349–355]. Furthermore, it has been shown in rodent experiments that SCFAs can be used as a mitochondrial energy source[356–358]. The contribution of SCFAs has also emerged associated with the maintenance of physical barriers (blood-brain and intestinal) through action on tight junctions[359–361].

Hence, since SCFAs can impact the host in a multitude of ways, it is not surprising that SCFAs are implicated in numerous functions. GI tract functions, lipid-, glucose-, and cholesterol-metabolism, blood pressure regulation, circadian rhythm, and immune function[362–368]. In this regard, it has emerged in recent decades that SCFAs could be crucial in the prevention and treatment of metabolic syndrome, intestinal disorders, and some cancers[369,370]. In clinical trials, for example, SCFAs administration had a positive impact on the treatment of ulcerative colitis, Crohn's disease, and antibiotic-associated diarrhea[371–374]. Concerning the gut-brain axis, it should be mentioned that SCFAs influence memory and learning processes, as well as the release of serotonin by the mucosa[375]. The amount of serotonin produced in the CNS is small compared with that in the gut, which is about 90% of the total. A substrate for serotonin production in the brain and gut is tryptophan, the metabolism of which is an essential modulator of the gut-brain axis. For example, depression and low mood conditions have been related to a reduction in tryptophan metabolism.

Also emotion processing and behavior involve microbially derived SCFAs: shreds of evidence report that butyrate improves cognitive impairments in vascular dementia model and a mouse model of obesity, while propionate reduces anticipated reward responses to high-energy foods in the human striatum[376–378].

3. Pain at gastrointestinal level

3.1 Pain

The definition of pain given by the International Association for the Study of Pain (IASP) is as follows: "*Pain is an unpleasant sensory and emotional experience associated with potential or actual tissue damage or described in terms of such damage*." Therefore, it may be inferred the subjective component of pain[379]. Indeed, the individual's response to pain is also influenced by the emotional, psychological state, and sociocultural environment in which it is experienced[380]. Experiencing pain implies not only consequences related to the proper physiology alteration, which may be more or less severe, but also psychological and social issues. Routines can be disrupted because of reduced mobility and poor appetite or sleep difficulties, even leading to anxiety and depression, which in turn aggravate the perception of pain itself[381]. When we refer to the patient's experience of total pain, we mean the set of etiologic components, but also the factors that influence the patient's perception such as social isolation, fear, anger, helplessness, and frustration[382].

Pain can be distinguished based on its origin into nociceptive, inflammatory or neuropathic, but also based on its duration, into acute or chronic[383]. Instead, if we refer to the area of onset, it is possible to distinguish between somatic and visceral. The latter category also includes abdominal pain, which together with diarrhea is the main GI symptom complained of by Fabry patients[84].

3.2 Visceral pain: characteristics, causes and comorbidity

Visceral pain is what comes from the internal organs as a result of activation of nociceptors in the thoracic, pelvic, or abdominal viscera[384]. Abdominal pain encompasses a range of even broader syndromes such as noncardiac chest pain, endometriosis, pancreatitis, chronic bowel and bladder pain, and not least abdominal pain[196].

Abdominal pain, common to GI pathologies like IBD and IBS, not only affect more than 50% of FD patients (neuropathic pain)[102,126,155], but also involve at least 10-15% of the general population. Moreover, it is also a growing problem associated with chronic opioid use[385–387].

If in some cases the pathophysiology underlying the pain onset is clear, in many others the mechanism has yet to be elucidated, which has led to them being referred to as idiopathic or functional disorders. Thus, at the origin of visceral pain there can be several causes, from inflammation, whether acute or chronic, to mechanical/functional damage (kidney stones, GI dysmotility), to neoplasms [196].

Although somatic and visceral pain share some points regarding information processing, important distinctions should also be clarified[384]. For example, visceral structures are not particularly sensitive to normal stimuli that evoke somatic pain, such as cutting or burning, but are sensitive to stretching, ischemia and inflammation[388]. Furthermore, visceral pain is poorly localized and often affects multiple organs simultaneously. Consequently, it is perceived more diffusely than noxious skin stimulation most likely owing to the low density of sensory afferents at the viscera level and the wide divergence of inputs at the intraspinal level[196,389,390]. Visceral pain localization generally refers to somatic structures, manifesting as secondary hyperalgesia at the superficial or deep tissue level, because of visceral-somatic confluence in common spinal levels[391,392]. Viscero-somatic convergence could explain why visceral pain often accompanies somatic pain conditions or vice versa. There is also visceral-visceral convergence whereby pain to one organ is perceived as pain to another[393]. Finally, clear autonomic experiences may accompany visceral pain. These include nausea, pallor, GI disturbances, altered heart rate, and blood pressure[389].

Contributing to the severely debilitating condition of visceral pain, as well as a very high socioeconomic cost, is the lack of effective treatments[394,395]. The main problem is the fact that opioid and/or nonsteroidal analgesic/anti-inflammatory drugs can cause major side effects in these patients, such as exacerbation of symptoms[393,396]. In addition, comorbidity with gut-brain axis mediated disorders (such as stress, anxiety and depression) increases its impact and complexity of management[397–401]. For example, in patients with IBS, it has been shown that anxiety and discomfort induced by scanner testing negatively impacted pain perception caused by colorectal distension[402]. Overall, it follows that effective management of patients with visceral pain involves cooperation between professionals from different fields[398].

3.2.1 Central modulation of visceral pain

There are two distinct anatomic spinal pathways along which colonic afferents flow. These are the splanchnic (lumbar-splanchnic nerves) and pelvic (sacral-pelvic nerves) afferents that have their cell bodies located in the thoracolumbar (T10-L2) and lumbosacral (L5-S1) spinal ganglia, respectively[403–405]. These sensory fibers interact in the dorsal horn of the spinal cord with excitatory and inhibitory interneurons and second-order neurons of the dorsal column, spinothalamic, and spinoparabrachial pathway. Autonomic and affective responses to pain are specific to the spinoparabrachial pathway, whose projections nourish the limbic and cognitive centers (amygdala, hypothalamus, and periaqueductal gray). Instead, for the discrimination and localization of pain, and partially also for

the emotional component of the response to it, there is the spinothalamic tract[393,406]. The thalamus sends signals to brain regions associated with emotional processing of pain such as amygdala, hippocampus and anterior cingulate cortex[407,408].

The brainstem descending antinociceptive circuit causes the release of inhibitory neurotransmitters in the dorsal horn of the spinal cord to regulate autonomic responses[393,406,409,410]. In fact, pain modulation in the CNS acts through descending pathways, with multiple areas involved, for example, the amygdala and hypothalamus. In this pathway, the periaqueductal gray region (PAG) via its projections to the medulla and amygdala is also involved[411]. The PAG also sends inputs to the rostral ventromedial medulla, which in concert with the raphe magnus and the nucleus reticularis projects to the dorsal spinal and medullary horns modifying the nociceptive signal. Proving this structure, it has also been found that injection of opioids into these brain areas offer an analgesic effect in animal models[412].

3.2.2 Stimuli perception, visceral hypersensitivity and its measurement

In the GI tract it is possible to distinguish between *high-threshold*, predominantly mechanical nociceptors, which function in the range of pain, and *low-threshold* nociceptors, which detect intensity by perceiving the stimulus from harmless to noxious. In chronic visceral pain, there are also silent nociceptors[413,414]. Hypersensitivity, a response to a stimulus that should be harmless as pain (allodynia), and hyperalgesia, an increased perception of a noxious stimulus, are the two components of GI pain[415]. Sensitization of a nociceptor is defined as a decrease in the activation threshold and an increase in the magnitude of the response[416]. This process generally occurs when there is a change in the chemical characteristics of the microenvironment at the site of the afferent endings. The responsive process can be triggered by the release of endogenous or synthesized molecules at the site of interest, attracted in response to the insult or translocated to the nociceptor membrane (receptors and ion channels)[417].

For visceral sensitivity analysis, one of the most widely used methods is the colorectal distension (CRD). The easy accessibility and large number of sensitive afferents make the rectum an ideal target for assessing visceral nociception[269]. This can be measured using an air-filled polyethylene bag attached to a barostat, which maintains a constant pressure and measure changes in rectal tone by recording variations in intra-rectal pressure and volume[418]. The intensity and quality of perception during the test can be assessed based on different parameters and using different scales[419,420].

For example in IBS, in which lowered rectal pain threshold is a hallmark, it has been noticed that about 50% of patients have increased visceral sensitivity to rectal balloon distension[421–423].

Initially, CRD was developed in rats by Ness and Gebhart (1988) and later in mice[424,425]. This technique has long been the method of choice for visceral pain studies. In rodents, responses to CRD are reliably intensity-dependent and duly attenuated by analgesics[424,426]. The same authors identified also peripheral and central neural pathways mediating the visceromotor response, later confirmed by Kyloh and colleagues (2011)[269,424]. By severing the lumbar splanchnic nerves the visceromotor responses or passive avoidance to CRD were unaffected, while resection of the pelvic rectal nerves nullified the responses, regardless of the presence or absence of the lumbar/hypogastric cut. This result revealed that nociceptive transmission to the spinal cord is mediated by the pelvic splanchnic nerves[269,427].

3.2.3 Microbiota and SCFAs effects on visceral pain

As detailed by Lomax and coworkers (2019) and other authors, the mutualistic relationship between bacteria and eukaryotes implies the ability of the gut microbiota to influence behavior and pain[428–431]. Early evidence that the microbiota might play a role on visceral pain comes from rodent studies in which antibiotic and probiotic treatments were used. These mice showed altered microbiota composition accompanied by increased inflammatory markers and visceral hypersensitivity (VHS) at CRD. However, when they were treated with the probiotic *Lactobacillus paracasei*, there was normalization of the parameters[432]. Still, other studies have shown that *Lactobacillus acidophilus* acting on opioid and cannabinoid receptors improves VHS[433]. In contrast, a reduction in Lactobacillus and butyrate production exacerbates colitis in mice[434]. Thus, the interaction between bacteria and nervous system is controversial. For instance, recent studies on skin show that *Staphylococcus aureus* can directly activate neurons in DRGs[435]. However, experiments carried out on germ-free mice indicate that the alteration in visceral sensitivity is not solely caused by a direct microbiota-neuron interaction, as a number of additional potentially confounding changes in immune development would also have to be considered[436]. Indeed, *in vivo* evidence has long supported a key role of epithelial and immune cells in mediating some effects of the microbiota on pain[437,438]. However, fecal transplantation from IBS patients into rats caused VHS in the absence of mucosal permeability damage or immune activation, thus leading to the hypothesis that bacterial metabolites may act directly on gut-brain signaling[439]. Just as bacterial dysbiosis has been associated with visceral sensitivity, consequently so are SCFAs. In particular, antibiotic- or dietary modulation-

induced decrease in SCFAs led to an increase in VHS[440–443]. However, when SCFAs were administered to rats with induced colitis, VHS was not improved by any of them. Actually, butyrate administration decreased the noxious pressure threshold in rats, indicating a pro-nociceptive effect[444]. These results were also supported by experiments in which sodium butyrate administered to rats induced VHS[445]. Overall, on the role of SCFAs in gut-brain mediation and visceral sensitivity there are contrasting findings that need further investigation.

3.3 Transient receptor ion channels in visceral hypersensitivity

The biophysical properties of ion channels influence responses to pain stimuli by regulating the action potential and excitability of neurons. Sodium (Na^+), calcium (Ca^{2+}) and potassium (K^+) channels, in particular, appear to play a critical role in neuropathic pain[446]. Many of these ion channels have also been studied in FD and found to be involved. These include voltage-gated sodium channels (NaV1.7 and NaV1.8); transient receptor potential (TRP) channels (TRPV1, TRPM8, TRPA1); voltage-gated calcium channels (VGCC); potassium/sodium-hyperpolarization-activated ion channel 2 (HCN2); voltage-gated potassium channels (KV); calcium-activated potassium channels (KCa1.1, KCa3.1); acid-sensing ion channels (ASIC1a), and Piezo channels[447].

Although the exact pathophysiological mechanisms of visceral hypersensitivity underlying the increased abdominal pain perception peculiar to FD and many other GI pathologies have yet to be elucidated, several studies have shown a role of the TRP channels[448].

To date, 28 TRP genes have been identified in mammals, organized into 6 subcategories: canonical (TRPC), melastatin (TRPM), vanilloid (TRPV), ankyrin (TRPA), mucolipin (TRPML) and polycystin (TRPP)[449]. TRP channels consist of four functional subunits that form the channel capable of opening and closing by conformational modifications[450,451]. The subunits have 6 transmembrane domains with a pore between the fifth and sixth[449,452]. TRP channels are only weakly sensitive to depolarization, but they open in response to temperature changes, ligand binding, or other alterations in the protein itself. These faintly depolarization-sensitive channels non-selectively conduct cations and open in response to binding to specific ligands, changes in the protein itself, or variations in temperature[449,452–454]. When they are active can cause an increase in intracellular Na^+ and Ca^{2+} concentrations and thus neuronal excitation and numerous cellular responses of various types[448]. Three main functions of TRP channels can be recognized: 1) to detect and transduce chemical and physical stimuli, as molecular sensors; 2) to act as downstream transducers of GPCR- or ion channel-mediated cellular activation; 3) to function as ion transporters, for example of Ca^{2+}

and magnesium (Mg^{2+}). Detected signals are transduced into effector responses either by local neuropeptide release or by transmission of signals to the CNS, resulting in sensitization[448,455].

In the GI tract, a wide variety of TRP channels (including TRPV1, TRPV4, TRPA1, TRPM8) are expressed by different cells. They cover several functions in this district, such as perception of food seasoning, thermal regulation and tissue protection, peristalsis, secretion, mucosal homeostasis, control of membrane potential and excitability of neurons, epithelial cells, muscle cells, and interstitial cells of Cajal, and visceral sensation[456].

A large literature demonstrates the linking between altered expression/function of TRP channels and GI disorders[268,457,458]. Experiments performed in TRP channels-muted transgenic mice and preclinical models through agonists would confirm their crucial role in the development and maintenance of colonic hypersensitivity[456,459,460]. Somatic pain and skin studies showed that the direct activation of TRP channels in sensory fibers triggers several protective mechanisms aimed at problem resolution. Failure to regulate these systems, in the long term, may lead to chronic sensitization of TRP channels, thus triggering sensitization[461].

3.3.1 Transient receptor potential vanilloid 1 (TRPV1)

TRPV1, known as the capsaicin receptor, is among the most studied and best characterized ion channels in the context of visceral pain. It is a voltage-gated outwardly rectifying cation channel and can be activated by a variety of stimuli: by high temperatures (> 43°C), acidosis (pH < 6), exogenous irritants such as the capsaicin found in hot peppers, allylisothiocyanate (AITC) found in the oil of mustard, horseradish or wasabi, and some endogenous lipid compounds, including anandamide and some lipoxygenase metabolites of arachidonic acids[462–466]. Pharmacological studies by gene deletions have revealed that TRPV1 channels play a key role in inflammatory and neuropathic pain[467]. Altered heat perception (heat hypersensitivity) associated with increased expression of the channel protein in DRG has also been reported in the mouse model of Fabry disease, the GLA KO mouse[468]. Again on Fabry mice, frontal paw skin, as well as primary neurons from DRG cultures, also showed increased levels of TRPV1 expression, as demonstrated by Lakomà and coworkers[94,95].

At GI level, TRPV1 is found expressed in intrinsic and extrinsic afferents as well as in epithelial and endocrine cells. Especially spinal and vagal primary fibers are rich in TRPV1 channels[469–474]. In addition, TRPV1 is expressed by small- and medium-sized neuronal cell bodies in DRGs and nodose ganglia[267,463,475–478]. Therefore, given the anatomical location, it is not surprising that TRPV1 may play a crucial role in nociception[470,479,480]. In general, altered expression and/or function of TRPV1

appears to be involved in VHS in several GI disorders, such as IBS, rectal hypersensitivity (Table 4). For example, it has been seen that IBS patients show a greater response to CRD during rectal application of capsaicin than controls. However, since the level of mRNA and rectal TRPV1 protein is comparable to that of healthy subjects, it seems that the VHS of patients is rather a consequence of sensitization and not up-regulation of the channel[481]. Accordingly, several inflammatory mediators, factors associated with hyperalgesia, and acidic pH have been shown to sensitize TRPV1 and increase the chance of channel gating by heat and capsaicin[482–484]. In addition, primary neurons from murine DRGs showed an increase in capsaicin-induced intracellular Ca^{2+} response following incubation with supernatants of submucosal rectal biopsies from IBS patients, suggesting the release by the latter of mediators capable of sensitizing TRPV1[485]. In addition, TRPV1-deficient mice in which acute colitis had been induced showed no inflammatory VHS[486]. Finally, in a rat model of maternal separation stress, VHS in adults was reversed by a TRPV1 antagonist, further emphasizing the role of the channel[487].

3.3.2 Transient receptor potential vanilloid 4 (TRPV4)

TRPV4 is a Ca^{2+} permeable cation channel that was once thought to be activated exclusively by hypoosmotic swelling[488–490]. However, recent evidence has revealed that there may be several stimuli causing its activation. These include stress, low pH, high temperatures (> 25°C), mechanical distention, phorbol esters and downstream metabolites of arachidonic acid[491–497]. In the GI tract, TRPV4 is mainly found expressed in the serosal and mesenteric layers by extrinsic afferents[498]. However, it can also be found in non-nervous cells, such as epithelial and endothelial cells (Table 4)[448]. Its expression is higher in DRG neurons projecting to the colon and recent evidences suggest its role in visceral nociception and also in GI motility by reducing NO-dependent Ca^{2+} release from enteric neurons[498,499]. For example, in patients with IBD, TRPV4 expression has been seen to be higher than in healthy people [498]. Similarly, in colonic lysates from patients with CD and ulcerative colitis, TRPV4 mRNA was highly enriched compared with healthy subjects[500]. Furthermore, a study on DRG neuron cultures showed that activation of protease-activated receptor 2 (PAR2) by mediators released from biopsies of patients with IBS, increases the response to TRPV4 agonists[495,501,502]. Finally, chemical activation of TRPV4 has also been shown to lead to allodynia and visceral hyperalgesia following CRD[503].

3.3.3 Transient receptor potential ankyrin 1 (TRPA1)

TRPA1 channel is activated by low temperatures (< 18°C) that are considered harmful. However, other stimuli trigger its activation, such as mechanical and chemical stimuli. These include some pungent compounds, such as cinnamaldehyde, menthol, AITC, allicin (in garlic), inflammatory fatty acids, prostaglandin metabolites, and hydrogen peroxide[504–509]. TRPA1 was originally thought to play a specific role in inner ear hair cells, however, experiments on TRPA1-silenced mice revealed normal hearing of the animals[510]. Instead, the function that has been demonstrated is in nociception, including in Fabry disease[511]. Studies have shown that TRPA1 is integral to mechanical sensitization in pain-related disorders resulting from peripheral inflammation, neuropathic pain, and diabetic neuropathy. However, in these disorders TRPA1 does not appear to underlie basic protective mechanical nociception, but its inhibition alleviates the perception of mechanical pain[512–514]. Miller and colleagues (2018) showed that in Fabry rats sensory neurons, blockade of TRAP1 reduced mechanical and nociceptive hypersensitivity[515].

At the GI level, TRPA1 is expressed by both the intrinsic and extrinsic innervation system[516]. Mainly it is found localized in mucosal and serosal and mesenteric afferents[517]. However, it can also be found in non-neuronal cells such as enterochromaffin, endocrine, and epithelial cells (Table 4)[518]. To date, much of the literature on the role of TRPA1 in the gut is linked to VHS, but also colorectal motility modulation should be considered[519,520]. For example, a study comparing mice colonically treated with a TRPA1 agonist and WT mice showed a significant increase in visceromotor response in the former, suggesting a role in VHS[517,521]. A nociceptive role also emerged in the rat DRG study by Yang and colleagues (2008), who, by intrathecal administration of antisense TRPA1 oligodeoxynucleotide to reduce TRPA1 expression, demonstrated a reduction in colitis-induced hyperalgesia to CRD and intracolonic mustard oil administration[519]. Finally, a recent study of biopsies from patients with IBD reported upregulation of TRPA1 mRNA expression, again suggesting that TRPA1 should be considered among potential targets for the treatment of VHS[522].

	Ligands	Physical Stimuli	Endogenous Stimuli	GI Tract Expression	GI Related Disorders
TRPV1	Capsaicin (red pepper) Piperine (black pepper) Gingerol (ginger) Resiniferatoxin (*Euphorbia poissonii*)	$T \geq 43\,°C$ Voltage Distension pH	Cannabinoids Anandamide Eicosanoids Acid Bradykinin Serotonin Histamine Proteases	Sensory neurons Enteric neurons Epithelial cells Enteroendocrine cells	IBS VH IBD CRC
TRPV4	4-α Phorbol (*C. tiglium*) Bisandrographolide A (*Andrographis paniculata*)	$T \geq 25\,°C$ Mechanical Osmolarity Distension pH	Anandamide Eicosanoids Bradykinin Citrate Arachidonic acids Histamine Proteases	Sensory neurons Epithelial cells	IBS VH IBD
TRPA1	Allicin (garlic) Carvacrol (oregano) Cinnamaldehyde (cinnamon) Diallyl disulfide (garlic) Gingerol (ginger) Ally isothiocyanate (mustard horseradish, wasabi)	$T \leq 18\,°C$ Mechanical Distension pH	Cannabinoids Bradykinin Nicotine Prostaglandins Histamine Proteases ROS 4-HNE	Sensory neurons Enteric neurons Epithelial cells Enteroendocrine cells	IBS VH IBD IF

Table 4 Principal characteristics of the analyzed ion channels. Modified from Alaimo at al. 2019

4. Gastrointestinal fluid and electrolyte transport

4.1 Ion Transport

In order to create a favorable environment for effective enzymatic digestion, ideal for nutrient absorption and fecal propulsion, ion transport is critical. In the GI tract, approximately 8 liters of fluid are secreted each day[523]. Most of this volume is reabsorbed, and only small traces remain in the expelled feces. So, we can infer how finely this process is regulated to preserve water and electrolyte balance[524]. Consequently, when this delicate absorption-secretion equilibrium is altered, several GI disorders are triggered. In particular, this is a common cause of symptoms associated with IBD and IBS, but also of serious consequences ranging from life-threatening diarrhea, for example in cholera, to constipation, as in cystic fibrosis[525–527].

4.1.1 Absorption mechanisms

In the absorption process, as reported in Figure 9, the solutes mainly involved are Na^+ and Cl^-.
As for Na^+, its uptake occurs by electroneutral ion exchangers. Three Na^+/H^+ (NHE) exchangers are expressed along the GI tract[528]. The first, NHE1 is located at the basolateral level and regulates intracellular pH and cell volume. The other two, NHE2 and NHE3, are expressed on the apical side[529]. Severe and chronic diarrhea was found in NHN3-deficient transgenic mice, thus suggesting its key role in intestinal absorption. Electrogenic Na^+ absorption occurs mainly in the colon at the apical level by amiloride-sensitive epithelial Na^+ channels (ENaC). ENaC, the main active ion channel for Na^+ reabsorption, has been shown to compensate for the loss of electrolytes associated with diarrhea in NHE3 KO mice[530].

Regarding Cl^- ions, their uptake is mediated mainly by two anion exchangers, DRA (down regulated in adenoma) and PAT-1 (putative anion transporter-1). Both, located apically, are Cl^-/HCO_3^- exchangers[531,532]. DRA is more highly expressed in the colon than in the small intestine, while PAT-1 shows an opposite expression pattern[533]. As evidence of the clinical importance of DRA, suffice it to say that its absence is associated with a rare form of Cl^- secretory congenital diarrhea[534].

Ion absorption can also occur through nutrient-coupled transporters, such as sodium-glucose transporter 1 (SGLT1) and SCFAs transporter, $SCFA/HCO_3^-$[535]. In the colon, SCFAs also affect Na^+ absorption and Cl^- secretion by promoting the expression of NHE3 and ENaC, as well as inhibiting cAMP- and cyclic guanosine monophosphate (cGMP)-mediated secretion[536–538].
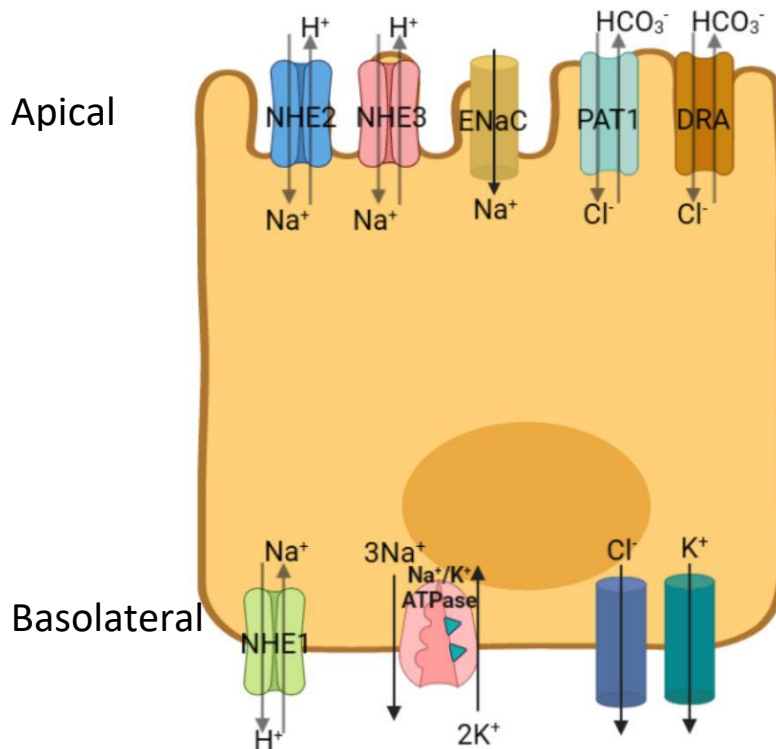
Figure 9 Absorption mechanisms in the GI tract. Na^+/H^+ cation exchangers 2 and 3 (NHE2, *blue;* NHE3, *pink*), along with down-regulated in adenoma (DRA, *ochre*) and putative anion transporter-1(PAT-1, *sage*) anion exchangers import Na^+ and Cl^- crossways the apical membrane into intestinal epithelial cells while exporting a H^+ and HCO_3^-. Basolaterally, Na^+/K^+ ATPase and NHE1 (*light green*) provide a gradient for the basolateral exit of ions and subsequent transport of water across the intestinal epithelium. Created by BioRender.

4.1.2 Secretion mechanisms

The secretion is also predominantly active. It involves intracellular Cl^- gradients and is regulated by apical ion channels and the activity of several basolateral transporters, as represented in Figure 10[523]. Indeed, Cl^- secretion is associated with paracellular Na^+ movement, that work to provide the osmotic source for water movement[539].

Three components are implicated in secretion: crypt epithelial cells (effectors); enterochromaffin cells or afferent neurons (sensors); and neural secretory reflex neurons. In summary, Cl^- accumulated within the cell via the basolateral sodium-potassium symporter (NKCC1) exits apically. The basal Na^+/K^+ ATPase pump recycles Na^+ and causes intracellular cytosolic Na^+ concentrations to remain low, thereby creating a net electronegative environment within the cell. This negativity is the driving force for apical extrusion of Cl^- [523,540,541]. The best known channel for Cl^- secretion is the cystic fibrosis membrane-regulatory Cl^- channel (CFTR), activated by cAMP or cGMP. However, in addition to CFTR channels, there are also alternative pathways for Cl^- extrusion. These include Ca^{2+}-activated Cl^- channels and cAMP-mediated ClC-2 channels, both of which are located on the apical

side of crypto-secreting cells. Experimental evidence has shown that cAMP-mediated Cl$^-$ secretion has slow kinetics, whereas Ca^{2+}-mediated Cl$^-$ secretion has a rapid start and is transient. Finally, on the basolateral side, there are also K$^+$ channels that promote Cl$^-$ expulsion by providing a favorable electrochemical gradient via K$^+$ output (Fig. 10)[540–542].
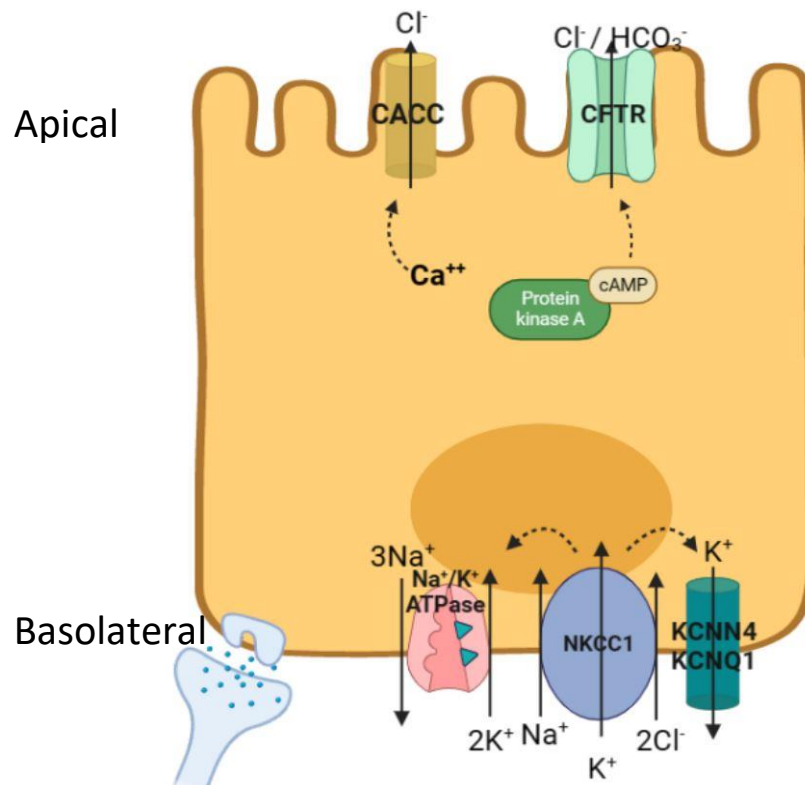
Figure 10 Secretion mechanisms in the gastrointestinal tract. Cl$^-$ ions are pumped into the cell via the Na$^+$/K$^+$/Cl$^-$ (NKCC1, *light blue*) symporter, the gradient for which is provided by the Na$^+$/K$^+$ ATPase which also recycles Na$^+$ out of the cell. Basolateral K$^+$ channels recycle K$^+$ out producing a negative intracellular charge and a push toward apical exit through cAMP activated cystic fibrosis transmembrane conductance regulator (CFTR, *green*) or calcium activated chloride channels (CACC). Created by BioRender.

The exchangers/channels involved in secretion mechanisms are described in more detail below, according to their basolateral or apical localization.

Basolateral membrane

- Na$^+$/K$^+$ ATPase. Structurally this is a heterodimer of α and β subunits. The ion transporter characteristics are embedded in the α subunit, whilst the β subunit seems to be involved in the placement of the pump at the membrane level[543,544]. Functionally, this is responsible for providing the energy for active Cl$^-$ secretion. Its function is based on the outward transport of three Na$^+$ ions in exchange of 2 K$^+$, after the hydrolysis of an ATP molecule[545,546]. Thus, its

activity maintains a low intracellular Na^+ concentration and a high K^+, making the interior of the cell electronegative. Such negativity is critical in providing the driving force for Cl^- egress.

- NKCC1. This is a $Na^+/K^+/2Cl^-$ cotransporter involved in Cl^- uptake. The protein is expressed in several cell types; however, it plays its specialized role in epithelia. In fact, its expression levels are 10- to 30-fold higher in secretory epithelial cells[547]. NKCC1 is often referred to as a secondary active transporter because it takes advantage of the ion gradients provided by the Na^+/K^+ ATPase. Because two Cl^- ions are transported in combination with two cations, the transport is electroneutral. However, the low intracellular Na^+ concentration causes an accumulation of Cl^- lower than the expected concentration by electrochemical equilibrium. To date, although the specifics are unknown, it is established that NKCC1 activity is stimulated by intracellular kinase cascades and phosphorylation[548,549]. Specifically, a kinase sensitive to Cl^- movement and cell volume may stimulate cotransporter phosphorylation caused by a decrease in intracellular Cl^-[550]. So, with this mechanism of communication between the basal and serosal sides, the apical loss of Cl^- would be compensated by an increase in incoming Cl^-, maximizing the rate of transport[551].

- K^+ channels. In Cl^- secretion there are at least two K^+ channels involved. One, dependent on intracellular Ca^{2+} levels, relatively insensitive to channel blocker; the other is instead presumed to be activated by increases in cAMP and is quite sensitive to barium[552–554]. Then there would be a third, described by Devor and coworkers (1998) in T84 cells that is activated by arachidonic acid[555].

Apical membrane

- CFTR. Cloning of this protein occurred in 1989, since which time numerous information about its structure and function has emerged[556–558]. It undoubtedly constitutes the main pathway of Cl^- excretion at the apical level. Structurally, CFTR is a large protein with several functional domains[559]. In addition to 12 membrane-crossing regions forming the channel pore, the protein also contains 2 nucleotide bonds and a large regulatory domain that contains consensus sequences for phosphorylation by several protein kinases[540].

Functionally, CFTR opening requires two steps: covalent modification of the R domain by cAMP-dependent PKA and binding followed by hydrolysis of the nucleotide in the nucleotide-binding domains[559–562]. In addition to this primary regulation, there are additional levels of regulation. One of these is provided by the delivery of preformed CFTR from subapical membrane vesicles at the expense of cAMP. This increases membrane channel density,

although this has not been observed in all Cl⁻ secreting cell types[563–565]. In addition, regulation of CFTR by other protein kinases has also been proposed. For example, it has been hypothesized that PKC activity may allow or enhance channel activation by PKA[566,567]. Finally, in GI tracts, CFTR also opens following increases in cGMP[568]. This could imply either a cross-activation of PKA by the high levels of cGMP induced by some agonists, or a direct effect of another cGMP-dependent protein kinase on CFTR[568–570].

- CaCC. Debate persists whether other Cl⁻ apical channels are involved in secretion at GI level. Several authors have reported that intestinal epithelial cells in situ, or cultured intestinal epithelial cells growing as confluent monolayers, show minimal, if any, Ca^{2+}-activated Cl⁻ conductance[571–573]. Furthermore, intestinal tissues from cystic fibrosis patients or mice with a targeted deletion of the CFTR gene do not exhibit cAMP- or Ca^{2+}-mediated Cl⁻ secretory responses, whereas the transport defect is limited to cAMP-mediated transport in the airways[571,574]. Based on these data, it has been suggested that the Cl⁻ secretory responses evoked in normal intestinal tissues by agonists that mobilize intracellular Ca^{2+} are actually driven primarily by the opening of a basolateral K⁺ channel, with Cl⁻ being able to exit the cell via the small fraction of CFTR Cl⁻ channels open at any given time.

  However, it is also suggested that Ca^{2+}-activated Cl⁻ channels may be significant for Cl⁻ excretion[575,576]. Treatment of intestinal epithelial cells with antisense oligonucleotides to the CFTR channel, sufficient to abolish cAMP-stimulated secretion, does not affect Ca^{2+}-mediated responses, so Ca^{2+}-activated Cl- secretion may be CFTR-independent. In addition, a subgroup of CFTR KO mice showed increased survival and reduced GI symptoms probably due to this alternative secretory pathway[577,578]. Several groups have shown the involvement of CaCCs in the process of viral and Vibrio parahaemolyticus-related diarrhea[579–581]. Finally, specific CaCC inhibitors shown to effectively decrease Cl⁻ secretion *in vitro*, but then *in vivo* experiments must be carried out[582].

4.2 Pharmacological secretagogues for the study of ion transport

Generally, the secretagogues are agents that promote the secretion of chemical neurotransmitters, hormones or molecules. They can have natural origin or be artificially synthesized. Their selectivity and specificity is determined by their and the receptors' structure[583]. The classic approach to investigating intestinal ion transport processes involves the use of these specific pharmacological

ligands with the ability to target and modulate ion channels, exchangers or effecter molecules of interest. In Figure 11 the secretagogues used in this project are represented.
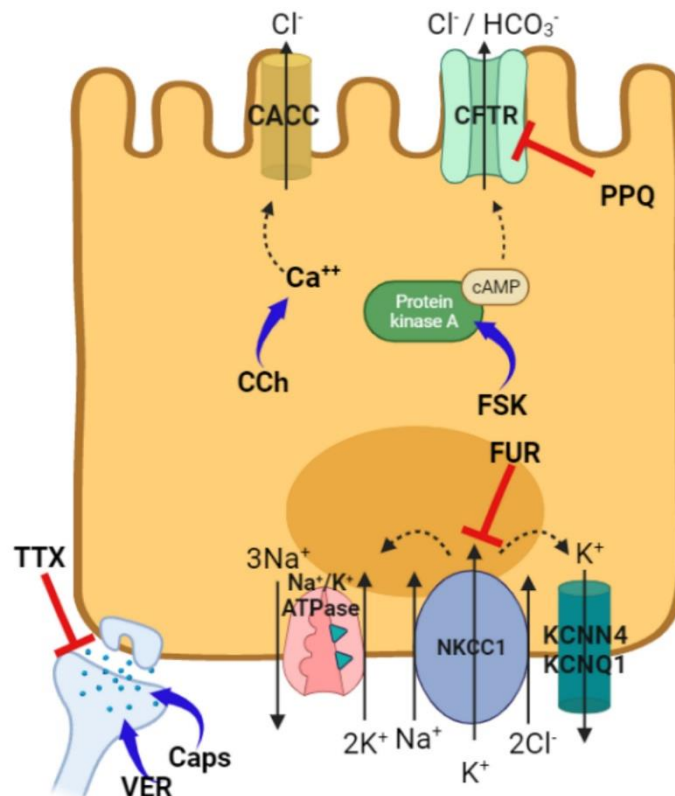
Figure 11 Secretagogues used for this research and their targets. The scheme shows the main components investigated at the apical and basolateral levels. Ca^{2+} activated chloride channel (CACC); Cystic Fibrosis Transmembrane Conductance Regulator (CFTR); $Na^+/K^+/Cl^-$ cotransporter (NKCC1) with its recyclers Na^+/K^+ ATPase and K^+ channels (KCNN4 and KCNQ1) are drawn with the secretagogues addressed to them. The activators/stimulants Carbachol (CCh), Forskolin (FSK), Capsaicin (Caps), and Veratridine (VER) are represented (*blue arrows*) where they act. As well, the blockers Pyrimido-pyrrolo-quinoxalinedione (PPQ), Furosemide (FUR) and Tetrodotoxin (TTX) (*red ticks*). Figure realized by BioRender.

4.2.1 Furosemide

Furosemide, an anthranilic acid derivative, is a highly efficacious loop diuretic drug which is common used for treatment of edema due to heart failure, hypertension, cirrhosis, and kidney disease[584,585]. It has been explained its inhibitory effect both on $Na^+/K^+/2Cl^-$ cotransporter isoform 2 (NKCC2) located on the apical membrane, and on NKCC1 ubiquitously distributed in epithelial and non-epithelial cells, and present at GI level in the basolateral membrane[586,587]. Therefore, in addition to the role of furosemide in enhancing urine output, some surveys have described its non-diuretic effects, such as its effects on airways, vascular smooth muscle, brain, and not least GI tract[588]. Some studies have displayed the side effects of furosemide on the GI tract including nausea, diarrhea, and constipation[589]. Moreover, given its blocking effect on NKCC1 channel, this secretagogue has been

56

widely used, and is still being used, to investigate the Cl⁻ secretion mechanisms at GI level , for example by Ussing Chamber[590]. This has also been employed in Organ Bath studies to evaluate the effect on contractility[591].

4.2.2 Pyrimido-pyrrolo-quinoxalinedione

Pyrimido-pyrrolo-quinoxalinedione (PPQ) [Patent Office EP2464354A4] is a potent inhibitor of CFTR, a cAMP-regulated Cl⁻ channel expressed in epithelial cells of the airway, intestine, testis, and other tissues. It is generally hypothesized that CFTR inhibitors may reduce fluid loss in secretory diarrhea, and slow the development of renal cysts in polycystic kidney disease, where fluid accumulation in renal cysts is CFTR-dependent[592–595]. PPQ owes its recent discovery as a CFTR inhibitor to Lukmanee Tradtrantip and Alan S. Verkman (2009)[596]. The authors, after identifying the potential of the PPQ class of compounds, performed a structure-activity analysis to identify the most potent CFTR inhibitors. Then, following further characterization and biological testing, they identified PPQ-102. To study the compound's potency, reversibility and specificity, they performed short-circuit current analysis of the Cl⁻ conductance of CFTR. Channel inhibition by PPQ-102 was about 100% at higher concentrations, with IC_{50} ~90 nM. At low concentrations, inhibition occurred for several minutes, suggesting an intracellular site of action. In addition, reversibility of inhibition emerged, as demonstrated by the complete restoration of Cl⁻ CFTR-dependent current after 30 min incubation with 2 μM PPQ-102 followed by 10 min washout. The advantage of PPQ is its voltage-independence, as confirmed by patch-clamp analysis, as it allows the potency of inhibition to be maintained even in negative cells[596]. Since its discovery, PPQ has not only been used for the treatment of polycystic kidney but also to investigate the role of CFTR in different epithelia.

4.2.3 Tetrodotoxin

Tetrodotoxin (TTX) is a well-known and potent neurotoxin synthesized by specific bacteria, which can be found in several animals, including pufferfish (in the ovary and liver)[597,598]. TTX as a pharmacological tool has been widely used on tissues to study the role of the neural component in the regulation of homeostatic function and external stimulus responses[599]. More generally in experiments aimed at understanding those mechanisms where voltage gated sodium channels (VGSCs) are potentially involved. In fact, TTX blocks VGSCs in a highly potent and selective manner without effects on any other receptor and ion channel systems. It acts from outside of the nerve membrane, through binding to the selectivity filter, thus preventing the influx of Na⁺ and the

propagation of action potentials. It does not impairs the channel gating mechanism[597]. Therefore, when this is administered, the result is blockade of associated neural or muscle function[600,601]. Some TTX-resistant Na^+ channels have been discovered in the nervous system and received much attention because of their role in pain sensation[599,602]. Specifically to GI function, it has been widely used in studies on intestinal tissues processed in Ussing chamber or organ baths to investigate neural components involved in motility and ion transport[603,604].

4.2.4 Carbachol

Carbachol (CCh), a quaternary ammonium compound, is a cholinergic agonist of ACh receptors, whose muscarinic and nicotinic actions it shares. However, it deactivates much more slowly than ACh and is not destroyed by cholinesterase[605,606].

This compound, along with bethanechol (it differs by a single β-methyl group), has been widely used to study cholinergic-induced intestinal epithelial ion transport in several species, including roditors[607–610]. Muscarinic receptors are Gq protein-coupled receptors that stimulate phospholipase C leading to the degradation of phosphatidylinositol 4-5 biphosphate (PIP2) to diacylglycerol (DAG) and inositol 1,4,5 triphosphate (IP3) that stimulate the release of intracellular Ca^{2+} stores from the endoplasmic. This Ca^{2+} release facilitates ion transport in the GI epithelium as Cl^- secretion. Like cAMP-induced Cl^- secretion, Ca^{2+} triggers basolateral K^+ channels that provide the driving force for apical Cl^- efflux through CaCCs[611].

4.2.5 Forskolin

Forskolin (FSK) is a labdane diterpenoid isolated from the roots of *Plectranthus barbatus*, an Indian plant better known as *Coleus forskohlii*. This, along with its derivatives, has also been widely used at the GI level as a pharmacological tool to investigate the role of cAMP[612,613]. Indeed, it is recalled that cAMP plays a key role in ion and fluid secretion, particularly by increasing CFTR channel-mediated Cl^- secretion[523]. Forskolin is considered a valuable tool (albeit not too selective) because it is able to increase the activity of adenylyl cyclase at the intracellular level, through the activation of 8 of the 9 present isoforms of the enzyme[613]. This enzyme is responsible for the conversion of ATP to cAMP and pyrophosphate, so the administration of FSK increases the levels of these products, with the resulting consequences[614]. Regarding intestinal ion transport, protein kinase A (PKA) is probably the best known and most relevant effector molecule downstream of cAMP. It should be noted that PKA phosphorylates NKCC1 basolaterally and CFTR on the mucosal side,

causing excretion of Cl⁻, and consequently water, into the lumen. In addition, cAMP can stimulate the recruitment of CFTR and NKCC1 to increase their density in the membrane[523]. Finally, through PKA-induced phosphorylation of NHE2/3 regulatory proteins, cAMP also inhibits uptake[615].

4.2.6 Veratridine

Veratridine (VER) is a natural plant alkaloid derived from *Veratrum*. It is a neurotoxin with a pan-neuronal function that acts by reversibly binding to Na^+ channels, causing continuous activation of action potentials in the nerve cell, thereby increasing its excitability[616].

As a result, it has been used for several studies of enteric regulation of ionic transport at the GI level, providing valuable functional insights into these processes[617].

For example, studies in submucosal tissue preparations have shown that exposure to veratridine causes the release of several enteric neurotransmitters, which in concert produce a potent and prolonged pro-secretory response causing an apical outflow of $NaCl$[610,617]. However, in whole GI tissues with extrinsic neural innervation, VER stimulation results in ion absorption[617].

4.2.7 Capsaicin

Capsaicin has already been mentioned as a TRPV1 channel agonist (see paragraph 3.3.1) . As noted above, it has long been used for the treatment of pain, but pharmacological studies on cardiovascular, respiratory, and GI tissues also described physiological effects[618,619]. In the GI tract, TRPV1 is mainly localized in primary sensory neurons and is thought to be responsible for the initial detection of noxious chemical and thermal stimuli, causing the typical burning sensation that follows activation with capsaicin (found, for example, in hot peppers)[463]. In studies conducted in the Ussing chamber on intestinal tissue, the effect of capsaicin on fluid transport was noticed. Specifically, exposure to the compound would activate sensory afferents, which in turn would activate secretomotor neurons to release pro-secretory neuropeptides (e.g., substance P) that can increase luminal efflux of Cl⁻ and thus water[620].

4.3 Ussing Chamber for measuring the GI ion transport

The Ussing Chamber was developed over 50 years ago by the Danish biologist Hans Henriksen Ussing as a method to investigate the active $NaCl$ transport[621–623]. The inventor and co-workers used frog skin as a model system since it can move $NaCl$ from the skin surface into the interstitium against concentration difference. However, distinguishing between the movement of ions actively

transported and the passive movement of ions represented a challenge. The problem was resolved by developing an experimental system whereby the tissue was placed between two halves of a chamber, each of which refilled with the same volume of identical electrolyte solutions (Fig. 12 A-B). Generally, bubbled Krebs solution is used as physiological buffer and the gas employed is a mixture of 95% O_2 and 5% CO_2 (carbogen). This oxygenates the solutions to a reasonably level of PO_2 , necessary to overcome the lack of hemoglobin distribution by arterial blood, and provides a PCO_2 approximately equivalent to venous blood, which maintains the HCO_3 buffer at pH 7[623]. This type of tissue assembly in the Ussing chamber allows the elimination of ionic movements powered by passive forces (transepithelial concentration, osmotic and hydrostatic gradients) by blocking the potential to zero via administering an external current passed through the epithelium (Fig. 12 C)[623]. This current, called short-circuit current (I_{sc}), corresponds to the summation of electrogenic ionic currents by active transport: $I_{sc}= I_{Na+}+I_{K+}+I_{Cl-}+I_{HCO3-}-I_K$. Hence, the I_{sc} in the Ussing chamber results from active transport[623,624]. Yet, I_{sc} alone is does not completely reflect the complexity of the system. Indeed, in many cases it's necessary a more precise interpretation. For example, I_{sc} alone does not give conclusive information on the direction of ion flux[625]. In order to have a comprehensive knowledge of the ionic nature of a response, further experimentation with pharmacological tools, as the secretagogues above mentioned, are often required. Moreover, we should consider the method of tissue preparation. For example, the stripped tissue (mucosal-submucosal preparation), lacking the MP and muscle layers, may provide an under estimated I_{sc} to certain stimulants, especially those involving a myenteric reflex, such as GABA-stimulated ion transport[626]. The Ussing chamber can also measure transepithelial resistance (TEER). TEER has been widely used to assess intestinal barrier integrity. However, it is a general measurement and represents para- and trans-cellular resistance in parallel. Consequently, while TEER is useful when used with I_{sc}, as a direct indicator of the physical tightness of the paracellular seal, it is not always a reliable marker of true paracellular permeability and barrier function. In fact, differences responsible for paracellular permeability to ions, solutes, and water do not always result in a change in TEER and barrier integrity, although they may affect transport[627].

Still to date, the Ussing chamber remains one of the most useful tools that provides a fairly precise method of measuring electrical and transport parameters in polarized tissue[621,623]. It has been utilized with every epithelium: reproductive tract, airway, eye, exocrine/endocrine ducts, choroid plexus, and of course intestine; as well as to cultured epithelial cells where tight junction integrity keeps apical and basolateral membrane polarity[628–632].
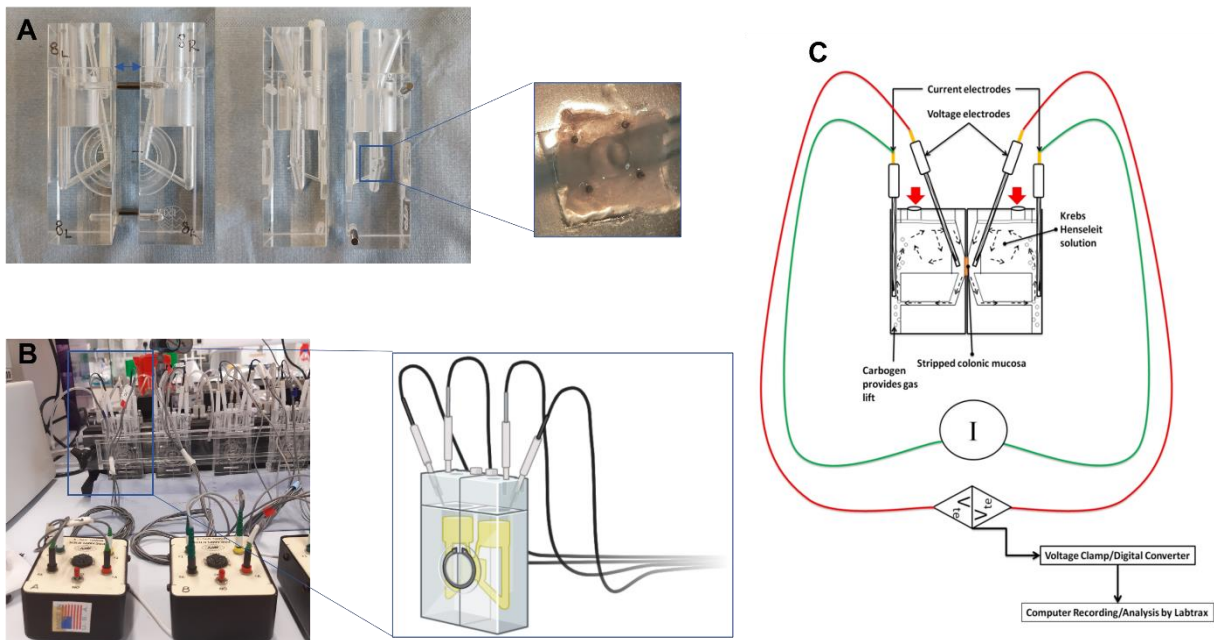
Figure 12 Representative photos and schematic illustration of Ussing Chamber operation. (A) Pictures of an open Ussing Chamber consisting of two halves. In the zoom (*blue box*) a piece of pinned mucosal-submucosal preparation in correspondence of the hole. (B) A picture of the functioning system entirely mounted and connected to carbogen-inflating tubes, that supply the necessary oxygen and maintains pH as well as providing gas lift to allow steady circulation of buffer and perfusion of the tissue. The chamber is kept at a constant temperature of 37°C. In the zoom (*blue box*) a graphic depiction of an equally filled chamber with Krebs buffer to eliminate osmotic and hydrostatic gradients. (C) Tissue is voltage clamped to 0V by sending a set current directly across the tissue via voltage electrodes (*red*). The amount of current required to maintain the tissue at 0V (Short circuit current) is measured by the current electrodes (*green)* and recorded electronically. Drugs can be added to either side of the chamber (*red arrows*). Created by personal photos, BioRender and Lomasney and Hyland 2014.

AIMS OF THE STUDY

FD is a rare X-linked genetic disorder caused by mutations in the GLA gene. This gene codes for the enzyme α-Gal A. When its metabolic function of cutting the alpha bond of neutral glycosphingolipids does not occur, the consequence is the accumulation of substrates in different cell types[5,79]. The two main molecules accumulated are Gb3 and its derivative lyso-Gb3. The resulting clinical picture is progressive and heterogeneous, involving several organs[6]. The first characteristic signs are pain and GI symptoms. Both are severely disabling and hurt patients' quality of life[82,84,87]. While there is copious literature regarding pain in FD and some underlying mechanisms have been elucidated, with regard to GI symptoms, on the other hand, the topic has yet to be fully elucidated. GI symptoms include abdominal pain, diarrhea, bloating, constipation, nausea, and vomiting. Because they can be indicative of many other disorders, they are often overlooked or misinterpreted, contributing to the delay in proper diagnosis. Moreover, although enzyme replacement therapy improves GI manifestations in most cases, about 50% of patients complain of disorders even during treatment or develop new ones[102,104,137]. Thus, there is an urgent need to improve knowledge of GI symptoms and their triggers in FD, and this is the main purpose of this work.

The laboratory where I conducted the experiments has been working for a long time on the α-Gal A -/0 (KO) mouse, many aspects of which have been characterized, making it a reliable model for the study of FD, particularly neuropathic pain[94,95,633]. In 2019, Masotti and colleagues performed the first morphologic characterization of the colonic tract of this mouse model and described several alterations, resembling the manifestations present in Fabry patients. These alterations include the confirmed presence of Gb3 deposits, as well as the thickening of muscle layers, reduction and rearrangement of nerve fibers innervating the mucosa, and enlargement of myenteric ganglia[131].

Building on these data, this thesis first objective (**AIM 1**) is to evaluate whether the α-Gal A -/0 mouse model also captures the functional GI problems experienced by Fabry patients and can be considered a valuable model for their investigation. Once the validity of the model is established, we attempt to identify potential mechanisms involved in the development and maintenance of GI symptoms in FD.

Moreover, given the growing scientific literature on the potential causal role of lyso-Gb3 in FD pathogenesis, the second aim (**AIM 2**) is the study of its effects on colonic electrolyte and fluid transport, sensory nerve activation, and contractility of adult healthy male mice[74–76].

To achieve **AIM 1**, the research has been organized into the following tasks:

TASK 1: Assessment of functional disorders through colonic motility and visceral sensitivity. The first is done by means of the analysis of fecal output, in terms of weight and water content. The second, by colorectal distention, is measured as visceromotor response (VMR) in sedated animals and as abdominal withdrawal reflex (AWR) in conscious mice.

TASK 2: Assessment of anxiety-like behavior by open-field and elevated plus maze tests.

TASK 3: Mapping the fecal microbiota. Bioinformatic analysis provides information on the indices of microbial diversity (alpha- and beta-diversity) and taxonomic classifications compared to healthy mice (phyla, families and genera levels). In addition, the profile of the predicted functional modules are explored to identify the pathways potentially involved. In particular, the gut-metabolic (GMM) and gut-brain (GBM) modules are used to draw attention to specific microbial functional changes and individual processes of production or degradation of neuroactive compounds, respectively.

TASK 4: Quantification of short-chain fatty acids (SCFAs), individually and as a total amount. It is carried out by gas chromatography technology coupled with mass spectrometry (GC-MS), and the amount of butyric acid, acetic acid, propionic acid, valeric acid, iso-butyric acid and iso-valeric acid are measured.

TASK 5: Qualitative and quantitative analysis of TRPV1, TRPV4 and TRPA1 ion channels. Transverse colonic cryosections, sections of lumbosacral DRGs and primary neurons from lumbosacral DRGs are stained by immunofluorescence with antibodies specific for the above mentioned channels together with a neuronal marker (Pgp9.5 or NeuN) to confirm the proper localization. The fluorescence signal is evaluated as both mere visual impact and corrected total cell fluorescence (CTCF).

This first experimental section is performed in parallel on male α-Gal A -/0 and α-Gal A +/0 mice (controls) at three different ages: 8-10 weeks, 16-20 weeks, and 12 months. Thus, a characterization of the model that also takes into account the progression of the pathology is provided. This allows for the identification of possible critical stages in certain aspects rather than others. Moreover, the planned experimental design may ultimately enable the validation of our mouse model for the study of the pathophysiological mechanisms underlying GI symptoms. Although this would already represent a relevant innovation with remarkable potential because it would open up its use for the

GI aspects, the first mapping of the fecal microbiota and metabolites is surely a cornerstone of this research. In this view, if the recognition of potential therapeutic targets is a key element in making progress in the management of Fabry-related GI symptoms, the identification of supportive integrative therapies, such as specific nutrition based on the patient's profile, may also be a breakthrough in the treatment of GI and probably anxiety-related disorders in FD.

As concerns **AIM 2**, the experiments were performed during my internship abroad, in Professor John Cryan's laboratory at APC Microbiome Ireland and University College of Cork, under the supervision of Professor Niall Hyland. Ussing Chamber and Organ Bath were employed to pursue the following tasks:

TASK 1: To evaluate the effect on short-circuit current (I_{sc}) and transepithelial electrical resistance (TEER) of lyso-Gb3 administered at increasing concentrations (30 nM, 100 nM, 300 nM, 1 µM, 3 µM, 10 µM) on mucosa-submucosa preparations of the mouse colon.

TASK 2: To investigate by whom the effect of lyso-Gb3 might be mediated and/or influenced by applying specific inhibitors. Namely, the following are used: tetrodotoxin (TTX), to block the TTX-sensitive voltage-dependent Na^+ channels; pyrimido-pyrrolo-quinoxalinedione (PPQ), to inhibit the chloride current of the cystic fibrosis transmembrane conductance regulator (CFTR); furosemide, to inhibit Na^+-K^+-Cl^- cotransporters (NKCC1).

TASK 3: To assess whether lyso-Gb3 can impact epithelium-mediated and/or neuro-mediated secretion by making use of activators/stimulants such as carbachol, to stimulate Ca^{2+}-mediated signaling pathways; forskolin, to promote cAMP-mediated signaling pathways; veratridine, to excite all intrinsic neurons expressing voltage-sensitive Na^+ channels; capsaicin, to activate a specific subset of sensory afferent neurons.

TASK 4: To test the impact of lyso-Gb3 on colonic contractility through Organ Bath.

The second experimental section is crucial in the pursuit of the mechanisms through which lyso-Gb3 acts on healthy colon, specifically on intestinal permeability and contractility. Noteworthy, in light of a unique *in vitro* study evaluating the effect of lyso-Gb3 at GI level [76], our project examines for the first time the causal role of the substrate in the pathogenesis mechanisms of the GI FD-related disorders by means of Ussing Chamber.

MATERIALS AND METHODS

1. Animals

For the experiments described in the present thesis, 6 groups of animals were used, based on genotype and age: 8-10 week-old (T1), 16-20 week-old (T2) and 12 month-old (T3) α-Gal A -/0 [knock-out (KO)] and α-Gal A +/0 [wild type (WT)] mice. Because of X-linked inheritance and greater severity in male patients, exclusively α-Gal A -/0 male mice have been analysed[92,95]. Heterozygous female α-Gal A +/− and wild type α-Gal A +/0 male mice (same JAX strain B6; 129Gla-tm1Kul/J) purchased from Charles River Laboratories Italia s.r.l. (stock number 003535; Jackson Laboratory; Bar Harbor, ME, USA) were crossed to give the F1 generation, thus obtaining females α-Gal A +/-, females α-Gal A +/+, male α-Gal A +/0 and KO males α-Gal A -/0[94,169]. These mice were used from the F1 to the F4 generation as heterozygous females (+/−, B6; 129-Glatm1Kul/J) crossed with WT males +/0, B6; 129-Glatm1Kul/J) of the same genetic background (B6; 129-Glatm1Kul/J). From the F4 generation, we obtained homozygous females α-Gal A −/− and hemizygous males α-Gal A -/0 mice that were compared to α-Gal +/+ and +/0 as controls[131]. KO and WT groups were separated after at least 4 generations that is known to be enough to stabilize the background and all the experiments were performed after more than 10 generations[173,177]. Therefore, well-established homozygous α-Gal A −/− and hemizygous α-Gal A -/0 mice compared to α-Gal A +/+ and +/0 controls were used.

Mice were housed in groups of six in individually ventilated cages (Tecniplast, Italia) with water and food ad libitum in controlled environmental conditions: lights on from 7.00 a.m. to 7.00 p.m., 22 ± 2°C temperature and 65% humidity. Once reached sexual maturity (21-28 days), males and females were separated. All efforts were made to minimize animal suffering and the number of animals used was kept to a minimum by the experimental design. All the procedures followed in this work were in compliance with the European Community Council Directive of November 24, 1986 (86/609/EEC) and were approved by the Ethical committee of the University of Bologna (prot. 141/2019 PR). Behavioral experiments were carried out at the Department of Medical and Clinical Sciences (DIMEC), University of Bologna, with the approval of the local ethical committee (Veterinary Service of the University of Bologna) and in agreement with the National Animal Welfare Act.

1.1 Genotyping

Genotyping is the process through which the genotype of the animals is defined. The protocol can be divided into three steps: I) DNA isolation from mice tails; II) Amplification of the gene of interest through polymerase chain reaction (PCR); III) Electrophoresis of amplified DNA fragments and their detection.

1.1.1 DNA extraction

DNA is extracted from an approximately 2-3 mm terminal portion of tail. Each sampling is performed using sterile scissors to avoid cross-contamination, and each animal in multiple cages is specifically ear-tagged to ensure its recognition post genotyping. Every mouse is monitored to guarantee the blood flow stop. The biopsies are put into an appropriately marked Eppendorf tube with Lysis Buffer (50 µL; 25 Mm NaOH, 0,2 Mm Na2 - EDTA; pH 12), a tissue digestion buffer with Proteinase K (pH ≈ 12), and placed into the thermocycler at 95 °C for 45 min. Then an equal volume of Neutralization Buffer (50µL; 40 Mm TRIS-HCl; pH 5.4) is added. Finally, samples are centrifugated (3 min, 4000 rpm, RT) and the supernatant, containing the extracted DNA, is transferred to a new Eppendorf tube. The extracted DNA is added to PCR mix.

1.1.2 PCR

The PCR master mix composition is shown in Table 5.

	Final concentration	Volume per sample (µL)
10X Buffer	1X	2
25 mM MgCl$_2$ Solution	2 mM	1,6
10 mM dNTP mix	0.2 mM	0,4
20 µM WT1 forward	1 µM	1
20 µM WT2 reverse	1 µM	1
20 µM Fabry mut.	1 µM	1
5 U/µL Taq Polymerase	0.02U/µL	0,08
H$_2$O Ultrapure		10,92
DNA template /H2O		2

Table 5 Master mix composition per sample. 10X PCR Buffer without MgCl$_2$ (Sigma, Burlington, Massachusetts, USA); 25 mM MgCl$_2$ Solution (Sigma); 10 mM dNTP, deoxynucleotide Mix (Sigma); 5 Units/µl Taq Polymerase from Thermus aquaticus; WT1 forward, MW: 6176.0 µg/µmole (Invitrogen, Carlsbad, California, USA); WT2 reverse, MW: 6045.0 µg/µmole (Invitrogen); mutant Fabry reverse, MW: 6159.0 µg/µmole (Invitrogen).

The PCR amplification program is shown in Table 6. The WT forward and reverse primers are oIMR$_{5947}$ (5'-AGGTCCACAGCAAAGGATTG-3') and oIMR$_{5948}$ (5'-GCAAGTTGCCCTCTGACTTC-3'),

respectively. They give two 296 bp-long bands in α-Gal A homozygous female mice (+/+) and one band in α-Gal A hemizygous males (+/0); whereas the mutant reverse primer oIMR$_{7415}$ (5'-GCCAGAGGCCACTTGTGTAG-3') gives two 202 bp-long bands in α-Gal A homozygous female mice (-/-) and one band in α-Gal A hemizygous male mice (-/0). The heterozygous female show both bands.

Program	Cycles	Time	Temperature
Starting Denaturation	1	3'	94°C
Denaturation		30''	94°C
Annealing	35	1'	64°C
Elongation		1'	72°C
Final elongation	1	2'	72°C

Table 6 PCR Amplification Program

1.1.3 Electrophoresis

Electrophoretic running is performed on agarose gel (1.8%) at 100V for about 30 minutes. The agarose powder is dissolved in TAE 1X buffer (40 mM Tris-acetate, 1 mM EDTA) and ethidium bromide (EtBr, 0.5 µg/ml) is added to allow UV light revelation (λ254 nm). The 10X loading dye buffer (0.9% SDS, 50% glycerol, 0.05% bromophenol blue, Takara) is added to DNA samples to follow the running. Samples are loaded joined by DNA size marker (MassRuler DNA Ladder Mix ready-to-use, Thermo Fisher Scientific, Waltham, Massachusetts, USA). The gel is exposed to UV trans illuminator for DNA bands visualization.

2. Evaluation of GI motility

2.1 Fecal output and water content

Fecal excretion was assessed for three consecutive days; the pellets were collected and weighted daily from 9:00 am. Each animal was individually housed in a clean, clear plastic cage and left there to become acclimatized the day before. According to the previously published methods Li et al. 2006, one-hour stool frequency was measured by monitoring constantly throughout the 60 minutes collection period[634]. Fecal pellets were collected immediately after expulsion and placed in sealed tubes to avoid evaporation. Fecal pellets were weighed (wet weight; mg), counted, dehydrated (60 °C, overnight), and weighed again (dry weight; mg). Fecal water content was calculated according to the equation: water content (%) = 100 (wet weight - dry weight)/wet weight. Similarly, total fecal output was assessed every 24 hours (n. of pellets, total weight). Fecal samples were then collected and frozen at -80 °C for SCFAs and microbiota analysis.

2.2 Statistical analysis

All experiments were carried out on 10 animals (n = 10) per genotype (WT - KO) per group (T1; T2; T3). Data were analyzed using GraphPad Prism for Windows (version 8, GraphPad Software, Inc. La Jolla, CA, USA). The data are represented as mean values ± SEM. Two-way analysis of variance (ANOVA) followed by Tukey's post hoc test for multiple comparisons were applied. $p < 0.05$ (*), $p < 0.01$ (**) and $p < 0.001$ (***) were chosen as indicating significance.

3. Assessment of colon sensitivity by Colorectal Distention (CRD) Technique

3.1 Visceromotor Response (VMR) to CRD and intraluminal pressure measurement

The Visceromotor Response (VMR) to CRD has been used as an objective evaluation of visceral sensitivity[635]. According to the previously described method by Lucarini and coworkers in 2020, two EMG electrodes wires (Teflon-coated stainless steel wire, diameter: 0.6 mm, length: 12-15 cm; Cooner wire, Chatsworth, California, USA) were sutured into the external oblique abdominal muscle under deep anesthesia and exteriorized at scruff level (Fig. 13 a-e)[636]. A week was allowed to elapse before measurement to ensure a full recovery from the surgery. During the experiment, the electrodes were relayed to a data acquisition system and the corresponding EMG signal was recorded, amplified, and filtered (Animal Bio Amp, ADInstruments, Colorado Springs, CO, USA) and digitized (PowerLab 4/35, ADInstruments, Colorado Springs, CO, USA). VMR assessment was carried out under light anesthesia (Isoflurane 2%; Ecuphar, Milan, Italy) and the whole protocol was performed keeping the mouse on a heating pad (about 37°C). A lubricated latex balloon was inserted trans-anally into the descending colon of mice. The balloon was assembled with an embolectomy catheter and connected to a syringe and a pressure sensor (Disposable Blood Pressure (BP) Transducer, ADInstruments, Dunedin, New Zealand). The distention was applied by filling the balloon through the syringe with increasing volumes of water (50, 100, 150/200, 300 µL). EMG signal was evaluated during the 30 seconds before and during the balloon distension, whereas the intraluminal colonic pressure only at the moment of distension (Fig. 13 f-h). The balloon was deflated at the end of each distension. Five minutes were allowed to elapse between each measurement. To quantify the magnitude of the VMR at each distension volume, the area under the curve (AUC) before the distension (30 s) was subtracted from the AUC during the balloon distension (30 s), and responses were expressed as a percentage increase from the baseline. Data were analyzed, and quantified using LabChart 8 (ADInstruments, Colorado Springs, CO, USA).
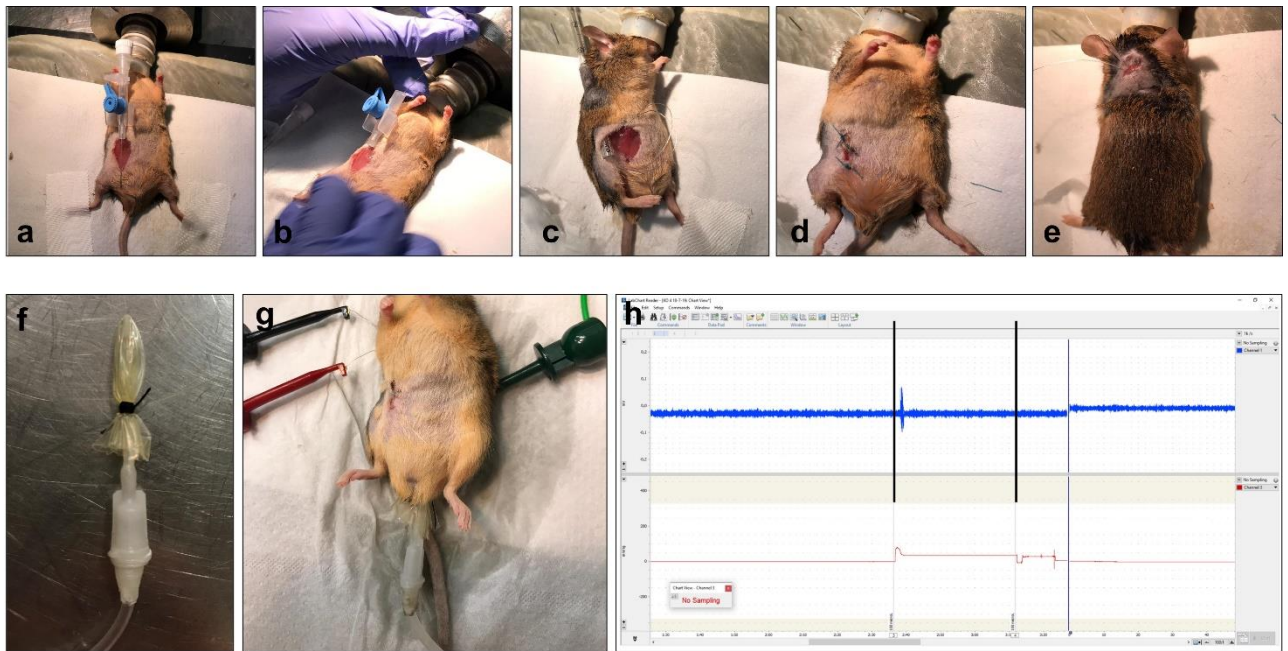
Figure 13 Method for implanting intramuscular electrode array and EMG recordings. Anesthetized mice were shaved in the abdominal area and at the back of the neck. By a sterile scalpel, a 1 cm incision was made in the skin in the lower right abdomen, and the skin around the incision was separated from the musculature. The two sterile electrodes were knotted in the terminal part and the Teflon coating was removed from the 0.3-0.5 cm. (a) 25-G needle was inserted into the oblique abdominal musculature and (b) the two electrodes were subsequently threaded through it so that the uncoated segments were completely inserted in parallel location. (c) To externalize the electrodes at the neck level, a 1 ml serological pipet was passed subcutaneously until the back of the neck, where a 1 cm incision was made in the skin and the two wires were then inserted into the pipet. The 3-0 Prolene and silk (Ethicon, Somerville, New Jersey, USA) were used to stitch the abdomen (d) and the back of the neck (e). Wounds were kept wet with sterile 0.9% NaCl during surgery and disinfected with Betadine at the end. The entire protocol was performed keeping the mouse on a heating pad (~ 37°C). (f) The balloon used to induce CRD connected to the embolectomy catheter connected to the pressure sensor (Disposable Blood Pressure (BP) Transducer, ADInstruments) needed for intraluminal colonic pressure recordings. (g) The balloon insertion and EMG electrodes connection (Cooner wire). The terminal part (0.3-0.5 cm) of the two electrodes was stripped from Teflon coating and connected to the system for EMG recordings via two connection wires (in *black* and *red*). The ground wire (in *green*) was leaned on the mouse side. The balloon was then inserted transanally into the descending colon of mice (total insertion distance, 25 mm). (h) Example of an EMG signal recording expressed as mV (*blue line*), and intraluminal colonic pressure, expressed as mmHg (*red line*), for VMR evaluation by CRD. The starting and ending points of distension (example with 100 µL) are shown by the first and second *black lines*. EMG signal was assessed during the 30 seconds before (*to the left of first black line*) and during (*in between the two black lines*) the distension, whereas the intraluminal colonic pressure only at the moment of distension (*pick*), by LabChart 8 software (ADInstruments).

3.2 Abdominal Withdrawal Reflex (AWR) to CRD

The Abdominal Withdrawal Reflex (AWR) is a behavioral response to CRD recorded in conscious animals, previously described on rats by Chen et al. (2014)[637]. This consists of visual observation of animal responses to CRD (in this context to: 50, 100, 150/200, 300 µL) by blinded viewers who

assigned a stabilized scores: (0) No behavioral response to colorectal distention; (1) Immobilization during colorectal distention with sporadic head movements; (2) Mild contraction of the abdominal muscles, but absence of abdomen lifting; (3) Strong contraction of the abdomen and lifting of it from the floor; (4) Arching of the body and lifting of the pelvic structures and scrotum. Briefly, mice were anesthetized, and the balloon was trans-anally inserted like previously described. The tubing was taped to the tail to hold the balloon in place. Then mice were allowed to recover from the anesthesia for about 30 min before the visual evaluation.

3.3 Statistical analysis

Behavioral measurements were performed on 10 animals (n = 10) for each genotype (WT – KO), per group (T1; T2; T3). Results were expressed as mean ± SEM. The analysis of variance (ANOVA) of data was performed by one-way ANOVA with Bonferroni's test for post hoc comparisons. p values ≤ 0.05 were considered significant. Data were analyzed using the "Origin 9" software (OriginLab, Northampton, MA).

4. Assessment of anxiety-like behavior and locomotor activity

The elevated plus maze (EPM), and the open field test (OF) were performed to assess anxiety-like behavior and locomotor activity. These tests were chosen to cover the expected range of intra-individual outcome variation. Animals (n = 8-11), from all three analyzed groups (T1, T2, T3) of both genotypes (WT-KO), were allowed to habituate to the testing room 1 hr before starting the tests.

4.1 Elevated Plus Maze (EPM) Test

The apparatus, raised off the ground (50 cm), consisted of two open arms and two closed arms (66,5 cm x 10 cm) separated by a junction area (10 cm x 10 cm). A video tracking system was fixed above the experimental platform. Then mice were placed individually in the middle of the apparatus, facing an open arm, and allowed to explore for 5 minutes. The maze was cleaned between each mouse with 30% ethanol to avoid leaving an abnormal odor. Data acquisition and analysis were performed by the software system Ethovision XT 15 Noldus (Wageningen, The Netherlands). The number of entries and the total time spent in open and close arms were determined.

4.2 Open Field (OF) Test

OF apparatus consists of a square arena (45cm × 45 cm), quietly lit up, and a ceiling-mounted camera to record the animals' movements. The arena is divided into two areas, the center zone

(11% of the total area) and the surrounding area. Behavior was analyzed using Ethovision XT 15 software system (Noldus, Wageningen, The Netherlands). Animals were gently introduced into the center of the arena one at a time and allowed to explore for 10 minutes. They were then removed and placed immediately back in their home cage. The arena was cleaned with 30% ethanol to avoid leaving an abnormal odor before placing the next animal inside. Data are expressed as number of entries and cumulative duration spent in border and total distance traveled (cm).

4.3 Statistical analysis

Behavioral measurements were performed on 8-11 animals (n=8-11) for each genotype (WT – KO), per group (T1; T2; T3). Results were expressed as mean ± SEM. Data were analyzed using Jamovi and GraphPad Prism for Windows (version 8, GraphPad Software, Inc. La Jolla, CA, USA). Test of homogeneity of variances (Levene) and normality (Shapiro-Wilk) were applied. Datasets with normal distribution were analyzed for significance using mixed model analysis of variance (ANOVA) with genotype and time as independent factors. Post hoc multiple comparisons were carried out using Tukey's post hoc test. A probability level of $p < 0.05$ was considered to be statistically significant.

5. Samples harvesting and preparation

5.1 Murine colon extraction and tissue processing

Mice were sacrificed by cervical dislocation previous halothane anesthesia[131]. Ventral incision was made using sterile scissors and forceps and the intestine was cut after the stomach and before the tail (at the end of the rectum) and removed with a clamp. Only the portion below the cecum (colon) was used in this thesis work. The colon content was gently flushed by inserting a round needle syringe with cold phosphate-buffered saline (PBS 1X, pH 7.4). Pieces of colon about 1 cm long, from proximal to distal were cut and fixed in 4% paraformaldehyde (PFA) in PBS, overnight at 4°C. The samples were washed with PBS (3 x 5 min, room temperature (RT), gently agitation) and stored in PBS with 0.1% sodium azide until use (short-term storage). The mesentery was eliminated by a sterile blade under the stereomicroscope (Nikon SMZ645, Tokyo, Japan). Samples were further cut into ~5 mm-long pieces and cryoprotected in PBS with 30% sucrose and 0.05% sodium azide (overnight, 4°C, agitation). Once sank to the well bottom, the tissue was embedded in Tissue Tek® O.C.T.™ Compound (O.C.T.= Optimal Cutting Temperature, Killik, Bio Optica, Milan, Italy) and sectioned by cryostat (Leica CM1850, Wetzlar, Germany) at -23 °C cutting temperature. Parafilm

cylinders fixed on the stubs were filled with O.C.T. and the pre-acclimated samples were placed inside, perpendicularly, in order to get transverse sections. 50 µm-thick cross free-floating sections were cut, collected and stored at 4°C in PBS/sodium azide (0.05%) to perform the immunofluorescence analysis.

5.2 Extraction of mouse DRGs: tissue sections and culturing of primary neurons

DRGs have been used in two ways: whole (as tissue), and as a source for primary cultures of neurons. The extraction procedure is the same, but the pre- and post-extraction steps change. In the first case, for whole DRGs, the animals (n = 3 per genotype, per group) were deeply anesthetized and transcardially perfused with 4% PFA (Sigma) in PBS (1X, pH 7.4). The spinal cord was extracted and the single DRGs removed (see description below) and subjected to post-fixation in 0.4% PFA at 4°C, overnight. The fixative solution was replaced with cryoprotective solution of 30% sucrose. DRGs cryo-sections (50 µm) were obtained from lumbo-sacral spinal cord segment (starting from T13 vertebral spine) and collected on slides (Superfrost Plus, Thermo Scientific).

Primary cultures of DRG neurons were prepared according to a previously described protocol with some modifications[95,633]. Mice were anesthetized by halothane before decapitation. The prone position mouse was sprinkled with ethanol, and by means of sterile forceps and scissors, the coat and underlying layers, internal organs, and excess skin and musculature were removed to isolate the spinal column (Fig. 14 a). Under the stereomicroscope, the lumbosacral portion of our interest was then cut with the scalpel (Fig. 14 b). The spine was longitudinally cut in the middle, so for each half one ganglion with its routs was obtained (Fig 14 c-e). The ganglia were transferred in ice cold DPBS 1x (Gibco) and the roots were cut using a sterile blade (Fig. 14 f). After rinsing in DMEM (Gibco), the ganglia were placed in DMEM containing 5000 U/mL type IV collagenase (Worthington) for 45–75 min (it depends on the animals' age) at 37 °C, 5% CO_2, washed twice with FBS-containing medium, and then gently mechanically dissociated with passages through 0.5 mm sterile needles. Cells were centrifuged for 10 min at low speed and then appropriately diluted in 1 mL of DMEM medium containing 10% FBS (Gibco), 50 ng/mL NGF (Gibco), and 1.5 µg/mL cytosine β-D-arabinofuranoside, (AraC, Sigma). For immunocytochemistry, 15.000 cell/ml were plated onto 18 mm round glass coverslips, pre-coated with poly-L-lysine and Laminin. Cell cultures were maintained in an incubator at 37°C, with 5% CO_2. Cells were maintained in DMEM, supplemented with 10% FBS in the presence of 50 ng/mL NGF, and 1.5 µg/mL cytosine β-D-arabinofuranoside, (AraC, Sigma) to reduce glial cell expression. Half volume of medium was changed every second day.
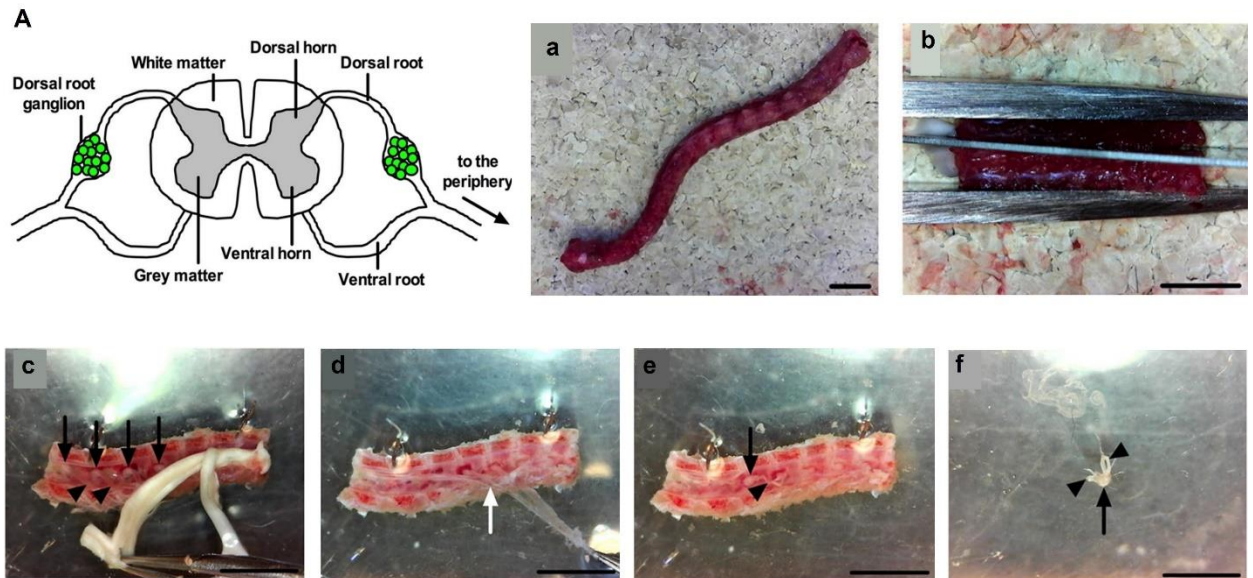
Figure 14 Dorsal Root Ganglia extraction. (A) Schematic representation of DRG localization: clusters of sensory neuron cell bodies located in the dorsal root of the spinal cord. (a) Mouse spinal cord exposure; (b) the spinal cord, blocked with thick tweezers to assure the dorsal position, is longitudinally cut into two halves along the midline; (c) peeling of the spinal cord in a rostro-caudal direction to expose the DRGs (*black arrows*); (d) the meninges (*withe arrows*) are carefully removed to expose the DRGs; (e) ganglia are visible (*black arrow*) with their roots (*black triangle*); (f) single ganglia (*arrow*) with their roots (*triangles*) are extracted.

6. Immunofluorescence (IF)

6.1 IF on colon and DRG cryosections

50µm-thick transverse free-floating sections of colon were put into 48-multi well plates (2 sections per well), whereas the DRGs were handled directly on slides by means of PAP Pen (Abcam). Samples were washed with PBS (5 min, RT) in order to remove the O.C.T. Sections were blocked with 5% BSA in PBS with 0.5% Triton X-100 (1 h, RT). Sections were incubated in humid chamber with primary antibodies diluted in PBS, 1% BSA, 0.5% Triton X-100 (overnight, 4°C). After washing (PBS, 4 x 20 min, RT), they were incubated with secondary antibodies in humid chamber (2 h, RT). From now on, all the steps were carried out in the dark. Sections were finally incubated with 4',6-diaminobenzidine-2-phenylindole (DAPI, Sigma-Aldrich) for 10 minutes at RT, washed (4x10 min, RT) and mounted with Fluoromount-G mounting medium (Sigma-Aldrich). The following antibodies were used: rabbit anti-PGP9.5 (1:1000; Abcam), guinea pig anti-PGP9.5 (1.1000; Millipore), rabbit anti-TRPV1 (1:200; Alomone, Jerusalem, Israel), rabbit anti-TRPV4 (1:300; Abcam), rabbit anti-TRPA1 (1:400; Novus Biologicals, Centennial, Colorado, USA); Cy2 donkey anti-rabbit (1:400; Jackson ImmunoResearch, Laboratories lnc., West Grove, Pennsylvania, USA), Alexa Fluour 488 Goat anti-guinea (1:1000; Invitrogen), Cy3-conjungated Fab fragments donkey anti-rabbit secondary antibody (1:100; Jackson ImmunoResearch), Cy3 donkey anti-rabbit (1:400; Jackson ImmunoResearch). The

specificity of each immunofluorescent signal was assured by incubation with only secondary antibody. The fluorescent signal of negative control samples was taken as threshold to detect the specific signal. For colon sections double immunostaining antibodies from the same host species (rabbit) were used. For this purpose, monovalent Fab Fragments of affinity-purified secondary antibodies was used, to achieve both labelling and the effective blocking of the first primary antibody, in order to prevent overlapping detection of antigens. In this case, samples were incubated (overnight, RT) with the primary antibody rabbit anti- TRPV1, TRPV4, or TRPA1. After washing, they were incubated (2 h, RT) with an excess of Cy3-conjungated Fab fragments donkey anti-rabbit (1:100; Jackson ImmunoResearch). The samples were then washed again and re-incubated (overnight, RT) with the second primary antibody, the rabbit anti-PGP9.5 (1:1000; Abcam). Finally, sections were incubated (2 h, RT) with the Cy2-donkey anti rabbit secondary antibody (1:400; Jackson ImmunoResearch) and stained with DAPI. Colon sections were transferred on polylysine-coated slides (Superfrost UltraPlus®, Thermo Fisher Scientific), whereas the DRG sections were covered.

6.2 IF on DRG neurons

Cells were fixed with 4% PFA (Sigma) in PBS (0.01 M, pH 7.4) for 20 min, RT and washed in 1X PBS (3 x 10 min, RT). Then they were incubated with blocking solution 5% BSA in PBS 1X plus 0.5% Triton X-100 (45 min, RT). Samples were then incubated with primary antibodies (over night, 4°C). In detail: mouse anti-NeuN (1:1000; Millipore), rabbit anti-TRPV1 (1:50; Santa Cruz), rabbit anti-TRPV4 (1:300; Abcam), rabbit anti-TRPA1 (1:400; Novus). The following day, after 1X PBS washes (3 x 15min), the incubation with the secondary antibodies was done (1h, RT, shaking). The secondary antibodies were: donkey anti-rabbit Cy3 (1:400; Jackson ImmunoResearch) and goat anti-mouse Cy2 (1:400; Jackson ImmunoResearch). After 1X PBS washes (3 x 15min), samples were mounted with Fluoroshield™ with DAPI (Sigma-Aldrich) on polylysine-coated slides (Superfrost UltraPlus®, Thermo Fisher Scientific).

7. Image acquisition and processing: confocal microscopy and ImageJ

7.1 Tissue sections acquisition

Images of transverse colon and DRG sections were taken on Nikon D-Eclipse C1 inverted laser scanning confocal microscope, at 40X magnification (Immersion oil, Sigma). The threshold value (gain) for each of the three channels of our interest (blue, green, red) was set based on the negative

control in order to eliminate nonspecific signals. Each experiment was performed in triplicate, and 4-6 sections per sample were acquired from each. Six or more images (depending on size) were taken to have the entire section (n = 3; WT and KO; T1, T2, T3). EZ-C1 3.90 FreeViewer and Image J software were used for image processing.

7.2 DRG neurons images and fluorescence quantification

Images of neurons from DRG were acquired by Nikon D-Eclipse C1 inverted laser scanning confocal microscope, at 40X magnification (Immersion oil, Sigma). The threshold values were set based on the negative control in order to eliminate nonspecific signals. Each experiment was performed in triplicate and 15 images per sample were acquired (n = 3; WT and KO; T1, T2, T3). ImageJ software was used to quantify the fluorescence of each neuron. Each 8-bit (black/white) transformed image was processed as follows: *Analyze → Set Measurements → Area, Mean gray value, Integrated density and Min and max gray value*. Then, using *Freehand selection*, the perimeter of each cell was manually outlined and *Analyze → Measure* provided the values of our interest. The same procedure was performed to set the values of the background, if any (Fig. 15). For data analysis, the values obtained were exported to Excel for calculation of Corrected Total Cell Fluorescence (CTCF) = Integrated density - (area of selected cell x average of background fluorescence) like previously described in McCloy et al. (2014)[638].
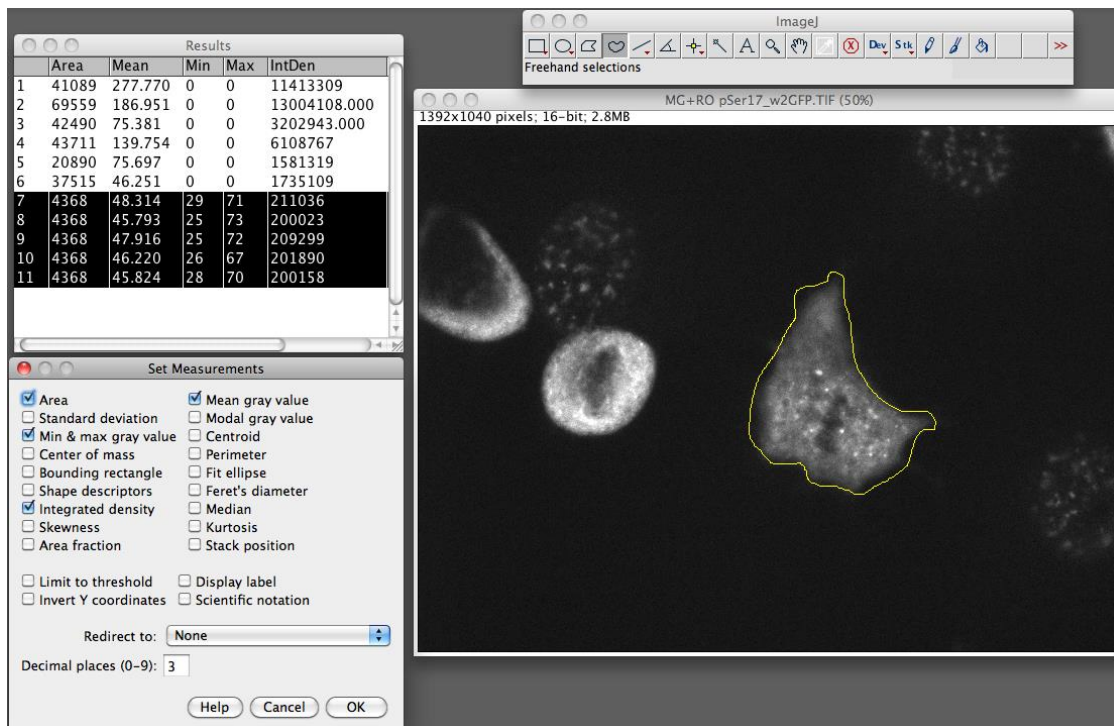
Figure 15 Quantitative fluorescence analysis on cells. The image illustrates the three steps to obtain the fluorescence quantity data. From the menu *Analyze*, *Measure,* and setting of the parameters (*bottom left*). Using the cursor the shape of the cells (*yellow line*) were drawn and one by one the measurement were taken. Finally, a region bordering the cell, which does not show fluorescence signals was measured to set the background values. From ImgaJ.com

8. Microbiota assessment

8.1 Fecal DNA extraction

DNA was extracted from the mouse fecal samples according to the protocol described by Eeckhout and Wullaert (2018)[639] with a few modifications as described below. It was performed using the QIAmp® DNA Stool Mini Kit (QIAGEN) giving the manufacturer's instructions with additional mechanical lysis by bead-beating. Briefly, 200-300 mg of feces were weighed for each sample, and 0.5 g of zirconia beads (0.1-mm diameter), 4 glass beads (3 mm-diameter) and 1.4 ml of ALS lysis buffer (QIAGEN) were added. Chemical lysis was supported by mechanical one performed with FastPrep Instrument (MP Biomedicals, Irvine, CA) through 3 homogenization steps of 1 min at 5 movements/s, interspersed with 5 min of incubation on ice. Then, samples were incubated at 95°C for 5 min to complete cell membrane lysis by heat shock and centrifuged at 13,000 rpm for 1 min at 4°C. The supernatants were incubated with half InhibitEX Tablet (QIAGEN) to remove inhibitory substances. After further centrifugation at 13,000 rpm for 3 min at room temperature, the supernatants were incubated with 15 µl of Proteinase K and 200 µl of AL buffer (QIAGEN) at 70°C for 10 min, to remove any residual protein. The DNA was then purified using the QIAGEN spin

columns, as per the manufacturer's instructions. Specifically, the DNA retained in the column was washed with 500 µl of AW1 buffer and then with 500 µl of AW2 buffer, which take advantage of different percentages of ethanol to allow the elimination of residual reagents, as well as to elute all cellular material co-extracted with the DNA; at each wash, the samples were centrifuged (13000 rpm, 2 min, RT). To remove all residual ethanol the samples were vacuum centrifugated (3 min, RT). To elute the DNA from the column, separating it from the resin, 50 µl of AE buffer was added and followed by centrifugation (13000 rpm, 1 min, RT). The same elution steps were repeated twice with 50 µl of AE buffer, eventually yielding an aliquot equal to 170 µl of genomic DNA for each starting fecal sample. The extracted DNA was quantified using the NanoDrop ND 100 spectrophotometer (NanoDrop Technologies, Wilmington, DE). Samples were diluted in DNase/RNase-Free Distilled Water (Roche, Basel, Switzerland) to a concentration of 5 ng/µl and stored at -20°C.

8.2 16S rRNA gene amplification and sequencing

The V3-V4 hyper-variable regions of the 16S rRNA gene were amplified using primers 341F and 785R including overhang adapter sequences for Illumina sequencing, according to the "16S Metagenomic Sequencing Library Preparation" protocol (Illumina, San Diego, CA, USA). Amplicons were purified using a magnetic bead-based system (Agencourt AMPure XP, Beckman Coulter, Brea, CA, USA) and indexed with Nextera technology by limited-cycle PCR. Briefly, each 25 µl PCR reaction contained 5 ng/µl microbial genomic DNA, 1 µM of forward primer (5'-TCGTCGGCAGCGTCAGATGTGTATAA GAGACAGCCTACGGGNGGCWGCA-3') and 1 µM reverse primer (5'-GTCTCGTGGGCTCGGAGAT GTGTATAAGAGACAGGACTACHVGGGTATCTAATCC-3') plus 12.5 µl 2X *Kapa HiFi Hot-start ReadyMix* (Kapa Biosystems) were added. The PCR conditions were as follows: initial denaturation at 95 ∘C × 3 min (melting); 30 cycles of 98°C for 20 sec (melting), 55°C 30 sec (annealing), 72°C 30 sec (elongation); and 72 °C × 5 min (final elongation). After further purification, the final libraries were prepared by pooling the samples at 4 nM, denaturing the pool with 0.2 NaOH and diluting it to 5 pM. Sequencing was performed on an Illumina MiSeq platform using a 2 × 300 bp paired-end protocol according to the manufacturer's instructions. Raw sequencing reads were deposited in the European Nucleotide Archive (ENA) under accession number PRJEB61216.

8.3 Bioinformatic and statistical analysis

Bioinformatic analysis of the sequences we obtained was performed in collaboration with the Microbiome Science And Biotechnology Unit led by Prof. Marco Candela (University of Bologna). After sequencing, the 16S rRNA gene sequences were returned in .fastq format. The reads in the

.fastq file were processed using PANDAseq[640]. PANDAseq aligned the forward (R1) and reverse (R2) pairs of reads; this was followed by merging and reconstruction of the actual sequence between R1 and R2, filtering the resulting sequences based on quality and length. An additional sequence cleaning step was conducted using QIIME2 (Quantitative Insights Into Microbial Ecology) software (https://qiime2.org), a bioinformatics platform that enables the analysis of complex microbial communities through a pipeline that includes the DADA2 (Divisive Amplicon Denoising Algorithm) plug-in[641,642]. The cleaned sequences, obtained from PANDAseq, were imported into a single file in .qza (QIIME zipped archive) format into the QIIME2 working environment. Through the DADA2 algorithm, a denoising process was carried out. In parallel, QIIME2 performed clustering of sequences into ASVs (Amplicon Sequence Variants) based on their sequence homology. During the DADA2 denoising process, the ASVs are filtered by quality, generating High-Quality ASVs with the undiscarded sequences. Using the VSEARCH program and the Greengenes database, taxonomic assignment of High-Quality ASVs was conducted and returned as ASV tables of which, for the purpose of analysis, 3 distinct levels of taxonomic classification were considered, namely: phylum, family, genus[643,644]. Relative abundance was reported for each taxonomic unit. The ASV tables obtained were analyzed to calculate the ecological indices of alpha-diversity and beta-diversity, intra-sample and inter-sample diversity, respectively. The α-diversity allows quantifying the degree of biodiversity of the individual sample as an independent variable, through the parameters of richness (number of species present) and distribution (percentages of relative abundance of species in the sample). To enable comparison of diversity among different samples, multiple rarefaction was performed. Rarefaction was performed until a plateau of taxonomic richness was reached, with a minimum number of ASVs for a normalized analysis of all samples. The metrics used in these analyses are divided into (1) phylogeny-based metrics and (2) non-phylogeny-based metrics: of the former, the PD-Whole Tree metric was used (defines diversity based on phylogenetic distances of observed species), for the latter, Chao1 (defines diversity by species richness in samples) and Observed ASVs (defines diversity by the number of observed ASVs per sample) were used. β-diversity was computed using the UniFrac metric to construct phylogenetic distance matrices from the ASVs tables[645]. The ASVs tables were subjected to biostatistical analysis using the open source software R (version 3.6.0, https://www.R-project.org/) and the program RStudio (version 1.2.1335, https://www.rstudio.com). Applying a selection filter, all taxonomic groups that did not have a relative abundance greater than 0.1% for at least two samples were discarded; the discarded taxa were then grouped into a single cluster named "Other" of the corresponding taxonomic

classification level of each ASV table (phylum, family, genus). To compare the microbial diversity and taxonomic composition among the different sampling time-points, a Kruskal-Wallis significance test was conducted for preliminary analysis, confirmation was then sought with the paired Wilcoxon rank-sum test method for correction of Type I errors due to running multiple tests on the same data. The results of these analyses were provided as box-plot, bar-plot, ring-plot or scatter-plot using R packages such as ggplot2 and plotrix[646,647]. Values of $p < 0.05$ were considered as significant.

In parallel, beta-diversity analysis highlights differences in gut microbiota composition among different samples, making it possible to represent them in a multi-dimensional graph. To make the distance matrices easy to read, the UniFrac weighted and unweighted files were graphed by multivariate Principal Coordinates Analysis (PCoA), performed with the vegan package (version 2.5-6; https://CRAN.Rproject.org/package=vegan) of R[648]. The Adonis function, from the same package, was used to assess the statistical significance of the results obtained through a permutation test.

Considering the absence of data in the literature regarding the microbiota of mice and Fabry patients, to validate and extend the analysis, it was decided to perform a second analysis from the High-Quality ASVs with the undiscarded sequences.

This analysis was conducted at the APC Microbiome Ireland – UCC University College of Cork (Laboratory of Prof. John Cryan) during my internship at the aforementioned host facility. Specifically, in this case, 300 base-pair paired-end reads were pre-filtered based on a quality score threshold of >30 and trimmed, filtered for quality and chimaeras using the DADA2 library in R (version 4.1.2). Only samples with >10,000 reads after QC were used in the analysis. Taxonomy was assigned with DADA2 against the SILVA SSURef database v138. Parameters recommended in the DADA2 manual were adhered to unless otherwise specified. ASVs were aggregated at the genus level. As ratios are invariant to sub-setting and this study employs compositional data analysis techniques, features that were unknown on the genus level were not considered in downstream analysis, as were genera that were only detected as non-zero in 10% or fewer total samples[649]. Genera that were never detected at a 2% relative abundance or higher were aggregated and defined as rare taxa for the stacked bar plots. These 'rare taxa' were not removed from statistical analysis. The iNEXT library was used to compute α-diversity for the first three hill numbers (Chao1, Shannon entropy and Simpson Index)[650]. Changes in α-diversity were assessed using linear models. Principal component analysis was per-formed on centred log-ratio (clr)-transformed counts as a visual companion to the beta diversity analysis. Zeroes were imputed using the "const" method[651]. Beta-diversity was computed as Aitchison distance (Euclidean distance of clr-transformed counts) and

differences were measured using the PERMANOVA implementation from the vegan library with 1000 permutations[652]. Differential abundance of taxa and functional modules was assessed by fitting linear models on the clr-transformed count tables. To correct for multiple testing in tests involving microbiome features, the Benjamini-Hochberg post hoc procedure was performed with a false discovery rate (FDR) q-value of 0.1 as a cut-off[653]. Plotting was handled using ggplot2. All R scripts are available online at https://github.com/thomazbastiaanssen/Tjazi[654]. PICRUSt2 was used on raw DADA2 output for functional inference from 16S rRNA gene sequence of microbiome samples in the form of KEGG orthologues[655]. Gut-Brain Modules (GBMs) and Gut-Metabolic Modules (GMMs) were calculated using the R version of the Gomixer tool[656]. Further data handling was done in R (version 4.1.2) with the RStudio GUI (version 1.4.1717).

9. Assessment of SCFAs in fecal samples

9.1 SCFAs quantification: Gas Chromatography - Mass Spectrometry

Quantification of SCFAs was performed by using a headspace solid-phase microextraction gas chromatography-mass spectrometry (HS-SPME GC-MS) method. For each fecal sample a 250-mg aliquot was weighed. Briefly, 250-mg aliquots of fecal samples were homogenized in 10% perchloric acid solution and then centrifuged at 15,000 rpm for 5 min at 4°C. Fifty microliters of supernatant were added with internal standard (IS, D8-butyric acid) and diluted 1:10 in water. We performed the calibration by analyzing spiked sample solutions and water standard solutions at scalar SCFA concentrations (external standardization). For acid identification and quantification, calibration solutions were prepared through Sigma commercial kit containing the internal standard and all standards of acetic, propionic, butyric and valeric acids. The obtained solutions underwent HS-SPME and GC-MS analysis. HS-SPME operated under the following conditions: temperature of 70°C, 10 min equilibration and 30 min extraction, 75 μm CarboxenTM/polydimethylsiloxane fiber (Supelco, Sigma-Aldrich, Italy, Milan). Analytes were desorbed in the GC injector at 250°C for 10 min. GC-MS analysis was performed with the TRACE GC Gas Chromatograph (Thermo Fisher Scientific, Waltham, MA, USA), interfaced with the GCQ Plus mass detector (Thermo Fisher Scientific) with an ionic trap analyzer, operating with a EI ion ionization source (70eV). The capillary column used for GC was a Phenomenex ZB-WAX (30m x 0.25mm ID, 0.15 μm). Helium (SIAD S.p.a.) was used as carrier gas at 1 ml/min. The thermal program was: 40°C for 5 min, increasing by 10°C / min until 220°C was reached and held for 5 minutes. The temperature of the electron impact (EI) source was maintained at 200°C, while the transfer line was maintained at 250°C. Injector base was at 250 °C in splitless

mode. Mass spectra were analyzed in full-scan (34-200 m/z) and in extract ion mode (EIM) on the EI-generated ions: 45 and 60 m/z for acetic acid, 55 and 73 m/z for propionic acid and isobutyric acid, 60 and 73 m/z for butyric and valeric acid, 60 and 87 m/z for isovaleric acid, 63 and 77 m/z for the internal standard (D8- butyric acid). The concentration of SCFAs was expressed in µmol/g stool. The range for the detection limit was between 4 and 68 nmol/g.

9.2 Statistical analysis

Samples were collected from 10 animals (n = 10) per genotype (WT-KO) per group (T1; T2; T3). Data were analyzed using GraphPad Prism for Windows (version 8, GraphPad Software, Inc. La Jolla, CA, USA). The data are represented as mean values ± SEM. Two-way analysis of variance (ANOVA) followed by Tukey's post hoc test for multiple comparisons were applied. $p < 0.05$ (*), $p < 0.01$ (**) and $p < 0.001$ (***) were chosen as indicating significance.

10. Assessment of lyso-Gb3 effect on electrolyte and fluid transport and sensory nerves activation by Ussing chamber and on contractility by organ bath

10.1 Animals

Adult C57BL/6 J male mice purchased from Harlan, UK, were group-housed and maintained on a 12 h – 12 h dark-light cycle with a room temperature of 22 ± 1 °C; standard rodent chow and water were available *ad libitum*. All experimental procedures were conducted in accordance with European Community Council Directive (86/609/EEC) and approved by the local University College Cork Animal Experimentation Ethics Committee.

10.2 Tissue preparation and Ussing Chamber

Mice were euthanized by decapitation, and the entire colon was removed and placed in cold Krebs solution (0.012 mM NaH2PO4, 1.16 M NaCl, 0.048 M KCl, 0,012 M MgCl2, 0,250 M NaHCO3, 2.5 mM CaCl2, and 10 mM D-glucose). Seromuscular stripping was carried out by dissection under a stereomicroscope, and both the longitudinal and circular muscle layers were removed. The resulting mucosal-submucosal preparations were mounted in Ussing chambers (Harvard Apparatus, Kent, UK, exposed tissue area of 0.12 cm^2) with 4 ml of Krebs solution at 37°C, and oxygenated with carbogen gas (95% O_2, 5% CO_2) in both the basolateral and luminal reservoirs as described previously[657]. Up to six preparations were obtained from each mouse and mounted in order from the proximal to distal part.

Tissues were voltage-clamped at 0 mV using an automatic voltage clamp (EVC 4000; World Precision Instruments, Sarasota, FL, USA); the short-circuit current (I_{sc}) required to maintain the potential at 0 mV was recorded as a reflection of the net active ion transport across the epithelium. Resistance was calculated using Ohm's law. Experiments were carried out simultaneously in chambers connected to a PC equipped with *DataTrax II s*oftware (World Precision Instruments). After mounting, the tissue was allowed to equilibrate (~30 min) until a stable baseline was achieved. Reagents were added to the basolateral or apical chamber as the following indicated. The change in the short circuit current (ΔI_{sc}) was calculated based on the value before and after the stimulation and was normalized as the current per unit area of the epithelium (mA/cm^2). Carbachol (CCh) and forskolin (FSK) were added at the end of each experiment to assess tissue viability and epithelial secretory function.

10.3 Treatment and Drugs

Serosal administration of lyso-Gb3 (synthetic - 860952P, Avanti Polar Lipids) was performed at increasing concentrations (30 nM – 100 nM – 300 nM – 1 µM – 3 µM - 10 µM) to test its effect in the acute setting and after 30 minutes of exposure on ΔI_{sc} and TEER. The final concentration of 3 µM lyso-Gb3 was chosen for the subsequent experimental protocols.

All drugs were obtained from Sigma-Aldrich unless otherwise stated. The following compounds were used, with the final concentration, side, and diluent in parenthesis: carbachol (CCh) (100 µM; serosal; in dH2O); forskolin (FSK) (10 µM; serosal; in DMSO); tetrodotoxin (TTX) (Tocris, 300 nM; serosal; in dH2O); veratridine (VER) (30 µM; serosal; in 70% ethanol); furosemide (FUR) (100 µM; serosal; in dH2O); Pyrimido-pyrrolo-quinoxalinedione (PPQ) (MCE, 50 µM; apical; in DMSO); capsaicin (3µM; serosal; in 70% ethanol). The administration protocol (order and time) for each compound will be indicated for each specific experiment.

10.4 Organ Bath

The proximal colon was excised from mice and the tissue was mounted to record the muscle contractility. The colonic tissue was suspended from a tension transducer in a tissue bath of carbogen-bubbled Krebs solution under 1 g of tension and allowed to equilibrate (20–30 min) before reagents were added to the bath. Changes in tension were recorded and analyzed using Powerlab and LabChart8 (AD Instruments Inc., Colorado Springs, CO, USA). Responses are reported as a percentage of the maximal response evoked by the cholinergic agonist carbachol (100 µM) in

each experiment. The tissue was exposed to carbachol before and after the administration of lyso-Gb3 (3µM).

10.5 Statistical Analysis

Data were analyzed using GraphPad Prism for Windows (version 8, GraphPad Software, Inc. La Jolla, CA, USA). The data are represented as mean values ± SD. Assuming a null hypothesis, Student's unpaired or paired t-tests were used when comparing two groups, and repeated-measures ANOVA with Bonferroni's multiple comparison post hoc test was used when comparing more than two groups. $p < 0.05$ (*), $p < 0.01$ (**) and $p < 0.001$ (***) were chosen as indicating significance.

RESULTS

1. Genotyping of murine colony

The experiments were performed on male α-Gal A KO mice and relative WT controls, then also named α-Gal A -/0 and α-Gal A +/0, respectively. Both of them were JAX strain B6;129-Glatm/1Kul/J. The choice to work only with male mice was dictated by the fact that the symptomatology is more severe and uniform in the latter than in the females. In particular, we considered three different time points: 8-10-week-old (T1); 16-20-week-old (T2); 12-month-old (T3). Thus, to confirm the genotype of animals used in experiments and carry out aimed breeding for murine colony maintaining, genotyping was periodically performed on both male and female mice. The electrophoresis gel of the DNA isolated from mice tails and amplified by PCR showed bands of 295 bp for α-Gal A +/0 and 202 bp for α-Gal A -/0 hemizygous male mice; both lines were shown in case of heterozygous female (Fig. 16).
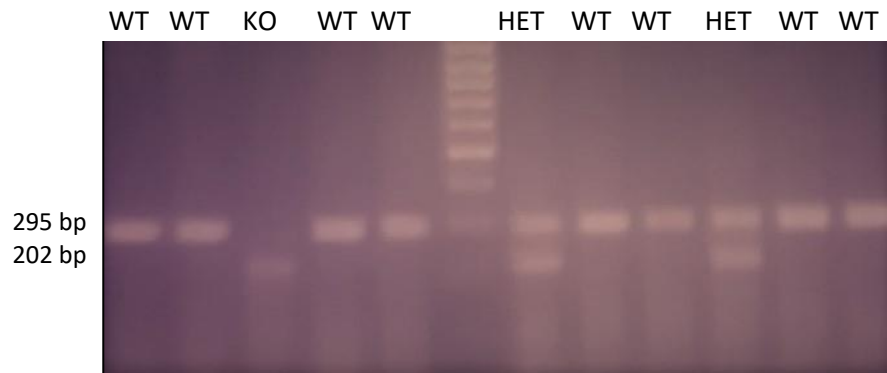
Figure 16 Representative image of DNA genotyping of α-Gal A +/0, α-Gal A -/0 and α-Gal A +/-. The DNA of 11 different animals was loaded along with the DNA ladder marker (lane 6) into an electrophoresis gel and revealed by UV transillumination. The DNA of α-Gal A -/0 mice (KO), separated in the third two lane, gave 202 bp-long bands, whereas the DNA of α-Gal A +/0 mice (WT), separated in lanes 1-2, 4-5, 8-9, 11-12, gave 295 bp-long bands. Heterozygous females (lanes 7, 10) gave both the bands at 202 and 295 bp.

2. Assessment of functional disorders at gastrointestinal level and dysbiosis in a murine model of Fabry disease: from visceral hypersensitivity to the first characterization of the fecal microbiota and its metabolites

2.1 Abnormal defecation parameters in α-Gal A -/0 mice: a diarrheal-like phenotype

Since the main GI symptoms complained by Fabry patients include diarrhea, we investigated whether our animal model reported any motility dysfunctions. Therefore, stool analysis was performed by assessing defecation parameters like the number of pellets, stool dry-weight (mg/24h), and water content (%). As shown in Figure 17, the α-Gal A -/0 mice compared to controls shown a significantly higher fecal output both with regard to the number of pellets (T1, α-Gal A -/0 VS α-Gal A +/0 p_{Tukey} < 0.001; T2, α-Gal A -/0 VS α-Gal A +/0 p_{Tukey} < 0.001; T3, α-Gal A -/0 VS α-Gal A +/0 p_{Tukey} = 0.03) (Fig. 17 A), and total weight, except in this case at 8-10- week old point (T1, α-Gal A -/0 VS α-Gal A +/0 p_{Tukey} = 0.41; T2, α-Gal A -/0 VS α-Gal A +/0 p_{Tukey} = 0.002; T3, α-Gal A -/0 VS α-Gal A +/0 p_{Tukey} < 0.001) (Fig. 17 B). Moreover, post-hoc analysis revealed that these increases in number of pellets and fecal output in KO mice were directly related to the age. In the first case, the effect of age was [$F_{(2, 42)}$ = 130, p < 0.001] and the interaction genotype*age [$F_{(2, 42)}$ = 11.7, p < 0.001]; and regarding the total weight, effect of age was [$F_{(2, 42)}$ = 4.23, p = 0.02] and the interaction genotype*age [$F_{(2, 42)}$ = 3.77, p = 0.03]. Similarly, the fecal water content in α-Gal A -/0 mice was significantly higher compared to controls in 8-10-week and 12-month old point (T1, α-Gal A -/0 VS α-Gal A +/0 p_{Tukey} < 0.001; T3, α-Gal A -/0 VS α-Gal A +/0 p_{Tukey} < 0.001) (Fig. 17 C). However, this alteration was not significant in 16-20- week old mice (T2, α-Gal A -/0 VS α-Gal A +/0 p_{Tukey} = 0.1). Furthermore, although there was both a genotype-dependent and age-dependent effect, the two did not appear to be statistically significantly correlated (effect of genotype [$F_{(1, 42)}$ = 63.5, p < 0.001]; age [$F_{(2, 42)}$ = 26.2, p < 0.001]; interaction genotype*age [$F_{(2, 42)}$ = 2.99, p = 0.06]). Overall, these findings confirm the presence of a diarrheal-like phenotype in the murine model. The complete statistical analysis is shown in Table 7.
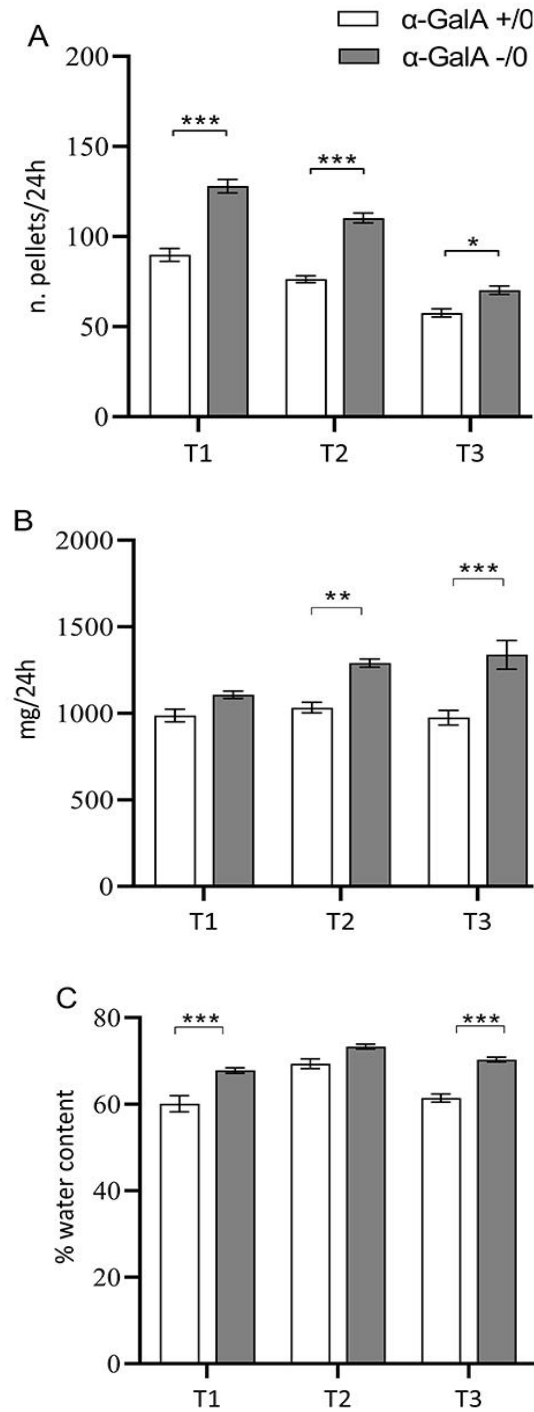
Figure 17 Diarrhea-like phenotype in α-Gal A -/0 mice. Stool analysis was carried out on α-Gal A -/0 mice (*gray bars*) and controls α-Gal A +/0 (*white bars*) at 8-10 weeks-old (T1), 16-20 weeks-old (T2), and 12 months-old (T3). The fecal output was measured as (A) number of pellets and (B) mg produced in 24h. (C) The water content was calculated according to the equation: water content (%) = 100 (wet weight - dry weight)/wet weight. Data are expressed as mean ± SEM of 10 animals per group (n = 10). GraphPad Prism 8 was used for the statistical analysis. Two-way ANOVA test with Bonferroni post-correction was used, *** $p <$ 0.001, ** $p <$ 0.01 and * $p <$ 0.05 vs α-Gal A +/0 animals.

Figure 17	Two-way ANOVA test with Bonferroni post-correction	
Panel A	**Comparisons**	**n. pellets/24h**
	genotype	F (1, 42) = 149; p<0.001
	age	F (2, 42) = 130; p<0.001
	genotype*age	F (2, 42) = 11.7; p<0.001
α-Gal A -/0 VS α-Gal A +/0	T1	p<0.001
	T2	p<0.001
	T3	P=0.04
α-Gal A -/0	T1 VS T2	p<0.001
	T1 VS T3	p<0.001
	T2 VS T3	p<0.001
α-Gal A +/0	T1 VS T2	p=0.02
	T1 VS T3	p<0.001
	T2 VS T3	p<0.001
Panel B	**Comparisons**	**mg/24h**
	genotype	F (1, 42) = 46.5; p<0.001
	age	F (2, 42) = 4.23; p=0.02
	genotype*age	F (2, 42) = 3.77; p=0.03
α-Gal A -/0 VS α-Gal A +/0	T1	ns
	T2	p=0.003
	T3	p<0.001
α-Gal A -/0	T1 VS T2	ns
	T1 VS T3	p=0.010
	T2 VS T3	ns
α-Gal A +/0	T1 VS T2	ns
	T1 VS T3	ns
	T2 VS T3	ns
Panel C	**Comparisons**	**% water content**
	genotype	F (1, 42) = 65.5; p<0.001
	age	F (2, 42) = 26.2; p<0.001
	genotype*age	F (2, 42) = 2.99; p=0.06
α-Gal A -/0 VS α-Gal A +/0	T1	p<0.001
	T2	ns
	T3	p<0.001
α-Gal A -/0	T1 VS T2	p=0.010
	T1 VS T3	Ns
	T2 VS T3	ns
α-Gal A +/0	T1 VS T2	p<0.001
	T1 VS T3	ns
	T2 VS T3	p<0.001

Table 7 Statistical analysis of fecal parameters in α-Gal A +/0 and α-Gal A -/0 mice at three different ages. Age-genotype-dependent correlations. 8-10 weeks-old (T1), 16-20 weeks-old (T2), and 12 months-old (T3); ns = not significant.

2.2 Visceral hypersensitivity in α-Gal A -/0 mice

To evaluate whether the diarrheal-like phenotype in α-Gal A -/0 mice was associated with differences in visceral sensitivity, we measured the Visceral Motor Response (VMR) and the Abdominal Withdrawal Reflex (AWR) to Colorectal Distension (CRD). Experiments were performed on 10 animals (n = 10) per genotype (α-Gal A -/0 VS α-Gal A +/0) per group (T1, T2, T3). It was performed through the insertion of a balloon inflated with increasing volumes in the range of 50-300 μL. The maximum distending volumes (150 μL at T1, 200 μL at T2 and 300 μL at T3) were chosen based on the animals age, to avoid injuring the colon.

Figure 18 shows that α-Gal A -/0 mice displayed higher abdominal responses to the colorectal stimuli compared to controls at each age analyzed. The VMR of α-Gal A -/0 mice was significantly increased in response to the balloon inflation with volumes ≥ 100 μL at all three time points (α-Gal A -/0 VS α-Gal A +/0; T1, 100 μL p = 0,004, 150 μL p =0,006; T2, 100 μL p < 0,001, 200 μL p < 0,001; T3, 100 μL p = 0,002, 200 μL p < 0,001; 300 μL p = 0,009) (Fig. 18 A-B-C). Similarly, by scoring the behavioral nocifensive response to CRD through the AWR assessment, α-Gal A -/0 mice showed a significantly greater sensitivity to controls, even at the lowest distension volume (50 μL), with an higher score to any applied stimulus (α-Gal A -/0 VS α-Gal A +/0; T1, 100 μL p < 0,001, 150 μL p < 0,001; T2, 100 μL p < 0,001, 200 μL p < 0,001; T3, 100 μL p = 0,032, 200 μL p = 0,005; 300 μL < 0,001) (Fig. 18 D-E-F), providing evidence of visceral hyperalgesia. The complete statistical analysis is reported in Table 8.
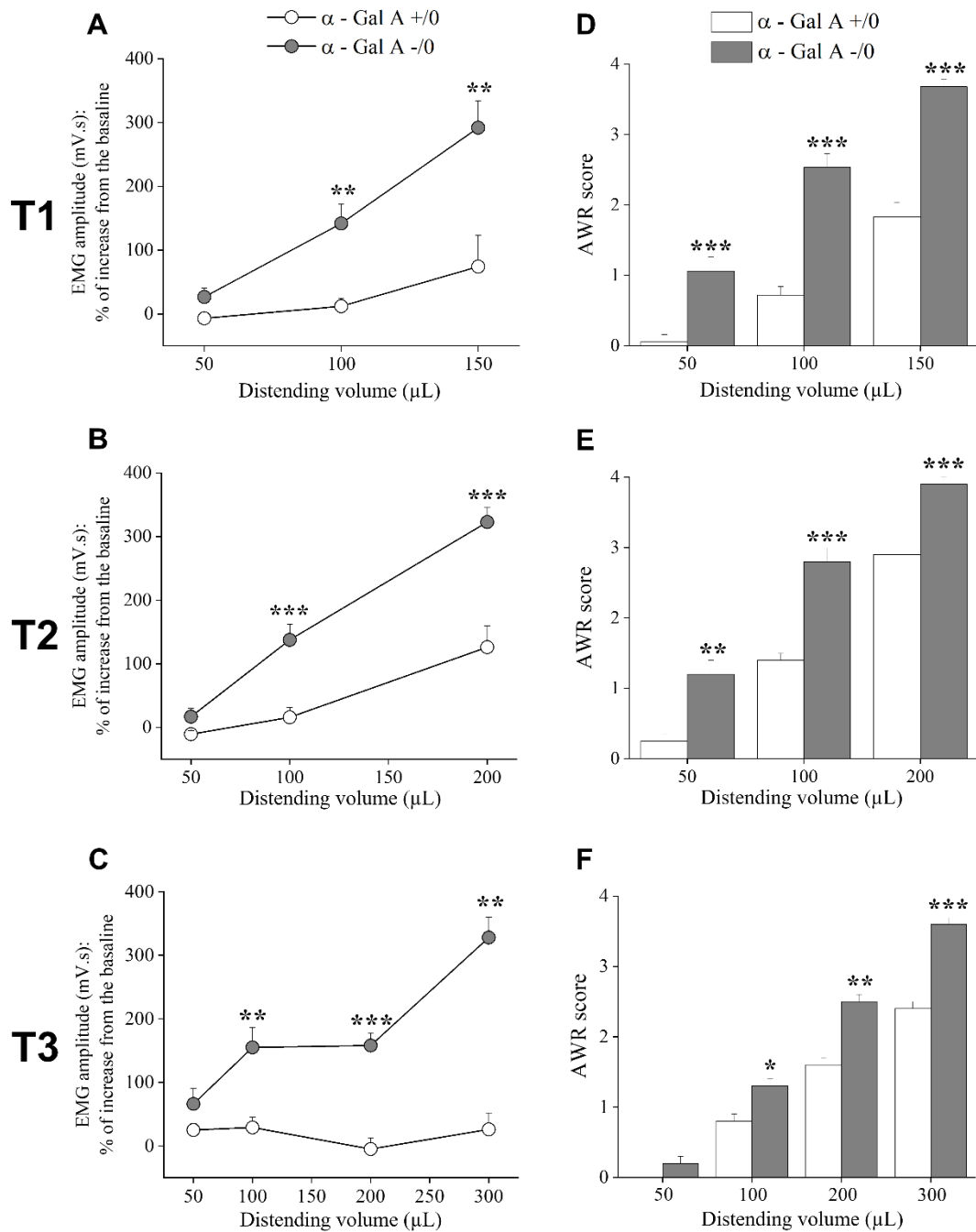
Figure 18 Assessment of Visceral hypersensitivity in α-Gal A -/0 mice by CRD. Visceral sensitivity was assessed in 8-10 weeks-old (T1), 16-20 weeks-old (T2), and 12 months-old (T3) α-Gal A -/0 (white) and controls α-Gal A +/0 (grey) mice, by measuring the electromyography (EMG) amplitude of abdominal contraction (VMR) under light anesthesia (*left panel*, A-B-C) and by scoring the behavioral responses (AWR) in conscious animals (*right panel*, D-E-F) to the CRD with increasing volumes (50-300 μL balloon inflation). Data are expressed as mean ± SEM of 10 animals per group (n = 10). *Origin 9* software (OriginLab, Northampton, MA) was used for the statistical analysis. One-way ANOVA followed by Bonferroni's post hoc test was applied. *** $p < 0.001$, ** $p < 0.01$ and * $p < 0.05$ vs α-Gal A +/0 animals.

Figure 18	Two-way ANOVA				
Panel A-B-C	**Two-way ANOVA statistics for VMR test**				
	Comparisons	**Colorectal Distending Volumes**			
		50 µL	**100 µL**	**150 µL**	**200 µL**	**300 µL**
	genotype	$F_{(1, 48)} =$ 9.1; $p=0.004$	$F_{(1, 48)} =$ 41.1; $p<0.001$	$F_{(1, 14)} =$ 85.2; $p<0.001$	$F_{(1, 36)} =$ 66.1; $p<0.001$	$F_{(1, 20)} =$ 51.4; $p<0.001$
	age	$F_{(2, 48)} =$ 4.1; $p=0.023$	$F_{(2, 48)} =$ 0.3; $p=0.754$	n.d.	$F_{(1, 36)} =$ 28.5; $p<0.001$	n.d.
	genotype*age	$F_{(2, 48)} =$ 0.4; $p=0.694$	$F_{(2, 48)} =$ 0.01; $p=0.987$	n.d.	$F_{(1, 36)} =$ 0.2; $p=0.647$	n.d.
α-Gal A -/0 VS α-Gal A +/0	**T1**	n.s	$p=0.004$	$p=0.006$	n.d.	n.d.
	T2	n.s	$p<0.001$	n.d.	$p<0.001$	n.d.
	T3	n.s	$p=0.002$	n.d.	$p<0.001$	$p=0.009$
Panel D-E-F	**Two-way ANOVA statistics for AWR test**				
		50 µL	**100 µL**	**150 µL**	**200 µL**	**300 µL**
	genotype	$F_{(1, 52)} =$ 36.5; $p<0.001$	$F_{(1, 52)} =$ 98.3; $p<0.001$	$F_{(1, 18)} =$ 41.2; $p<0.001$	$F_{(1, 36)} =$ 82.7; $p<0.001$	$F_{(1, 20)} =$ 106.2; $p<0.001$
	age	$F_{(2, 52)} =$ 11.5; $p<0.001$	$F_{(2, 52)} =$ 26.9; $p<0.001$	n.d.	$F_{(1, 36)} =$ 162.2; $p<0.001$	n.d.
	genotype*age	$F_{(2, 52)} =$ 5.7; $p=0.005$	$F_{(2, 52)} =$ 9.4; $p<0.001$	n.d.	$F_{(1, 36)} =$ 0.2; $p=0.652$	n.d.
α-Gal A -/0 VS α-Gal A +/0	**T1**	n.s	$p<0.001$	$p<0.001$	n.d.	n.d.
	T2	n.s	$p<0.001$	n.d.	$p<0.001$	n.d.
	T3	n.s	$p=0.032$	n.d.	$P=0.005$	$p<0.001$

Table 8 Statistical analysis of visceral sensitivity in α-Gal A +/0 and α-Gal A -/0 mice at three different ages. Age-genotype-dependent correlations. 8-10 weeks-old (T1), 16-20 weeks-old (T2), and 12 months-old (T3); n.s. = not significant; n.d. = not detected.

2.3 Anxiety-like behavior traits and reduced locomotor activity in α-Gal A -/0 mice

Given the different results between α-Gal A -/0 and α-Gal A +/0 mice in motility and visceral hypersensitivity, we decided to investigate the role of the gut-brain axis. To do that, the anxiety and locomotor activity were investigated by the Elevated Plus Maze (EPM) Test and Open Field (OF) Test, evaluators of fear and anxious-like behavior. In particular, the first was mainly used to test anxiety-like behavior, the second to assess a more generalized anxious trait, locomotor activity and explorative behavior. In fact, in this regard, it has been argued that emotionality is not one-dimensional but rather has the ability to vary along different axes in multidimensional space. This

means that different environments, such as open spaces, lighted or elevated areas, can provide different behavioral responses[658].

With regards to the EPM, between α-Gal A -/0 and α-Gal A +/0 mice, for the same total entries (effect of genotype [$F (1, 48) = 0.199$, $p = 0.66$]; age [$F (2, 48) = 1.59$, $p = 0.21$]; interaction genotype*age [$F (2, 48) = 0.574$, $p = 0.57$]) (Fig. 19 A) no significant differences were found in either the frequency of entry into the closed arms (effect of genotype [$F (1, 47) = 0.415$, $p = 0.52$]; age [$F (2, 47) = 2.25$, $p = 0.117$]; interaction genotype*age [$F (2, 47) = 0.824$, $p = 0.45$]) (Fig. 19 B-C) or the time spent in them; even if for the latter in α-Gal A -/0 mice there was a time-dependent decrease (effect of genotype [$F (1, 47) = 3.53$, $p = 0.07$]; age [$F (2, 47) = 15.0$, $p < 0.001$]; interaction genotype*age [$F (2, 47) = 1.27$, $p = 0.29$]). In particular, 12-month-old KO mice spent less time in close arms compared to the same genotype younger mice, both at 8-10 week-old and 16-20 week-old (T3 α-Gal A -/0 VS T1 α-Gal A -/0 $p_{Tukey} = 0.001$; T3 α-Gal A -/0 VS T2 α-Gal A -/0 $p_{Tukey} = 0.002$).

On the other hand, by OF test, we observed that α-Gal A -/0 mice showed a significant decrease in frequency in the periphery at all the three ages (effect of genotype [$F (1, 51) = 68.37$, $p < 0.001$]; age [$F (2, 51) = 9.78$, $p < 0.001$]; interaction genotype*age [$F (2, 51) = 1.26$, $p = 0.293$]; α-Gal A -/0 VS α-Gal A +/0 T1, $p_{Tukey} < 0.001$; T2, $p_{Tukey} = 0.002$; T3, $p_{Tukey} = 0.005$) (Fig. 20 A). However, the time spent in border by α-Gal A -/0 was significantly increased (effect of genotype [$F (1, 45) = 53.38$, $p < 0.001$]; age [$F (2, 45) = 5.97$, $p = 0.005$]; interaction genotype*age [$F (2, 45) = 0.075$, $p = 0.93$]; α-Gal A -/0 VS α-Gal A +/0 T1, $p_{Tukey} = 0.008$; T2, $p_{Tukey} < 0.001$; T3, $p_{Tukey} = 0.002$) (Fig. 20 B), indicating an anxiety-like behavior trait in Fabry mice. Furthermore, we observed that α-Gal A -/0 mice exhibited decreased spontaneous activity in the OF arena compared to control littermates only at T3 (α-Gal A -/0 VS α-Gal A +/0 $p_{Tukey} = 0.002$) (Fig.20 C). This alteration was not observed at 8-10- and 16-20-week old (8-10-week old, α-Gal A -/0 VS α-Gal A +/0 $p_{Tukey} = 0.517$; 16-20-week old, α-Gal A -/0 VS α-Gal A +/0 $p_{Tukey} = 1.000$). Post-hoc analysis revealed that this reduction in locomotor activity observed in α-Gal A -/0 mice is directly related to the age (effect of age [$F (2, 47) = 7.21$, $p = 0.002$]; interaction genotype*age [$F (2, 47) = 9.39$, $p < 0.001$]). The complete OF statistical analysis is shown in Table 9.
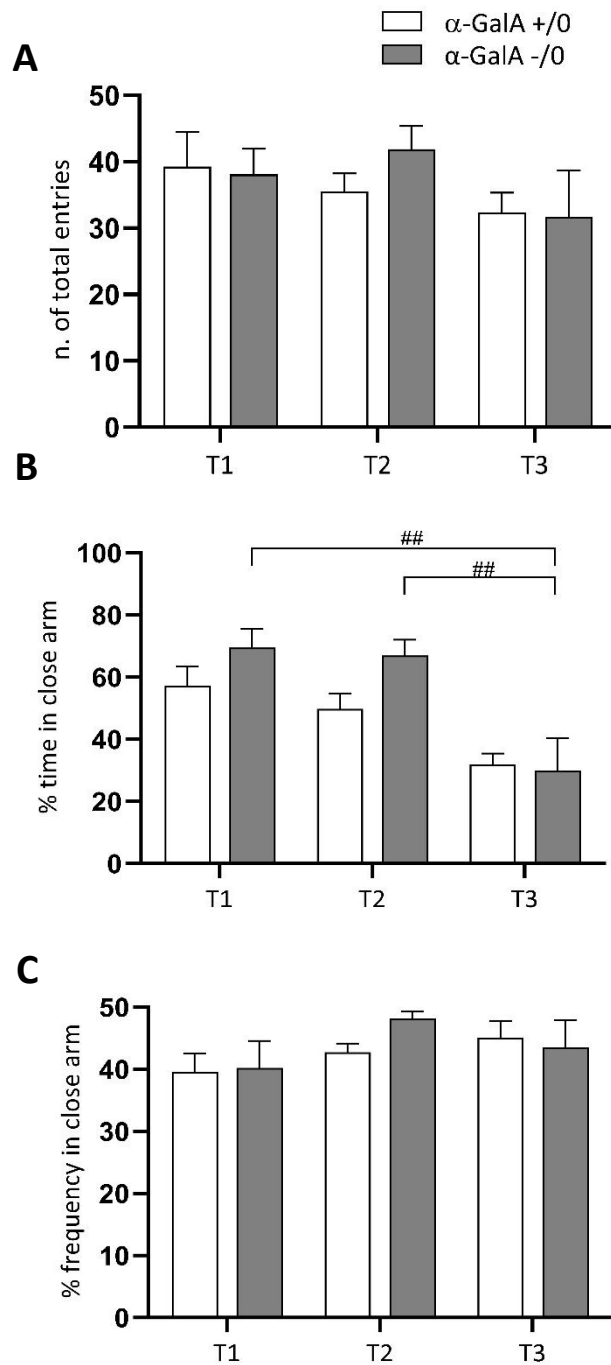
Figure 19 Assessment of anxiety-like behavior in α-Gal A +/0 and α-Gal A -/0 mice by Elevated Plus Maze Test. Experiments were carried out on 8-10 weeks-old (T1), 16-20 weeks-old (T2), and 12 months-old (T3) α-Gal A -/0 (*grey*) and controls α-Gal A +/0 (*white*) mice. Data are representative of at least three independent experiments performed on 7-11 animals (n = 7-11) per group per genotype. Anxiety-like behavior was measured as (A) Number of total entries (B) Time in close arms (C) Frequency in close arms. Values represent means ± SEM. 2-Way ANOVA followed by Tukey's post hoc test. *## p* < 0.01; *### p* < 0.001 vs same genotype.
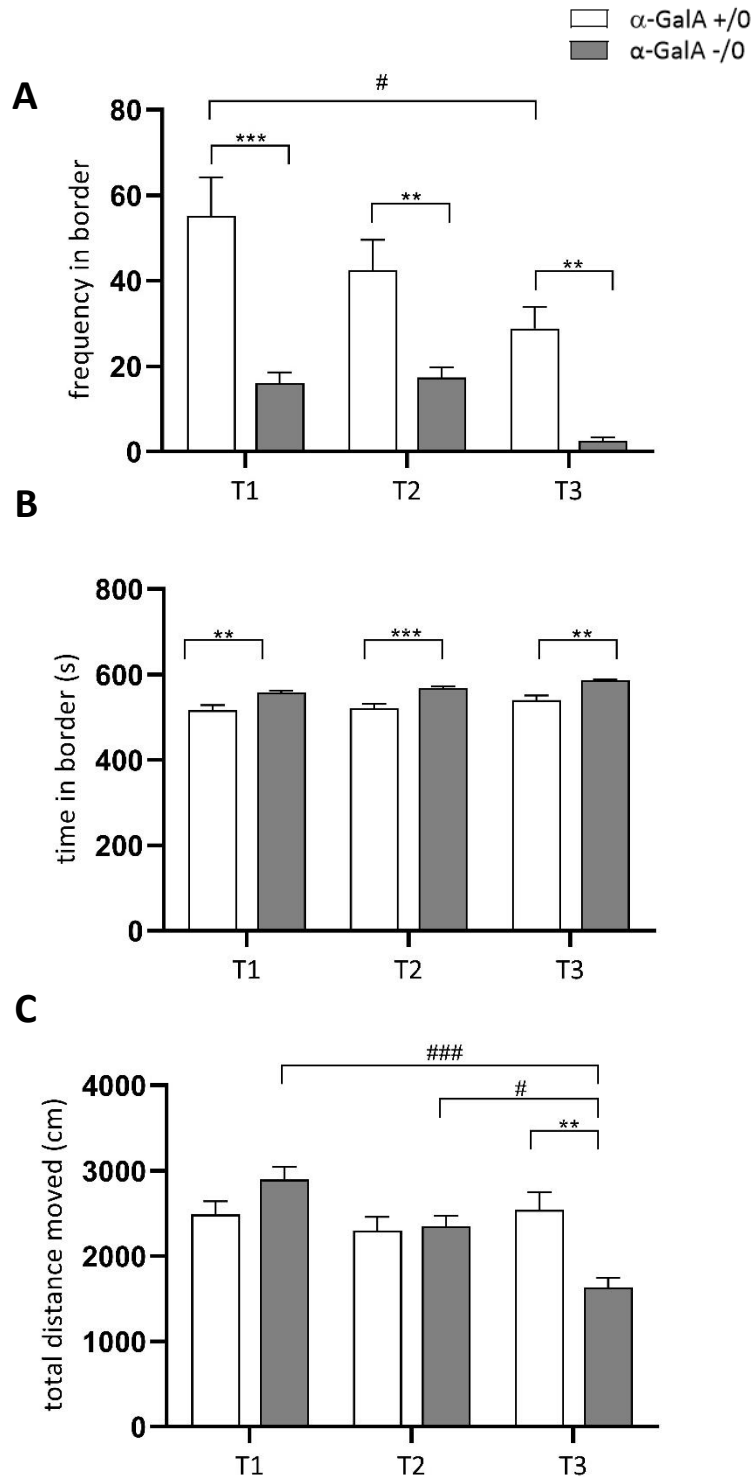
Figure 20 Assessment of anxiety-like behavior and locomotor activity in α-Gal A +/0 and α-Gal A -/0 mice by Open Field Test. Experiments were carried out on 8-10 weeks-old (T1), 16-20 weeks-old (T2), and 12 months-old (T3) α-Gal A -/0 (*grey*) and controls α-Gal A +/0 (*white*) mice. Data are representative of at least three independent experiments performed on 7-11 animals (n = 7-11) per group per genotype. Anxiety-like behavior was measured as (A) Frequency in border; (B) Time in border; (C) total distance moved. Values represent means ± SEM. 2-Way ANOVA followed by Tukey's post hoc test was applied. * $p < 0.05$; ** $p < 0.01$; *** $p < 0.001$ vs α-Gal A +/0; ## $p < 0.01$; ### $p < 0.001$ vs same genotype.

Figure 20	Two-Way ANOVA followed by Tukey's *post hoc*	
Panel A	**Comparisons**	**Frequency in border**
	genotype	F (1, 51) = 68.37; p<0.001
	age	F (2, 51) = 9.78; p<0.001
	genotype*age	F (2, 51) = 1.26; p=0.293
α-Gal A -/0 VS α-Gal A +/0	**T1**	p<0.001
	T2	P=0.002
	T3	P=0.05
α-Gal A -/0	**T1 VS T2**	n.s.
	T1 VS T3	n.s.
	T2 VS T3	n.s.
α-Gal A +/0	**T1 VS T2**	n.s.
	T1 VS T3	P=0.02
	T2 VS T3	n.s.
Panel B	**Comparisons**	**Time in border (s)**
	genotype	F (1, 45) = 53.38; p<0.001
	age	F (2, 45) = 5.97; p=0.005
	genotype*age	F (2, 45) = 0.075; p=0.930
α-Gal A -/0 VS α-Gal A +/0	**T1**	P=0.008
	T2	p<0.001
	T3	P=0.002
α-Gal A -/0	**T1 VS T2**	n.s.
	T1 VS T3	n.s.
	T2 VS T3	n.s.
α-Gal A +/0	**T1 VS T2**	n.s.
	T1 VS T3	n.s.
	T2 VS T3	n.s.
Panel C	**Comparisons**	**Total distance moved (cm)**
	genotype	F (1, 47) = 1.41; p<0.24
	age	F (2, 47) = 7.21; p=0.002
	genotype*age	F (2, 47) = 9.39; p<0.001
α-Gal A -/0 VS α-Gal A +/0	**T1**	n.s.
	T2	n.s.
	T3	P=0.002
α-Gal A -/0	**T1 VS T2**	n.s.
	T1 VS T3	p<0.001
	T2 VS T3	P=0.01
α-Gal A +/0	**T1 VS T2**	n.s.
	T1 VS T3	n.s.
	T2 VS T3	n.s.

Table 9 Statistical analysis of Open Field Test in α-Gal A +/0 and α-Gal A -/0 mice at three different ages. Age-genotype-dependent correlations. 8-10 weeks-old (T1), 16-20 weeks-old (T2), and 12 months-old (T3); n.s. = not significant.

2.4 Compositional and functional dysbiosis of the gut microbiota in α-Gal A -/0 mice

2.4.1 Alpha and beta diversity

The 16S rRNA amplicon sequencing yielded a total of 570,308 reads (mean ± SD, 9,505 ± 1,624), binned into 3,630 ASVs. Alpha diversity describes the complexity of a community in terms of the number of species represented (richness) and the equality between species (evenness) and was analyzed at the genus level. Alpha diversity increased with age in both α-Gal A -/0 and α-Gal A +/0 mice, but at 16-20 weeks it was significantly higher in the former (p_{Tukey} = 0.007). In more detail, on the Chao1 index of microbial richness α-Gal A -/0 mice showed relevant differences compared to controls, especially at the first two time point (effect of genotype [F (1, 54) = 16.31, p < 0.001]). α-Gal A -/0 mice exhibited a consistent increase at T2 also in evenness as measured by Shannon entropy, in a time-dependent way (effect of genotype [F (1, 54) = 0.53, p = 0.46]; age [F (2, 54)= 27.93, p < 0.001]; interaction genotype*age [F (2, 54) = 12.25, p < 0.001]). Even for Simpson index the most relevant difference was detected at T2, as increment in α-Gal A -/0 mice (effect of genotype [F (1, 54) = 6.495, p = 0.013]; age [F (2, 54)= 23.75, p < 0.001]; interaction genotype*age [F (2, 54) = 7.65, p < 0.001]) (Fig. 21 A). As for beta diversity, which describes differences in the overall composition of communities, Aitchison-based principal coordinates analysis (PCA) showed significant separation over time for both α-Gal A -/0 and α-Gal A +/0 mice, especially within Gal A -/0 mice the shift over time is marked (Gal A -/0 T2 VS Gal A -/0 T1, p < 0.001; Gal A -/0 T3 VS Gal A -/0 T2, p < 0.001; Gal A -/0 T3 VS Gal A -/0 T1, p < 0.001). As well as between the two genotypes at all ages the separation is significantly evident (PERMANOVA, p < 0.005) (effect of genotype [F (1, 54) = 6.944, p < 0.001]; age [F (2, 54)= 4.773, p < 0.001]; interaction genotype*age [F (2, 54) = 3.16, p < 0.001]) (Fig. 21 B).
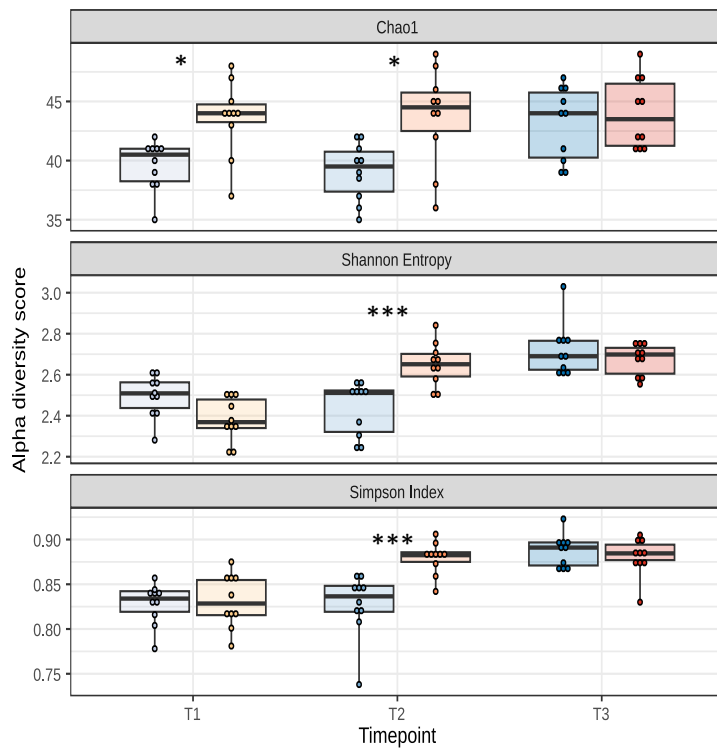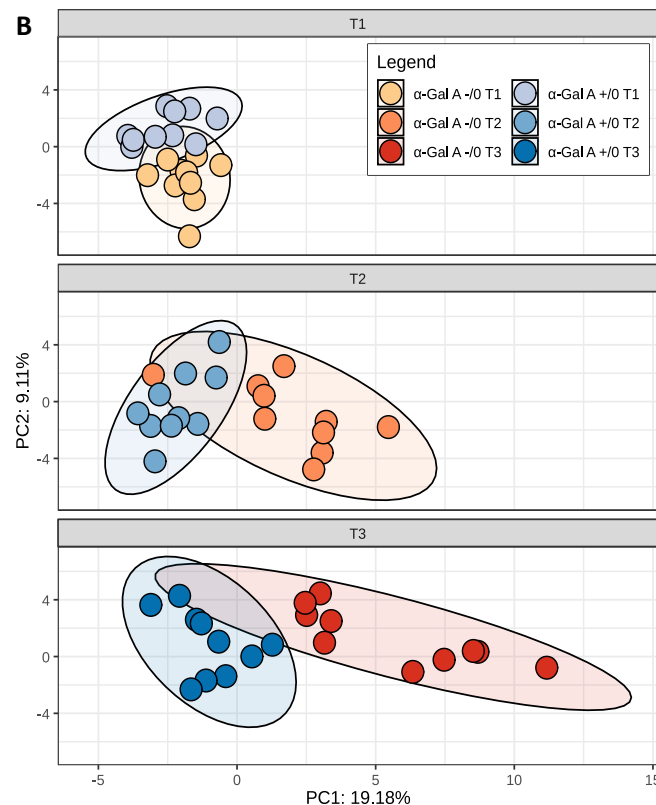
Figure 21 Alpha and beta diversity of the gut microbiota in α-Gal A -/0 mice. (A) Boxplots showing the distribution of alpha diversity, according to Chao1, Shannon entropy and Simpson index, in the gut microbiota of α-Gal A -/0 mice and α-Gal A +/0 controls at 8-10 weeks (T1), 16-20 weeks (T2), and 12 months (T3). Tukey test, * $p < 0.05$; ** $p < 0.01$ ** $p < 0.001$. (B) Principal Coordinates Analysis of beta diversity, based on Aitchison distance, of all fecal samples. A significant separation was found between groups of mice at each age and within each mouse group over time (PERMANOVA, $p < 0.005$).

2.4.2 Signs of gut microbiota dysbiosis in α-Gal A -/0 mice at phylum, family and genus level

From the taxonomic standpoint, α-Gal A -/0 mice and α-Gal A +/0 mice differed from each other and over time, even at the phylum level. In particular, at 8-10 weeks, α-Gal A -/0 mice showed increased proportions of *Deferribacteres* and *Firmicutes*, while reduced proportions of *Bacteroidetes* compared to α-Gal A +/0 mice (Wilcoxon test, $p < 0.05$), but these changes disappeared at 1 year of age (Fig. 22 A-B). The main families involved were those belonging to the phylum *Bacteroidetes*, with particularly *Porphyromonadaceae* and *Rikenellaceae* being enriched and *Bacteroidales S24-7 group* depleted in α-Gal A -/0 mice at 8-10 weeks compared to α-Gal A +/0 mice ($p < 0.016$) (Fig. 23 A-B). Again, the proportions of these taxa varied over time, no longer being distinct from those of controls at 12 months. α-Gal A -/0 mice were also discriminated by a higher relative abundance of *Bacteroidaceae* at 12 months, as well as a temporal increase in *Prevotellaceae* ($p < 0.03$). It is also worth noting that α-Gal A -/0 mice showed an increase with age in *Erysipelotrichaceae* and *Streptococcaceae*, while a decrease in *Lachnospiraceae* (which was overrepresented at T1 compared to controls) and *Helicobacteraceae* ($p < 0.03$). The major discriminating genera included *Alistipes*, *Bacteroides*, *Ruminococcaceae* UCG-014, *Helicobacter*, and *Lachnospiraceae* UCG-001, of which the former two were overrepresented (at T1 and T3, respectively) and the latter three underrepresented (at T1, T3 and T3, respectively) in α-Gal A -/0 mice compared with counterparts ($p < 0.03$) (Fig. 24-25-26).

Figure 22 Bacterial distribution at phylum level and significant differences between α-Gal A -/0 mice and α-Gal A +/0 mice at three ages. 8-10 weeks-old (T1), 16-20 weeks-old (T2), and 12 months-old (T3) α-Gal A -/0 (panel B, *orange nuance*) and controls α-Gal A +/0 (panel B, *blue nuance*) mice were considered. (A) Pie-plots showing the differences in microbial compositions at the phylum level at the various time-points in α-Gal A -/0 (*right*) and controls (*left*). (B) Boxplots showing the relative abundance distribution of differentially represented phyla between α-Gal A -/0 mice and α-Gal A +/0 controls at each age and within each mouse group over time (Wilcoxon test, * $p < 0.05$; ** $p < 0.01$).
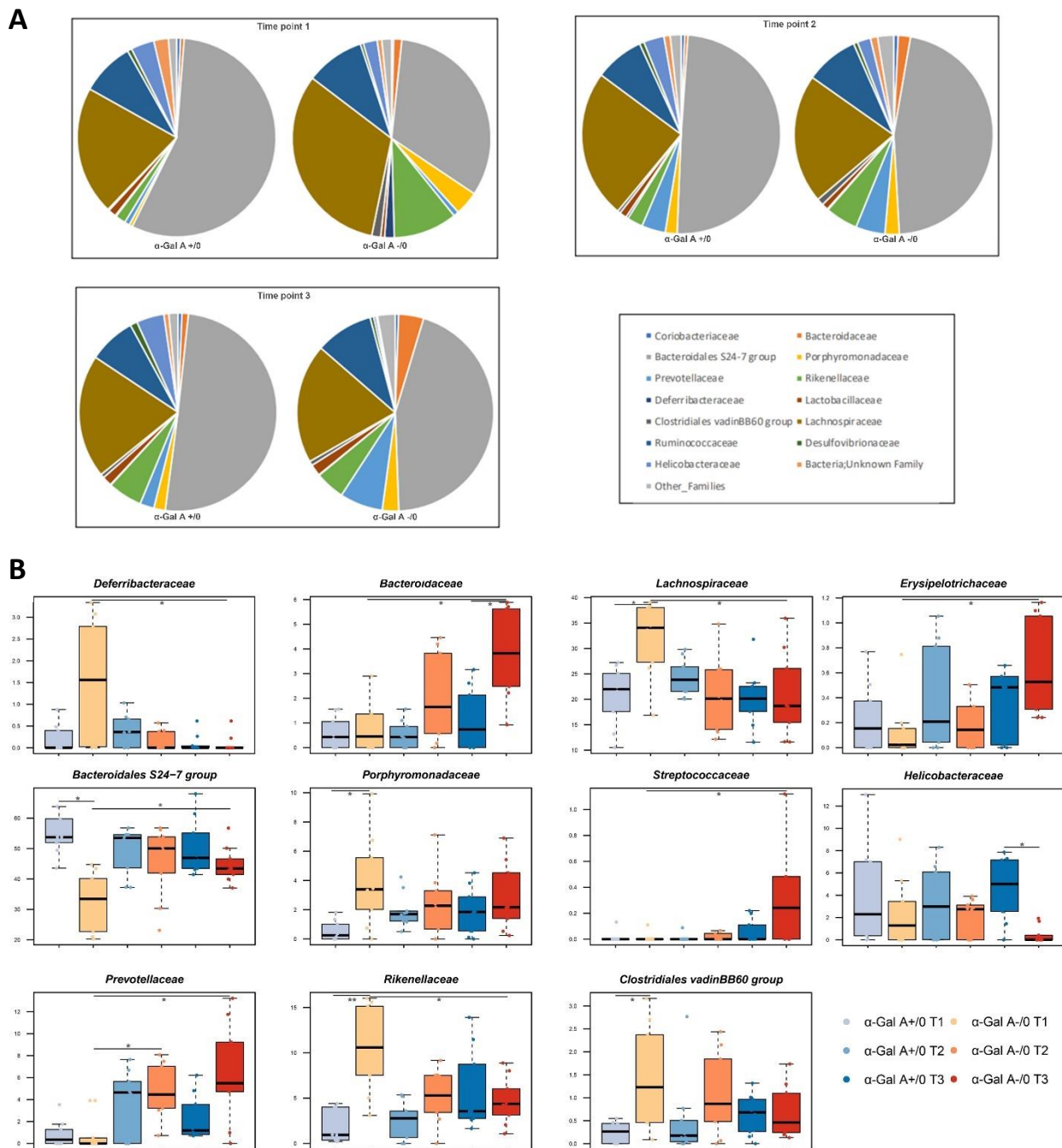
Figure 23 Bacterial distribution at family level and relevant differences between α-Gal A -/0 mice and α-Gal A +/0 mice at three ages. 8-10 weeks-old (T1), 16-20 weeks-old (T2), and 12 months-old (T3) α-Gal A -/0 (panel B, *orange nuance*) and controls α-Gal A +/0 (panel B, *blue nuance*) mice were considered. (A) Pie-plots showing the differences in microbial compositions at the family level at the various time-points in α-Gal A -/0 (*right*) and controls (*left*). (B) Boxplots showing the relative abundance distribution of differentially represented families between α-Gal A -/0 and α-Gal A +/0 mice at each time-point and within each mouse group over time (Wilcoxon test, * $p < 0.05$; ** $p < 0.01$).
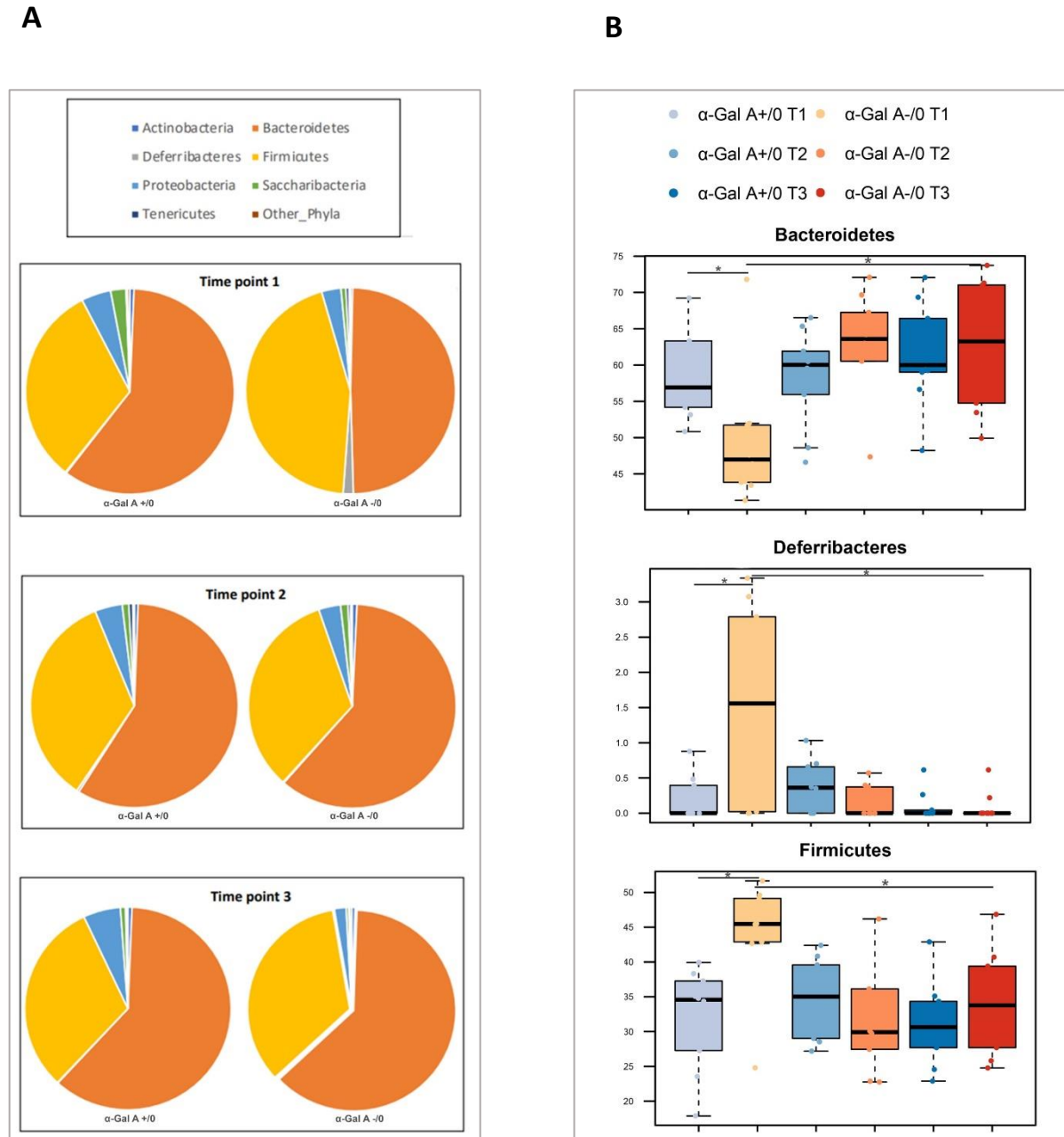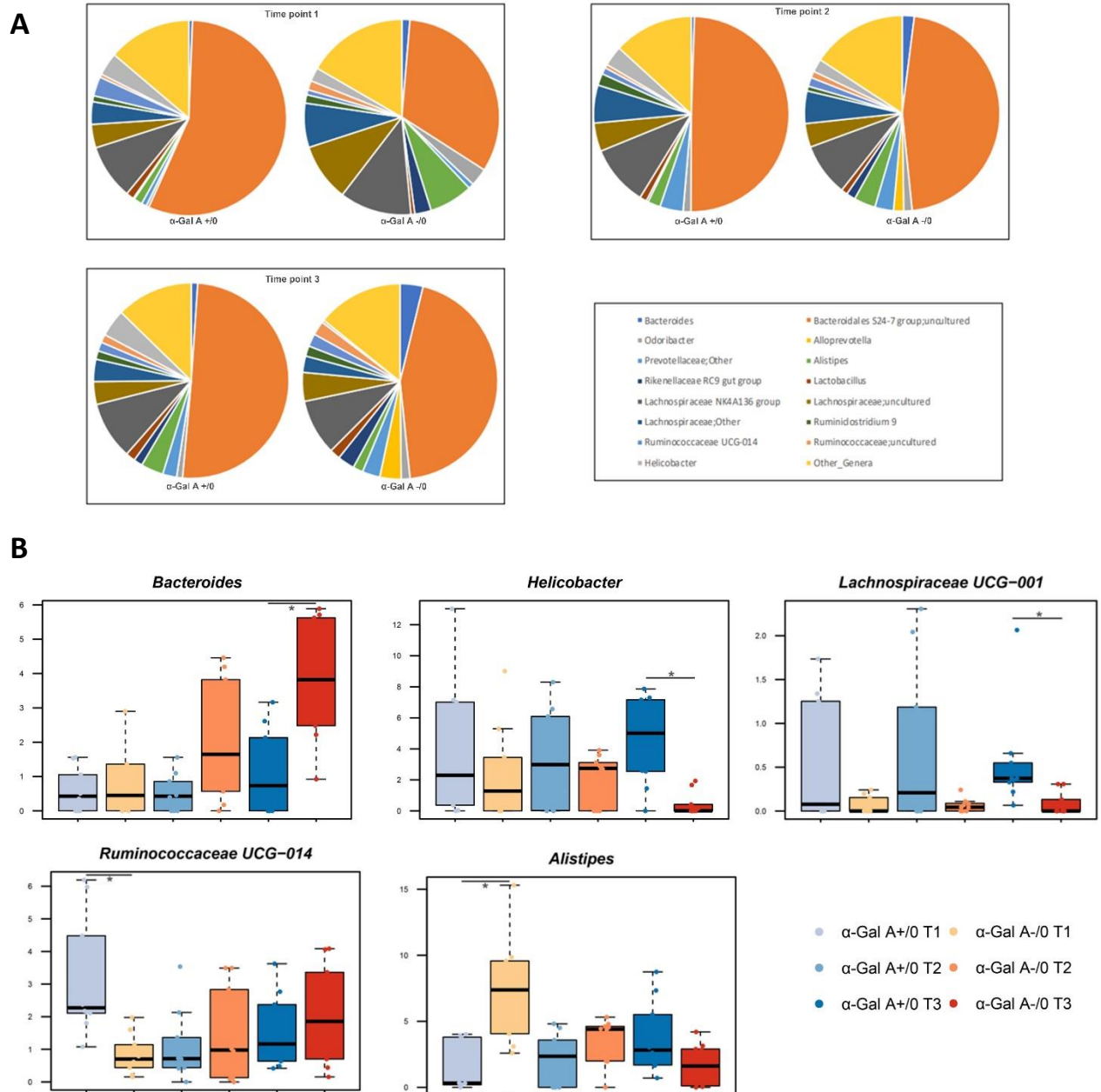
Figure 24 Bacterial distribution at genus level and relevant differences between α-Gal A -/0 mice and α-Gal A +/0 mice at three ages. 8-10 weeks-old (T1), 16-20 weeks-old (T2), and 12 months-old (T3) α-Gal A -/0 (panel B, *orange nuance*) and controls α-Gal A +/0 (panel B, *blue nuance*) mice were considered. (A) Pie-plots showing the differences in microbial compositions at the genus level at the various time-points in α-Gal A -/0 (*right*) and controls (*left*). (B) Boxplots showing the relative abundance distribution of differentially represented genera between α-Gal A -/0 and α-Gal A +/0 mice at each time-point and within genotype over time (Wilcoxon test, * $p < 0.05$; ** $p < 0.01$).

A

Taxonomy Key

- Bacteroidaceae Bacteroides
- Marinifilaceae Odoribacter
- Prevotellaceae Alloprevotella
- Prevotellaceae Prevotellaceae UCG 001
- Rikenellaceae Alistipes
- Rikenellaceae Rikenella
- Rikenellaceae Rikenellaceae RC9 gut group
- Helicobacteraceae Helicobacter
- Lachnospiraceae GCA 900066575
- Lachnospiraceae Lachnospiraceae AC2044 group
- Lachnospiraceae Lachnospiraceae NK4A136 group
- Oscillospiraceae Colidextribacter
- Oscillospiraceae Oscillibacter
- Saccharimonadaceae Candidatus Saccharimonas
- Rare Taxa

B

Figure 25 Taxonomy analysis at genus level on α-Gal A -/0 and α-Gal A +/0 mice at three ages. 8-10 weeks-old (T1), 16-20 weeks-old (T2), and 12 months-old (T3) α-Gal A -/0 and controls α-Gal A +/0 mice were considered. (A) bar-graph showing the taxonomy distribution at the various time-points in α-Gal A -/0 (*below*) and controls (*above*). (B) Heatmap showing the relative abundance distribution of differentially represented genera between genotypes at each time-point. Colors indicates effect size, with blue indicating higher in α-Gal A +/0 and red indicating higher abundances in α-Gal A -/0. * $p < 0.01$; ** $p < 0.01$; *** $p < 0.001$.
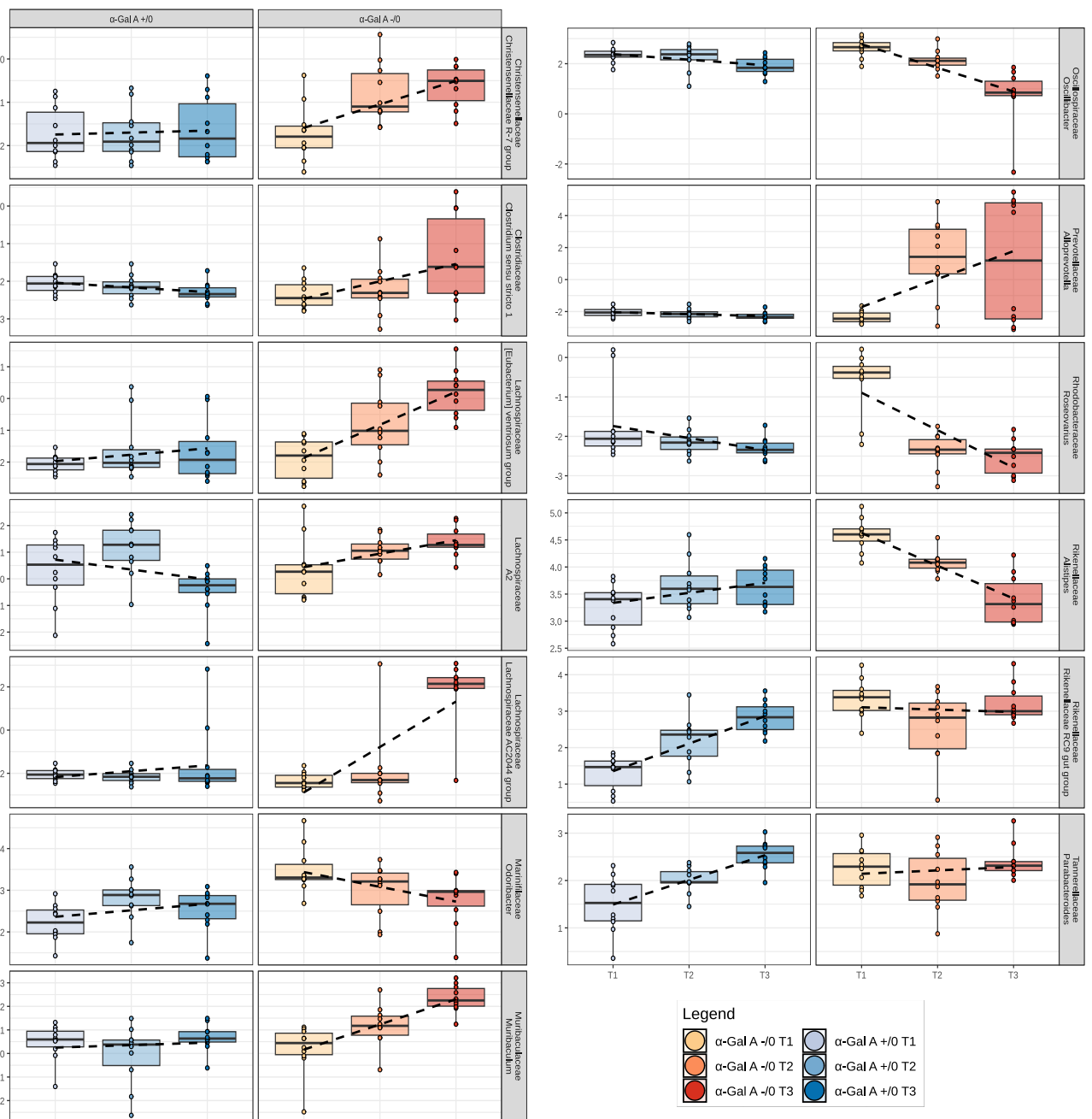
Figure 26 Comparison between α-Gal A -/0 and α-Gal A +/0 mice of selected genera with a specific trend over time. Significant differences at the genus level in Gal A -/0 (*orange nuance)* mice and α-Gal A +/0 (*blue nuance*) over time: 8-10 weeks-old (T1), 16-20 weeks-old (T2), and 12 months-old (T3). Dotted lines highlight the slope of increasing or decreasing trend over time.

2.4.3 Alterations in predicted gut microbiota functions related to the gut-brain axis and gut-metabolomic-axis

In order to obtain functional insights into gut microbiota dysbiosis of α-Gal A -/0 mice, 16S rRNA gene sequencing data were used to predict microbiota functionalities in the form of KEGG orthologues, using PICRUSt2[655]. In particular, compared to controls, α-Gal A -/0 mice at 8-10 weeks showed an overrepresentation of functions involved in the dissimilatory sulfate reduction, and degradation of urea and the amino acids aspartate, glutamine, histidine, lysine, proline, and tryptophan ($p < 0.05$). The tryptophan and lysine degradation pathways were also overabundant at 16-20 weeks and 1 year of age, respectively ($p < 0.05$). On the other hand, compared to controls, α-Gal A -/0 mice at 8-10 weeks were overall depleted in functions involved in the degradation of other amino acids (*i.e.*, arginine, cysteine, threonine, and tyrosine), mucin and sugars (arabinose, fructose, maltose, sucrose, trehalose, and xylose), as well as in other metabolic functionalities related to energy production (e.g., those involved in glycolysis and the citrate cycle) ($p < 0.05$). At 16-20 weeks, the two groups of mice did not show substantial differences, while at 1 year of age, they still differed for some of the aforementioned predicted functions but also for rhamnose and fucose degradation, which were enriched in α-Gal A -/0 mice, and arginine and threonine degradation, and *Bifidobacterium* shunt, which were instead enriched in α-Gal A +/0 mice ($p < 0.03$) (Fig. 27). With specific regard to modules related to the gut-brain axis (Fig. 28), it is worth noting that at 8-10 weeks, α-Gal A -/0 mice were discriminated by an overrepresentation of functions involved in GABA degradation and synthesis, g-hydroxybutyric acid degradation, butyrate synthesis, and menaquinone synthesis, and by underrepresentation of nitric oxide degradation ($p < 0.03$). The changes in the latter module as well as in the synthesis of GABA, butyrate and menaquinone, were maintained even at 16-20 weeks ($p < 0.05$). At 16-20 weeks, several other differences appeared between α-Gal A -/0 mice and α-Gal A +/0 mice, including especially an overabundance of biosynthetic functions for p-cresol, propionate, acetate, iso-valeric acid, glutamate, DOPAC, S-adenosylmethionine, quinolinic acid, and inositol in the former ($p < 0.05$). At this age, α-Gal A -/0 mice also showed increased degradation of quinolinic acid, while reduced degradation of p-cresol and kynurenine synthesis ($p < 0.05$). At 12 months, the overrepresentation of functions involved in propionate synthesis persisted ($p = 0.0008$). These data suggest that phenotypic differences in the Fabry gut microbiota may have effects on functional pathways that encode the metabolism of neuroactive molecules essential for gut-brain communication.

Figure 27 Differences between and within genotypes over time by gut-metabolic modules predictions in α-Gal A -/0 and α-Gal A +/0 mice. Samples: 8-10 weeks-old (T1), 16-20 weeks-old (T2), and 12 months-old (T3) α-Gal A -/0 and α-Gal A +/0 mice. (A) Heatmap showing the relative abundance of main differences in gut-metabolic axis-involved pathways. Colors indicates effect size, with *blue* indicating higher in α-Gal A +/0 and *red* indicating higher abundances in α-Gal A -/0. Stars indicate Benjamini-Hochberg-adjusted p-values (* padj < 0.1, ** padj < 0.01, *** padj < 0.001).. (B) Bar-plots representing the most significantly different biochemical routs over time between α-Gal A +/0 (*blue nuance*) and α-Gal A -/0 (*orange nuance*) . Dotted lines highlight the slope of increasing or decreasing trend over the three time points.
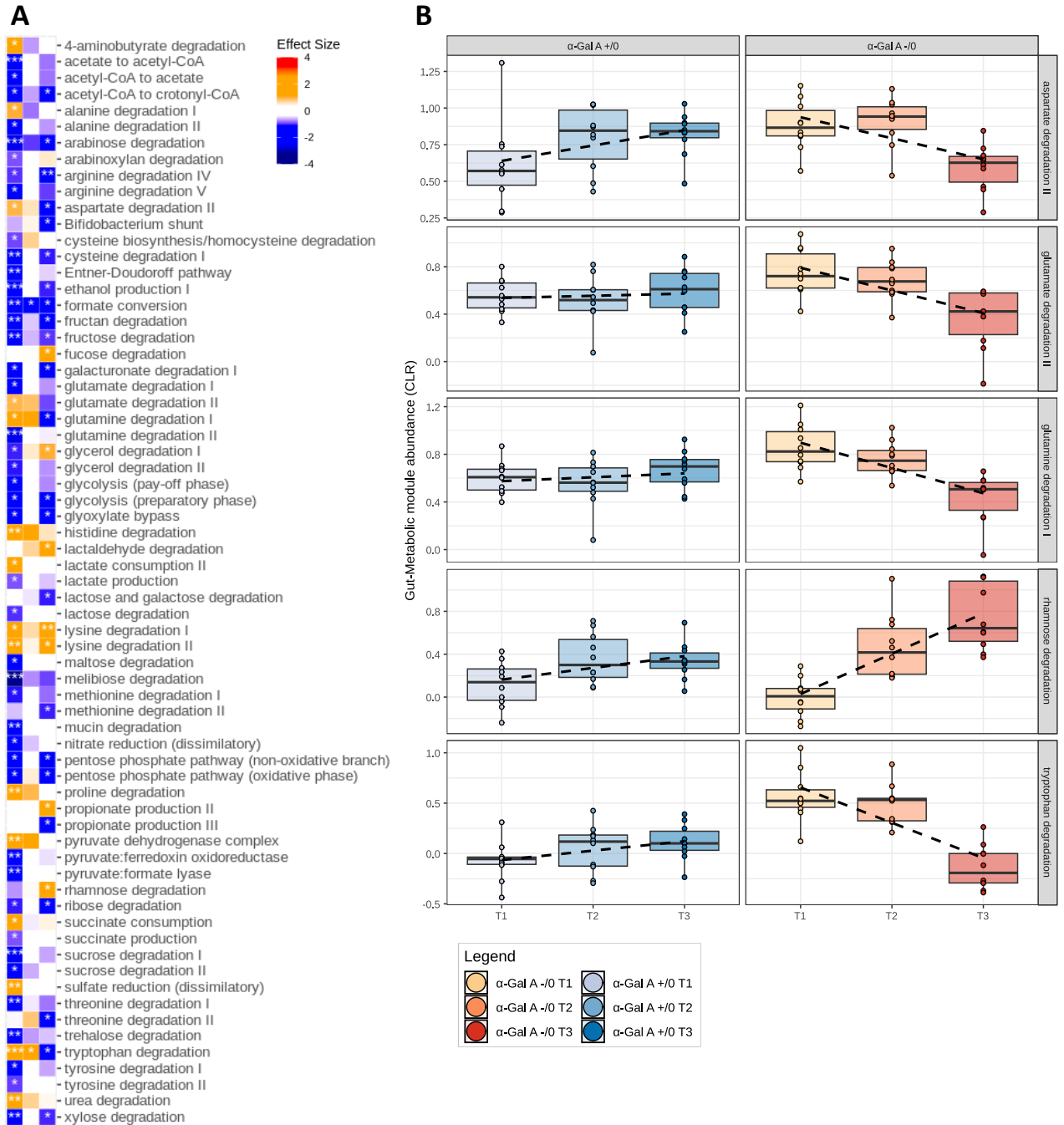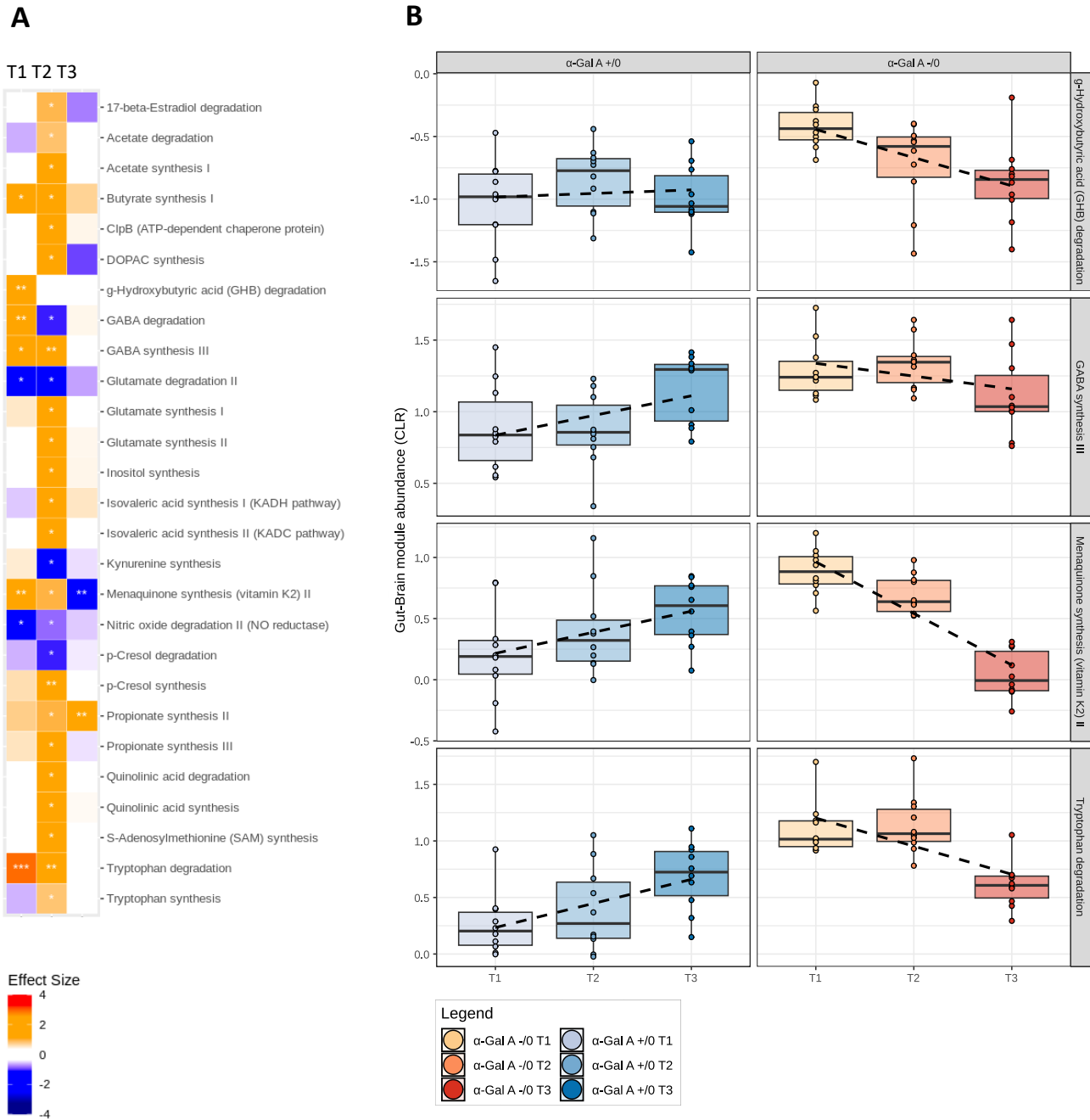
Figure 28 Differences between and within genotypes over time by gut-brain modules predictions in α-Gal A -/0 and α-Gal A +/0 mice. Samples: 8-10 weeks-old (T1), 16-20 weeks-old (T2), and 12 months-old (T3) α-Gal A -/0 and α-Gal A +/0 mice. (A) Heatmap showing the differential abundance of significantly altered neuroactive gut-brain modules. Colors indicates effect size, with blue indicating higher in α-Gal A +/0 and red indicating higher abundances in α-Gal A -/0. Stars indicate Benjamini-Hochberg-adjusted p-values (* padj < 0.1, ** padj < 0.01, *** padj < 0.001). (B) Bar-plots representing the most significantly different biochemical pathways over time between α-Gal A +/0 (blue nuance) and α-Gal A -/0 (orange nuance) . The dotted lines highlight the slope of increasing or decreasing trend over the three time points.

2.5 Imbalance of SCFAs: increased propionic and butyric acid in α-Gal A -/0 mice

To correlate the taxonomic changes in α-Gal A -/0 mice to their disease-promoting functionality, we performed a GC–MS analysis of fecal SCFAs of α-Gal A +/0 and α-Gal A -/0 mice at 8-10 weeks old (T1), 16-20 weeks-old (T2), and 12 months-old (T3). The results are shown in Figure 29. The total amount of SCFAs (μmol/g) was found to be gradually increasing in α-Gal A -/0 mice compared to α-Gal A +/0. In fact, even though there were no significant differences at T1 and only a slight increase at T2, in older mice the difference was found to be significant (α-Gal A -/0 VS α-Gal A +/0 at T3, p_{Tukey} <0.001). The enhancement of SCFAs total amount in old Fabry mice is such that it is statistically significant also compared to the amount at T1 of the same genotype (α-Gal A -/0 at T3 VS α-Gal A -/0 VS at T1, p_{Tukey} <0.001). Hence, it might be said that the SCFAs increase is both genotype and time-related (effect of genotype [$F_{(1, 54)}$ = 11.1, p = 0.002]; age [$F_{(2, 54)}$= 5.54, p = 0.006]; interaction genotype*age [$F_{(2, 54)}$ = 4.95, p = 0.01]) (Fig. 29 A). Going more into detail, the analysis of single fatty acids revealed that butyric acid in α-Gal A -/0 mice is consistently higher than in α-Gal A +/0 at all three time points, although only in younger mice the increase is significant (α-Gal A -/0 VS α-Gal A +/0 at T1, p_{Tukey} = 0.05; effect of genotype [$F_{(1, 54)}$ = 19.3, p < 0.001]) (Fig. 29 B). Its isomer, iso-butyric acid, exhibited an entirely similar trend, with a constant increment in α-Gal A -/0 mice compared to α-Gal A +/0, but significant exclusively at T1 (α-Gal A -/0 VS α-Gal A +/0 at T1, p_{Tukey} = 0.03) (Fig. 29 E). Regarding the acetic acid no substantial differences were found between the two genotypes, however while α-Gal A +/0 mice maintained constant levels over time, α-Gal A -/0 mice showed a significant age-dependent increase (effect of time [$F_{(2, 54)}$ = 7.05, p = 0.002]; α-Gal A -/0 at T3 VS α-Gal A -/0 at T1, p_{Tukey} = 0.04) (Fig. 29 C). The third most extensively produced fatty acid is propionic acid, which exhibited among all a peculiar trend that should be considered in the context of Fabry dysbiosis. Propionic acid was found to undergo both a genotype- and time-dependent effect (effect of genotype [$F_{(1, 54)}$ = 71.0, p <0.001]; age [$F_{(2, 54)}$= 11.9, p <0.001]; interaction genotype*age [$F_{(2, 54)}$ = 6.40, p = 0.003]) (Fig. 29 D). In particular, in α-Gal A -/0 mice its amount is progressively greater than in controls (α-Gal A -/0 VS α-Gal A +/0 at T1, p_{Tukey} = 0.18; at T2, p_{Tukey} <0.001; at T3, p_{Tukey} <0.001). The increase is markedly different even within the same genotype at the different times analyzed (α-Gal A -/0 at T2 VS α-Gal A -/0 at T1, p_{Tukey} = 0.1; α-Gal A -/0 at T3 VS α-Gal A -/0 at T1, p_{Tukey} < 0.001; α-Gal A -/0 at T3 VS α-Gal A -/0 at T2, p_{Tukey} = 0.02), in contrast to α-Gal A +/0 mice, in which propionic acid levels remain constant over time.

Finally, valeric and isovaleric acid were assessed and no differences were uncovered between healthy and affected animals. The complete statistical analysis is reported in Table 10.
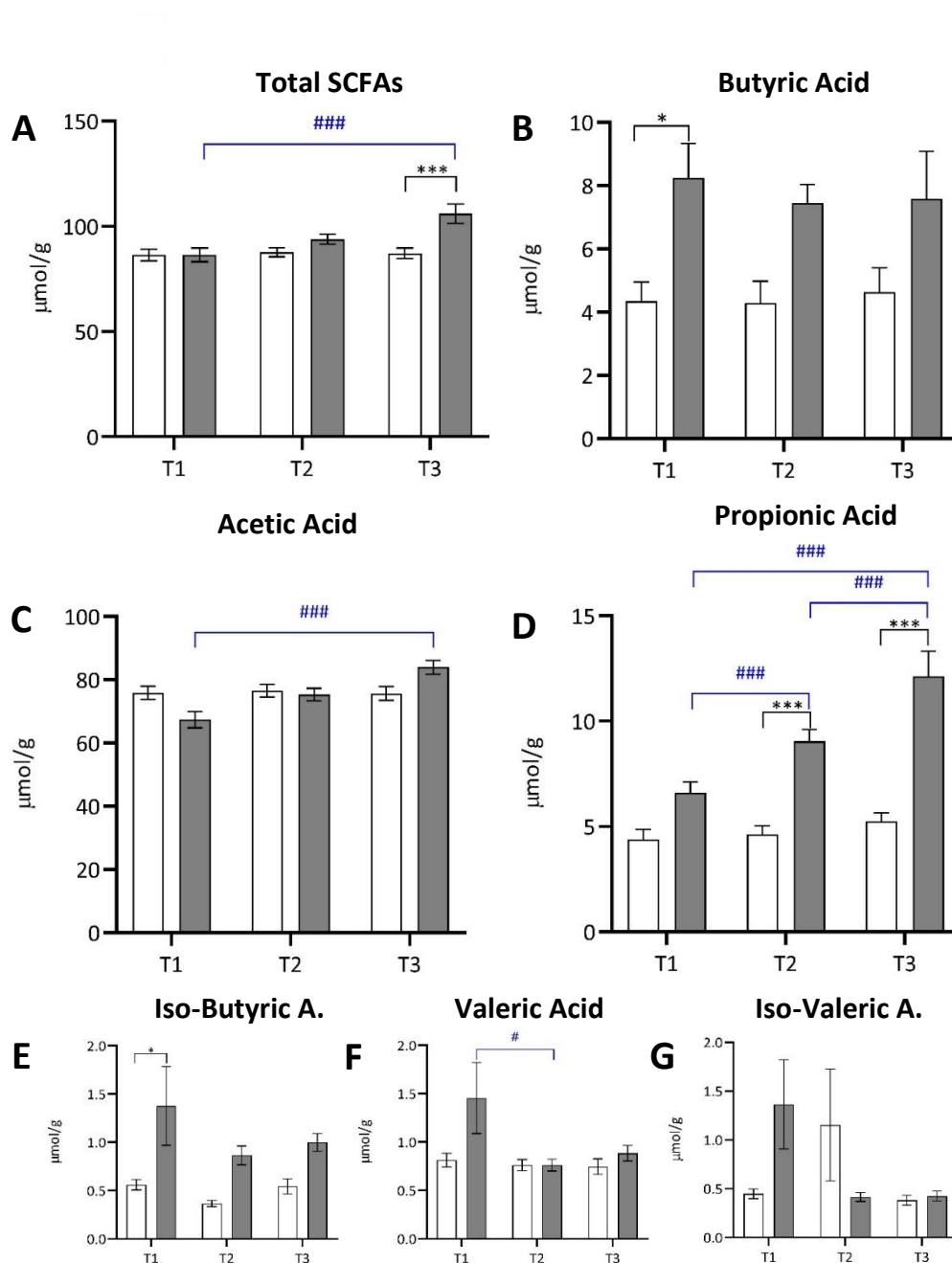
Figure 29 Alterations in fecal short-chain fatty acid (SCFA) levels in α-Gal A -/0 mice. Experiments were carried out on 8-10 weeks-old (T1), 16-20 weeks-old (T2), and 12 months-old (T3) α-Gal A -/0 (*grey*) and controls α-Gal A +/0 (*white*) mice. SCFAs levels were measured in μmol/g.(A) Total amount of SCFAa; (B) Butyric Acid amount; (C) Acetic Acid amount; (D) Propionic Acid amount; (E) Iso-butyric Acid amount; (F) Valeric Acid amount; (G) Isovaleric Acid amount. Data are shown as means ± SEM. 2-Way ANOVA followed by Tukey's post hoc test was applied (n = 10, per genotype, per group). *$p < 0.05$; ** $p < 0.01$; *** $p < 0.001$ vs α-Gal A +/0; # $p < 0.05$ ## $p < 0.01$; ### $p < 0.001$ vs same genotype.

Figure 29	Two-way ANOVA followed by Tukey's *post-hoc*	
Panel A	**Comparisons**	**SCFAs total amount (µmol/gr)**
	genotype	$F_{(1, 54)} = 11.1$; p=0.002
	age	$F_{(2, 54)} = 5.54$; p=0.006
	genotype*age	$F_{(2, 54)} = 4.95$; p=0.01
α-Gal A -/0 VS α-Gal A +/0	T1	n.s.
	T2	n.s
	T3	p<0.001
α-Gal A -/0	T1 VS T2	n.s.
	T1 VS T3	p<0.001
	T2 VS T3	n.s.
α-Gal A +/0	T1 VS T2	n.s.
	T1 VS T3	n.s.
	T2 VS T3	n.s.
Panel B	**Comparisons**	**Butyric acid (µmol/gr)**
	genotype	$F_{(1, 54)} = 19.3$; p<0.001
	age	$F_{(2, 54)} = 0.107$; p=0.90
	genotype*age	$F_{(2, 54)} = 0.143$; p=0.87
α-Gal A -/0 VS α-Gal A +/0	T1	p=0.05
	T2	n.s
	T3	n.s
α-Gal A -/0	T1 VS T2	n.s.
	T1 VS T3	n.s
	T2 VS T3	n.s.
α-Gal A +/0	T1 VS T2	n.s.
	T1 VS T3	n.s.
	T2 VS T3	n.s.
Panel C	**Comparisons**	**Acetic acid (µmol/gr)**
	genotype	$F_{(1, 54)} = 0.0627$; p=0.8
	age	$F_{(2, 54)} = 7.05$; p=0.002
	genotype*age	$F_{(2, 54)} = 7.57$; p=0.001
α-Gal A -/0 VS α-Gal A +/0	T1	n.s.
	T2	n.s
	T3	n.s
α-Gal A -/0	T1 VS T2	n.s.
	T1 VS T3	P<0.001
	T2 VS T3	n.s.
α-Gal A +/0	T1 VS T2	n.s.
	T1 VS T3	n.s.
	T2 VS T3	n.s.
Panel D	**Comparisons**	**Propionic acid (µmol/gr)**
	genotype	$F_{(1, 54)} = 71.0$; p<0.001
	age	$F_{(2, 54)} = 11.9$; p<0.001
	genotype*age	$F_{(2, 54)} = 6.40$; p=0.003
α-Gal A -/0 VS α-Gal A +/0	T1	n.s
	T2	p<0.001
	T3	p<0.001
α-Gal A -/0	T1 VS T2	p<0.001
	T1 VS T3	P<0.001
	T2 VS T3	p<0.001

α-Gal A +/0	T1 VS T2	n.s.
	T1 VS T3	n.s.
	T2 VS T3	n.s.
Panel E	Comparisons	Isobutyric acid (µmol/gr)
	genotype	$F_{(1, 54)} = 16.2$; $p<0.001$
	age	$F_{(2, 54)} = 1.94$; $p=0.15$
	genotype*age	$F_{(2, 54)} = 0.597$; $p=0.55$
α-Gal A -/0 VS α-Gal A +/0	T1	$p=0.03$
	T2	n.s.
	T3	n.s.
α-Gal A -/0	T1 VS T2	n.s.
	T1 VS T3	n.s.
	T2 VS T3	n.s.
α-Gal A +/0	T1 VS T2	n.s.
	T1 VS T3	n.s.
	T2 VS T3	n.s.
Panel F	Comparisons	Valeric acid (µmol/gr)
	genotype	$F_{(1, 54)} = 3.82$; $p=0.06$
	age	$F_{(2, 54)} = 3.09$; $p=0.05$
	genotype*age	$F_{(2, 54)} = 2.14$; $p=0.13$
α-Gal A -/0 VS α-Gal A +/0	T1	n.s.
	T2	n.s.
	T3	n.s.
α-Gal A -/0	T1 VS T2	$p=0.04$
	T1 VS T3	n.s.
	T2 VS T3	n.s.
α-Gal A +/0	T1 VS T2	n.s.
	T1 VS T3	n.s.
	T2 VS T3	n.s.
Panel G	Comparisons	Isovaleric acid (µmol/gr)
	genotype	$F_{(1, 54)} = 0.0889$; $p=0.77$
	age	$F_{(2, 54)} = 1.51$; $p=0.23$
	genotype*age	$F_{(2, 54)} = 3.76$; $p=0.03$
α-Gal A -/0 VS α-Gal A +/0	T1	n.s.
	T2	n.s.
	T3	n.s.
α-Gal A -/0	T1 VS T2	n.s.
	T1 VS T3	n.s.
	T2 VS T3	n.s.
α-Gal A +/0	T1 VS T2	n.s.
	T1 VS T3	n.s.
	T2 VS T3	n.s.

Table 10 Statistical analysis of fecal SCFAs levels in α-Gal A +/0 and α-Gal A -/0 mice at three different ages. Age-genotype-dependent correlations. 8-10 weeks-old (T1), 16-20 weeks-old (T2), and 12 months-old (T3); n.s. = not significant.

3. Qualitative and quantitative evaluation of the expression of TRP ion channels involved in visceral sensitivity in tissue and cells of a mouse model of Fabry disease.

3.1 TRPV1 overexpression in colon, lumbosacral DRG and primary DRG neurons in Fabry mice

Given the extensive literature relating TRPV1 channel alteration to GI disorders and visceral pain, to assess whether there were alterations in its expression in our FD murine model, we performed a qualitative and quantitative analysis by immunofluorescence. The staining were performed on tissue sections (colon and DRG) (Fig 30-31-32) and cells (neurons from lumbosacral DRGs) (Fig 33) of α-Gal A +/0 and α-Gal A -/0 mice at three different ages (8-10 weeks-old (T1), 16-20 weeks-old (T2), and 12 months-old (T3)). Pan neuronal marker Pgp9.5 or nuclear specific neuronal marker NeuN (in green), and antibodies against TRPV1 channel (red) were used. As shown in Fig 30, in reconstructed images of colon transverse sections, the fluorescence signal of TRPV1 channel in α-Gal A -/0 mice looked higher than in α-Gal A +/0, especially in myenteric plexus. By an higher magnification analysis (objective 40X) performed in triplicate on three animals (n=3 per genotype, per age; 4 sections per animals and 4 pictures per sections), TRPV1 intensification in α-Gal A -/0 mice seemed to be confirmed at all three time points analyzed (Fig. 31 A, B, C). In this context, given the role of lumbosacral innervation, it was deemed appropriate to evaluate the expression of TRPV1 upstream, at the level of the DRGs. As shown in Figure 32, qualitative analysis revealed that α-Gal A -/0 mice had an enhanced fluorescence signal of TRPV1.

TRPV1 expression was also evaluated in primary cultures of neurons from lumbosacral DRGs (Fig. 33). A preliminary qualitative analysis of TRPV1 fluorescence intensity confirmed the increase in α-Gal A -/0 mice compared with α-Gal A +/0 mice, as reported at the tissue level. However, in this case, due to the defined cell shape, it was possible to quantify this signal by corrected total cell fluorescence (CTCF). The blinded analysis was performed on three mice (n = 3, for each genotype and age), and 15 fields were acquired for each slide. The analysis indicated increased CTCF of TRPV1 in α-Gal A -/0 mice compared to Gal A +/0 mice, especially at T2 and T3 (α-Gal A -/0 VS α-Gal A +/0 in T1, p_{Tukey} = 0.76; α-Gal A -/0 VS α-Gal A +/0 in T2, p_{Tukey} = 0.007; α-Gal A -/0 VS α-Gal A +/0 in T3, p_{Tukey} = 0.03) (Fig. 33). In addition, there was an age-dependent increase in TRPV1 fluorescence in α-Gal A -/0 animals (α-Gal A -/0 T1 VS α-Gal A -/0 at T2, p_{Tukey} = 0.02; α-Gal A -/ T1 VS α-Gal A -/0 at

T3, p_{Tukey} = 0.04), which did not occur in WT animals, where the levels appear to be fairly constant over time.
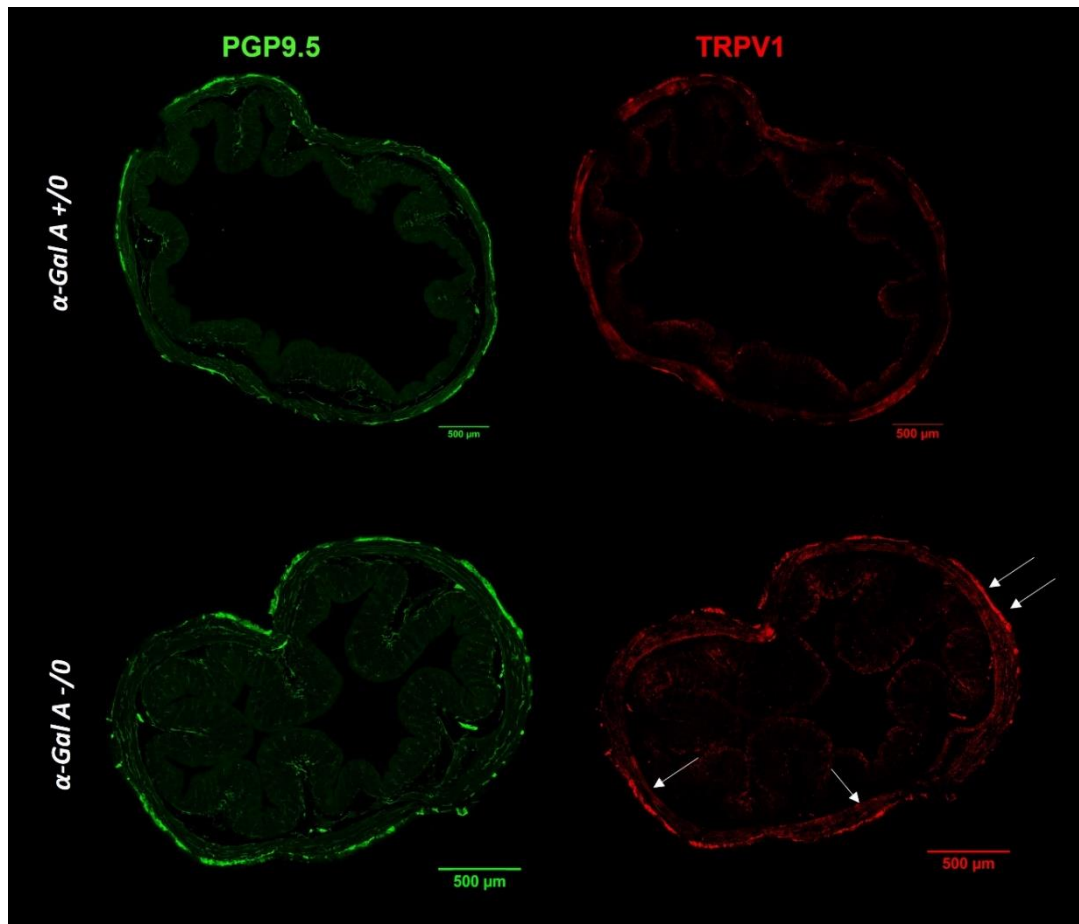
Figure 30 Representative reconstructed immunofluorescence staining images of PGP9.5 and TRPV1 on transverse colon cryosections of α-Gal A +/0 and α-Gal A -/0 mice. PGP9.5 (*green*) and TRPV1 (*red*) were detected by IF in 50μm-thick transverse cryo-sections of 8- to 10-week-old, 16- to 20-week-old, and 12-month-old (*here represented*) α-Gal A -/0 and α-Gal A +/0 male mice colon. Fluorescent images were captured on a Nikon D-Eclipse C1 inverted laser scanning confocal microscope. Representative images were taken as single confocal sections at 40X magnification and separately for each channel. Image J (NIH, http://rsb.info.nih.gov/ij/) software was used for image analysis. Scale bar: 500 μm.

Figure 31 Representative images of PGP9.5 and TRPV1 immunofluorescence staining on colon sections of *α-Gal A +/0* and *α-Gal A -/0* mice at three time point. . PGP9.5 (*green*; a, d) and TRPV1 (*red*; b, e) were detected by IF in 50μm-thick transverse cryo-sections of 8-10-week-old (A; T1), 16-20-week-old (B; T2), and 12-month-old (C; T3) α-Gal A -/0 and α-Gal A +/0 male mice colon. The enhanced TRPV1 fluorescence signal (*red*) in α-Gal A (-/0) is showed (*white arrows*). Images were captured on a Nikon D-Eclipse C1 inverted laser scanning confocal microscope. Images were taken as single confocal sections at 40X magnification and separately for each channel. Image J (NIH, http://rsb.info.nih.gov/ij/) software was used for image analysis and merge. Scale bar: 50 μm.
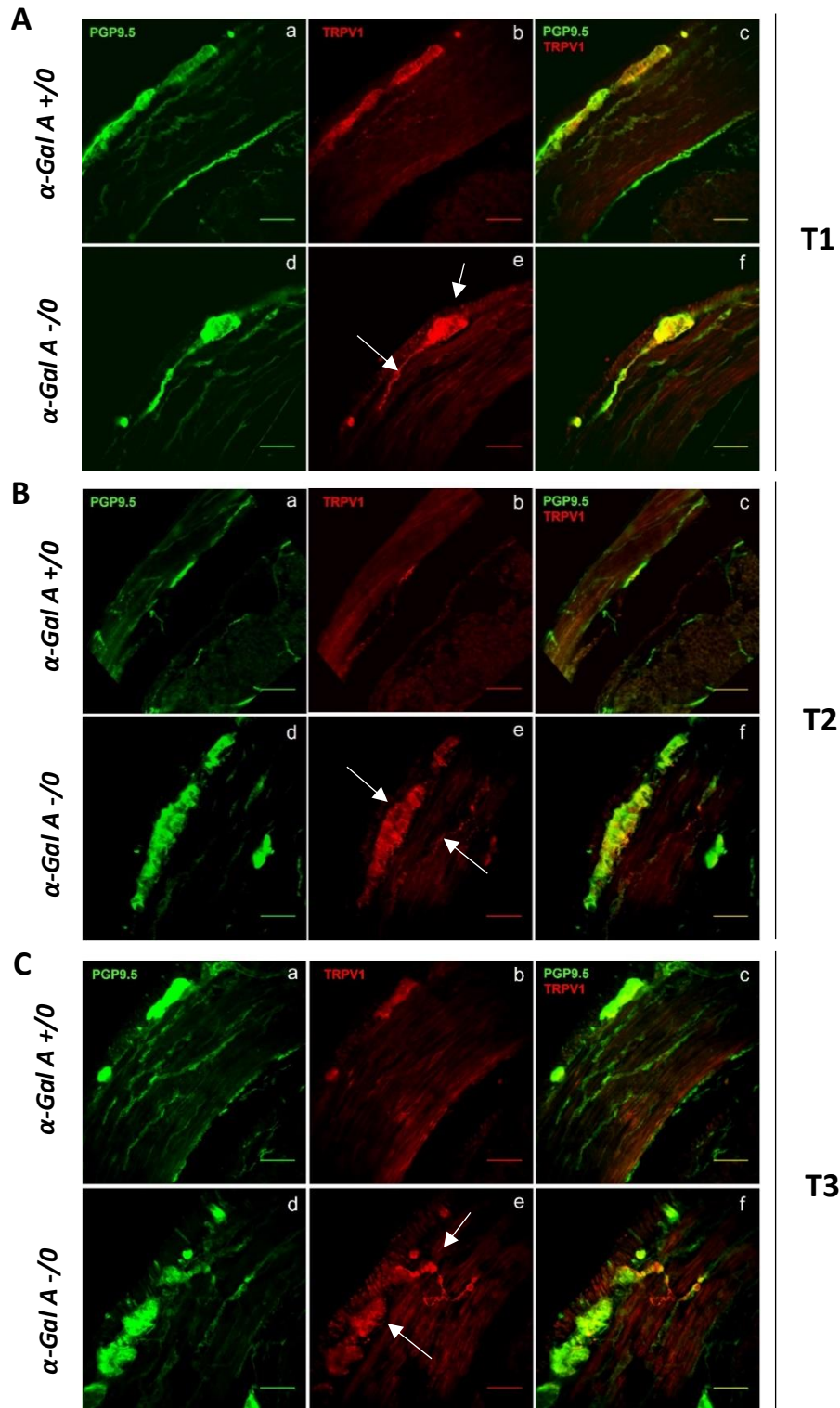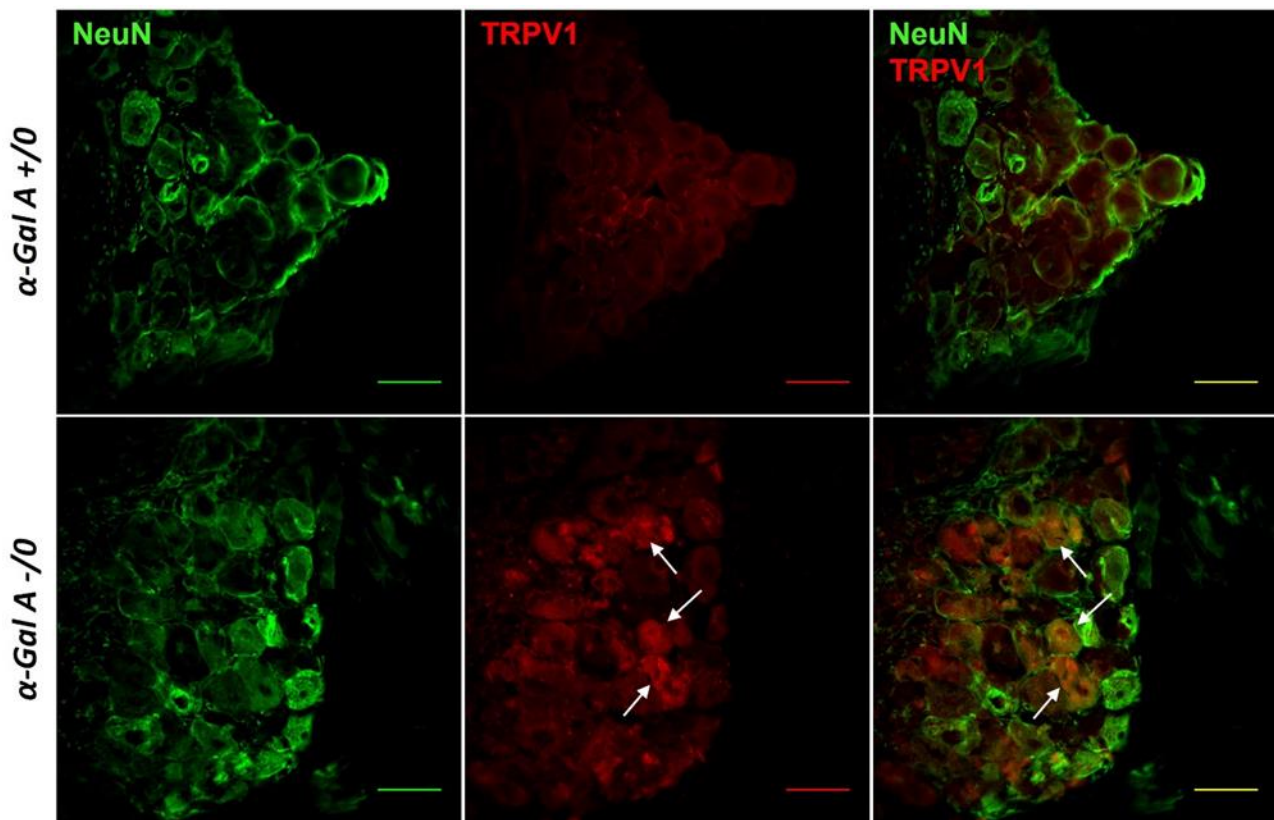
Figure 32 Representative images of NeuN and TRPV1 immunofluorescence staining on DRG (L6) sections of α-Gal A +/0 and α-Gal A -/0 mice. NeuN (*green*) and TRPV1 (*red*) were detected by IF in 50µm-thick transverse cryo-sections of 8-10-week-old, 16- 20-week-old, and 12-month-old (*here represented*) α-Gal A +/0 and α-Gal A -/0 male mice colon. TRPV1 positive staining (*red*) in α-Gal A (-/0) is indicated (*white arrows*). Images were captured on a Nikon D-Eclipse C1 inverted laser scanning confocal microscope. Images were taken as single confocal sections at 40X magnification and separately for each channel. Image J (NIH, http://rsb.info.nih.gov/ij/) software was used for image analysis and merge. Scale bar: 50 µm.
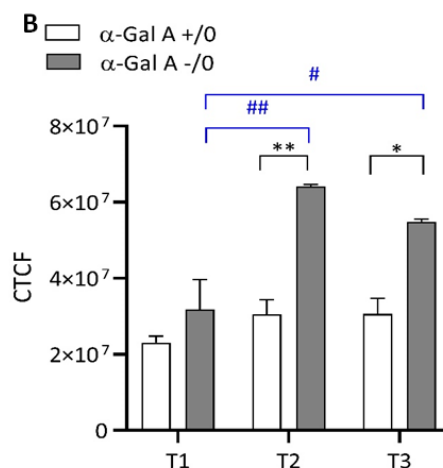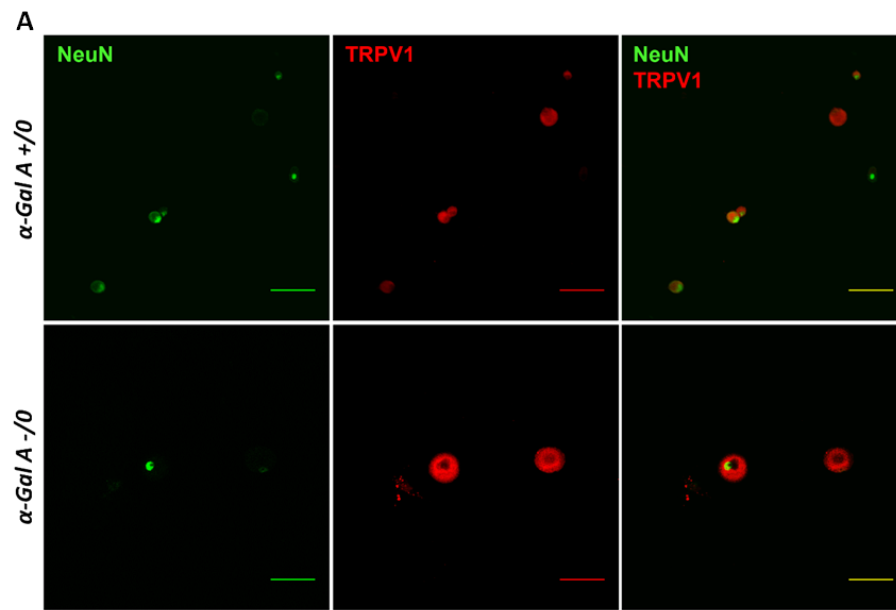
Figure 33 Qualitative and quantitative analysis of TRPV1 fluorescence in neuronal cells from lumbosacral DRGs of α-Gal A +/0 and α-Gal A -/0 mice at three time points. In A, representative images of NeuN and TRPV1 staining by immunofluorescence on primary neurons from lumbosacral DRGs of α-Gal A +/0 and α-Gal A -/0 mice at 8-10-week-old (T1), 16-20-week-old (T2), and 12-month-old (T3; *here represented*). Images were acquired with Nikon D-Eclipse C1 microscope, 40X objective. Scale bar=50 μm. ImageJ software was used for image processing. In B, the graph showing the statistical analysis of TRPV1 fluorescence signal expressed as CTCF in α-Gal A +/0 (*white*) and α-Gal A -/0 (*grey*) animals at T1, T2, T3. GraphPad Prism 8 software was used to perform statistical analysis. Data are shown as means ± SEM. 2-Way ANOVA followed by Tukey's post hoc test was applied (n = 3, per genotype, per group). * $p < 0.05$; ** $p < 0.01$; *** $p < 0.001$ vs α-Gal A +/0; # $p < 0.05$ ## $p < 0.01$; ### $p < 0.001$ vs same genotype.

3.2 Increased TRPV4 expression in old α-Gal A -/0 mice

To improve the understanding of mechanisms involved in visceral nociception and have an overview of the TRP channels expression in FD colon, TRPV4 was also analyzed, with an approach quite similar to that used for TRPV1. The immunofluorescence analysis were performed on colon and DRG sections (Fig. 34) as well as on primary neurons from lumbosacral DRGs (Fig. 35) of α-Gal A +/0 and α-Gal A -/0 mice at the three selected ages (8-10 weeks-old (T1), 16-20 weeks-old (T2), and 12 months-old (T3)). Pan neuronal marker Pgp9.5 or nuclear specific neuronal marker NeuN (in *green*), and antibody against TRPV4 channel (*red*) were employed.

From the qualitative evaluation of the pictures captured by confocal microscope (objective 40X; (n = 3 per genotype, per age; 4 sections per animals and 4 pictures per sections), looking at colon sections, TRPV4 was not markedly different in terms of fluorescence intensity between the genotypes at none of the three ages; however, by observing the DRG sections, especially at T3 (Fig. 34 B) α-Gal A -/0 DRGs appeared with ah higher number of cells intensively TRPV4 positive compared to α-Gal A +/0. This observation, as shown in Figure 35, was also confirmed by the staining on neurons, whose fluorescence intensity was definitively higher in Fabry than in WT. This increment in the oldest mice was validated by the quantitative analysis by CTCF. The analysis reported a significant increased CTCF in α-Gal A -/0 compared to Gal A +/0 mice exclusively at T3 (α-Gal A -/0 VS α-Gal A +/0 at T3, p_{Tukey} = 0.03). Regarding the other two time points, no differences between genotypes were recorded, however, it is noteworthy the huge intra-genotype increase at T3 in α-Gal A -/0 mice compared with healthy animals, in which, on the other hand, the values remain constant over time (α-Gal A -/0 T3 VS α-Gal A +/0 at T1, p_{Tukey} = 0.04; α-Gal A -/0 T3 VS α-Gal A +/0 at T2, p_{Tukey} = 0.03).
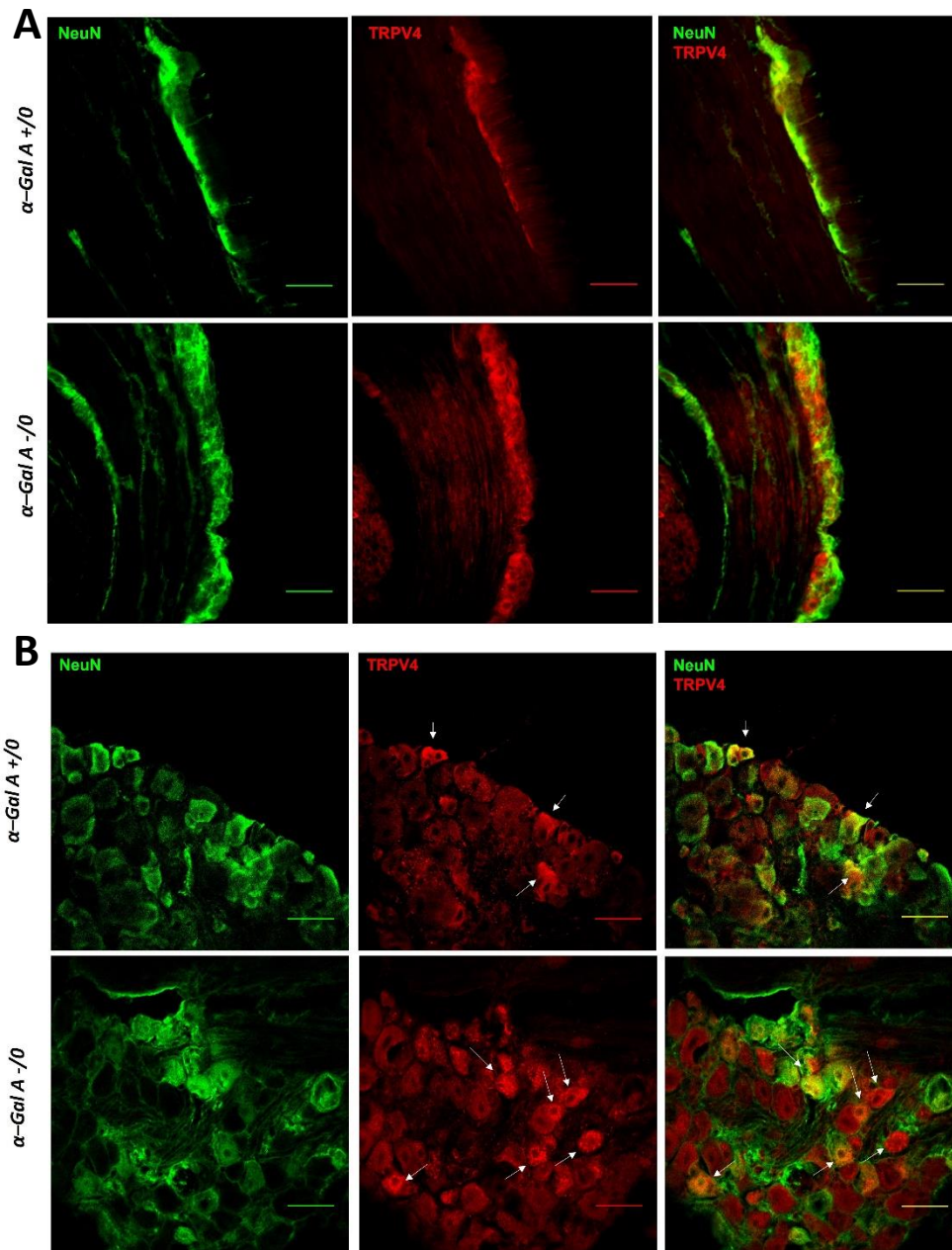
Figure 34 Representative images of Pgp.5/NeuN and TRPV4 immunofluorescence staining on colon and DRG (L6) sections of α-Gal A +/0 and α-Gal A -/0 mice. Pgp9.5 or NeuN (*green*) and TRPV1 (*red*) were detected by IF in 50µm-thick cryo-sections of 8-10-week-old, 16-20-week-old, and 12-month-old (*here represented*) α-Gal A +/0 and α-Gal A -/0 male mice colon (A) and lumbosacral DRGs (B). The TRPV4 positive staining (*red*) in α-Gal A (-/0) is indicated (*white arrows*). Fluorescent images were captured on a Nikon D-Eclipse C1 inverted laser scanning confocal microscope. Images were taken as single confocal sections at 40X magnification and separately for each channel. Image J (NIH, http://rsb.info.nih.gov/ij/) software was used for image analysis and merge. Scale bar: 50 µm.
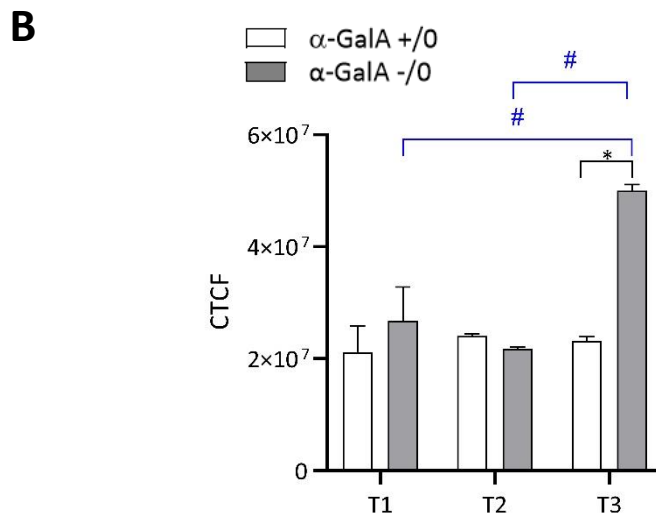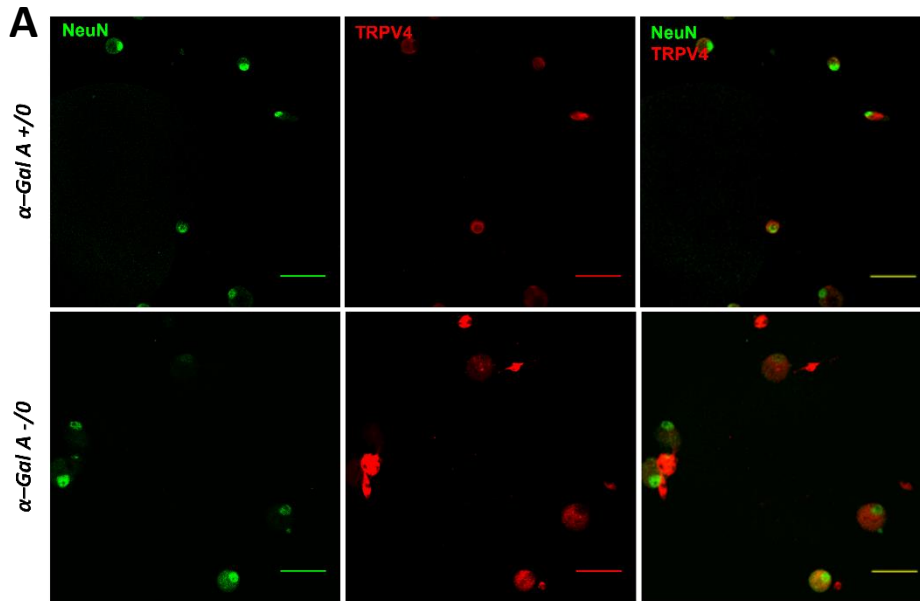
Figure 35 Qualitative and quantitative analysis of TRPV4 fluorescence in neuronal cells from lumbosacral DRGs of α-Gal A +/0 and α-Gal A -/0 mice. In A, representative images of NeuN (*green*) and TRPV4 (*red*) staining by immunofluorescence on primary neurons from lumbosacral DRGs of α-Gal A +/0 and α-Gal A -/0. Images were acquired with Nikon D-Eclipse C1 microscope, 40X objective. Scale bar = 50 μm. ImageJ software was used for image processing. In B, the graph showing the statistical analysis of TRPV4 fluorescence signal expressed as CTCF in α-Gal A +/0 (*white*) and α-Gal A -/0 (*grey*) animals at 8-10-week-old (T1), 16-20-week-old (T2), and 12-month-old (T3; *here represented*). GraphPad Prism 8 software was used to perform statistical analysis. Data are shown as means ± SEM. 2-Way ANOVA followed by Tukey's post hoc test was applied (n = 3, per genotype, per group).* $p < 0.05$ vs α-Gal A +/0; # $p < 0.05$ vs same genotype.

3.3 Progressive increase of TRPA1 expression in α-Gal A -/0 mice

The staining were performed on colon, DRG sections (Fig. 36) and lumbosacral DRG neurons (Fig. 37) from α-Gal A +/0 and α-Gal A -/0 mice at the three different ages (n=3 per genotype, per age; 4 sections per animals and 4 pictures per sections). Pan neuronal marker Pgp9.5 or nuclear specific

neuronal marker NeuN (in *green*), and antibodies against TRPA1 channel (*red*) were used. As shown in Figure 36 A, the TRPA1 fluorescence signal in α-Gal A -/0 mice colon sections appeared stronger than in α-Gal A +/0, especially in MP, where the ganglia were also enlarged. Accordingly, also the qualitative analysis performed on sections of lumbosacral DRGs also seemed to indicate a trend of increasing TRPA1 expression in α-Gal A -/0 animals (Fig. 36 B). Furthermore, TRPA1 fluorescence signal was assessed in neurons primary cultures from lumbosacral DRGs. The qualitative analysis of TRPA1 expression confirmed the increase in α-Gal A -/0 mice compared to controls, as reported at tissue level. Noteworthy, in α-Gal A -/0 mice the channel was also expressed along the neuronal branches, which was not the case for the other channels studied. However, for the quantification of CTCF, as in previous analyses, only fluorescence at the level of the neuronal bodies was considered. Blinded analysis was performed on three mice (n = 3, for each genotype and age), and 10-15 fields were acquired for each slides. In spite of fluorescence images appearance, the statistical analysis reported that the TRPA1 increment was not parallelized by a significant CTCF increase in α-Gal A -/0 (effect of genotype [$F_{(1,9)}$ = 0.87, p = 0.37]; age [$F_{(2, 9)}$= 0.566, p = 0.59]; interaction genotype*age [$F_{(2, 9)}$ = 8.63, p = 0.008). However, it has to be noted the opposite trend over time between Gal A -/0 and Gal A +/0. The former tended to grow with increasing age (α-Gal A -/0 T3 VS α-Gal A -/0 at T1, p_{Tukey} = 0.1), while the latter to decrease (α-Gal A +/0 T3 VS α-Gal A +/0 at T1, p_{Tukey} = 0.15).
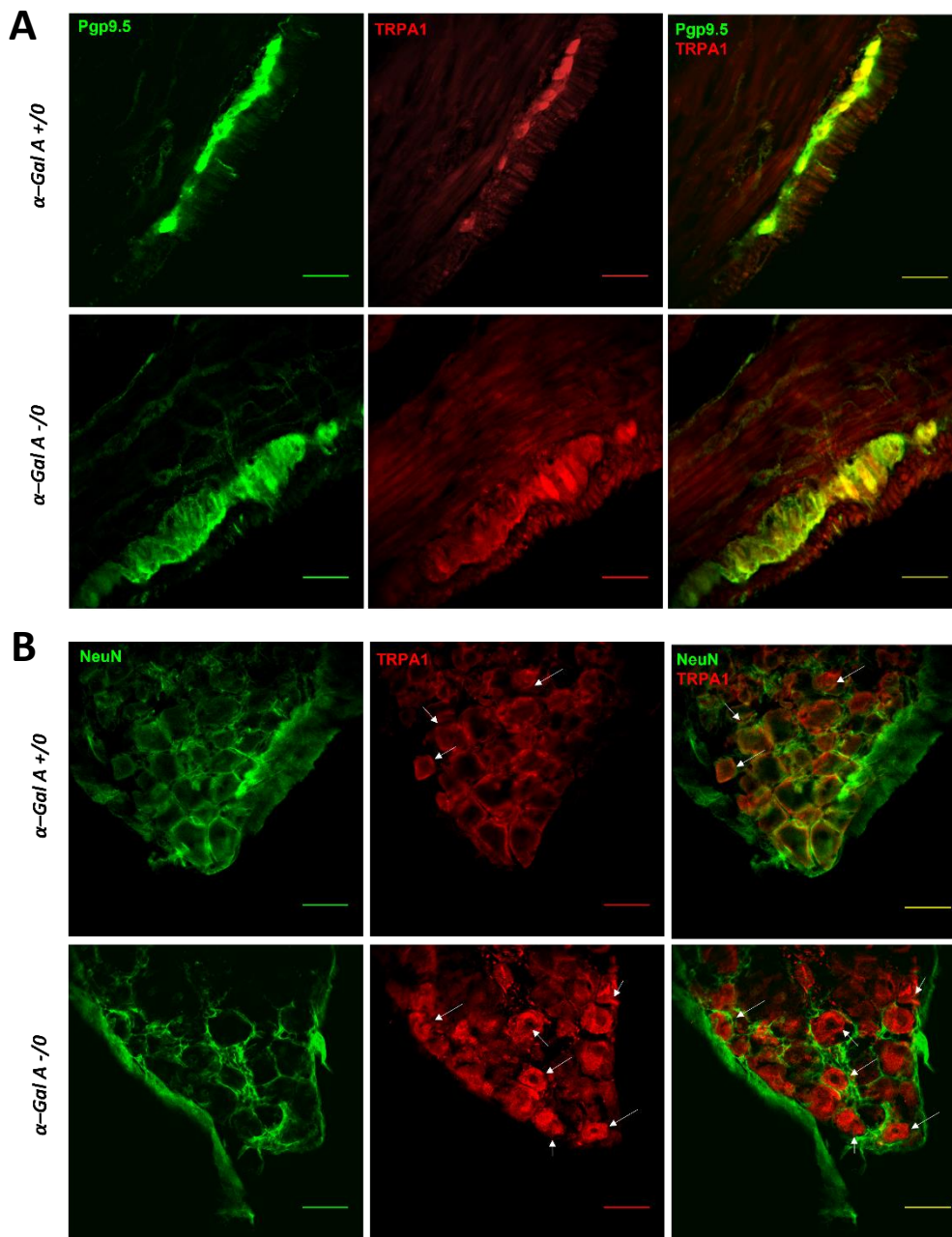
Figure 36 Representative images of Pgp.5/NeuN and TRPA1 immunofluorescence staining on colon and DRG (L6) sections of α-Gal A +/0 and α-Gal A -/0 mice. Pgp9.5 or NeuN (*green*) and TRPV1 (*red*) were detected by IF in 50μm-thick cryo-sections of 8-10-week-old, 16-20-week-old, and 12-month-old (*here represented*) α-Gal A +/0 and α-Gal A -/0 male mice colon (A) and lumbosacral DRGs (B). The TRPA1 positive staining (*red*), especially in α-Gal A -/0 is indicated (*white arrows*). Fluorescent images were captured on a Nikon D-Eclipse C1 inverted laser scanning confocal microscope. Images were taken as single confocal sections at 40X magnification and separately for each channel. Image J (NIH, http://rsb.info.nih.gov/ij/) software was used for image analysis and merge. Scale bar: 50 μm.
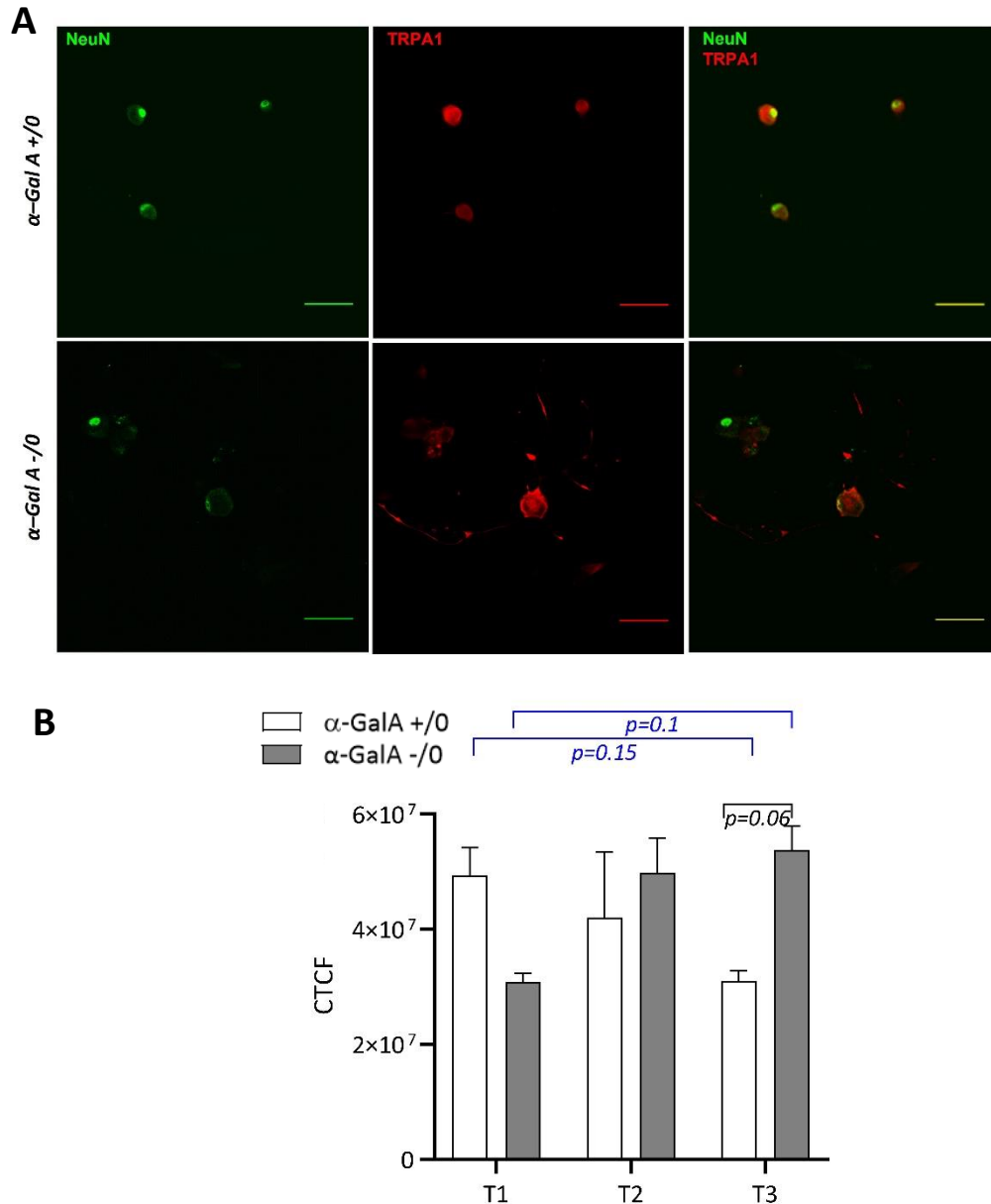
Figure 37 Qualitative and quantitative analysis of TRPA1 fluorescence in neuronal cells from lumbosacral DRGs of α-Gal A +/0 and α-Gal A -/0 mice. In A, representative images of NeuN (*green*) and TRPA1 (*red*) staining by immunofluorescence on primary neurons from lumbosacral DRGs of α-Gal A +/0 and α-Gal A -/0. Images were acquired with Nikon D-Eclipse C1 microscope, 40X objective. Scale bar = 50 μm. ImageJ software was used for image processing. In B, the graph showing the statistical analysis of TRPA1 fluorescence signal expressed as CTCF in α-Gal A +/0 (*white*) and α-Gal A -/0 (*grey*) animals at 8-10-week-old (T1), 16-20-week-old (T2), and 12-month-old (T3; *here represented*). GraphPad Prism 8 software was used to perform statistical analysis. Data are shown as means ± SEM. 2-Way ANOVA followed by Tukey's post hoc test was applied (n = 3, per genotype, per group).* $p < 0.05$ was chosen as significant.

3.4 Neurons from lumbosacral DRGs of α-Gal A -/0 mice develop in larger size

Interestingly, genotype-specific phenotype of the neuronal bodies size from the lumbosacral DRGs was noticed. The analysis of cell body area (μm^2) was performed on neurons from 8-10-week-old (T1), 16- 20-week-old (T2), and 12-month-old (T3) α-Gal A +/0 and α-Gal A -/0 mice (n = 9; for each genotype and age). As shown in Figures 38, in addition to the physiological reduction in size in older mice that is visible in both genotypes (cultures of neurons from DRGs become progressively more complicated to set up and slower in development the older the starting animal), it is interesting to note that α-Gal A -/0 mice compared to α-Gal A +/0 mice, at the same age and days of culture develop in larger dimensions (α-Gal A -/0 VS α-Gal A +/0 at T1, p = 0.004; α-Gal A -/0 VS α-Gal A +/0 at T2, p = 0.03; α-Gal A -/0 VS α-Gal A +/0 at T3, p= 0.01).
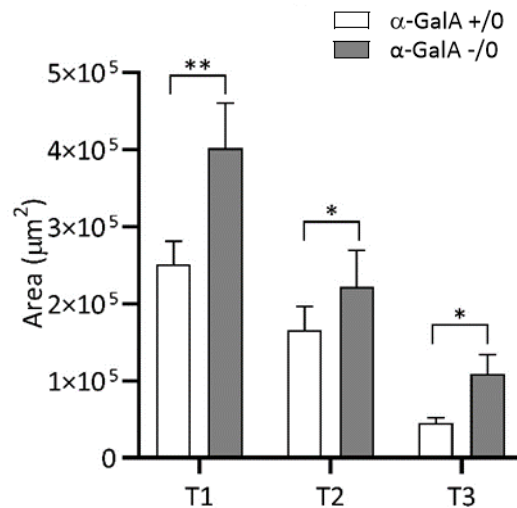
Figure 38 Statistical analysis of neuronal size from lumbosacral DRGs of α-Gal A +/0 and α-Gal A -/0 animals at three ages. Immunofluorescence images of primary neurons from lumbosacral DRGs of α-Gal A +/0 and α-Gal A -/0 mice at 8-10-week-old (T1), 16-20-week-old (T2), and 12-month-old (T3) were used for the cell body area evaluation. ImageJ software was used for image processing. Nuclear-specific neuronal marker NeuN was employed to draw the perimeter. GraphPad Prism 8 software was used to perform statistical analysis. Data are shown as means ± SEM. Paired Student t-test was applied (n = 9, per genotype, per group). * p < 0.05; ** p < 0.002 vs α-Gal A +/0.

4. Evaluation of lyso-Gb3 effects on ion transport and sensory nerves activation by Ussing chamber and on contractility by organ bath

In the image below, to make clear the experimental design, a graphical summary of the tests carried out employing Ussing Chamber is provided. The experiments were performed on stripped adult mouse colon. The purpose was to identify a possible effect of lyso-Gb3 on I_{sc}, and the upstream mechanisms and downstream effects of this lyso-Gb3-mediated impact. For this purpose, as shown in the Figure 39, we employed secretagogues commonly used as blockers or activators in this kind of approach.
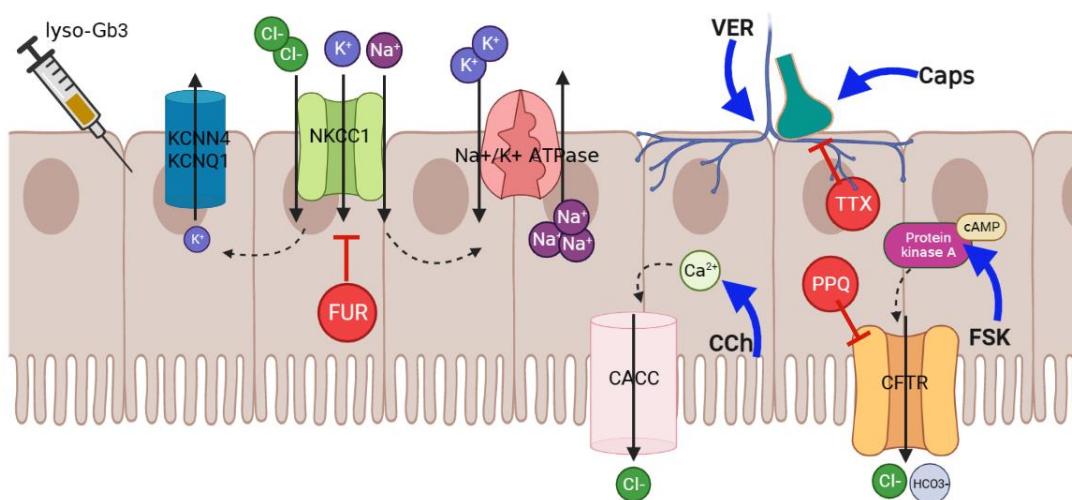
Figure 39 Graphical abstract of tests conducted by Ussing Chamber to investigate the action mechanism and effect of lyso-Gb3. The scheme shows the main components investigated at the apical and basolateral levels. In particular, Ca^{2+} activated Cl^- channel (CACC); Cystic Fibrosis Transmembrane Conductance Regulator (CFTR); $Na^+/K^+/Cl^-$ cotransporter (NKCC1) with its recyclers Na^+/K^+ ATPase and K^+ channels (KCNN4 and KCNQ1). The activators/stimulants Carbachol (CCh), Forskolin (FSK), Capsaicin (Caps), and Veratridine (VER) are represented (*blue arrows*) where they act. As well, the blockers Pyrimido-pyrrolo-quinoxalinedione (PPQ), Furosemide (FUR) and Tetrodotoxin (TTX) (*red ticks*). Figure realized by *BioRender.*

4.1 Lyso-Gb3 affects the baseline short circuit current (I_{sc})

To investigate whether lyso-Gb3 impacts basal I_{sc} and TEER, it was administrated into basolateral reservoir at increasing concentrations: 30 nM – 100 nM – 300 nM – 1 µM – 3 µM - 10 µM. All the experiments were carried on mucosal-submucosal preparation of adult male mice colon. For each test, the control tissue from the same animal was treated in an adjacent chamber, with the respective amount of vehicle (DMSO). According to the schematic protocol reported in Figure 41 A, the I_{sc} was assessed right afterward the administration (acute effect; ΔI_{sc} t = 0) and after 30 minutes (long-lasting phase; ΔI_{sc} t = 30) comparing to the mean value over a period of 6 min; also the TEER

before and after the treatment was taken. As shown in Figure 40, the lower concentrations tested (from 30 nM to 1 µM) did not exhibit statistically significant differences in the either acute or long term, despite an increasing trend (Fig. 40 A-B). Surprisingly, not even the highest lyso-Gb3 concentration tested (10 µM) was found to alter the basal I_{sc}, most likely due to the impact on saturation of the system (Fig. 40 C-D).
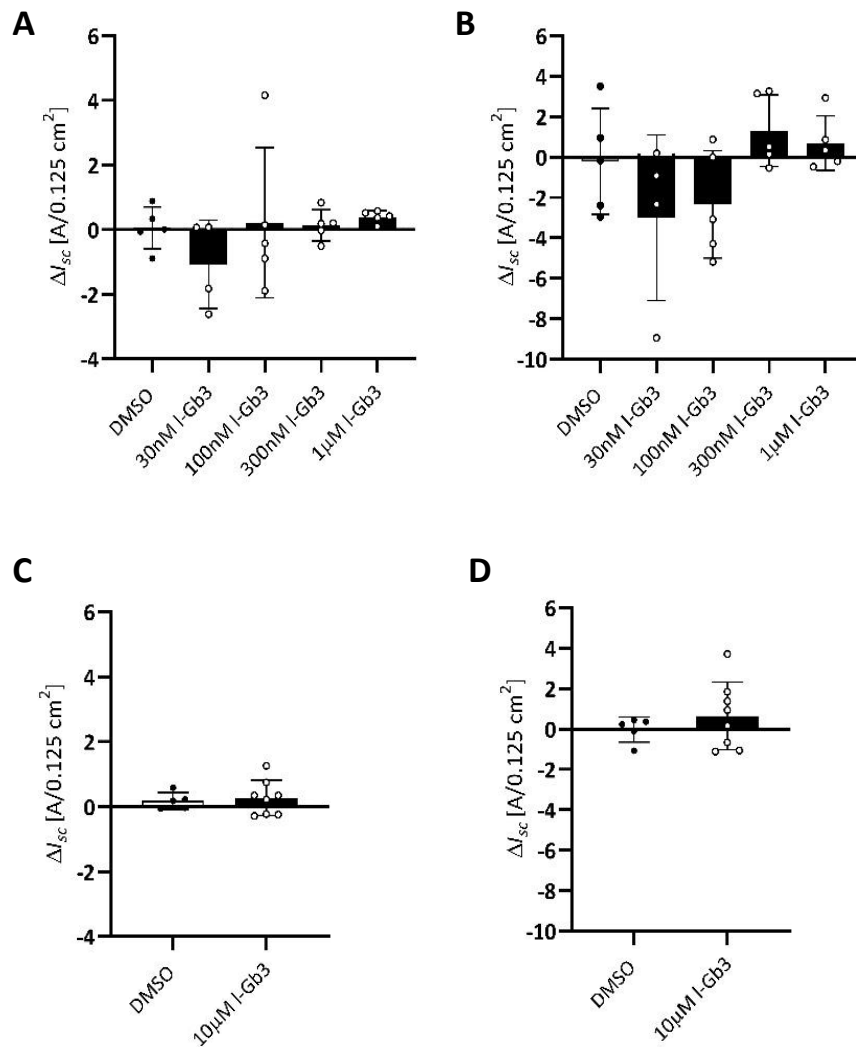
Figure 40 Effect on I_{sc} of 30 nM, 100 nM, 300 nM, 1 µM and 10 µM lyso-Gb3 in acute and long-lasting. Lyso-Gb3 (30 nM, 100 nM, 300 nM, 1 µM and 10 µM) and the vehicle (DMSO) were added to the basolateral reservoir in adjacent chambers to adult male mice colon mucosal-submucosal preparations. The I_{sc} was measured acutely, right after the administration of lyso-Gb3 (A-C), and after 30 minutes (B-D). GraphPad Prism 8 software was used to perform statistical analysis. Data are shown as means ± SD. Paired Student t - test was applied (n = 5-8, one dot); no significance. Values of $p < 0.05$ were chosen as significant.

However, the addition of 3 µM lyso-Gb3 significantly affected I_{sc} causing an increment both acutely (n = 9; means ± SEM, $\Delta I_{sc\ (DMSO)}$ = -0.3 ± 0.2 µA.0,12cm^{-2}, $\Delta I_{sc\ (lyso-Gb3)}$ = 0.6 ± 0.2 µA.0,12cm^{-2}; Paired t-test, p = 0.047) and after 30 min (n = 9; means ± SEM, $\Delta I_{sc\ (DMSO)}$ = -0.7 ± 0.6 µA.0,12cm^{-2}, $\Delta I_{sc\ (lyso-Gb3)}$ = 0.8 ± 0.5 µA.0,12cm$^{-2;}$; Paired t-test, p = 0.031) (Fig. 41). This increment was detected along the entire length of the colon with no segmental differences from proximal to distal. TEER was not impacted by any of the concentrations tested after 30 min of incubation (*data not shown*). This proved that lyso-Gb3 does not affect tissue integrity. Given the results obtained, we established to use the 3 µM concentration for all following experiments aimed at identifying the mediators (upstream) of this increase given by lyso-Gb3, and the effects (downstream) on epithelium- and neuro-mediated secretion.
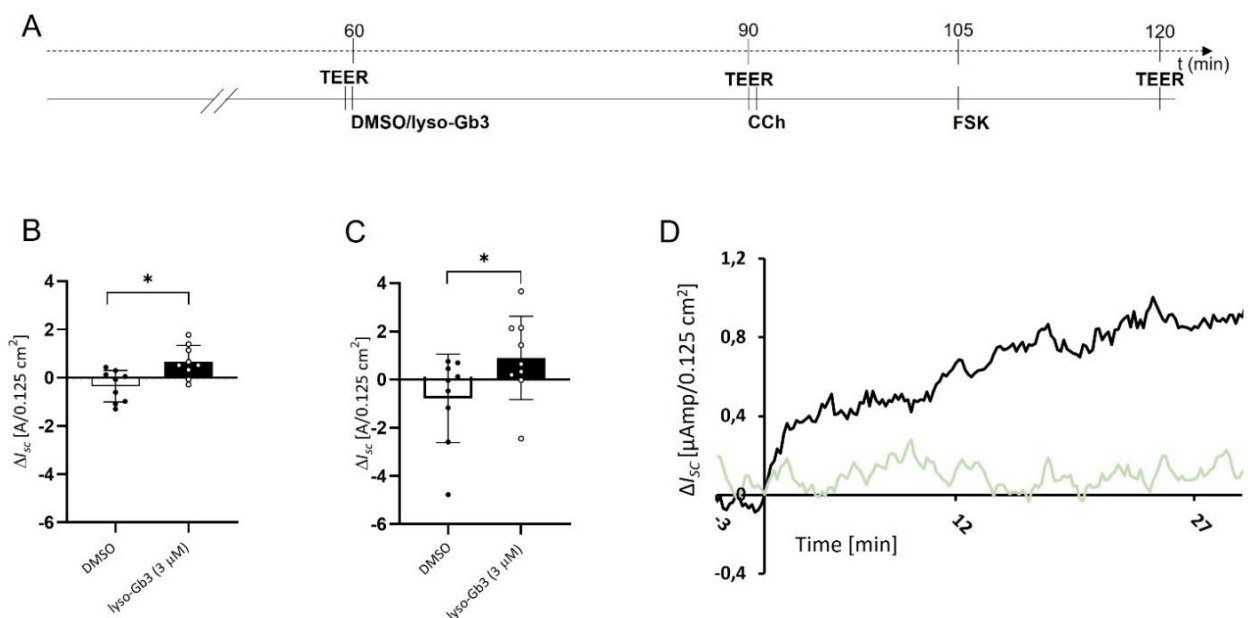
Figure 41 Protocol and effect on I_{sc} of lyso-Gb3 administration. (A) Experimental protocol: lyso-Gb3 (3 µM) and the vehicle (DMSO) were added to the basolateral reservoir in adjacent chambers to adult male mice colon mucosal-submucosal preparations. TEER was recorded before the administration and after 30 minutes. (B-C) Lyso-Gb3 significantly affects the baseline I_{sc} causing an increase both acute (B) and long-lasting (C). GraphPad Prism 8 software was used to perform statistical analysis. Data are shown as means ± SD. Paired Student t -test was applied (n = 9). * $p < 0.05$; ** $p < 0.01$; *** $p < 0.001$ vs control. (D) Representative trances of DMSO- *(green)* and lyso-Gb3-treatment *(black)* responses measured by DataTrax II software (World Precision Instruments).

4.2 The lyso-Gb3-induced increase in I_{sc} is mediated neither by TTX-sensitive enteric neurons nor by CFTR, but NKCC1 blockade affects the responses.

To investigate the mechanism by which lyso-Gb3-induced increase in baseline I_{sc} occurs, some specific inhibitors were applied before the application of lyso-Gb3. In particular, tetrodotoxin (TTX)

(300nM) that inhibits the Na^+ activation mechanism of nerve impulse, to examine if it was mediated via a neuronal pathway, and Pyrimido-pyrrolo-quinoxalinedione (PPQ) (50 µM) and furosemide (FUR) (100 µM) to inhibit CFTR and NKCC1 respectively to assess the transporters' role at basolateral and apical levels for the ion components involved. As reported in Fig. 42, the analysis showed that the TTX-induced blockade did not prevent the lyso-Gb3 effect either acutely or after 30 minutes (n = 12; acutely, means ± SEM, $\Delta I_{sc\,(H2O)}$ = 0.39 ± 0.08 µA.0,12cm^{-2}, $\Delta I_{sc\,(TTX)}$ = 0.4 ± 0.08 µA.0,12cm^{-2}; Paired t-test, p = 0.5; long-lasting, means ± SEM, $\Delta I_{sc\,(H2O)}$ = 0.42 ± 0.4 µA.0,12cm^{-2}, $\Delta I_{sc\,(TTX)}$ = 1.04 ± 0.32 µA.0,12cm$^-$2; Paired t-test, p = 0.14), suggesting that the lyso-Gb3 increase in basal I_{sc} was not ENS mediated.
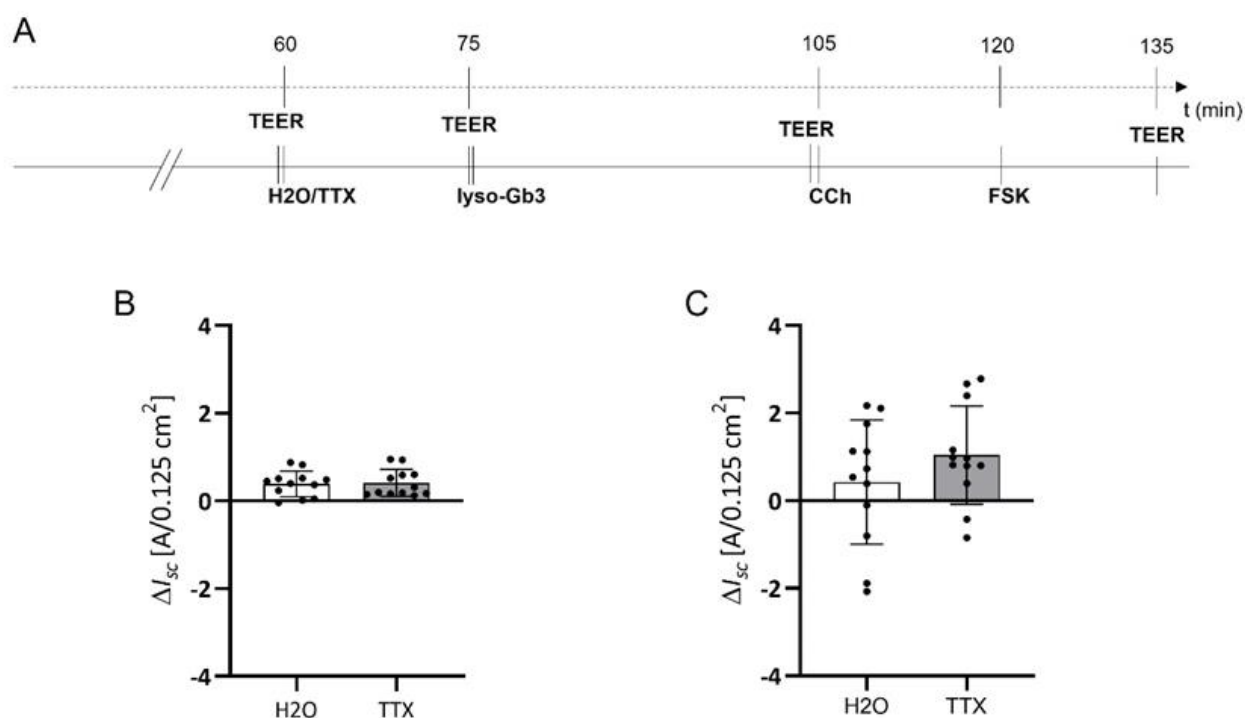
Figure 42 Effect of TTX-sensitive enteric neurons blockage on lyso-Gb3-evoked increase in I_{sc}. (A) Experimental protocol: tetrodotoxin (TTX; 300nM) or vehicle (H_2O) were added to the basolateral bathing solution (15 min) before the treatment with lyso-Gb3 (3 µM) in adjacent chambers to mucosal-submucosal preparations. Carbachol (CCh) and Forskolin (FSK) were added to confirm the tissue vitality after 30 min of lyso-Gb3 treatment. (B-C) Graphs represent lyso-Gb3 I_{sc} after the pre-treatment both acutely (B) and after 30 min (C). GraphPad Prism 8 software was used to perform statistical analysis. Data are shown as mean ± SD. Values of $p < 0.05$ were chosen as significant. TTX pre-treatment does not significantly affect the lyso-Gb3 I_{sc} (n = 12, Paired t-test, no significance).

However, although the blockade of CFTR did not impact the activity of lyso-Gb3 either in the acute or in the long-lasting response (n = 7; acutely, means ± SEM, $\Delta I_{sc\ (DMSO)}$ = 0.6 ± 0.22 µA.0,12cm^{-2}, $\Delta I_{sc\ (PPQ)}$ = 0.39 ± 0.1 µA.0,12cm^{-}2; Paired t-test, p = 0.2; long-lasting, means ± SEM, $\Delta I_{sc\ (DMSO)}$ = 1.32 ± 0.36 µA.0,12cm^{-2}, $\Delta I_{sc\ (PPQ)}$ = 1.17 ± 0.64 µA.0,12cm^{-2}; Paired t-test, p = 0.14) (Fig. 43 A-B), the pre-treatment with the NKCC1-blocker FUR elicited a progressive increase in I_{sc} induced by lyso-Gb3. Already acutely with a clear, albeit non-significant increase and even more clearly and significantly in the long term (n = 6; acutely, means ± SEM, $\Delta I_{sc\ (H2O)}$ = 0.2 ± 0.11 µA.0,12cm^{-2}, $\Delta I_{sc\ (FUR)}$ = 0.44 ± 0.06 µA.0,12cm^{-2}; Paired t-test, p = 0.2; long-lasting, means ± SEM, $\Delta I_{sc\ (H2O)}$ = 0.26 ± 0.19 µA.0,12cm^{-}2, $\Delta I_{sc\ (FUR)}$ = 1.2 ± 0.26 µA.0,12cm^{-}2; Paired t-test, p = 0.002) (Fig. 43 C-D).
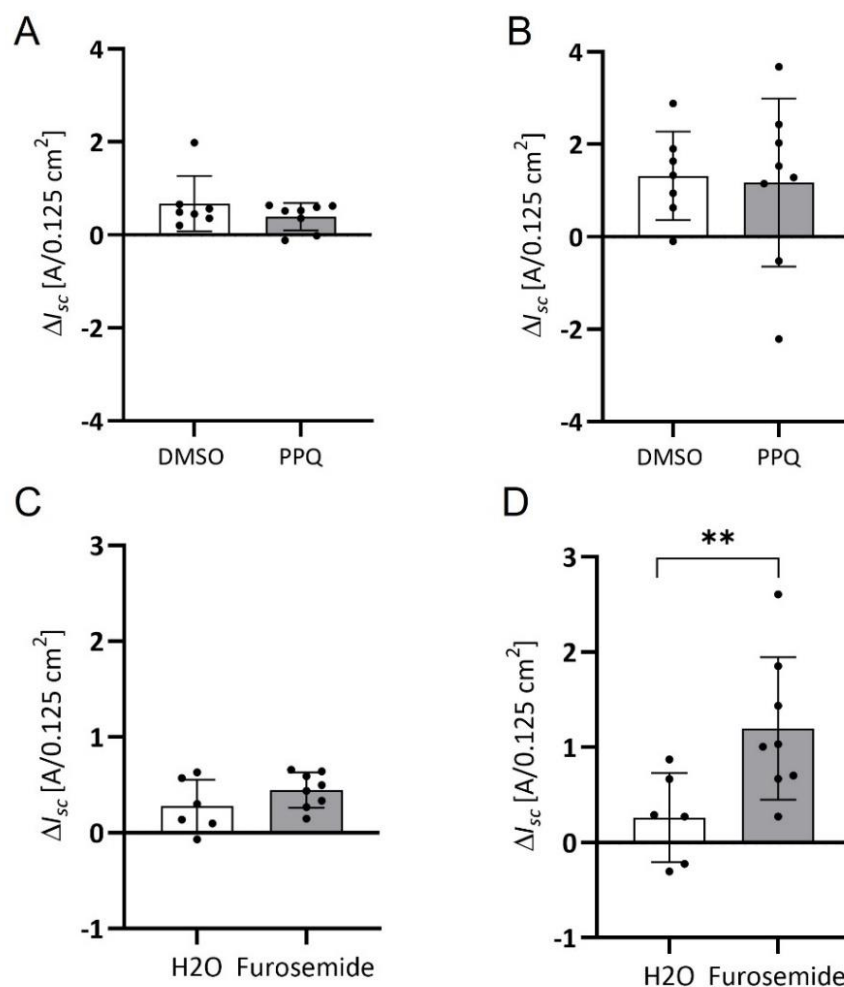
Figure 43 Effect of CFTR-inhibitor (PPQ) and NKCC1 blockage via Furosemide (FUR) on lyso-Gb3 response in I$_{sc}$. (A-B) Pre-treatment with PPQ (15 min, apically) does not significantly affect the lyso-Gb3 increase in I$_{sc}$ (n = 7, Paired *t-test*, no significance) neither acutely (A) nor after 30 min. (B). Pre-treatment with FUR (15 min, basolateral) significantly enhances the lyso-Gb3 long-lasting increase in I_{sc} (n =6, Paired *t-test*, p=0.002) (D) but not the acute one (n =6, Paired *t-test*, no significance) (C). GraphPad Prism 8 software was used to perform statistical analysis. Data are shown as mean ± SD. * p < 0.05; ** p < 0.01; *** p < 0.001 vs vehicle.

4.3 Treatment with lyso-Gb3 does not affect the epithelial-mediated secretion

As an excessive activation of Cl$^-$ secretion triggers diarrheal disorders, the mechanisms implicated are of interest for targeted pharmacotherapy. Thus, to investigate whether lyso-Gb3-dependent I$_{sc}$ changings impacted the Cl$^-$ epithelial-mediated secretion, carbachol (Cch) (100 µM) and forskolin (FSK) (10 µM) were sequentially serosal added to mucosal-submucosal preparations pre-treated with lyso-Gb3 (3 µM). The former, a cholinergic agonist, was used to stimulate Ca^{2+}-dependent Cl$^-$ secretion, the latter, administrated during the plateau phase of the I$_{sc}$ induced by CCh, to activate cAMP-dependent Cl$^-$ secretion. The CCh adding led to the usual rapid but transient increase in I$_{sc}$, which return to the basal level within 15 min (Fig.44). Since the responses' size presents substantial segmental differences in the expression of Ach, all the experiments were performed almost in the middle of the colon[659]. Similarly, the response to cAMP-dependent secretagogue FSK are characterized by a rapid and high I$_{sc}$ peak which exceeds even the previous CCh one (Fig. 44 A). As shown in Figure 44 (Fig. 44B-C) lyso-Gb3 appeared to influence neither Ca^{2+}-dependent nor cAMP-dependent Cl$^-$ secretion (n = 9; CCh: means ± SEM, ΔI$_{sc\ (DMSO)}$ = 9.49 ± 1.62 µA.0,12cm-2, ΔI$_{sc\ (lyso\text{-}Gb3)}$ = 9.07 ± 1.16 µA.0,12cm^{-2}; unpaired t-test, p = 0.83; FSK: means ± SEM, ΔI$_{sc\ (DMSO)}$ = 40.8 ± 3.15 µA.0,12cm^{-2}, ΔI$_{sc\ (lyso\text{-}Gb3)}$ = 42.6 ± 3.81 µA.0,12cm-2; unpaired t-test, p = 0.72). These experiments demonstrate that lyso-Gb3 increase in I$_{sc}$ does not affect epithelial-mediated secretion.
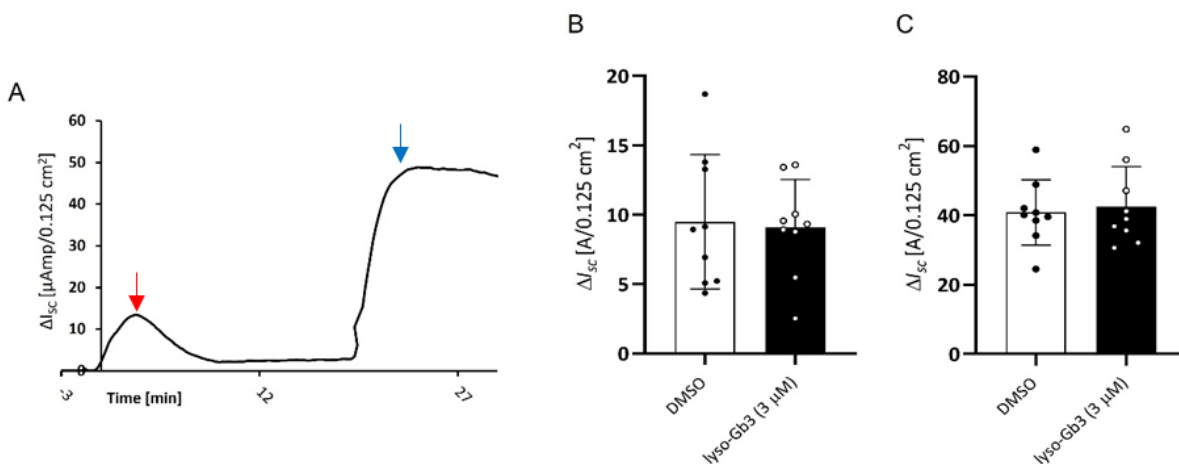
Figure 44 Effect of lyso-Gb3-dependent *I$_{sc}$* increase on the Cl$^-$ epithelial-mediated secretion. Carbachol (CCh, 100 µM) and Forskolin (FSK, 10 µM) were consecutively serosal added to mucosal-submucosal preparations pre-treated with lyso-Gb3 (3 µM) or vehicle (DMSO). (A) Representative trace of CCh- *(red arrow)* and FSK- *(blue arrow)* responses recorded by *DataTrax II* software (World Precision Instruments). (B-C) Graphs of the statistical analysis of CCh (B) and FSK (C) responses after lyso-Gb3 (*black column*) or vehicle (DMSO; *white column*). GraphPad Prism 8 software was used to perform statistical analysis. Data are shown as mean ± SD. Values of *p* < 0.05 were chosen as significant (n = 9, unpaired t-test, no significance).

4.4 Treatment with lyso-Gb3 increases neuronal-mediated secretion

Since lyso-Gb$_3$ has been demonstrated to modulate neuronal excitability and the enteric neurons are crucial regulators of epithelial ion transport, we wondered whether the exposure to lyso-Gb$_3$ could interfere with neuron-induced epithelial secretion. We applied veratridine (VER) (30 μM) and capsaicin (3 μM) in order to activate the majority of neurons. They were put on in the basolateral side at the end of lyso-Gb3 treatment. To reduce the VER off-target effects, we applied a concentration within the range known to activate voltage-gated Na$^+$ channels and in line with others previous studies of VER-stimulated electrogenic ion transport in mouse colon[610]. As illustrated in Figure 45 (Fig. 45A-B), though the growing trend of the response to VER in lyso-Gb3 pre-treated tissues compared to controls, there was no significant difference (n = 7; means ± SEM, $\Delta I_{sc\ (DMSO)}$ = 8.51 ± 0.86 μA.0,12cm^{-2}, $\Delta I_{sc\ (lysO\text{-}Gb3)}$ = 10.12 ± 0.84 μA.0,12cm^{-2}; unpaired t-test, p = 0.2).

Regarding the subgroup of capsaicin-sensitive sensory nerves, they constitutes another important neural network modulating GI function. Exposure to capsaicin activates sensory afferent neurons which in turn activate submucosal secretomotor neurons to release pro-secretory neuropeptides which can then cause an increase in luminal Cl$^-$ efflux. Since the capsaicin modulates intestinal ion transport markedly differently along colonic segments, statistical analyses were performed taking into account the absolute value of the reported ΔI_{sc} (Fig. 45 C-D). The outcomes proved that lyso-Gb3 (3 μM) pre-treatment significantly increased capsaicin sensitivity (n = 5-8; means ± SEM, $\Delta I_{sc\ (DMSO)}$ = 1.31 ± 0.18 μA.0,12cm^{-2}, $\Delta I_{sc\ (lysO\text{-}Gb3)}$ = 2.51 ± 0.41 μA.0,12cm^{-2}; unpaired t-test, p = 0.01). Therefore, these results demonstrate that lyso-Gb3 may modulate specific neuronal pathways involved in the regulation of GI physiology, especially it enhances neuron-mediated secretagogue induced secretion, specifically capsaicin-mediated and only partially veratridine-mediated.
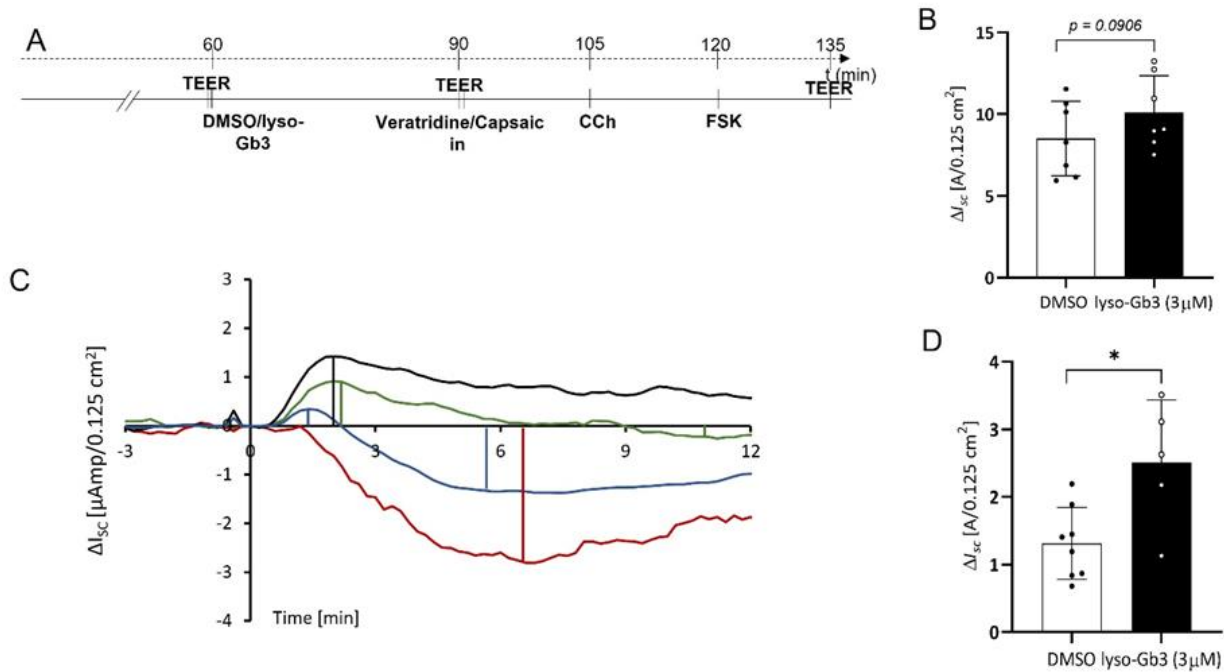
Figure 45 Effect of lyso-Gb3 treatment on neuronal-mediated secretion (A) Experimental protocol: after 30 min of lyso-Gb3 (3 µM) treatment, veratridine (VER) (30 µM) was added to the serosal reservoir (15 min). Then, CCh and FSK were added to assess the tissue vitality. (B) Veratridine responses to lyso-Gb3 pre-treatment compared to controls; (C) Typical traces of capsaicin-response along the different colonic segments, from proximal (*black*) to distal (*red*). The considered absolute value of Δ*Isc* in the different portions is drawn with the lines. (D) Capsaicin responses to lyso-Gb3 pre-treatment compared to controls. GraphPad Prism 8 software was used to perform statistical analysis. Data are shown as mean ± SD. Unpaired t-test; * p < 0.05; ** p < 0.01; *** p < 0.001 vs vehicle (DMSO).

4.5 Lyso-Gb3 does not modulate colonic contractility

Given the effects of lyso-Gb3 on ion transport and sensitization to secretory stimuli, we wondered whether lyso-Gb3 could act directly on muscle-mediated contractility, because alterations of GI motility represent another essential cause for diarrhea/constipation. Therefore, we examined whether the compound affected colonic motility in a vertical organ bath chamber set-up. The experiments were performed on male mouse no-stripped colon tissue, to preserve the muscle layers involved in contractility process. As reported in Figure 46, the application of lyso-Gb$_3$ (3 µM) to the bath did not significantly affect acute tension or spontaneous contractility (AUC), even if there might be a decreasing trend in lyso-Gb3 treated mice (n = 6-7; means ± SEM, AUC/s $_{(DMSO)}$ = 0.026 ± 0.005 µA.0.12cm^{-2}, ΔI_{sc} $_{(lysO-Gb3)}$ = 0.014 ± 0.0025 µA.0.12cm^{-2}; unpaired t-test, p = 0.07) (Fig. 46). To check the quality of the tissue, CCh (100 µM) was put into the bath and it induced contractions reproducible to those of colon tissues. Then, we evaluated whether the magnitude of the CCh-induced contraction was different between lyso-Gb$_3$ and DMSO-treated tissues. The traces did not

reported any substantial changes between the samples. Overall, these findings suggest that FD-associated GI dysfunctions are not primarily generated via lyso-Gb$_3$ targeting muscle contractility but rather through effects on ion transport and sensitivity to secretory stimuli.
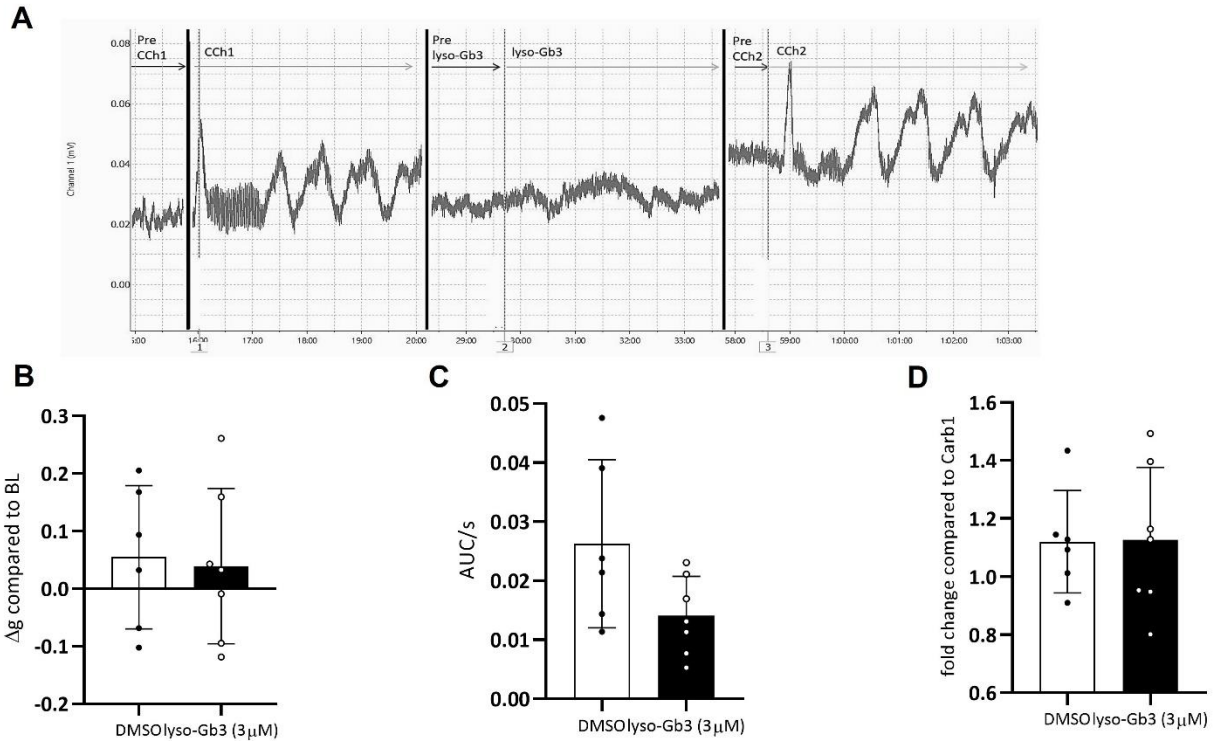
Figure 46 Lyso-Gb3 (3 µM) effect on colon contractility tested by Organ Bath. (A) Excerpt of representative traces and order of administration of Carbachol before (CCh1) and after (CCh2) lyso-Gb3 treatment. Powerlab and LabChart8 (AD Instruments Inc., Colorado Springs, CO, USA) were used for recording and analyzing. (B) Acute tension; (C) Spontaneous contractility (Area Under the Curve; AUC); (D) fold change between CCh1 and CCh2. GraphPad Prism 8 software was used to perform statistical analysis. Data are shown as mean ± SD. Values of $p < 0.05$ were chosen as significant (n = 5-7, unpaired t-test, no significance).

DISCUSSION

The main purpose of this thesis was to expand knowledge regarding gastrointestinal symptoms in FD, both in terms of functional characterization and identification of mechanisms potentially involved in their onset. The need for increased awareness of gastrointestinal complaints in Fabry patients stems from the fact that these are among the most prevalent and disabling early signs of the disease in children (60.8%) and adults (49.8%); however, they are paradoxically the same ones that contribute to the delay in the proper diagnosis because of their misinterpretation even today[84]. Once the diagnosis is confirmed, this is compounded by the lack of effectiveness in the management of GI problems by commonly used treatments. This is reflected in a relevant negative impact on the patient's quality of life as well as in a burden on the healthcare system. Hence, there is a pressing need for greater understanding aimed at identifying new potential therapeutic targets[123].

To date, two main hypotheses have been formulated regarding the pathophysiological mechanisms underpinning the onset of GI symptoms in FD. The first involves an alteration of the ANS (impacting motility), and the second concerns vascular dysfunction and/or ischemia caused by damage to the muscle wall or endothelial cells, reasonably associated with Gb3 deposits[660]. Gb3 accumulation in enteric vessels and neurons and inflammation would trigger ANS dysregulation and damage the functionality of the enteric neurons, responsible for regulating intestinal motility[661]. In addition to causing ischemia, Gb3 would modify cell signaling pathways, inducing hypertrophy, myopathy, and extracellular matrix production by vascular smooth muscle cells ultimately leading to vascular remodeling[119]. In turn, impaired blood flow would act on inflammation[137]. Although these assumptions are strongly supported by the literature, the complexity and multicausality that characterize the symptomatology are not fully elucidated. As well as the struggle in distinguishing between cause and effect. Hence, the idea of exploring traits not yet investigated in FD but common to other GI disorders, such as bacterial dysbiosis, or reported in FD but not at the GI level, as ion channel expression. In addition, given the increasing importance of the causal role played by lyso-Gb3, which is no longer just a diagnostic marker, it was deemed appropriate to also evaluate its effect at the GI level, particularly on ion and water permeability.

The murine model of the disease (α-Gal A -/0 mouse) was used to achieve this goal. This model has been validated to mirror the GI morphological changes of Fabry patients[131,178] and has already proven to be a valuable model for the study of neuropathic pain[94,95,662]. Because of the X inactivation process might have impaired the reproducibility, and because FD is more severe in male patients,

in this study we decided to use exclusively male mice[633]. All experiments presented here directly involving the intestine were performed on the colon, although the other tracts (duodenum, jejunum, and ileum) were also collected for future analysis. The choice to focus specifically on this portion was dictated primarily by the availability of the relevant scientific literature; in fact, the only characterization of the GI tract in this mouse model reporting the presence of Gb3 deposits was performed on the colon. In addition to the limitation dictated by some of the techniques used, such as that to test the visceral sensitivity technique (CRD). This is compounded by the generally greater availability of scientific literature focused on the murine colon rather than on other portions of the intestine.

The first part of the work focused on a comprehensive characterization of functional and behavioral disorders in the animals. Since diarrhea (57%) and abdominal pain (56%) are the two main GI symptoms reported by patients, we started by investigating these in the α-Gal A -/0 mouse model[155]. Quantifying fecal output and assessing the fecal water content showed that Fabry mice exhibit impairment comparable to a diarrheal phenotype. Furthermore, from a time-dependent but intragenotype point of view, it is interesting to note that although the fecal output in terms of number of pellets is significantly and progressively decreasing, as is the case at the physiological level, it does not occur with regard to weight expressed in mg. This trend would thus corroborate the finding that the Fabry adult animals have a higher water content. This might suggest that in the oldest affected, the diarrheal phenotype may be even more pronounced than in the juvenile, suggesting the involvement of a progressive mechanism underlying the disturb.

Diarrhea is still a diagnostic and therapeutic challenge, probably because of its multiple origins, not only for FD[663]. Certainly, secretory function and motility represent two crucial aspects and both can contribute to its onset[664]. Regarding the former, the amount of fluid in stool is determined by its solute content, which in diarrhea is insufficiently absorbed and actively secreted. The function of the epithelial barrier in stool dehydration is also relevant. Although a reduction in its effectiveness is not a sufficient condition to cause diarrhea, when it is associated with defective ion transport and fluid accumulation in the lumen, the efficiency of absorption may be compromised[663]. For example, this mechanism has been proposed as a possible pathogenesis of IBD (with which Fabry shares some characteristics) but it may also contribute to chronic watery diarrhea[665,666]. Regarding the latter, clinical studies have indicated that impaired motility is also a key component. Motility disorders would cause diarrhea by accelerating or slowing GI transit. Among the most common forms of

diarrhea related to these alterations are autonomic neuropathies, such as diabetic neuropathy (with which Fabry is often allied) or IBD, both of which are associated with accelerated transit or an increased number of high-amplitude propagated contractions[420,667,668]. Nevertheless, what seems to emerge from our finding of increased water-rich fecal output (Fig. 17), taking into account also the previous observations on the thickening of the muscle layer and alteration of the nerve fibers innervating the mucosa, is that diarrhea in the Fabry mouse might be the result of a number of factors that together contribute to the onset of the symptom operating simultaneously from different parts.

Our next step was the first ever known assessment of visceral sensitivity and pain in α-Gal A -/0 mice. Indeed, while somatic pain is a hallmark of FD, widely described in the literature nothing is known about visceral pain in Fabry mice[85,87].

The quantitative measure of visceral sensitivity was obtained from VMR to CRD since the magnitude of the abdominal contraction is directly proportional to the animals' intrinsic sensitivity[270,635]. The results at the same age reported an increase in the VMRs of α-Gal A -/0 mice compared with controls (Fig. 18). Results that would confirm a visceral hypersensitivity (VHS) in Fabry animals, consistent with the symptomatology reported by patients. Furthermore, in the interpretation of these data, we should account for the similar results of VHS obtained from rodents treated with GI disorders-inducing compounds[669,670]; as well as at the opposite end, data reporting reduced VMR in animals lacking TRPV1 or ASIC3[671]. Indeed, this association leads to the hypothesis that in the onset of VHS found in Fabry mice, similar mechanisms, such as alterations in ion channel expression, may be involved. However, it should be added that despite its usefulness as a quantitative measure, the VMR presents some limits. Indeed, it is performed on sedated animals, thus excluding the cognitive and emotional components of pain. For this reason, the VMR was combined with the evaluation of the AWR to CRD in conscious animals, as described by Chen et al. (2014)[637]. This allowed for a more in-depth examination of this pain and confirmed visceral hyperalgesia in Fabry mice at all three ages considered (Fig. 18). Moreover, even in this case, there appears to be not a waning of symptoms, but rather a progression, probably also prompted by the fact that progressively the pathology leads to the appearance of other conditions that contribute to the reduced tolerability of the pain stimulus. These results possibly reflect the severe abdominal pain experienced by patients and provide further evidence that the male α-Gal A -/0 mouse is a reliable model for studying pain in FD, including visceral pain. Moreover, in light of previous results obtained on the same animals, from which a reduction in the number of nerve fibers innervating the mucosa and a scattered pattern of

these had emerged[131], we might speculate that a neuropathic pain component could also be in the context of visceral hypersensitivity. Nevertheless, multifactorial origin seems to be the most trustworthy hypothesis, given the alteration of a set of co-presenting factors.

Furthermore, in studying the mechanisms underlying the perception of visceral pain, it is important to consider that also the emotional component plays a relevant role[672–674]. To date, this *pain – GI alteration - emotional influence* interconnection is well-established. Numerous scientific pieces of evidence have reported that people suffering from chronic diarrhea, nausea, vomiting, irritable bowel or stomach pain often experience also related psychological issues, anxiety and depression[675–678]. Alander and colleagues have reported that patients with GI diseases manifest higher levels of stress and psychological complications than healthy people[679]. Stress has also been found to be a strong predictor of the level of severity in patients with diabetes[680]. A critical role in the pathophysiology of mood disorders is also played by inflammation[681,682]. For this reason, it has been hypothesized and then confirmed that inflammatory conditions are linked to an increased risk of mood disorders, as with IBS and IBD, also characterized by functional disorders, such as chronic abdominal pain or discomfort and altered bowel habits[683]. For instance, the prevalence of affective illnesses in IBS patients is estimated to be as high as 94%[684]. FD patients are also considered to be at higher risk of developing neuropsychiatric symptoms, such as depression or neuropsychological deficits[685–687]. However, the mechanisms underpinning these processes have not yet been fully elucidated. In particular, it is not defined whether the onset of behavioral disorders is the consequence or the cause. Indeed, a key question is whether affective and cognitive indicators are part of the disease pathogenesis or a reactive event that comes as a response to a painful, chronic, and life-threatening disorder[174]. These behavioral aspects may be caused by the comorbidity with pain or discomfort. Then again, long-term stress enhances pain perception and sensitizes pain pathways, causing a loop that stimulates chronic visceral pain[688]. Besides, it supports the benefit given by antidepressant treatment in affected people[689]. For their part, antidepressants and antiepileptic drugs able to reestablish neuronal activity (i.e. *Pregabalin*) have been demonstrated to be more efficient than anti-inflammatories. Similarly, it takes place in neuropathic pain conditions[690,691]. However, the major limitation of current clinical studies dealing with the correlation between pain and affective disorders in FD is the fact that neuropsychological changes during treatment are mostly secondary end-points that may be influenced by the improvement in organ function associated with treatment[174]. Therefore, the study of emotional attitudes we performed on the mouse model could also represent an alternative. In fact, to date to the best of

our knowledge, the literature offers only one study, by Hoffmann and colleagues (2017) in which α-Gal A -/0 mice were characterized for anxiety and depression behaviors[174].

Specifically, in the present thesis, the focus was on anxiety, which, according to the largest and most recent survey of 106 Italian patients, is reported by 66.7%, without distinction between the elderly and young. Using the EQ-5D questionnaire, it was found that 50.9% feel "moderately" anxious or depressed and 6.6% "extremely." In this, a major role is played by the pain itself. A high number of patients report being "fairly or very" concerned about potential impairment of vital organs (83.9%), increased severity of symptoms (74.5%), possible onset of physical disability (68.9%), and physical pain management (63.3%)[108]. This would suggest a not so much genetic factor in the onset of anxiety- and depression-related disorders in FD, but rather environmental and social. Indeed, the results obtained might be in line with both this hypothesis and what Hoffmann and colleagues have previously shown[174]. What accordingly emerged from our investigation, although the ages considered are different from those analyzed by the other group, is that α-Gal A -/0 mice exposed to EPM do not show significant differences from healthy controls either genotype- or age-dependent. The only feasible observation is related to a slight but not significant increase in the time spent in the closed arm by α-Gal A -/0 mice, and a decrease in it intra-genotype at increasing age (Fig. 19). However, no conclusions can be drawn from this observation, except that it is in line with what occurs physiologically, but in a more pronounced way, which is probably to be attributed to a reduced mobility of the animal and not to a strictly genetic factor.

Regarding OF, comparably to Hoffmann and coworkers (2017)[174], we also found a different response between healthy and KO animals, which could delineate an anxious-like behavior of the latter. Surprisingly, α-Gal A -/0 mice show a significantly lower frequency in borders than controls, with a physiological age-dependent reduction over time (Fig. 20A). However, such apparently abnormal behavior is clarified when looking at the time spent in the periphery of the arena. Indeed, although α-Gal A -/0 mice enter the borders less, when they do they spend significantly more time there than controls, at all three ages analyzed and steadily over time (Fig. 20B). Regarding the mobility of the animals, it can be said that no major genotype-dependent differences were found, except at time point three, where α-Gal A -/0 mice move less than α-Gal A +/0 mice. What is confirmed, however, is a progressive and significant reduction in mobility of Fabry mice, which does not occur in controls (Fig. 20C). This is not surprising considering that 28.3% of FD patients report difficulty moving and another 0.9% being bedridden[108].

The different results between EPM and OF for anxiety behaviors can probably be attributed to the different environmental settings of the two tests, demonstrating the need to apply both[174]. Most researchers agree that none of the existing anxiety tests provide a definite rate of emotional reactivity and that every single test assesses only a portion of the affecting profile[692,693]. The OF, as a behavioral test aims more at identifying a generalized anxious trait and assessing locomotor and exploratory skills, as well as stereotypical behaviors[694]. Such behaviors include those that are repetitive, invariant, and seemingly purposeless. For example, mice that prefer to stay close to walls are described as exhibiting thigmotaxis, which, as in the case of Fabry mice, is pronounced in animals showing signs of anxious-like behavior[695–697]. On the other hand, the EPM has a more complex structure. In the EPM test the amount of time spent in the closed arms is compared to that spent in the open ones as a degree of anxiety or fear. The test exploits the normal inclination of mice to avoid open or elevated places compensated by their natural tendency to explore new areas. A less anxious animal goes into the open arms more often, whereas an anxious mouse tends to spend more time in the closed arms[698,699]. Data from correlational studies, despite being partially contradictory, often indicate little correlation between anxious behaviors evaluated by different tests. This lack of correlation is explained as a probable difference in the psychobiological meanings of various tests[700–702]. However, since it is impossible for one animal to perform multiple tests at the same time as well as to detect whether these measures only temporary emotional states, it can not be affirmed with certainty that the inconsistency between the tests is due to real structural differences between tests or temporal changes in the emotional state of an animal exposed to different tests at different times[658,701,703]. Thus, although the mouse model fails to mimic the anxiety effect dependent on what we might call social/human aspects, it nevertheless seems to be able to reflect the traits of anxiety probably due to the presence of chronic pain, which also limits physical abilities. For instance, it is known that patients with fibromyalgia or neuropathic pain syndromes (e.g., diabetic peripheral neuropathy) may have impaired cognitive and consequently also emotional functions related to anxiety and depression[704,705].

In light of the functional and behavioral GI alterations found in our mouse model, the study continued with the analysis of the fecal microbiota. This GI tract-CNS connection also includes endocrine, humoral, metabolic, and immune routes of communication[682]. In support, a growing body of evidence demonstrates the bidirectional communication between gut microbiota and the brain. Gut bacterial communities are dynamic and can change in both composition and activity during life and as a reaction to host factors, such as age and genetics, and environmental factors[706].

Indeed, the configuration of the gut microbiota on the one hand may be associated with host health benefits, including maintenance of gut homeostasis, peristalsis, mucosal integrity, protection from pathogens, and triggering of immune responses, on the other with many GI disorders, such as IBS IBD, or VHS[398]. Furthermore, modifications in microbiota diversity and composition have been linked to extraintestinal diseases. Many articles, mostly still in the preclinical stage, show that a rearrangement of bacterial communities could also lead to alterations in behavioral/cognitive responses. Indeed, alteration of the microbial profile has also been proposed to be implicated in several CNS pathologies, such as anxiety, depression, autism, Alzheimer's disease, stroke or brain injury, and Parkinson's disease [329,334,354,397,428,429,706–709].

Therefore, we started by assessing indices of microbial diversity, and then profiling the taxonomic and metabolomic composition, of α-Gal A +/0 and α-Gal A -/0 mice to investigate whether, as already found in the many disorders above mentioned, there might be microbiota involvement in FD. In this regard, it is worth mentioning that since this is the first analysis of the microbiota about FD, either on a mouse or human model, comparison with previous analyses is not possible and is therefore to be done based on what are the GI and behavioral alterations most akin to it. While this might be a major limitation of the proposed research, it represents a pivotal innovative element in the study of GI- and non-FD-related disorders and a starting point for new research approaches. Indeed, albeit mechanistic studies of how this extensive community of microorganisms may influence ENS and CNS function, motility, mood, cognition and learning are still in their infancy, it offers itself as a potentially important site for future therapeutic interventions[710]. Moreover, our double bioinformatic analysis carried out with different databases and approaches, thanks to the collaboration reported in the relative section of "Materials and Methods" with two laboratories specialized in bioinformatic analysis, corroborates and reinforces the validity of our data.

Specifically, the measurement of microbial diversity between α-Gal A +/0 and α-Gal A -/0 mice was initially assessed by α- and β-diversity respectively used to describe the diversity within the sample and between samples. By α-diversity it meant the average of all relevant subunits; however, it must be considered that this may vary depending on what is assumed as species diversity. Hence, the use of multiple diversity indices, each based on distinct aspects. *Chao1* assesses community richness and is based more on relative abundance, while *Shannon* and *Simpson* consider community diversity and are based on measuring the concentration degree, still contemplating both species richness and abundance. What emerged is a picture of a clear unbalance between healthy and Fabry mice which seems to decrease with increasing age (Fig. 21A). Instead, looking at β-diversity an explicit gut

ecosystem fluctuation profile both genotype- and age-dependent emerged. In α-Gal A -/0 animals there is a clear progressive population shift, with a cluster increasingly distanced from that of the α-Gal A +/0 mice, which not only remains much more constant over time (it is gradually more distant from the α-Gal A -/0), but tends less toward dispersion. Indeed, what is important to note is the growth in individual-specific diversity marked by the augmented dispersion of cluster constituent points that occurs in Fabry mice over time (Fig. 21B). This might lead us to speculate that there is a strongly individual-dependent pattern in FD, and thus to reason in terms of personalized therapies. From cross-sectional studies in humans, although the factors are unclear, there is a growing awareness that changes in the diversity and relative abundances of the microbiota and microbial metabolites are linked to a wide range of disorders. The results of these studies, however, have been inconsistent and lacking evidence establishing causality for the gut microbiome[710,711].

The microbiota modulates the homeostasis and behavior of its host acting through chemical communication. This includes "direct" signaling (such as SCFAs that may impact the CNS by regulating neuroplasticity, epigenetic and gene expression, and the immune system) and "indirect" signaling, by modulation of the neuroendocrine system and neurotransmitter concentration[375,712–715]. For example, several microorganisms (such as *Bacteroides* and *Bifidobacterium*) are known to produce GABA, others noradrenaline and dopamine, and still others would influence the production and secretion of 5-HT[353]. As for our gut microbiota composition analysis on α-Gal A +/0 and α-Gal A -/0 mice, 7 bacterial phyla were identified with *Bacteroidetes*, *Firmicutes* and *Proteobacteria* dominant in both groups in the three time points considered (Fig. 22). *Deferribacteres,* though represents a phylotype exclusive to mice and present at a considerably lower percentage, is also relevant in terms of differences between the two genotypes. Although the dominant phyla are the same between the two genotypes, the differences in quantitative terms are marked, especially among younger mice, that show a clear imbalance between *Bacteroidetes* and *Firmicutes*. In fact, in healthy mice, the former prevails over the latter considerably, whereas in Fabry mice *Bacteroidetes* is significantly less present and the gap is filled by an increase in *Firmicutes*, which consequently is more abundant than in α-Gal A +/0. Again in young mice, the difference in *Deferribacteres* is quite striking, with a significantly greater presence in α-Gal A -/0 mice. With increasing age, the differences at the phyla level seem to smooth out, and the ratio of *Bacteroidetes* to *Firmicutes* balance, with a net increase in *Bacteroidetes* accompanied by a decrease in *Firmicutes* in α-Gal A -/0 mice. At time point 3, a significant presence of *Proteobacteria* in healthy mice that is not paralleled in α-Gal A -/0 mice is also remarkable. Consistent with our results, numerous studies have

shown that *Bacteroidetes* and *Firmicutes* are the two numerically most prevalent bacteria in the human and murine intestines[716]. *Bacteroidetes* inhabit the mucosal surface where they regulate even immune and intestinal functions maintaining a generally beneficial relationship with the host. Several papers have reported a reduction in *Bacteroidetes* in association with IBD, similar to that found in our young Fabry mice. However, other studies have found no significant alterations or even reported an increase in abundance, which in the Fabry appears to occur in old age[717–719].

Such an evident difference even at the phylum level and mainly accounted for by dominant taxa of the mouse core microbiota suggests a deeply destructured microbial assembly and trajectory[720–722]. In particular, as reported in Figure 23, young α-Gal A -/0 mice were featured by higher proportions of the families *Rikenellaceae* (particularly *Alistipes*) and *Porphyromonadaceae*, while lower proportions of *Bacteroidales S24-7 group* (recently renamed *Muribaculaceae*)[723]. *Porphyromonadaceae* and *Rikenellaceae* although found to be associated with positive modulation of adiposity, were also shown to be increased in IBS [724,725]. Moreover, recently Huang and colleagues (2019) identified *Porphyromonadaceae* and *Rikenellaceae* as key IBD-related bacteria[726]. Among them, *Alistipes* is a relatively new bacterial genus, whose role in disease is not yet well understood[727]. However, some species are known to trigger gut barrier dysfunction and inflammation and have been implicated in anxiety and depressive disorders, possibly through the degradation of tryptophan to indole (and thus reduced tryptophan availability for serotonin production) and increased production of GABA[728–730]. Various species of intestinal bacteria belonging to the genus *Alistipes* have been isolated from patients with appendicitis and abdominal and rectal abscess. In addition, *Alistipes* has been found to be pathogenic in patients with colorectal cancer or depression[731]. However, this may have protective effects against some diseases, such as liver fibrosis, colitis, cancer immunotherapy, and cardiovascular disease[732]. Other *Bacteroidetes* families were involved as well, including *Bacteroidaceae* and *Prevotellaceae*, which increased with age in α-Gal A -/0 mice (Fig. 25-26). It should be noted that all these families include the major gut microbiota producers of propionate, an SCFA whose fecal levels were consistently found to be increased in α-Gal A -/0 mice, especially with advancing age (Fig. 29)[733]. Although generally considered a beneficial molecule, when in excess, propionate may be related to metabolic and neurodegenerative disorders, possibly through impairment of the urea cycle, as well as the citrate cycle and related enzymes[365,734]. Not least, elevated endogenous levels of SCFAs, particularly propionate, have been found in the IBS mouse model and IBS patients (particularly those with the diarrhea-predominant subtype), and suggested to be involved in the pathogenesis through the

alteration of the gut serotonergic system, with increased motility, and induction of visceral hypersensitivity[735–738]. For example, Shaidullov and colleagues demonstrated in a mouse model of IBS that had visceral hypersensitivity to CRD, diarrhea, and increased concentration of SCFAs, quite similar to what we found in our Fabry model, that the increased transit rate was associated with a disbalance of activating and inhibiting the action of SCFAs due to chronically elevated SCFAs[736]. In addition, it was seen that SCFAs could also act at the epigenetic level. Specifically, intracellular butyrate and propionate as well as acetate would inhibit the activity of HDACs, promoting hyperacetylation of histones. HDACs are involved in brain development and several neuropsychiatric diseases, including depression, schizophrenia, Alzheimer's disease, and addiction. Preclinical studies in rodents suggest also that HDAC inhibitors act as cognitive enhancers in processes related to fear, anxiety, and trauma[739–741]. Finally, propionate can increase levels of certain hormones linked to the hallmarks of metabolic syndrome, like insulin resistance, hyperinsulinemia and hyperglycemia, typical of diabetes. Indeed, what has emerged is that chronic exposure to the toxic ingredient not only induces insulin resistance in mice but also causes gradual weight gain[742].

Young α-Gal A -/0 mice also had higher proportions of *Deferribacteraceae*, a family potentially linked to intestinal inflammation, while older ones had higher proportions of other taxa with pathogenic potential, such as *Streptococcaceae* and *Erysipelotrichaceae*, and smaller amounts of *Helicobacter,* another genus recognized as part of the healthy core gut microbiota of mice (Fig. 24-25-26)[721]. Collectively, the compositional alterations found in the FD model were reflected in a sharply distinct predicted metagenome, which among others exhibited increased dissimilatory sulfate reduction, propionate synthesis and proteolytic capabilities (i.e., degradation of amino acids, especially tryptophan), while reduced core metabolic activities and housekeeping functions, such as those related to sugar degradation, glycolysis and the citrate cycle (Fig. 27). It should be remembered that the dissimilatory sulfate reduction pathway leads to the production of hydrogen sulfide, a highly toxic compound that induces inflammatory responses and DNA damage, and has already been associated with GI symptoms, also in the context of IBS and IBD[743,744]. As regards tryptophan, its increased degradation combined with the reduced kynurenine synthesis and the increased synthesis/degradation of quinolinic acid seem to suggest an increased disposal of this amino acid via the kynurenine pathway and therefore its reduced availability for enteric production of serotonin[745]. Finally, α-Gal A -/0 mice also showed increased degradation of gamma-hydroxybutyric acid (a neurotransmitter that inhibits intestinal peristalsis) and increased synthesis (and reduced

degradation) of p-cresol (Fig. 28), a microbial metabolite resulting from tyrosine, which has been hypothesized to impair the central dopamine balance and social reward circuit, possibly inducing autistic-like behaviours in mice[746,747].

As we hypothesized, gut microbiota results in FD provided evidence of an early compositional and functional dysbiosis of the gut microbiota in Fabry mice, which partly persisted with advancing age. Interestingly, most of the dysbiotic features suggested a disruption of gut homeostasis and impaired communication along the gut-brain axis.

Given the several evidences concerning the microbiota-CNS interactions, including, for example, in the development of visceral and neuropathic pain it is reasonable to speculate that the gut microbiota may also be linked to the pain modulation physiology via pain receptors, comprising TRPs channels[428,436]. Albeit the exact mechanism is not fully understood, it is believed that upregulation and/or sensitization of nociceptors, including opioid and cannabinoid receptors play a crucial role in altering pain signaling[493,748,749]. In the context of FD, the study of pain-associated ion channel expression is a hot topic that has been widely addressed, but not at the GI level. The same laboratory in which the results of the present work were collected had demonstrated an over-expression of TRPV1 in epidermal neuronal fibers of forepaws and DRG neurons correlated with heat hyperalgesia in young α-Gal A -/0 mice[94,95]. Subsequently, an increase in neuronal TRPV1 immunoreactivity in DRG neurons associated with heat hypersensitivity in young α-Gal A -/0 mice, which may turn into heat hyposensitivity with aging due to stress-induced degeneration of peripheral afferents, was also demonstrated[172,750]. However, alterations in the expression or function of TRPs may not only be a cause of neuropathic pain, but also of GI visceral pain. Indeed, it is well known that TRP channels are expressed throughout the GI tract and act as sensors and molecular transducers, playing a role in regulating several GI functions[748,751]. Several studies have shown that they are expressed by primary afferent sensory neurons arising from the ganglia and enteric neurons[456,752]. Emerging evidence also demonstrated their presence in non-neuronal GI cells, including enterocytes and enterochromaffin cells[753]. The implication of TRP channels in the pathophysiological mechanisms of the GI tract and the changes in their expression and activity related to VHS, IBS, IBD, intestinal fibrosis, and GI cancers aroused interest in their therapeutic exploitation[453,754,755]. Indeed, growing data indicate TRP channels as potential targets for novel effective analgesics in GI pathologic conditions. Hence the recent interest of several companies in research screening to identify TRP modulators. So far, TRPV1, TRPV4, TRPA1 and TRPM8 channels have been largely studied for their implication in visceral pain[458].

As we described, the FD mouse model exhibits diarrhea and VHS. The pathogenesis of VHS is complex and multifactorial, involving neuronal, immune, and endocrine signaling pathways, but may also result from altered signaling between the gut and CNS, and consequently even TRP channels[756]. Thus, to investigate the involvement of ion channels, we assessed TRPV1, TRPV4 and TRPA1 expression in colon and DRG sections and in lumbosacral DRG neurons. Although aware of the limitation given by quantifying expression in terms of fluorescence, which does not necessarily overlap with the activity, the expression of these channels reported an altered pattern, with expressions generally increased in α-Gal A -/0 mice compared with controls. In particular, TRPV1 was found to be the most involved. Starting from the youngest mice up to T3, its fluorescence is markedly increased in affected mice compared with controls at both tissue and neuronal levels (Fig. 30-33). TRPV1 is probably the most extensively studied subtype with regard to both somatic and visceral pain processing. It has been found to play a role in gut inflammation, pain and hyperalgesia. In addition, TRPV1 is upregulated and sensitized during episodes of inflammation, and its expression at the mucosal level has been discovered to be pain severity-related in functional disorders, including IBS, ulcerative colitis, and Crohn's disease[757]. In addition, colorectal pain sensitivity decreases with the use of TRPV1 antagonists and in TRPV1-KO mice[671,758]. It has also been shown that TRPV1 upregulation and sensitization causing hyperalgesia are also influenced by inflammatory mediators and endocrine factors produced by the gut microbiota such as histamine, serotonin, and nerve growth factor[457,485]. Similarly, biopsies from patients with functional inflammatory disorders also show channel upregulation in nociceptive afferent neurons. It has been reported that in the mouse colon, TRPV1 allows upregulated release of CGRP and SP neuropeptides[757,759]. Therefore, it is reasonable to assume that its involvement may also occur in the Fabry mice. Since there is abundant evidence that TRPV1 activity is crucial in colorectal sensation and neurogenic inflammation of pathologies similar to what occurs in the α-Gal A -/0 mouse colon, we might hypothesize that it represents an attractive target for pharmacological treatment of Fabry-related GI symptoms. However, further investigation into the functionality of the channel would be appropriate, as would also be of interest to assess mRNA levels to understand whether this increase is a pre- or post-transcriptional event. Furthermore, considering the proximity between TRPV1 positive sensory neurons and the gut microbiota[760] and given the compositional alteration found in Fabry mice, it is plausible to assume that factors secreted by it may somehow play a relevant role. As for TRPV4, expressed by primary afferent sensory neurons, epithelial cells, and inflammatory cells infiltrating the intestine[761,762], differences between α-Gal A -/0 and α-Gal A +/0 were not found at

T1 and T2, but at T3 the increase in Fabry animals is marked, suggesting a role for the channel only at later ages (Fig. 34-35). Unlike TRPV1, which has been extensively studied in FD, TRPV4, to the best of our knowledge, has never been studied in relation to FD even at the somatic level, making parallels more complicated. However, increasing evidence supports that TRPV4 activation may trigger VHS by playing a key role in hyperalgesia and exert a pro-inflammatory effect[448,503]. The hypothesis, also potentially translatable to our murine model, is that TRPV4 potentiates the pro-algetic effects of histamine and serotonin and co-localizes with protease-activated receptor-2, causing mechanical hyperalgesia in the mouse colon[493,498,763]. In addition, TRPV4 overexpression emerged in the colitis-inflamed tissue and its activation induced somatic and visceral pain[503,764]; in fact, in recent studies the potential use of two TRPV4 antagonists in the treatment of VHS has been suggested. Further, *in vitro* studies on TRPV4 expressed by epithelial cells have also shown that its activation triggers IL-8 production in mucosal cells, also suggesting a role in inflammation through a non-neuronal mechanism[765]. Again, as with TRPV1, further functional studies could help the understanding of the exact pathophysiological mechanism in FD as well, and explain the late onset of such increased expression.

Finally, looking at TRPA1 expression, even though the differences in statistical terms between α-Gal A -/0 and α-Gal A +/0 mice are not so marked, it is interesting to note the trend over time (Fig. 36-37). Indeed, Fabry mice show a progressive increase in channel expression, whereas healthy animals a decrease with increasing age. In addition, it should be noted that this quantification of expression was done by considering only fluorescence of the cellular body and not of the fibers, which in this case were instead found to be TRPA1-positive in α-Gal A -/0, resulting in a likely underestimation of the true expression. Despite not being at the GI level, the study of TRPA1 has already been addressed in relation to FD. In fact, Miller and colleagues (2018) demonstrated that TRPA1 is sensitized in Fabry rat sensory neurons and that its antagonists reversed the behavioral mechanical sensitization. They concluded that TRPA1 might be a potentially novel target to treat the pain experienced by patients with FD[515]. It is also of interest to mention that TRPV1 and TRPA1 channels interact with each other in controlling the sensitization of DRG neurons[766]. Recent studies have recognized that TRPA1 participates in inflammatory responses and the establishment of mechanical and chemical hypersensitivity in the colon[456,767]. Stimulation of TRPA1 induces Ca^{2+}-mediated secretion of substance P, CGRP, and other transmitters from afferent nerve fibers, which ultimately results in inflammation and VHS[768]. TRPA1 channels can be also activated by bacterial lipopolysaccharide, by inducing acute intestinal inflammation and visceral pain, associating gut

microbiota-epithelium interactions with the potential role of microorganisms and microbial metabolites[769]. Moreover, higher levels of TRPA1 were identified in the intestines of colitis or Crohn's disease murine models[770]. Similarly, mouse models of IBS exhibit increased TRPA1 function in the sensory ganglia and colon[771]. These observations, taken together with our observed progressive age-dependent increase in TRPA1 expression in α-Gal A -/0 mice suggest a role for the channel in the progression and subsistence of VHS in FD.

Overall, the collected data on the expression of these channels at the GI level provide an initial semi-quantitative characterization in Fabry mice, mirroring clear alterations. Therefore, the countless shreds of evidence associated with other GI disorders largely akin to FD suggest that an altered pattern of their expression may underlie the GI pathogenesis mechanisms. In this context, in support of the hypothesized significant role of ion channels, it could be hypothesized that such general overexpression of fluorescence in KO mice is probably due to a greater number of channels/receptors present in them than in WT. This is because, although affected mice show significantly larger neuronal bodies from a size point of view (Fig. 38), at the time of analysis on DRG neurons, the value obtained has been normalized for their area; moreover, in previous morphological analyses on cross-sections of the colon, an enlargement of the ganglia had been found that was not accompanied by a numerical proportional increase in neuronal cells within them. However, not only will it be necessary to proceed to more precise quantification of their expression, pre- and post-transcriptionally (for example by PCR-quantitative and western blot), but also to assess their functionality by calcium-imaging and electrophysiology. In addition, it will be interesting to investigate the expression of other ion channels known to be drawn into pain perception and GI disorders, such as NaV 1.7, NaV 1.8 and NaV 1.9. Indeed, several members of this family are altered in several functional GI disorders and their expression and functionality were found to be changed in different murine models of FD, even if not at GI level[94,772,773].

To conclude by addressing what was our AIM 2, it is necessary to take a step back. Notwithstanding, as previously mentioned there are no studies in which the characteristic microbial profile of the disease has been evaluated, the idea of its involvement is not new. Indeed, in a study by Aguilera-Correa and colleagues (2019), it had been hypothesized that the metabolic imbalance that occurs in FD could act directly on the biology of gut bacteria[76]. However, the aim of the study was not to characterize the Fabry microbiota but to assess whether a clinically relevant concentration of lyso-Gb3, a diagnostic marker of the disease, could influence its composition. In addition, the study was not performed directly on human or animal samples, but through *in vitro* models far from mimicking

148

the complexity of the pathology[76,774]. For this reason, the comparison between the two studies is ineffective. What emerged from their analysis was increased growth of *Bacteroides fragilis* in individual and multispecies biofilm assays and in simulated suspensions of microbiota. Additionally, lyso-Gb3 altered the amount of SCFAs, mainly butyrate. The authors postulated that the reduction of butyrate releases from histone deacetylase inhibition allowed inflammation. Besides, it could trigger the Gb3 synthase, thus increasing the formation of lyso-Gb3, and worsening kidney and heart conditions[76,775]. But the authors themselves point out that other Fabry-related glycosphingolipids, such as Gb3 or lactosylceramide, which could theoretically be present in bile or within sloughing enterocytes, could also modulate the microbiota[71,72,776]. Indeed, our results on microbiota and SCFAs directly from the murine model show different findings.

However, this work is the first to reveal a possible direct relationship between lyso-Gb3 and GI conditions in FD. It has previously been reported that plasma lyso-Gb3, which can increase up to several hundred-fold to normal control values, compared to the 2-fold increase observed in serum Gb3, contributes to the pathogenesis of renal, vascular, and neuronal injury[777]. Lyso-Gb3 has been shown to promote Notch1-mediated inflammatory and fibrogenic responses in podocytes[75]. Furthermore, direct administration of lyso-Gb3 to sensory neurons *in vitro* has been observed to greatly potentiate voltage-dependent Ca^{2+} channels and lead to enhanced intracellular Ca^{2+} levels[70]. Also in the tissues, an important growth in lyso-Gb3 concentrations has been described in the liver and intestine of FD mice, significantly exceeding plasma levels[71]. However, to date, though the fact that GI symptoms stem from the deposits within intestinal tissues is now widely accepted, the effects of lyso-Gb3 on GI physiology had not been examined yet[137]. So this thesis work represents the first in which its direct effects on intestinal epithelium and ENS are examined.

In the first set of experiments, as reported in Figure 41, we observed that 3 µM lyso-Gb3 gradually increased basal I_{sc}. Instead, higher or lower concentrations, albeit trending in a similar direction, did not have a significant effect (Fig. 40), suggesting that there is a specific concentration range at which lyso-Gb3 itself induces intestinal dysfunction. Whilst this might appear surprising, it is likely that, at higher concentrations, counteracting pathways are activated leading to an apparent saturation of the system. This may include a lyso-Gb3-mediated inhibition of α-Gal A leading to the accumulation of Gb3 in the cell and, although it hasn't been shown for enterocytes, likely induces cell dysfunction and cell-death[61,775]. Since I_{sc}, or the net sum of all ionic currents across the epithelium, requires intact epithelial cells and enteric neurons, Gb3-induced cell damage could reduce lyso-Gb3-induced currents[542]. Nevertheless, the fluctuations in this parameter are considered an indicator that the

net fluid transport across the epithelium has changed. Indeed, in Ussing chambers, an increase of I_{sc} indicates an increase in cation absorption and anion secretion and/or a decrease in cation secretion and anion absorption. In the colon, changes in I_{sc} are mostly due to changes in Cl^- and Na^+ currents, with an increase usually representing Cl^- secretion and/or Na^+ absorption[623]. However, that I_{sc} alone is a relatively simple measure that cannot reflect the complexity of physiology is known[625]. To further investigate the ionic nature of the changes, pharmacological tools such as those applied in the present study may be useful. In addition, we should consider the limit given by the use of stripped tissue, lacking the MP and associated muscle layers, which while affecting viability, may lead to an underestimation of I_{sc} responses to certain stimulants, particularly those involving a myenteric reflex, such as GABA-stimulated ion transport[626,657]. Moreover, the impacts of tissue preparation and dissection could also activate stretch receptors and the subsequent release of potentially confounding compounds. However, the administration of CCh and FSK, together with the measurement of TEER (two operations that were always performed in the experiments presented and reported no difference between treated and untreated tissues) provide a useful tool to verify tissue viability and integrity. Briefly, TEER represents an overall measurement of the entire exposed area and consists of para-cellular (between cells) and trans-cellular (regulated by basal/apical transporters) resistance in parallel. Therefore, while it is usefully used as a direct indicator of physical "tightness," it is not always so for permeability and barrier function. Indeed, differences at the level of tight junctions involved in paracellular permeability do not always translate into a change in TEER and barrier integrity, although they may affect transport function[665].

Thus, once the direct effect of the metabolite on transepithelial ion transport was identified, we wondered by whom the impact of lyso-Gb3 on basal I_{sc} was mediated and whether this could in turn have an effect on either epithelium-mediated or neuro-mediated secretion. In order to do this, we applied blockers prior to lyso-Gb3 treatment to assess whether the lack of function of certain components, such as CTCF, neurons and NKCC1, could alter the response to lyso-Gb3.

Firstly, we blocked the TTX-sensitive neurons (Fig. 42) and no effect was recorded on the lyso-Gb3-induced current compared to controls; hence, the TTX-sensitive neuronal mediation was ruled out. Then, we tested the involvement of CFTR-mediated Cl^- secretion using PPQ (Fig. 43 A-B). PPQ however was unable to inhibit lyso-Gb3-induced I_{sc}. The notion that lyso-Gb3-induced I_{sc} is not mediated by Cl^- secretion is also supported by our finding that the induced current was larger when basolateral Cl^- absorption through NKCC1 (leading to less available secretory Cl^-) was inhibited using furosemide (Fig. 43 C-D). Since furosemide and its paralogue bumetanide inhibit NKCC (and KCC),

they do not only affect Cl⁻but also K^+ and Na^+ homeostasis, leading to a decrease of baseline current under NKCC-inhibition and in NKCC1-deficient mice in the cecum and early distal colon as well as a decrease of most secretory stimuli including FSK-, CCh and propionate-induced currents[778–780]. However, FSK still induces a significant increase in I_{sc} in bumetanide-treated and NKCC1-KO ceca which suggests that colonic epithelial secretion is at least in part mediated by other anions. Indeed, it has been found that propionate-induced bumetanide-insensitive current is dependent upon HCO_3^- and that FSK-induced currents in NKCC1-deficient animals are also driven by HCO_3^-. Apical HCO_3^- secretion is mediated either through CFTR or Cl⁻/ HCO_3^- exchanger pendrin. Since CFTR inhibition with PPQ did not reduce lyso-Gb3-induced current, it would appear that lyso-Gb3 induces an HCO_3^- - current which increased in the presence of furosemide because of the relatively higher concentration of HCO_3^- in the cells and the need for non-NKCC1-mediated Cl⁻. Although the importance of pendrin-dependent Cl⁻/HCO_3^-- exchange is still somewhat unclear, future research will investigate this by using pharmacological targeting of non-CFTR Cl⁻ channels and ion displacement approaches.

In support of this hypothesis, we need to remind that among the main anions in the faces there are SCFAs and HCO_3^- [781,782]. Several observations indicate that HCO_3^- secretion is also important in both normal individuals and those with diarrhea[783]. Stool water in most diarrheal disorders frequently has a high HCO_3^- concentration, whereas the metabolic acidosis observed in some patients with severe diarrhea is caused by sustained stool bicarbonate losses[784]. Furthermore, in *in vivo* studies, HCO_3^- concentrations are high in experimentally induced fluid secretion[785].

The colon has an important function in regulating fecal water content and stool consistency. To reduce water content in the stool, sodium chloride is actively absorbed to create an osmotic gradient for water. This occurs through DRA-mediated (down-regulated in adenoma) HCO_3^- anion exchange with Cl⁻ which is coupled with the NHE-mediated Na^+/H^+ exchange to allow electroneutral absorption of sodium chloride and water[786]. Entry of HCO_3^- for secretion across the apical membrane is mediated by NaHCO3 cotransporters at the basolateral membrane, or is generated intracellularly via spontaneous and catalyzed hydrolysis of CO_2[787]. Diffusion of CO_2 and its hydration by cellular anhydrases, intracellular metabolism, or entry from plasma via transport of HCO_3^- coupled anions or cations from the basal membrane can contribute to the HCO_3^- intracellularly influx. In turn, HCO_3^- secretion may occur via channels or related to the inward movement of Cl⁻ in the small intestine and proximal colon through Cl⁻/HCO_3^- exchange and through HCO_3^-/SCFA- exchange in the colon[782,788,789].

Overall, our data suggest that FD-associated diarrhea may be directly caused by lyso-Gb3-induced modulation of this process. We observed a CFTR-independent current that was bigger when NKCC1 was inhibited compared to control conditions suggesting that it might involve DRA anion exchanger. In addition to understanding the acute effects of lyso-Gb$_3$ on baseline I$_{sc}$, one of the tasks was to investigate how exposure to lyso-Gb$_3$ would modulate well-characterized secretion-inducing pathways, to model lyso-Gb$_3$ accumulation in FD patients. Neuronal regulation of ion transport is an essential homeostatic mechanism for maintaining fluid and electrolyte balance. The ENS exerts control of secretory and absorptive processes via tonically active submucosal secretomotor neurons. These neurons release cholinergic and noncholinergic neurotransmitters from nerve endings surrounding the basement membrane of the enterocyte and stimulate a Cl$^-$-dependent secretory response. These neurons are modulated by neural inputs from other intrinsic neurons and by inhibitory inputs from extrinsic sympathetic nerves. In addition, there is evidence that capsaicin-sensitive sensory nerves may constitute an important neural network that modulates GI function. We found that lyso-Gb$_3$ increased veratridine- and capsaicin-induced secretion. Regarding the former, as reported in Figure 45 B, the effect is not significant but the involvement is clearly discernable. Instead, as the latter (Fig. 45 C-D) the impact is likely to be significant. Veratridine evokes neuron-mediated secretory currents by depolarizing intrinsic neurons via increased permeability through voltage-gated Na$^+$ channels. This secretory response is caused by a net increase in Cl$^-$ secretion[790]. It has been shown to stimulate the release of enteric neurotransmitters such as substance P, VIP and Ach. Secretomotor neurons immunoreactive to VIP in the submucosal plexus are involved in mediating bacterial toxin-induced hypersecretion leading to diarrhea. VIP neurons become hyperexcitable after mucosal exposure to cholera toxin, suggesting that manipulating the excitability of these neurons could be therapeutic[791]. As for the capsaicin, the results suggest a very specific effect on TRPV1-expressing neurons. Regarding the role of TRPV1 in visceral pain and GI disorders in general, including those related to diarrhea, it has already been discussed extensively in the section on ion channels. Here, we might propose that lyso-Gb3 is able to modulate capsaicin-mediated secretion, either directly or through the activation of enteric secretomotor neurons. Moreover, whilst traditionally TRPV1 expression is linked to neurons, more recently it has been demonstrated that epithelial cells also express this ion channel suggesting that increased capsaicin-induced signals could also be mediated by lyso-Gb$_3$-induced changes within the epithelial cell. However, given that neither the response to FSK nor CCh were altered following pre-

treatment with lyso-Gb$_3$ (Fig. 44), we hypothesized that it indeed acts through modulation of neuronal secretion.

Taken together our findings indicate an effect of lyso-Gb3 on I$_{sc}$, hypothetically mediated by HCO$_3^-$, (or at any rate not by CFTR or the TTX-sensitive neuronal component) which impacts capsaicin-induced secretion, suggesting a key role of the compound in altered permeability and diarrheal disorders. However, the comprehension of the mechanisms remains to be elucidated and needs further investigation. Nevertheless, it is reasonable to think that the altered secretion or absorption mechanisms are those that lead to the onset of lyso-Gb3-dependent diarrhea, rather than changes in contractile capacity since the null effect observed on Organ Bath (Fig. 46). In addition, although these results are indicative of a potential direct effect of lyso-Gb3 on GI disturbances in FD, it would be worthwhile to evaluate basal I$_{sc}$ on the colon of our mouse model, to assess whether other products of the lipid metabolism involved in addition to lyso-Gb3 may play a role in the pathogenesis of FD GI disorders.

CONCLUSIONS & FUTURE PERSPECTIVES

The α-Gal A -/0 murine model of FD is validated as a model for the study of GI symptoms enabling its use in research to investigate the pathogenetic mechanisms.

It is reasonable to speculate on a future key role of the microbiota for the development of individual-specific diets to adjuvant the common therapies, although further investigations are needed especially in patients. To this end, a collaborative project is already ongoing with "Bellaria Hospital" in Bologna to analyze the fecal microbiota of Fabry patients.
In this context, some of our preliminary findings on the CNS and the memory and learning capacities in Fabry mice, as well as neuroinflammation and neurogenesis, suggest and enhance the gut-brain axis involvement in FD.

The different ion channels' molecular expression in the gut wall and ENS neurons of Fabry mice, makes the ion channels an attractive potential target for the development of pharmacological treatments specifically designed for GI symptoms of Fabry patients.
Additionally, along with a quantification of their expression by molecular methods more sensitive (such as qPCR or ddPCR), to consolidate the knowledge of their function in the GI tract of the mouse model, the future goal is to characterize them electro-physiologically. To this end, we have recently developed a primary neuronal cultures protocol from ENS of adult mice, which will allow us to analyze the functionality by patch-clamp and calcium imaging. Moreover, it will then be possible to characterize neuronal and glial populations at the level of the myenteric and submucosal plexuses to highlight any differences between α-Gal A -/0 and α-Gal A +/0 mice.

By staying in the context of possible molecular players which contribute to the altered molecular/functional changes found, it is important to keep in mind that the ion channels investigated here may in all likelihood not be the only ones involved, and the picture could be much more complex. Therefore, a genome-wide trascriptional approach could be envisioned in the future to extend the horizon of investigation.

Finally, lyso-Gb3 once again emerges not only as a simple marker of pathology. Its potentially causal role in gastrointestinal pathogenesis, with a direct impact on the control of ion and electrolyte secretion, and thus fluid secretion, occurs overwhelmingly. Given these initial findings, it will be

interesting to evaluate in the Ussing chamber the responses of the Fabry mouse colonic epithelium to also assess the effect of the co-presence of deposits of other substrates, such as Gb3.

REFERENCES

1. Wanner C, Germain DP, Hilz MJ, Spada M, Falissard B, Elliott PM. Therapeutic goals in Fabry disease: Recommendations of a European expert panel, based on current clinical evidence with enzyme replacement therapy. *Mol Genet Metab*. 2019;126(3):210-211. doi:10.1016/J.YMGME.2018.04.004

2. Lenders M, Brand · Eva. Fabry Disease: The Current Treatment Landscape. *Drugs*. 2021;81:635-645. doi:10.1007/s40265-021-01486-1

3. Michaud M, Mauhin W, Belmatoug N, et al. Maladie de Fabry : quand y penser ? *Rev Med Interne*. 2021;42(2):110-119. doi:10.1016/J.REVMED.2020.08.019

4. Ortiz A, Germain DP, Desnick RJ, et al. Fabry disease revisited: Management and treatment recommendations for adult patients. *Mol Genet Metab*. 2018;123(4):416-427. doi:10.1016/J.YMGME.2018.02.014

5. Germain DP. Fabry disease. *Orphanet J Rare Dis*. 2010;5(1). doi:10.1186/1750-1172-5-30

6. Tuttolomondo A, Pecoraro R, Simonetta I, Miceli S, Pinto A, Licata G. Anderson-Fabry Disease: A Multiorgan Disease. *Curr Pharm Des*. 2013;19(33):5974-5996. doi:10.2174/13816128113199990352

7. Schiffmann R, Warnock DG, Banikazemi M, et al. Fabry disease: progression of nephropathy, and prevalence of cardiac and cerebrovascular events before enzyme replacement therapy. *Nephrology Dialysis Transplantation*. 2009;24(7):2102. doi:10.1093/NDT/GFP031

8. Vedder AC, Linthorst GE, van Breemen MJ, et al. The Dutch Fabry cohort: diversity of clinical manifestations and Gb3 levels. *J Inherit Metab Dis*. 2007;30(1):68-78. doi:10.1007/S10545-006-0484-8

9. Germain DP. General aspects of X-linked diseases. *Fabry Disease: Perspectives from 5 Years of FOS*. Published online 2006. Accessed December 5, 2022. https://pubmed.ncbi.nlm.nih.gov/21290690/

10. de Onis M. X-chromosome inactivation: role in skin disease expression. *Acta Paediatr Suppl*. 2006;95(451):16-26. doi:10.1080/08035320600618775

11. Wilcox WR, Oliveira JP, Hopkin RJ, et al. Females with Fabry disease frequently have major organ involvement: Lessons from the Fabry Registry. *Mol Genet Metab*. 2008;93(2):112-128. doi:10.1016/J.YMGME.2007.09.013

12. Echevarria L, Benistan K, Toussaint A, et al. X-chromosome inactivation in female patients with Fabry disease. *Clin Genet*. 2016;89(1):44-54. doi:10.1111/CGE.12613

13. Baldacci Amici P Bonola E Betto G Fogliani E Refatti EA, Fooolt A, Agraria Milano J. Gene Action in the X-chromosome of the Mouse (Mus musculus L.). *Nature 1961 190:4773*. 1961;190(4773):372-373. doi:10.1038/190372a0

14. Miller JJ, Kanack AJ, Dahms NM. Progress in the understanding and treatment of Fabry disease. *Biochim Biophys Acta Gen Subj*. 2020;1864(1). doi:10.1016/j.bbagen.2019.129437

15. Mehta A, Hughes DA. Fabry Disease Synonyms: Alpha-Galactosidase A Deficiency, Anderson-Fabry Disease. Published online 2002:1993-2022.

16.   Spada M, Pagliardini S, Yasuda M, et al. High Incidence of Later-Onset Fabry Disease Revealed by Newborn Screening. *Am J Hum Genet*. 2006;79(1):31. doi:10.1086/504601

17.   Gragnaniello V, Burlina AP, Polo G, et al. Newborn Screening for Fabry Disease in Northeastern Italy: Results of Five Years of Experience. *Biomolecules*. 2021;11(7). doi:10.3390/BIOM11070951

18.   Wittmann J, Karg E, Turi S, et al. Newborn Screening for Lysosomal Storage Disorders in Hungary. *JIMD Rep*. 2012;6:117. doi:10.1007/8904_2012_130

19.   Mechtler TP, Stary S, Metz TF, et al. Neonatal screening for lysosomal storage disorders: feasibility and incidence from a nationwide study in Austria. *Lancet*. 2012;379(9813):335-341. doi:10.1016/S0140-6736(11)61266-X

20.   Colon C, Ortolano S, Melcon-Crespo C, et al. Newborn screening for Fabry disease in the north-west of Spain. *Eur J Pediatr*. 2017;176(8):1075-1081. doi:10.1007/S00431-017-2950-8

21.   Burton BK, Charrow J, Hoganson GE, et al. Newborn Screening for Lysosomal Storage Disorders in Illinois: The Initial 15-Month Experience. *J Pediatr*. 2017;190:130-135. doi:10.1016/J.JPEDS.2017.06.048

22.   Hinton CF, Homer CJ, Thompson AA, et al. A framework for assessing outcomes from newborn screening: on the road to measuring its promise. *Mol Genet Metab*. 2016;118(4):221. doi:10.1016/J.YMGME.2016.05.017

23.   Hwu WL, Chien YH, Lee NC, et al. Newborn screening for Fabry disease in Taiwan reveals a high incidence of the later-onset GLA mutation c.936+919G>A (IVS4+919G>A). *Hum Mutat*. 2009;30(10):1397-1405. doi:10.1002/HUMU.21074

24.   α-Galactosidase A Deficiency: Fabry Disease | The Online Metabolic and Molecular Bases of Inherited Disease | OMMBID | McGraw Hill Medical. Accessed December 5, 2022. https://ommbid.mhmedical.com/content.aspx?bookid=2709&sectionid=225546984

25.   Bishop DF, Kornreich R, Desnick RJ. Structural organization of the human alpha-galactosidase A gene: further evidence for the absence of a 3' untranslated region. *Proc Natl Acad Sci U S A*. 1988;85(11):3903-3907. doi:10.1073/PNAS.85.11.3903

26.   Kornreich R, Desnick RJ, Bishop DF. Nucleotide sequence of the human alpha-galactosidase A gene. *Nucleic Acids Res*. 1989;17(8):3301-3302. doi:10.1093/NAR/17.8.3301

27.   Ioannou YA, Zeidner KM, Grace ME, Desnick RJ. Human alpha-galactosidase A: glycosylation site 3 is essential for enzyme solubility. *Biochem J*. 1998;332 (Pt 3)(Pt 3):789-797. doi:10.1042/BJ3320789

28.   Stenson PD, Mort M, Ball E v., et al. The Human Gene Mutation Database: towards a comprehensive repository of inherited mutation data for medical research, genetic diagnosis and next-generation sequencing studies. *Hum Genet*. 2017;136(6):665-677. doi:10.1007/S00439-017-1779-6

29.   Ortiz A, Germain DP, Desnick RJ, et al. Fabry disease revisited: Management and treatment recommendations for adult patients. *Mol Genet Metab*. 2018;123(4):416-427. doi:10.1016/J.YMGME.2018.02.014

30.   Garman SC, Garboczi DN. The molecular defect leading to fabry disease: Structure of human α-galactosidase. *J Mol Biol*. 2004;337(2):319-335. doi:10.1016/j.jmb.2004.01.035

31.   Desnick RJ. Fabry disease: α-galactosidase A deficiency. In: *Rosenberg's Molecular and Genetic Basis of Neurological and Psychiatric Disease: Volume 1*. Elsevier; 2020:575-587. doi:10.1016/B978-0-12-813955-4.00042-8

32.   Passaglia Bernardes T, Foresto RD, Kirsztajn GM. Fabry disease: genetics, pathology, and treatment. *REV ASSOC MED BRAS*. 2020;66(1):10-16. doi:10.1590/1806-9282.66.S1.10

33.   Desnick RJ, Wasserstein MP, Banikazemi M. Fabry disease (alpha-galactosidase A deficiency): renal involvement and enzyme replacement therapy. *Contrib Nephrol*. 2001;136(136):174-192. doi:10.1159/000060184

34.   Oder D, Liu D, Hu K, et al. α-Galactosidase A Genotype N215S Induces a Specific Cardiac Variant of Fabry Disease. *Circ Cardiovasc Genet*. 2017;10(5). doi:10.1161/CIRCGENETICS.116.001691

35.   Germain DP, Oliveira JP, Bichet DG, et al. Use of a rare disease registry for establishing phenotypic classification of previously unassigned GLA variants: a consensus classification system by a multispecialty Fabry disease genotype-phenotype workgroup Genotype-phenotype correlations. *J Med Genet*. 2020;57:542-551. doi:10.1136/jmedgenet-2019-106467

36.   Oder D, Liu D, Üçeyler N, et al. Clinical impact of the alpha-galactosidase A gene single nucleotide polymorphism -10C>T: A single-center observational study. *Medicine (United States)*. 2018;97(21). doi:10.1097/MD.0000000000010669

37.   Caputo F, Lungaro L, Galdi A, et al. Gastrointestinal involvement in anderson-fabry disease: A narrative review. *Int J Environ Res Public Health*. 2021;18(6). doi:10.3390/ijerph18063320

38.   di Martino MT, Scionti F, Sestito S, et al. Genetic variants associated with gastrointestinal symptoms in Fabry disease. *Oncotarget*. 2016;7(52):85895-85904. doi:10.18632/ONCOTARGET.13135

39.   Encyclopedia of Biological Chemistry II | ScienceDirect. Accessed December 5, 2022. https://www.sciencedirect.com/referencework/9780123786319/encyclopedia-of-biological-chemistry-ii

40.   Comprehensive Glycoscience | ScienceDirect. Accessed December 5, 2022. https://www.sciencedirect.com/referencework/9780444519672/comprehensive-glycoscience

41.   Garman SC. Structure-function relationships in alpha-galactosidase A. *Acta Paediatr*. 2007;96(455):6-16. doi:10.1111/J.1651-2227.2007.00198.X

42.   Engelking LR. Sphingolipids. *Textbook of Veterinary Physiological Chemistry*. Published online January 1, 2015:378-383. doi:10.1016/B978-0-12-391909-0.50059-1

43.   Sueoka H, Aoki M, Tsukimura T, Togawa T, Sakuraba H. Distributions of Globotriaosylceramide Isoforms, and Globotriaosylsphingosine and Its Analogues in an α-Galactosidase A Knockout Mouse, a Model of Fabry Disease. Published online 2015. doi:10.1371/journal.pone.0144958

44.   Zelnik ID, Ventura AE, Kim JL, Silva LC, Futerman AH. The role of ceramide in regulating endoplasmic reticulum function. *Biochim Biophys Acta Mol Cell Biol Lipids*. 2020;1865(1). doi:10.1016/J.BBALIP.2019.06.015

45.   Funakoshi T, Yasuda S, Fukasawa M, Nishijima M, Hanada K. Reconstitution of ATP- and cytosol-dependent transport of de novo synthesized ceramide to the site of sphingomyelin synthesis in semi-intact cells. *J Biol Chem*. 2000;275(39):29938-29945. doi:10.1074/JBC.M004470200

46. Hanada K, Kumagai K, Yasuda S, et al. Molecular machinery for non-vesicular trafficking of ceramide. *Nature*. 2003;426(6968):803-809. doi:10.1038/NATURE02188

47. Merrill AH. Sphingolipid and glycosphingolipid metabolic pathways in the era of sphingolipidomics. *Chem Rev*. 2011;111(10):6387-6422. doi:10.1021/CR2002917

48. El-Abassi R, Singhal D, England JD. Fabry's disease. *J Neurol Sci*. 2014;344(1-2):5-19. doi:10.1016/j.jns.2014.06.029

49. Importance of glycosylation in enzyme replacement therapy - PubMed. Accessed December 5, 2022. https://pubmed.ncbi.nlm.nih.gov/21290695/

50. Ghosh P, Dahms NM, Kornfeld S. Mannose 6-phosphate receptors: new twists in the tale. *Nature Reviews Molecular Cell Biology 2003 4:3*. 2003;4(3):202-213. doi:10.1038/nrm1050

51. D'Angelo G, Capasso S, Sticco L, Russo D. Glycosphingolipids: synthesis and functions. *FEBS J*. 2013;280(24):6338-6353. doi:10.1111/FEBS.12559

52. Yamashita T, Wada R, Sasaki T, et al. A vital role for glycosphingolipid synthesis during development and differentiation. *Proc Natl Acad Sci U S A*. 1999;96(16):9142-9147. doi:10.1073/PNAS.96.16.9142

53. Hakomori S itiroh. Structure and function of glycosphingolipids and sphingolipids: recollections and future trends. *Biochim Biophys Acta*. 2008;1780(3):325-346. doi:10.1016/J.BBAGEN.2007.08.015

54. Schnarr RL, Kinoshita T. Glycosphingolipids. *Essentials of Glycobiology*. 2015;5:1-12. doi:10.1101/GLYCOBIOLOGY.3E.011

55. Lindberg AA, Brown JE, Strömberg N, Westling-Ryd M, Schultz JE, Karlsson KA. Identification of the carbohydrate receptor for Shiga toxin produced by Shigella dysenteriae type 1. *Journal of Biological Chemistry*. 1987;262(4):1779-1785. doi:10.1016/S0021-9258(19)75706-8

56. Hakomori SI. Tumor-associated carbohydrate antigens defining tumor malignancy: basis for development of anti-cancer vaccines. *Adv Exp Med Biol*. 2001;491:369-402. doi:10.1007/978-1-4615-1267-7_24

57. Kovbasnjuk O, Mourtazina R, Baibakov B, et al. The glycosphingolipid globotriaosylceramide in the metastatic transformation of colon cancer. *Proc Natl Acad Sci U S A*. 2005;102(52):19087-19092. doi:10.1073/PNAS.0506474102

58. Mangeney M, Lingwood CA, Taga S, Caillou B, Tursz T, Wiels J. Apoptosis induced in Burkitt's lymphoma cells via Gb3/CD77, a glycolipid antigen. *Cancer Res*. 1993;53(21):5314-5319. Accessed December 5, 2022. https://pubmed.ncbi.nlm.nih.gov/8221667/

59. Johansson D, Kosovac E, Moharer J, et al. Expression of verotoxin-1 receptor Gb3 in breast cancer tissue and verotoxin-1 signal transduction to apoptosis. *BMC Cancer*. 2009;9. doi:10.1186/1471-2407-9-67

60. Kang J, Rajpert-De Meyts E, Skakkebæk N, Wiels J. Expression of the glycolipid globotriaosylceramide (Gb3) in testicular carcinoma in situ. *Virchows Arch*. 1995;426(4):369-374. doi:10.1007/BF00191346

61. Sueoka H, Ichihara J, Tsukimura T, Togawa T, Sakuraba H. Nano-LC-MS/MS for Quantification of Lyso-Gb3 and Its Analogues Reveals a Useful Biomarker for Fabry Disease. *PLoS One*. 2015;10(5):e0127048. doi:10.1371/JOURNAL.PONE.0127048

62. Ikeda K, Taguchi R. Highly sensitive localization analysis of gangliosides and sulfatides including structural isomers in mouse cerebellum sections by combination of laser microdissection and

hydrophilic interaction liquid chromatography/electrospray ionization mass spectrometry with theoretically expanded multiple reaction monitoring. *Rapid Communications in Mass Spectrometry*. 2010;24(20):2957-2965. doi:10.1002/RCM.4716

63. Lee MH, Choi EN, Jeon YJ, Jung SC. Possible role of transforming growth factor-β1 and vascular endothelial growth factor in Fabry disease nephropathy. *Int J Mol Med*. 2012;30(6):1275-1280. doi:10.3892/IJMM.2012.1139/HTML

64. Satoh K. Globotriaosylceramide induces endothelial dysfunction in fabry disease. *Arterioscler Thromb Vasc Biol*. 2014;34(1):2-4. doi:10.1161/ATVBAHA.113.302744/FORMAT/EPUB

65. Choi S, Kim JA, Na HY, et al. Globotriaosylceramide induces lysosomal degradation of endothelial K Ca3.1 in fabry disease. *Arterioscler Thromb Vasc Biol*. 2014;34(1):81-89. doi:10.1161/ATVBAHA.113.302200/FORMAT/EPUB

66. Mehta A, Beck M, Eyskens F, et al. Review Fabry disease: a review of current management strategies. *Q J Med*. 2010;103:641-659. doi:10.1093/qjmed/hcq117

67. Mills K, Morris P, Lee P, et al. Measurement of urinary CDH and CTH by tandem mass spectrometry in patients hemizygous and heterozygous for Fabry disease.

68. Perrone A, Mohamed S, Donadio V, Liguori R, Contin M. A rapid and simple uhplc-ms/ms method for quantification of plasma globotriaosylsphingosine (Lyso-gb3). *Molecules*. 2021;26(23). doi:10.3390/molecules26237358

69. E Y, K M, P M, et al. Is globotriaosylceramide a useful biomarker in Fabry disease? *Acta Paediatr Suppl*. 2005;94(447):51-54; discussion 37. doi:10.1111/J.1651-2227.2005.TB02112.X

70. Choi L, Vernon J, Kopach O, et al. The Fabry disease-associated lipid lyso-Gb3 enhances voltage-gated calcium currents in sensory neurons and causes pain. *Neurosci Lett*. 2015;594:163-168. doi:10.1016/J.NEULET.2015.01.084

71. Aerts JM, Groener JE, Kuiper S, et al. *Elevated Globotriaosylsphingosine Is a Hallmark of Fabry Disease*.; 2008. www.pnas.orgcgidoi10.1073pnas.0712309105

72. Duro G, Zizzo C, Cammarata G, et al. Mutations in the GLA Gene and LysoGb3: Is It Really Anderson-Fabry Disease? *International Journal of Molecular Sciences Article Int J Mol Sci*. 2018;19:3726. doi:10.3390/ijms19123726

73. Simonetta I, Tuttolomondo A, Daidone M, Pinto A. Molecular Sciences Review Biomarkers in Anderson-Fabry Disease. doi:10.3390/ijms21218080

74. Nowak A, Beuschlein F, Sivasubramaniam V, Kasper D, Warnock DG. Lyso-Gb3 associates with adverse long-term outcome in patients with Fabry disease. *J Med Genet*. Published online 2021. doi:10.1136/jmedgenet-2020-107338

75. Sanchez-Niño MD, Carpio D, Sanz AB, Ruiz-Ortega M, Mezzano S, Ortiz A. Lyso-Gb3 activates Notch1 in human podocytes. Published online 2015. doi:10.1093/hmg/ddv291

76. Aguilera-Correa JJ, Madrazo-Clemente P, Martínez-Cuesta M del C, et al. Lyso-Gb3 modulates the gut microbiota and decreases butyrate production. *Sci Rep*. 2019;9(1). doi:10.1038/s41598-019-48426-4

77. Vedder AC, Strijland A, vd Bergh Weerman MA, Florquin S, Aerts JMFG, Hollak CEM. Manifestations of Fabry disease in placental tissue. *J Inherit Metab Dis*. 2006;29(1):106-111. doi:10.1007/S10545-006-0196-0

78. Popli S, Leehey DJ, Molnar Z v., Nawab ZM, Ing TS. Demonstration of Fabry's disease deposits in placenta. *Am J Obstet Gynecol*. 1990;162(2):464-465. doi:10.1016/0002-9378(90)90410-9

79. Mehta A, Hughes DA. Fabry Disease. *GeneReviews®*. Published online January 27, 2022. Accessed December 4, 2022. https://www.ncbi.nlm.nih.gov/books/NBK1292/

80. Nakao S, Kodama C, Takenaka T, et al. Fabry disease: detection of undiagnosed hemodialysis patients and identification of a "renal variant" phenotype. *Kidney Int*. 2003;64(3):801-807. doi:10.1046/J.1523-1755.2003.00160.X

81. Elleder M, Bradová V, Smíd F, et al. Cardiocyte storage and hypertrophy as a sole manifestation of Fabry's disease. *Virchows Archiv A 1990 417:5*. 1990;417(5):449-455. doi:10.1007/BF01606034

82. Hopkin RJ, Bissler J, Banikazemi M, et al. Characterization of Fabry disease in 352 pediatric patients in the Fabry Registry. *Pediatr Res*. 2008;64(5):550-555. doi:10.1203/PDR.0B013E318183F132

83. Wilcox WR, Oliveira JP, Hopkin RJ, et al. Females with Fabry disease frequently have major organ involvement: lessons from the Fabry Registry. *Mol Genet Metab*. 2008;93(2):112-128. doi:10.1016/J.YMGME.2007.09.013

84. Hoffmann B, Keshav S. Gastrointestinal symptoms in Fabry disease: Everything is possible, including treatment. In: *Acta Paediatrica, International Journal of Paediatrics*. Vol 96. ; 2007:84-86. doi:10.1111/j.1651-2227.2007.00216.x

85. Üçeyler N, Ganendiran S, Kramer D, Sommer C. Characterization of pain in fabry disease. *Clinical Journal of Pain*. 2014;30(10):915-920. doi:10.1097/AJP.0000000000000041

86. Charrow J. A 14-year-old boy with pain in hands and feet. *Pediatr Ann*. 2009;38(4):190-192. doi:10.3928/00904481-20090401-01

87. Politei JM, Bouhassira D, Germain DP, et al. Pain in Fabry Disease: Practical Recommendations for Diagnosis and Treatment. *CNS Neurosci Ther*. 2016;22(7):568-576. doi:10.1111/cns.12542

88. Cole AL, Lee PJ, Hughes DA, Deegan PB, Waldek S, Lachmann RH. Depression in adults with Fabry disease: a common and under-diagnosed problem. *J Inherit Metab Dis*. 2007;30(6):943-951. doi:10.1007/S10545-007-0708-6

89. Miners AH, Holmes A, Sherr L, Jenkinson C, MacDermot KD. Assessment of health-related quality-of-life in males with Anderson Fabry Disease before therapeutic intervention. *Qual Life Res*. 2002;11(2):127-133. doi:10.1023/A:1015009210639

90. Burlina AP, Sims KB, Politei JM, et al. Early diagnosis of peripheral nervous system involvement in Fabry disease and treatment of neuropathic pain: The report of an expert panel. *BMC Neurol*. 2011;11. doi:10.1186/1471-2377-11-61

91. Üçeyler N, He L, Schönfeld D, et al. Small fibers in Fabry disease: baseline and follow-up data under enzyme replacement therapy. *J Peripher Nerv Syst*. 2011;16(4):304-314. doi:10.1111/J.1529-8027.2011.00365.X

92.	Biegstraaten M, Binder A, Maag R, Hollak CEM, Baron R, van Schaik IN. The relation between small nerve fibre function, age, disease severity and pain in Fabry disease. *European Journal of Pain*. 2011;15(8):822-829. doi:10.1016/J.EJPAIN.2011.01.014

93.	Liguori R, di Stasi V, Bugiardini E, et al. Small fiber neuropathy in female patients with fabry disease. *Muscle Nerve*. 2010;41(3):409-412. doi:10.1002/MUS.21606

94.	Lakomá J, Rimondini R, Donadio V, Liguori R, Caprini M. Pain related channels are differentially expressed in neuronal and non-neuronal cells of glabrous skin of fabry knockout male mice. *PLoS One*. 2014;9(10). doi:10.1371/journal.pone.0108641

95.	Lakomá J, Rimondini R, Montiel AF, Donadio V, Liguori R, Caprini M. Increased expression of trpv1 in peripheral terminals mediates thermal nociception in fabry disease mouse model. *Mol Pain*. 2016;12:1-16. doi:10.1177/1744806916663729

96.	Möhrenschlager M, Braun-Falco M, Ring J, Abeck D. Fabry disease: recognition and management of cutaneous manifestations. *Am J Clin Dermatol*. 2003;4(3):189-196. doi:10.2165/00128071-200304030-00005

97.	Germain DP. Fabry disease: Clinical and genetic aspects. Therapeutic perspectives. *Revue de Medecine Interne*. 2000;21(12):1086-1103. doi:10.1016/S0248-8663(00)00269-1

98.	Orteu CH, Jansen T, Lidove O, et al. Fabry disease and the skin: data from FOS, the Fabry outcome survey. *Br J Dermatol*. 2007;157(2):331-337. doi:10.1111/J.1365-2133.2007.08002.X

99.	Eng CM, Germain DP, Banikazemi M, et al. Fabry disease: guidelines for the evaluation and management of multi-organ system involvement. *Genet Med*. 2006;8(9):539-548. doi:10.1097/01.GIM.0000237866.70357.C6

100.	Lee S, Chun S il. Generalized anhidrosis associated with Fabry's disease. *J Am Acad Dermatol*. 1987;17(5):883-887. doi:10.1016/S0190-9622(87)70274-6

101.	Sodi A, Ioannidis AS, Mehta A, Davey C, Beck M, Pitz S. Ocular manifestations of Fabry's disease: data from the Fabry Outcome Survey. *Br J Ophthalmol*. 2007;91(2):210-214. doi:10.1136/BJO.2006.100602

102.	Politei J, Thurberg BL, Wallace E, et al. Gastrointestinal involvement in Fabry disease: So important, yet often neglected. *Clin Genet*. 2016;89(1):5-9. doi:10.1111/cge.12673

103.	Pensabene L, Sestito S, Nicoletti A, Graziano F, Strisciuglio P, Concolino D. Gastrointestinal Symptoms of Patients with Fabry Disease. Published online 2016. doi:10.1155/2016/9712831

104.	Lenders M, Brand E. Fabry disease–a multisystemic disease with gastrointestinal manifestations. *Gut Microbes*. 2022;14(1). doi:10.1080/19490976.2022.2027852

105.	Hilz MJ, Arbustini E, Dagna L, et al. Non-specific gastrointestinal features: Could it be Fabry disease? *Digestive and Liver Disease*. 2018;50(5):429-437. doi:10.1016/j.dld.2018.02.011

106.	Morand Jack Johnson Jerry Walter Leone Atkinson Gregory Kline Aline Frey Juan Politei Raphael Schiffmann O. Symptoms and Quality of Life in Patients with Fabry Disease: Results from an International Patient Survey. *Adv Ther*. 36. doi:10.6084/m9

107.	Jerndal P, Ringström G, Agerforz P, et al. Gastrointestinal-specific anxiety: An important factor for severity of GI symptoms and quality of life in IBS. *Neurogastroenterology and Motility*. 2010;22(6). doi:10.1111/J.1365-2982.2010.01493.X

108. Polistena B, Rigante D, Sicignano LL, et al. Survey about the Quality of Life of Italian Patients with Fabry Disease. *Diseases*. 2021;9(4):72. doi:10.3390/diseases9040072

109. MacDermot KD, Holmes A, Miners AH. Anderson-Fabry disease: clinical manifestations and impact of disease in a cohort of 98 hemizygous males. *J Med Genet*. 2001;38(11):750-760. doi:10.1136/JMG.38.11.750

110. Ortiz A, Oliveira JP, Waldek S, Warnock DG, Cianciaruso B, Wanner C. Nephropathy in males and females with Fabry disease: cross-sectional description of patients before treatment with enzyme replacement therapy. *Nephrol Dial Transplant*. 2008;23(5):1600-1607. doi:10.1093/NDT/GFM848

111. Shah JS, Hughes DA, Sachdev B, et al. Prevalence and clinical significance of cardiac arrhythmia in Anderson-Fabry disease. *Am J Cardiol*. 2005;96(6):842-846. doi:10.1016/J.AMJCARD.2005.05.033

112. Okeda R, Nisihara M. An autopsy case of Fabry disease with neuropathological investigation of the pathogenesis of associated dementia. *Neuropathology*. 2008;28(5):532-540. doi:10.1111/J.1440-1789.2008.00883.X

113. Mitsias P, Levine SR. Cerebrovascular complications of Fabry's disease. *Ann Neurol*. 1996;40(1):8-17. doi:10.1002/ANA.410400105

114. Sims K, Politei J, Banikazemi M, Lee P. Stroke in Fabry disease frequently occurs before diagnosis and in the absence of other clinical events: natural history data from the Fabry Registry. *Stroke*. 2009;40(3):788-794. doi:10.1161/STROKEAHA.108.526293

115. Doheny D, Srinivasan R, Pagant S, Chen B, Yasuda M, Desnick RJ. Fabry Disease: prevalence of affected males and heterozygotes with pathogenic GLA mutations identified by screening renal, cardiac and stroke clinics, 1995-2017. *J Med Genet*. 2018;55(4):261-268. doi:10.1136/JMEDGENET-2017-105080

116. Scheidt W von, Eng CM, Fitzmaurice TF, et al. An atypical variant of Fabry's disease with manifestations confined to the myocardium. *N Engl J Med*. 1991;324(6):395-399. doi:10.1056/NEJM199102073240607

117. Marchesoni CL, Roa N, Pardal AM, et al. Misdiagnosis in Fabry disease. *J Pediatr*. 2010;156(5):828-831. doi:10.1016/J.JPEDS.2010.02.012

118. Reisin R, Perrin A, García-Pavía P. Time delays in the diagnosis and treatment of Fabry disease. *Int J Clin Pract*. 2017;71(1). doi:10.1111/IJCP.12914

119. Zar-Kessler C, Karaa A, Sims KB, Clarke V, Kuo B. Understanding the gastrointestinal manifestations of Fabry disease: Promoting prompt diagnosis. *Therap Adv Gastroenterol*. 2016;9(4):626-634. doi:10.1177/1756283X16642936

120. rn Hoffmann B, Reinhardt D, Koletzko B. *Effect of Enzyme-Replacement Therapy on Gastrointestinal Symptoms in Fabry Disease*. Vol 16. Lippincott Williams & Wilkins; 2004.

121. Hoffmann B, Reinhardt D, Koletzko B. Effect of enzyme-replacement therapy on gastrointestinal symptoms in Fabry disease. *Eur J Gastroenterol Hepatol*. 2004;16(10):1067-1069. doi:10.1097/00042737-200410000-00020

122. Schiffmann R, Pastores GM, Lien YHH, et al. Agalsidase alfa in pediatric patients with Fabry disease: a 6.5-year open-label follow-up study. *Orphanet J Rare Dis*. 2014;9:169. doi:10.1186/S13023-014-0169-6

123. Radulescu D, Crisan D, Militaru V, et al. Gastrointestinal Manifestations and Treatment Options in Fabry Disease Patients. A Systematic Review. *Journal of Gastrointestinal and Liver Diseases*. 2022;31(1):98-106. doi:10.15403/jgld-3855

124. Hoffmann B, Schwarz M, Mehta A, Keshav S. Gastrointestinal symptoms in 342 patients with Fabry disease: prevalence and response to enzyme replacement therapy. *Clin Gastroenterol Hepatol*. 2007;5(12):1447-1453. doi:10.1016/J.CGH.2007.08.012

125. Eng CM, Fletcher J, Wilcox WR, et al. Fabry disease: Baseline medical characteristics of a cohort of 1765 males and females in the Fabry Registry. *J Inherit Metab Dis*. 2007;30(2):184-192. doi:10.1007/S10545-007-0521-2

126. Martins AM, Cabrera G, Molt F, et al. The clinical profiles of female patients with Fabry disease in Latin America: A Fabry Registry analysis of natural history data from 169 patients based on enzyme replacement therapy status. *JIMD Rep*. 2019;49(1):107-117. doi:10.1002/JMD2.12071

127. Hopkin RJ, Feldt-Rasmussen U, Germain DP, et al. Improvement of gastrointestinal symptoms in a significant proportion of male patients with classic Fabry disease treated with agalsidase beta: A Fabry Registry analysis stratified by phenotype. *Mol Genet Metab Rep*. 2020;25. doi:10.1016/J.YMGMR.2020.100670

128. Nampoothiri S, Yesodharan D, Bhattacherjee A, et al. Fabry disease in India: A multicenter study of the clinical and mutation spectrum in 54 patients. *JIMD Rep*. 2020;56(1):82-94. doi:10.1002/JMD2.12156

129. Germain DP, Nicholls K, Giugliani R, et al. Efficacy of the pharmacologic chaperone migalastat in a subset of male patients with the classic phenotype of Fabry disease and migalastat-amenable variants: data from the phase 3 randomized, multicenter, double-blind clinical trial and extension study. *Genet Med*. 2019;21(9):1987-1997. doi:10.1038/S41436-019-0451-Z

130. O'brien BD, Shnitka TK, McDougall R, et al. Pathophysiologic and Ultrastructural Basis for Intestinal Symptoms in Fabry's Disease. *Gastroenterology*. 1982;82(5):957-962. doi:10.1016/S0016-5085(82)80262-X

131. Masotti M, Delprete C, Dothel G, et al. Altered globotriaosylceramide accumulation and mucosal neuronal fiber density in the colon of the Fabry disease mouse model. *Neurogastroenterol Motil*. 2019;31(3). doi:10.1111/NMO.13529

132. Rombach SM, Twickler TB, Aerts JMFG, Linthorst GE, Wijburg FA, Hollak CEM. Vasculopathy in patients with Fabry disease: current controversies and research directions. *Mol Genet Metab*. 2010;99(2):99-108. doi:10.1016/J.YMGME.2009.10.004

133. Urquhart BL, Tirona RG, Kim RB. Nuclear receptors and the regulation of drug-metabolizing enzymes and drug transporters: implications for interindividual variability in response to drugs. *J Clin Pharmacol*. 2007;47(5):566-578. doi:10.1177/0091270007299930

134. Pereira CS, Azevedo O, Maia ML, Dias AF, Sa-Miranda C, Macedo MF. Invariant natural killer T cells are phenotypically and functionally altered in Fabry disease. *Mol Genet Metab*. 2013;108(4):241-248. doi:10.1016/j.ymgme.2013.01.018

135. Kang JJ, Shu L, Park JL, Shayman JA, Bodary PF. Endothelial nitric oxide synthase uncoupling and microvascular dysfunction in the mesentery of mice deficient in-galactosidase A. *Am J Physiol Gastrointest Liver Physiol*. 2014;306:140-146. doi:10.1152/ajpgi.00185.2013.-A

136. Buda P, Ksiazyk J, Tylki-Szymaska A. Gastroenterological complications of Anderson-Fabry disease. *Curr Pharm Des*. 2013;19(33):6009-6013. doi:10.2174/13816128113199990347

137. Hilz MJ, Arbustini E, Dagna L, et al. Non-specific gastrointestinal features: Could it be Fabry disease? *Dig Liver Dis*. 2018;50(5):429-437. doi:10.1016/J.DLD.2018.02.011

138. Cozma-Petrut A, Loghin F, Miere D, Dumitrascu DL. Diet in irritable bowel syndrome: What to recommend, not what to forbid to patients! *World J Gastroenterol*. 2017;23(21):3771-3783. doi:10.3748/WJG.V23.I21.3771

139. Guo Y bin, Zhuang KM, Kuang L, Zhan Q, Wang XF, Liu S de. Association between Diet and Lifestyle Habits and Irritable Bowel Syndrome: A Case-Control Study. *Gut Liver*. 2015;9(5):649-656. doi:10.5009/GNL13437

140. Murray K, Wilkinson-Smith V, Hoad C, et al. Differential effects of FODMAPs (Fermentable Oligo-, Di-, Mono-Saccharides and Polyols) on small and large intestinal contents in healthy subjects shown by MRI. *American Journal of Gastroenterology*. 2014;109(1):110-119. doi:10.1038/AJG.2013.386

141. Staudacher HM, Whelan K. The low FODMAP diet: recent advances in understanding its mechanisms and efficacy in IBS. *Gut*. 2017;66(8):1517-1527. doi:10.1136/GUTJNL-2017-313750

142. Michaud M, Mauhin W, Belmatoug N, et al. When and How to Diagnose Fabry Disease in Clinical Pratice. *Am J Med Sci*. 2020;360(6):641-649. doi:10.1016/J.AMJMS.2020.07.011

143. Gal A, Hughes DA, Winchester B. Toward a consensus in the laboratory diagnostics of Fabry disease - recommendations of a European expert group. *J Inherit Metab Dis*. 2011;34(2):509-514. doi:10.1007/S10545-010-9261-9

144. Togawa T, Kodama T, Suzuki T, et al. Plasma globotriaosylsphingosine as a biomarker of Fabry disease. *Mol Genet Metab*. 2010;100(3):257-261. doi:10.1016/J.YMGME.2010.03.020

145. Schiffmann R, Fuller M, Clarke LA, Aerts JMFG. Is it Fabry disease? *Genet Med*. 2016;18(12):1181-1185. doi:10.1038/GIM.2016.55

146. Azevedo O, Fernandes Gago M, Miltenberger-Miltenyi G, Sousa N, Cunha D. Molecular Sciences Fabry Disease Therapy: State-of-the-Art and Current Challenges. Published online 2020. doi:10.3390/ijms22010206

147. Parenti G, Pignata C, Vajro P, Salerno M. New strategies for the treatment of lysosomal storage diseases (review). *Int J Mol Med*. 2013;31(1):11-20. doi:10.3892/IJMM.2012.1187

148. Ramaswami U, Whybra C, Parini R, et al. Clinical manifestations of Fabry disease in children: data from the Fabry Outcome Survey. *Acta Paediatr*. 2006;95(1):86-92. doi:10.1080/08035250500275022

149. Beck M, Hughes D, Kampmann C, et al. Long-term effectiveness of agalsidase alfa enzyme replacement in Fabry disease: A Fabry Outcome Survey analysis. *Mol Genet Metab Rep*. 2015;3:21-27. doi:10.1016/J.YMGMR.2015.02.002

150. Mehta A, Clarke JTR, Giugliani R, et al. Natural course of Fabry disease: changing pattern of causes of death in FOS - Fabry Outcome Survey. *J Med Genet*. 2009;46(8):548-552. doi:10.1136/JMG.2008.065904

151. Schiffmann R, Swift C, Wang X, Blankenship D, Ries M. A prospective 10-year study of individualized, intensified enzyme replacement therapy in advanced Fabry disease. *J Inherit Metab Dis*. 2015;38(6):1129-1136. doi:10.1007/S10545-015-9845-5

152. Schiffmann R, Askari H, Timmons M, et al. Weekly enzyme replacement therapy may slow decline of renal function in patients with Fabry disease who are on long-term biweekly dosing. *J Am Soc Nephrol*. 2007;18(5):1576-1583. doi:10.1681/ASN.2006111263

153. Ramaswami U, Beck M, Hughes D, et al. Cardio- Renal Outcomes With Long- Term Agalsidase Alfa Enzyme Replacement Therapy: A 10- Year Fabry Outcome Survey (FOS) Analysis. *Drug Des Devel Ther*. 2019;13:3705-3715. doi:10.2147/DDDT.S207856

154. Eng CM, Guffon N, Wilcox WR, et al. Safety and efficacy of recombinant human alpha-galactosidase A replacement therapy in Fabry's disease. *N Engl J Med*. 2001;345(1):9-16. doi:10.1056/NEJM200107053450102

155. Hopkin RJ, Feldt-Rasmussen U, Germain DP, et al. Improvement of gastrointestinal symptoms in a significant proportion of male patients with classic Fabry disease treated with agalsidase beta: A Fabry Registry analysis stratified by phenotype. *Mol Genet Metab Rep*. 2020;25. doi:10.1016/J.YMGMR.2020.100670

156. Wanner C, Feldt-Rasmussen U, Jovanovic A, et al. Cardiomyopathy and kidney function in agalsidase beta-treated female Fabry patients: a pre-treatment vs. post-treatment analysis. *ESC Heart Fail*. 2020;7(3):825-834. doi:10.1002/EHF2.12647

157. Ortiz A, Kanters S, Hamed A, et al. Agalsidase beta treatment slows estimated glomerular filtration rate loss in classic Fabry disease patients: results from an individual patient data meta-analysis. *Clin Kidney J*. 2020;14(4):1136-1146. doi:10.1093/CKJ/SFAA065

158. Desnick RJ, Schuchman EH. Enzyme replacement and enhancement therapies: lessons from lysosomal disorders. *Nat Rev Genet*. 2002;3(12):954-966. doi:10.1038/NRG963

159. Parenti G, Andria G, Valenzano KJ. Pharmacological Chaperone Therapy: Preclinical Development, Clinical Translation, and Prospects for the Treatment of Lysosomal Storage Disorders. *Mol Ther*. 2015;23(7):1138-1148. doi:10.1038/MT.2015.62

160. Brogden G, Shammas H, Maalouf K, et al. Case study on the pathophysiology of Fabry disease: abnormalities of cellular membranes can be reversed by substrate reduction in vitro. *Biosci Rep*. 2017;37(2). doi:10.1042/BSR20160402

161. Abe A, Gregory S, Lee L, et al. Reduction of globotriaosylceramide in Fabry disease mice by substrate deprivation. *J Clin Invest*. 2000;105(11):1563-1571. doi:10.1172/JCI9711

162. Heare T, Alp NJ, Priestman DA, et al. Severe endothelial dysfunction in the aorta of a mouse model of Fabry disease; partial prevention by N-butyldeoxynojirimycin treatment. *J Inherit Metab Dis*. 2007;30(1):79-87. doi:10.1007/S10545-006-0473-Y

163. Ziegler RJ, Yew NS, Li C, et al. Correction of enzymatic and lysosomal storage defects in Fabry mice by adenovirus-mediated gene transfer. *Hum Gene Ther*. 1999;10(10):1667-1682. doi:10.1089/10430349950017671

164. Ziegler RJ, Lonning SM, Armentano D, et al. AAV2 vector harboring a liver-restricted promoter facilitates sustained expression of therapeutic levels of alpha-galactosidase A and the induction of immune tolerance in Fabry mice. *Mol Ther*. 2004;9(2):231-240. doi:10.1016/J.YMTHE.2003.11.015

165. Khan A, Barber DL, Huang J, et al. Lentivirus-mediated gene therapy for Fabry disease. *Nat Commun*. 2021;12(1). doi:10.1038/S41467-021-21371-5

166. Tuttolomondo A, Simonetta I, Pinto A. Gene Therapy of Anderson-Fabry Disease. *Curr Gene Ther*. 2019;19(1):3-5. doi:10.2174/1566523219999190415160632

167. Zhu X, Yin L, Theisen M, et al. Systemic mRNA Therapy for the Treatment of Fabry Disease: Preclinical Studies in Wild-Type Mice, Fabry Mouse Model, and Wild-Type Non-human Primates. *Am J Hum Genet*. 2019;104(4):625-637. doi:10.1016/J.AJHG.2019.02.003

168. Schiffmann R, Goker-Alpan O, Holida M, et al. Pegunigalsidase alfa, a novel PEGylated enzyme replacement therapy for Fabry disease, provides sustained plasma concentrations and favorable pharmacodynamics: A 1-year Phase 1/2 clinical trial. *J Inherit Metab Dis*. 2019;42(3):534-544. doi:10.1002/JIMD.12080

169. Ohshima T, Murray GJ, Swaim WD, et al. *Galactosidase A Deficient Mice: A Model of Fabry Disease*. Vol 94.; 1997. www.pnas.org.

170. Burand AJ, Stucky CL. Fabry disease pain: patient and preclinical parallels. *Pain*. 2021;162(5):1305-1321. doi:10.1097/j.pain.0000000000002152

171. Rodrigues LG, Ferraz MJ, Rodrigues D, et al. Neurophysiological, behavioral and morphological abnormalities in the Fabry knockout mice. *Neurobiol Dis*. 2009;33(1):48-56. doi:10.1016/j.nbd.2008.09.001

172. Üçeyler N, Biko L, Hose D, Hofmann L, Sommer C. Comprehensive and differential long-term characterization of the alpha-galactosidase A deficient mouse model of Fabry disease focusing on the sensory system and pain development. *Mol Pain*. 2016;12. doi:10.1177/1744806916646379

173. Formaggio F, Rimondini R, Delprete C, et al. L-Acetylcarnitine causes analgesia in mice modeling Fabry disease by up-regulating type-2 metabotropic glutamate receptors. *Mol Pain*. 2022;18:174480692210870. doi:10.1177/17448069221087033

174. Hofmann L, Karl F, Sommer C, Üçeyler N. Affective and cognitive behavior in the alpha-galactosidase A deficient mouse model of Fabry disease. *PLoS One*. 2017;12(6). doi:10.1371/journal.pone.0180601

175. Spitzel M, Wagner E, Breyer M, et al. Dysregulation of Immune Response Mediators and Pain-Related Ion Channels Is Associated with Pain-like Behavior in the GLA KO Mouse Model of Fabry Disease. *Cells*. 2022;11(11). doi:10.3390/CELLS11111730/S1

176. Torvin Møller A, Winther Bach F, Feldt-Rasmussen U, et al. Functional and structural nerve fiber findings in heterozygote patients with Fabry disease. *Pain*. 2009;145(1-2):237-245. doi:10.1016/J.PAIN.2009.06.032

177. Fontaine DA, Davis DB. Attention to Background Strain Is Essential for Metabolic Research: C57BL/6 and the International Knockout Mouse Consortium. *Diabetes*. 2016;65(1):25-33. doi:10.2337/DB15-0982

178. Bangari DS, Ashe KM, Desnick RJ, et al. α-Galactosidase A knockout mice: progressive organ pathology resembles the type 2 later-onset phenotype of Fabry disease. *Am J Pathol*. 2015;185(3):651-665. doi:10.1016/J.AJPATH.2014.11.004

179. Nguyen TLA, Vieira-Silva S, Liston A, Raes J. How informative is the mouse for human gut microbiota research? *Dis Model Mech*. 2015;8(1):1-16. doi:10.1242/DMM.017400

180. Dethlefsen L, McFall-Ngai M, Relman DA. An ecological and evolutionary perspective on human-microbe mutualism and disease. *Nature*. 2007;449(7164):811-818. doi:10.1038/NATURE06245

181.	Jena S, Chawla S. The Anatomy and Physiology of Laboratory Mouse. *Essentials of Laboratory Animal Science: Principles and Practices*. Published online 2021:159-185. doi:10.1007/978-981-16-0987-9_8/COVER

182.	Hoyt RE, Hawkins J v., St Clair MB, Kennett MJ. Mouse Physiology. *The Mouse in Biomedical Research*. 2007;3:23-90. doi:10.1016/B978-012369454-6/50056-X

183.	Casteleyn C, Rekecki A, van der Aa A, Simoens P, van den Broeck W. Surface area assessment of the murine intestinal tract as a prerequisite for oral dose translation from mouse to man. *Lab Anim*. 2010;44(3):176-183. doi:10.1258/LA.2009.009112

184.	Treuting PM, Dintzis SM, Montine KS. *Comparative Anatomy And Histology: A Mouse, Rat, And Human Atlas Second Edition*. Mica Haley; 2018. Accessed December 11, 2022. http://www.sciencedirect.com:5070/book/9780128029008/comparative-anatomy-and-histology

185.	Nishiyama K, Sugiyama M, Mukai T. Adhesion Properties of Lactic Acid Bacteria on Intestinal Mucin. *Microorganisms*. 2016;4(3). doi:10.3390/MICROORGANISMS4030034

186.	Treuting PM, Dintzis SM, Montine KS. Comparative Anatomy and Histology. *Comparative Anatomy and Histology*. Published online 2012. doi:10.1016/C2009-0-61166-1

187.	Cunliffe RN, Rose FRAJ, Keyte J, Abberley L, Chan WC, Mahida YR. Human defensin 5 is stored in precursor form in normal Paneth cells and is expressed by some villous epithelial cells and by metaplastic Paneth cells in the colon in inflammatory bowel disease. *Gut*. 2001;48(2):176-185. doi:10.1136/GUT.48.2.176

188.	Spencer NJ, Hu H. Enteric nervous system: sensory transduction, neural circuits and gastrointestinal motility. *Nat Rev Gastroenterol Hepatol*. 2020;17(6):338-351. doi:10.1038/s41575-020-0271-2

189.	Haller A von,. *A Dissertation on the Sensible and Irritable Parts of Animals*. Johns Hopkins Press,; 1936.

190.	Wood JD. Enteric Nervous System: Physiology. *The Curated Reference Collection in Neuroscience and Biobehavioral Psychology*. Published online January 1, 2017:1103-1113. doi:10.1016/B978-0-12-809324-5.01834-4

191.	Trendelenburg P. Physiological and pharmacological investigations of small intestinal peristalsis. Translation of the article "Physiologische und pharmakologische Versuche über die Dünndarmperistaltik", Arch. Exp. Pathol. Pharmakol. 81, 55-129, 1917. *Naunyn Schmiedebergs Arch Pharmacol*. 2006;373(2):101-133. doi:10.1007/S00210-006-0052-7

192.	Costa M, Furness JB. The peristaltic reflex: an analysis of the nerve pathways and their pharmacology. *Naunyn Schmiedebergs Arch Pharmacol*. 1976;294(1):47-60. doi:10.1007/BF00692784

193.	Constantinescu M. The enteric nervous system. In: *Neuro-Immuno-Gastroenterology*. Springer International Publishing; 2016:23-38. doi:10.1007/978-3-319-28609-9_2

194.	Furness JB. The enteric nervous system and neurogastroenterology. *Nat Rev Gastroenterol Hepatol*. 2012;9(5):286-294. doi:10.1038/NRGASTRO.2012.32

195.	Grundy D. Neuroanatomy of visceral nociception: vagal and splanchnic afferent. *Gut*. 2002;51 Suppl 1(Suppl 1). doi:10.1136/GUT.51.SUPPL_1.I2

196. Grundy L, Erickson A, Brierley SM. Annual Review of Physiology Visceral Pain. *The Annual Review of Physiology is online at*. 2019;5000:261-284. doi:10.1146/annurev-physiol-020518

197. Furness JBarton. The enteric nervous system. Published online 2006:274.

198. Toumi F, Neunlist M, Cassagnau E, et al. Human submucosal neurones regulate intestinal epithelial cell proliferation: evidence from a novel co-culture model. *Neurogastroenterol Motil*. 2003;15(3):239-242. doi:10.1046/J.1365-2982.2003.00409.X

199. Lakhan SE, Kirchgessner A. Neuroinflammation in inflammatory bowel disease. *J Neuroinflammation*. 2010;7. doi:10.1186/1742-2094-7-37

200. Furness JB, Jones C, Nurgali K, Clerc N. Intrinsic primary afferent neurons and nerve circuits within the intestine. *Prog Neurobiol*. 2004;72(2):143-164. doi:10.1016/j.pneurobio.2003.12.004

201. Berthoud HR. Neural control of appetite: cross-talk between homeostatic and non-homeostatic systems. *Appetite*. 2004;43(3):315-317. doi:10.1016/J.APPET.2004.04.009

202. Berthoud HR. The vagus nerve, food intake and obesity. *Regul Pept*. 2008;149(1-3):15-25. doi:10.1016/J.REGPEP.2007.08.024

203. Berthoud HR, Blackshaw LA, Brookes SJH, Grundy D. Neuroanatomy of extrinsic afferents supplying the gastrointestinal tract. *Neurogastroenterol Motil*. 2004;16 Suppl 1(SUPPL. 1):28-33. doi:10.1111/J.1743-3150.2004.00471.X

204. Furness JB, Kunze WAA, Bertrand PP, Clerc N, Bornstein JC. Intrinsic primary afferent neurons of the intestine. *Prog Neurobiol*. 1998;54(1):1-18. doi:10.1016/S0301-0082(97)00051-8

205. Brehmer A, Rupprecht H, Neuhuber W. Two submucosal nerve plexus in human intestines. *Histochem Cell Biol*. 2010;133(2):149-161. doi:10.1007/S00418-009-0657-2

206. Timmermans JP, Adriaensen D. Outer Submucous Plexus: An Intrinsic Nerve Network Involved in Both Secretory and Motility Processes in the Intestine of Large Mammals and Humans. Published online 2001. doi:10.1002/1097-0185

207. Furness JB, Costa M, Keast JR. Choline acetyltransferase- and peptide immunoreactivity of submucous neurons in the small intestine of the guinea-pig. *Cell Tissue Res*. 1984;237(2):329-336. doi:10.1007/BF00217152

208. Furness JB, Alex G, Clark MJ, Lal V v. Morphologies and projections of defined classes of neurons in the submucosa of the guinea-pig small intestine. *Anat Rec A Discov Mol Cell Evol Biol*. 2003;272(2):475-483. doi:10.1002/AR.A.10064

209. Richardson KC. Electronmicroscopic observations on Auerbach's plexus in the rabbit, with special reference to the problem of smooth muscle innervation. *American Journal of Anatomy*. 1958;103(1):99-135. doi:10.1002/AJA.1001030105

210. Furness JB. The enteric nervous system: normal functions and enteric neuropathies. *Neurogastroenterology & Motility*. 2008;20(SUPPL. 1):32-38. doi:10.1111/J.1365-2982.2008.01094.X

211. Nurgali K, Stebbing MJ, Furness JB. Correlation of Electrophysiological and Morphological Characteristics of Enteric Neurons in the Mouse Colon. *Journal of Comparative Neurology*. 2004;468(1):112-124. doi:10.1002/cne.10948

212. Wong V, Blennerhassett M, Vanner S. Electrophysiological and morphological properties of submucosal neurons in the mouse distal colon. *Neurogastroenterol Motil*. 2008;20(6):725-734. doi:10.1111/J.1365-2982.2008.01117.X

213. Furness JB, Jones C, Nurgali K, Clerc N. Intrinsic primary afferent neurons and nerve circuits within the intestine. *Prog Neurobiol*. 2004;72(2):143-164. doi:10.1016/j.pneurobio.2003.12.004

214. Furness JB. *Types of Neurons in the Enteric Nervous System*. Vol 81.; 2000. www.elsevier.com/locate/jans

215. Spencer NJ, Smith TK. Mechanosensory S-neurons rather than AH-neurons appear to generate a rhythmic motor pattern in guinea-pig distal colon. *J Physiol*. 2004;558(2):577-596. doi:10.1113/JPHYSIOL.2004.063586

216. Spencer NJ, Costa M, Hibberd TJ, Wood JD. Advances in colonic motor complexes in mice. *Am J Physiol Gastrointest Liver Physiol*. 2021;320(1):G12-G29. doi:10.1152/AJPGI.00317.2020

217. Furness JB. Intestinofugal neurons and sympathetic reflexes that bypass the central nervous system. *Journal of Comparative Neurology*. 2003;455(3):281-284. doi:10.1002/CNE.10415

218. Kirchgessner AL, Tamir H, Gershon MD. Identification and stimulation by serotonin of intrinsic sensory neurons of the submucosal plexus of the guinea pig gut: activity-induced expression of Fos immunoreactivity. *J Neurosci*. 1992;12(1):235-248. doi:10.1523/JNEUROSCI.12-01-00235.1992

219. Bertrand PP, Kunze WAA, Bornstein JC, Furness JB, Smith ML. Analysis of the responses of myenteric neurons in the small intestine to chemical stimulation of the mucosa. *Am J Physiol*. 1997;273(2 Pt 1). doi:10.1152/AJPGI.1997.273.2.G422

220. Kunze WAA, Furness JB, Bertrand PP, Bornstein JC. Intracellular recording from myenteric neurons of the guinea-pig ileum that respond to stretch. *undefined*. 1998;506(3):827-842. doi:10.1111/J.1469-7793.1998.827BV.X

221. Furness JB, Jones C, Nurgali K, Clerc N. Intrinsic primary afferent neurons and nerve circuits within the intestine. *Prog Neurobiol*. 2004;72(2):143-164. doi:10.1016/J.PNEUROBIO.2003.12.004

222. Fantaguzzi CM, Thacker M, Chiocchetti R, Furness JB. Identification of neuron types in the submucosal ganglia of the mouse ileum. doi:10.1007/s00441-009-0773-2

223. Quinson N, Robbins H, Clark M, Furness J. Calbindin immunoreactivity of enteric neurons in the guinea-pig ileum. *Cell Tissue Res*. 2001;305(1):3-9. doi:10.1007/S004410100395

224. Iyer V, Bornstein JC, Costa M, Furness JB, Takahashi Y, Iwanaga T. Electrophysiology of guinea-pig myenteric neurons correlated with immunoreactivity for calcium binding proteins. *J Auton Nerv Syst*. 1988;22(2):141-150. doi:10.1016/0165-1838(88)90087-2

225. Furness JB, Keast JR, Pompolo S, et al. Immunohistochemical evidence for the presence of calcium-binding proteins in enteric neurons. *Cell Tissue Res*. 1988;252(1):79-87. doi:10.1007/BF00213828

226. Van L, Ae N, Ae MW, et al. Cytoplasmic, but not nuclear, expression of the neuronal nuclei (NeuN) antibody is an exclusive feature of Dogiel type II neurons in the guinea-pig gastrointestinal tract. doi:10.1007/s00418-005-0019-7

227. Chiocchetti R, Poole DP, Kimura H, et al. Evidence that two forms of choline acetyltransferase are differentially expressed in subclasses of enteric neurons. *Cell Tissue Res*. 2003;311(1):11-22. doi:10.1007/S00441-002-0652-6

228. Li ZS, Furness JB. Immunohistochemical localisation of cholinergic markers in putative intrinsic primary afferent neurons of the guinea-pig small intestine. *Cell Tissue Res*. 1998;294(1):35-43. doi:10.1007/S004410051154

229. Foong JPP, Tough IR, Cox HM, Bornstein JC. Properties of cholinergic and non-cholinergic submucosal neurons along the mouse colon. *Journal of Physiology*. 2014;592(4):777-793. doi:10.1113/jphysiol.2013.265686

230. Mazzoni M, Caremoli F, Cabanillas L, et al. Quantitative analysis of enteric neurons containing choline acetyltransferase and nitric oxide synthase immunoreactivities in the submucosal and myenteric plexuses of the porcine colon HHS Public Access. *Cell Tissue Res*. 2021;383(2):645-654. doi:10.1007/s00441-020-03286-7

231. Chiocchetti R, Grandis A, Bombardi C, et al. Extrinsic and intrinsic sources of calcitonin gene-related peptide immunoreactivity in the lamb ileum: a morphometric and neurochemical investigation. *Cell Tissue Res*. 2005;323(2):183-196. doi:10.1007/S00441-005-0075-2

232. Furness JB, Robbins HL, Xiao J, Stebbing MJ, Nurgali K. Projections and chemistry of Dogiel type II neurons in the mouse colon. *undefined*. 2004;317(1):1-12. doi:10.1007/S00441-004-0895-5

233. Sang Q, Young HM. The identification and chemical coding of cholinergic neurons in the small and large intestine of the mouse. *Anat Rec*. 1998;251(2):185-199. doi:10.1002/(sici)1097-0185(199806)251:2<185::aid-ar6>3.0.co;2-y

234. Costa M, Keightley LJ, Hibberd TJ, et al. Motor patterns in the proximal and distal mouse colon which underlie formation and propulsion of feces. *Neurogastroenterol Motil*. 2021;33(7). doi:10.1111/NMO.14098

235. Lomax AE, Furness JB. Neurochemical classification of enteric neurons in the guinea-pig distal colon. *Cell Tissue Res*. 2000;302(1):59-72. doi:10.1007/S004410000260

236. Durnin L, Sanders KM, Mutafova-Yambolieva VN. Differential release of β-NAD(+) and ATP upon activation of enteric motor neurons in primate and murine colons. *Neurogastroenterol Motil*. 2013;25(3). doi:10.1111/NMO.12069

237. Vanner S, Macnaughton WK. *Submucosal Secretomotor and Vasodilator Reflexes*.

238. Furness JB. The enteric nervous system and neurogastroenterology. *Nat Rev Gastroenterol Hepatol*. 2012;9(5):286-294. doi:10.1038/nrgastro.2012.32

239. Beyer J, Jabari S, Rau TT, Neuhuber W, Brehmer A. Substance P- and choline acetyltransferase immunoreactivities in somatostatin-containing, human submucosal neurons. *Histochem Cell Biol*. 2013;140(2):157-167. doi:10.1007/S00418-013-1078-9/FIGURES/7

240. Hens J, Vanderwinden JM, de Laet MH, Scheuermann DW, Timmermans JP. Morphological and neurochemical identification of enteric neurones with mucosal projections in the human small intestine. *J Neurochem*. 2001;76(2):464-471. doi:10.1046/J.1471-4159.2001.00032.X

241. Hu H, Spencer NJ. Enteric Nervous System Structure and Neurochemistry Related to Function and Neuropathology. In: *Physiology of the Gastrointestinal Tract, Sixth Edition*. Vol 1. Elsevier; 2018:337-360. doi:10.1016/B978-0-12-809954-4.00014-1

242. Costa M, Brookes SJH, Hennig GW. *Anatomy and Physiology of the Enteric Nervous System*. www.gutjnl.com

243. Smith TK, Spencer NJ, Hennig GW, Dickson EJ. Recent advances in enteric neurobiology: mechanosensitive interneurons. *Neurogastroenterol Motil*. 2007;19(11):869-878. doi:10.1111/J.1365-2982.2007.01019.X

244. Dickson EJ, Spencer NJ, Hennig GW, et al. An Enteric Occult Reflex Underlies Accommodation and Slow Transit in the Distal Large Bowel. *Gastroenterology*. 2007;132(5):1912-1924. doi:10.1053/j.gastro.2007.02.047

245. Porter AJ, Wattchow DA, Brookes SJH, Costa M. The neurochemical coding and projections of circular muscle motor neurons in the human colon. *Gastroenterology*. 1997;113(6):1916-1923. doi:10.1016/S0016-5085(97)70011-8

246. Griffith SG, Burnstock G. Serotoninergic neurons in human fetal intestine: An immunohistochemical study. *Gastroenterology*. 1983;85(4):929-937. doi:10.1016/0016-5085(83)90446-8

247. Brookes SJ, Ewart WR, Wingate DL. Intracellular recordings from myenteric neurones in the human colon. *J Physiol*. 1987;390(1):305-318. doi:10.1113/JPHYSIOL.1987.SP016702

248. Porter AJ, Wattchow DA, Brookes SJH, Costa M. Cholinergic and nitrergic interneurones in the myenteric plexus of the human colon. *Gut*. 2002;51(1):70-75. doi:10.1136/gut.51.1.70

249. Brehmer A, Schrödl F, Neuhuber W. Morphological phenotyping of enteric neurons using neurofilament immunohistochemistry renders chemical phenotyping more precise in porcine ileum. *Histochemistry and Cell Biology 2002 117:3*. 2002;117(3):257-263. doi:10.1007/S00418-001-0373-Z

250. Hibberd TJ, Zagorodnyuk VP, Spencer NJ, Brookes SJH. Identification and mechanosensitivity of viscerofugal neurons. *Neuroscience*. 2012;225:118-129. doi:10.1016/J.NEUROSCIENCE.2012.08.040

251. Miller SM, Szurszewski JH. Circumferential, not longitudinal, colonic stretch increases synaptic input to mouse prevertebral ganglion neurons. *Am J Physiol Gastrointest Liver Physiol*. 2003;285(6). doi:10.1152/AJPGI.00292.2003

252. Miller SM, Szurszewski JH. Colonic mechanosensory afferent input to neurons in the mouse superior mesenteric ganglion. *Am J Physiol Gastrointest Liver Physiol*. 1997;272(2 35-2):G357-G366. doi:10.1152/AJPGI.1997.272.2.G357

253. Szurszewski JH, Ermilov LG, Miller SM. Prevertebral ganglia and intestinofugal afferent neurones. *Gut*. 2002;51 Suppl 1(Suppl 1). doi:10.1136/GUT.51.SUPPL_1.I6

254. Lomax AE, Zhang JY, Furness JB. Origins of cholinergic inputs to the cell bodies of intestinofugal neurons in the guinea pig distal colon. *J Comp Neurol*. 2000;416(4):451-460. doi:10.1002/(sici)1096-9861(20000124)416:4<451::aid-cne3>3.0.co;2-e

255. Miller SM, Szurszewski JH. Circumferential, not longitudinal, colonic stretch increases synaptic input to mouse prevertebral ganglion neurons. *Am J Physiol Gastrointest Liver Physiol*. 2003;285(6). doi:10.1152/AJPGI.00292.2003

256. Furness JB, Callaghan BP, Rivera LR, Cho HJ. The enteric nervous system and gastrointestinal innervation: integrated local and central control. *Adv Exp Med Biol*. 2014;817:39-71. doi:10.1007/978-1-4939-0897-4_3

257. Gebhart GF, Bielefeldt K. Physiology of Visceral Pain. *Compr Physiol*. 2016;6(4):1609-1633. doi:10.1002/CPHY.C150049

258. Brierley SM, Jones RCW, Gebhart GF, Blackshaw LA. Splanchnic and pelvic mechanosensory afferents signal different qualities of colonic stimuli in mice. *Gastroenterology*. 2004;127(1):166-178. doi:10.1053/j.gastro.2004.04.008

259. Brookes SJH, Spencer NJ, Costa M, Zagorodnyuk VP. Extrinsic primary afferent signalling in the gut. *Nature Reviews Gastroenterology & Hepatology 2013 10:5*. 2013;10(5):286-296. doi:10.1038/nrgastro.2013.29

260. Furness JB. Integrated neural and endocrine control of gastrointestinal function. *Adv Exp Med Biol*. 2016;891:159-173. doi:10.1007/978-3-319-27592-5_16

261. Furness JB, Rivera LR, Cho HJ, Bravo DM, Callaghan B. The gut as a sensory organ. *Nat Rev Gastroenterol Hepatol*. 2013;10(12):729-740. doi:10.1038/NRGASTRO.2013.180

262. Raybould HE. Gut chemosensing: interactions between gut endocrine cells and visceral afferents. *Auton Neurosci*. 2010;153(1-2):41-46. doi:10.1016/J.AUTNEU.2009.07.007

263. Thai J, Kyloh M, Travis L, Spencer NJ, Ivanusic JJ. Identifying spinal afferent (sensory) nerve endings that innervate the marrow cavity and periosteum using anterograde tracing. *J Comp Neurol*. 2020;528(11):1903-1916. doi:10.1002/CNE.24862

264. Spencer NJ, Kyloh M, Duffield M. Identification of different types of spinal afferent nerve endings that encode noxious and innocuous stimuli in the large intestine using a novel anterograde tracing technique. *PLoS One*. 2014;9(11). doi:10.1371/JOURNAL.PONE.0112466

265. Zagorodnyuk VP, Chen BN, Costa M, Brookes SJH. Mechanotransduction by intraganglionic laminar endings of vagal tension receptors in the guinea-pig oesophagus. *Journal of Physiology*. 2003;553(2):575-587. doi:10.1113/jphysiol.2003.051862

266. Zagorodnyuk VP, Chen BN, Brookes SJH. Intraganglionic laminar endings are mechano-transduction sites of vagal tension receptors in the guinea-pig stomach. *J Physiol*. 2001;534(Pt 1):255-268. doi:10.1111/J.1469-7793.2001.00255.X

267. Tan LL, Bornstein JC, Anderson CR. Distinct chemical classes of medium-sized transient receptor potential channel vanilloid 1-immunoreactive dorsal root ganglion neurons innervate the adult mouse jejunum and colon. *Neuroscience*. 2008;156(2):334-343. doi:10.1016/J.NEUROSCIENCE.2008.06.071

268. Akbar A, Yiangou Y, Facer P, Walters JRF, Anand P, Ghosh S. Increased capsaicin receptor TRPV1-expressing sensory fibres in irritable bowel syndrome and their correlation with abdominal pain. *Gut*. 2008;57(7):923-929. doi:10.1136/gut.2007.138982

269. Kyloh M, Nicholas S, Zagorodnyuk VP, Brookes SJ, Spencer NJ. Identification of the visceral pain pathway activated by noxious colorectal distension in mice. *Front Neurosci*. 2011;(FEB). doi:10.3389/fnins.2011.00016

270. Larsson M, Arvidsson S, Ekman C, Bayati A. A model for chronic quantitative studies of colorectal sensitivity using balloon distension in conscious mice -- effects of opioid receptor agonists. *Neurogastroenterol Motil*. 2003;15(4):371-381. doi:10.1046/J.1365-2982.2003.00418.X

271. Zagorodnyuk VP, Kyloh M, Nicholas S, et al. Loss of visceral pain following colorectal distension in an endothelin-3 deficient mouse model of Hirschsprung's disease. *Journal of Physiology-London*. 2011;589(7):1691-1706. doi:10.1113/JPHYSIOL.2010.202820

272.   Brookes SJ, Dinning PG, Gladman MA. Neuroanatomy and physiology of colorectal function and defaecation: from basic science to human clinical studies. *Neurogastroenterol Motil*. 2009;21 Suppl 2(SUPPL. 2):9-19. doi:10.1111/J.1365-2982.2009.01400.X

273.   Shimizu Y, Chang EC, Shafton AD, et al. Evidence that stimulation of ghrelin receptors in the spinal cord initiates propulsive activity in the colon of the rat. *J Physiol*. 2006;576(1):329-338. doi:10.1113/JPHYSIOL.2006.116160

274.   Gabella G. Fine structure of the myenteric plexus in the guinea-pig ileum. *J Anat*. 1972;111(Pt 1):69. Accessed December 14, 2022. https://www.ncbi.nlm.nih.gov/pmc/articles/PMC1271115/

275.   Seguella L, Gulbransen BD. Enteric glial biology, intercellular signalling and roles in gastrointestinal disease. *Nat Rev Gastroenterol Hepatol*. 2021;18(8):571-587. doi:10.1038/s41575-021-00423-7

276.   Gabella G. Ultrastructure of the nerve plexuses of the mammalian intestine: the enteric glial cells. *Neuroscience*. 1981;6(3):425-436. doi:10.1016/0306-4522(81)90135-4

277.   Hoff S, Zeller F, von Weyhern CWH, et al. Quantitative assessment of glial cells in the human and guinea pig enteric nervous system with an anti-Sox8/9/10 antibody. *J Comp Neurol*. 2008;509(4):356-371. doi:10.1002/CNE.21769

278.   Young HM, Bergner AJ, Müller T. Acquisition of neuronal and glial markers by neural crest–derived cells in the mouse intestine. *Journal of Comparative Neurology*. 2003;456(1):1-11. doi:10.1002/CNE.10448

279.   Jessen KR, Mirsky R. Glial cells in the enteric nervous system contain glial fibrillary acidic protein. *Nature*. 1980;286(5774):736-737. doi:10.1038/286736A0

280.   Ferri GL, Probert L, Cocchia D, Michetti F, Marangos PJ, Polak JM. Evidence for the presence of S-100 protein in the glial component of the human enteric nervous system. *Nature*. 1982;297(5865):409-410. doi:10.1038/297409A0

281.   Neunlist M, Rolli-Derkinderen M, Latorre R, et al. Enteric glial cells: recent developments and future directions. *Gastroenterology*. 2014;147(6):1230-1237. doi:10.1053/J.GASTRO.2014.09.040

282.   Coelho-Aguiar J de M, Bon-Frauches AC, Gomes ALT, et al. The enteric glia: identity and functions. *Glia*. 2015;63(6):921-935. doi:10.1002/GLIA.22795

283.   Boesmans W, Lasrado R, vanden Berghe P, Pachnis V. Heterogeneity and phenotypic plasticity of glial cells in the mammalian enteric nervous system. *Glia*. 2015;63(2):229-241. doi:10.1002/GLIA.22746

284.   Rosenberg HJ, Rao M. iScience Enteric glia in homeostasis and disease: From fundamental biology to human pathology. Published online 2021. doi:10.1016/j.isci

285.   Grubišić V, Gulbransen BD. Enteric glia: the most alimentary of all glia. *Journal of Physiology*. 2017;595(2):557-570. doi:10.1113/JP271021

286.   Lucarini E, Seguella L, Vincenzi M, et al. Role of Enteric Glia as Bridging Element between Gut Inflammation and Visceral Pain Consolidation during Acute Colitis in Rats. Published online 2021. doi:10.3390/biomedicines9111671

287.   Delvalle NM, Fried DE, Rivera-Lopez G, Gaudette L, Gulbransen BD. Cholinergic activation of enteric glia is a physiological mechanism that contributes to the regulation of gastrointestinal motility. *Am J Physiol Gastrointest Liver Physiol*. 2018;315(4):G473-G483. doi:10.1152/AJPGI.00155.2018

288. Rao M, Rastelli D, Dong L, et al. Enteric Glia Regulate Gastrointestinal Motility but Are Not Required for Maintenance of the Epithelium in Mice. *Gastroenterology*. 2017;153(4):1068-1081.e7. doi:10.1053/J.GASTRO.2017.07.002

289. Savidge TC, Newman P, Pothoulakis C, et al. Enteric glia regulate intestinal barrier function and inflammation via release of S-nitrosoglutathione. *Gastroenterology*. 2007;132(4):1344-1358. doi:10.1053/J.GASTRO.2007.01.051

290. Grubišić V, McClain JL, Fried DE, et al. Enteric Glia Modulate Macrophage Phenotype and Visceral Sensitivity following Inflammation. *Cell Rep*. 2020;32(10). doi:10.1016/J.CELREP.2020.108100

291. Ibiza S, García-Cassani B, Ribeiro H, et al. Glial-cell-derived neuroregulators control type 3 innate lymphoid cells and gut defence. *Nature*. 2016;535(7612):440-443. doi:10.1038/NATURE18644

292. Abdo H, Derkinderen P, Gomes P, et al. Enteric glial cells protect neurons from oxidative stress in part via reduced glutathione. *FASEB J*. 2010;24(4):1082-1094. doi:10.1096/FJ.09-139519

293. Brun P, Giron MC, Qesari M, et al. Toll-like receptor 2 regulates intestinal inflammation by controlling integrity of the enteric nervous system. *Gastroenterology*. 2013;145(6):1323-1333. doi:10.1053/J.GASTRO.2013.08.047

294. Joseph NM, He S, Quintana E, Kim YG, Núñez G, Morrison SJ. Enteric glia are multipotent in culture but primarily form glia in the adult rodent gut. *J Clin Invest*. 2011;121(9):3398-3411. doi:10.1172/JCI58186

295. Laranjeira C, Sandgren K, Kessaris N, et al. Glial cells in the mouse enteric nervous system can undergo neurogenesis in response to injury. *J Clin Invest*. 2011;121(9):3412-3424. doi:10.1172/JCI58200

296. Rao M, Gershon MD. Neurogastroenterology: The dynamic cycle of life in the enteric nervous system. *Nat Rev Gastroenterol Hepatol*. 2017;14(8):453-454. doi:10.1038/nrgastro.2017.85

297. Morales-Soto W, Gulbransen BD. Enteric Glia: A New Player in Abdominal Pain. *Cell Mol Gastroenterol Hepatol*. 2019;7(2):433-445. doi:10.1016/J.JCMGH.2018.11.005

298. Yamamoto M, Nishiyama M, Iizuka S, et al. Transient receptor potential vanilloid 1-immunoreactive signals in murine enteric glial cells. *World J Gastroenterol*. 2016;22(44):9752-9764. doi:10.3748/wjg.v22.i44.9752

299. D'Aldebert E, Cenac N, Rousset P, et al. Transient receptor potential vanilloid 4 activated inflammatory signals by intestinal epithelial cells and colitis in mice. *Gastroenterology*. 2011;140(1):275-285.e3. doi:10.1053/J.GASTRO.2010.09.045

300. de Schepper S, Verheijden S, Aguilera-Lizarraga J, et al. Self-Maintaining Gut Macrophages Are Essential for Intestinal Homeostasis. *Cell*. 2018;175(2):400-415.e13. doi:10.1016/J.CELL.2018.07.048

301. Obata Y, Castaño Á, Boeing S, et al. Neuronal programming by microbiota regulates intestinal physiology. *Nature*. 2020;578(7794):284-289. doi:10.1038/S41586-020-1975-8

302. Devos D, Lebouvier T, Lardeux B, et al. Colonic inflammation in Parkinson's disease. *Neurobiol Dis*. 2013;50(1):42-48. doi:10.1016/j.nbd.2012.09.007

303. Fu H, Bartz JD, Stephens RL, McCarty DM. Peripheral nervous system neuropathology and progressive sensory impairments in a mouse model of Mucopolysaccharidosis IIIB. *PLoS One*. 2012;7(9). doi:10.1371/JOURNAL.PONE.0045992

304. Wood JD. The first nobel prize for integrated systems physiology: Ivan Petrovich Pavlov, 1904. *Physiology (Bethesda)*. 2004;19(6):326-330. doi:10.1152/PHYSIOL.00034.2004

305. Gibbons CH. Basics of autonomic nervous system function. *Handb Clin Neurol*. 2019;160:407-418. doi:10.1016/B978-0-444-64032-1.00027-8

306. Westfall S, Lomis N, Kahouli I, Dia SY, Singh SP, Prakash S. Microbiome, probiotics and neurodegenerative diseases: deciphering the gut brain axis. *Cell Mol Life Sci*. 2017;74(20):3769-3787. doi:10.1007/S00018-017-2550-9

307. Furness JB, Callaghan BP, Rivera LR, Cho HJ. The enteric nervous system and gastrointestinal innervation: integrated local and central control. *Adv Exp Med Biol*. 2014;817:39-71. doi:10.1007/978-1-4939-0897-4_3

308. Foster JA. Modulating brain function with microbiota. *Science*. 2022;376(6596):936-937. doi:10.1126/SCIENCE.ABO4220

309. Hunt SP, Mantyh PW. The molecular dynamics of pain control. *Nat Rev Neurosci*. 2001;2(2):83-91. doi:10.1038/35053509

310. Palecek J, Willis WD. The dorsal column pathway facilitates visceromotor responses to colorectal distention after colon inflammation in rats. *Pain*. 2003;104(3):501-507. doi:10.1016/S0304-3959(03)00075-7

311. Bester H, Matsumoto N, Besson J marie, Ois Bernard J franç. *Further Evidence for the Involvement of the Spinoparabrachial Pathway in Nociceptive Processes: A c-Fos Study in the Rat*. Vol 383. Wiley-Liss, Inc; 1997.

312. Bonaz B, Sinniger V, Pellissier S. Vagus Nerve Stimulation at the Interface of Brain-Gut Interactions. *Cold Spring Harb Perspect Med*. 2019;9(8). doi:10.1101/CSHPERSPECT.A034199

313. Cryan JF, O KJ, M Cowan CS, et al. The Microbiota-Gut-Brain Axis. *Physiol Rev*. 2019;99:1877-2013. doi:10.1152/physrev.00018.2018.-The

314. Ogbonnaya ES, Clarke G, Shanahan F, Dinan TG, Cryan JF, O'Leary OF. Adult Hippocampal Neurogenesis Is Regulated by the Microbiome. *Biol Psychiatry*. 2015;78(4):e7-e9. doi:10.1016/J.BIOPSYCH.2014.12.023

315. Luczynski P, Whelan SO, O'Sullivan C, et al. Adult microbiota-deficient mice have distinct dendritic morphological changes: differential effects in the amygdala and hippocampus. *Eur J Neurosci*. 2016;44(9):2654-2666. doi:10.1111/EJN.13291

316. Erny D, de Angelis ALH, Jaitin D, et al. Host microbiota constantly control maturation and function of microglia in the CNS. *Nat Neurosci*. 2015;18(7):965-977. doi:10.1038/NN.4030

317. Neufeld KM, Kang N, Bienenstock J, Foster JA. Reduced anxiety-like behavior and central neurochemical change in germ-free mice. *Neurogastroenterol Motil*. 2011;23(3). doi:10.1111/J.1365-2982.2010.01620.X

318. Kelly JR, Borre Y, O' Brien C, et al. Transferring the blues: Depression-associated gut microbiota induces neurobehavioural changes in the rat. *J Psychiatr Res*. 2016;82:109-118. doi:10.1016/J.JPSYCHIRES.2016.07.019

319. Qin J, Li R, Raes J, et al. A human gut microbial gene catalogue established by metagenomic sequencing. *Nature*. 2010;464(7285):59-65. doi:10.1038/NATURE08821

320. Zoetendal EG, Akkermans ADL, Akkermans-van Vliet WM, de Visser JAGM, de Vos WM. The Host Genotype Affects the Bacterial Community in the Human Gastrointestinal Tract. *Microb Ecol Health Dis*. 2001;13(3):129-134. doi:10.1080/089106001750462669

321. Abubucker S, Segata N, Goll J, et al. Metabolic reconstruction for metagenomic data and its application to the human microbiome. *PLoS Comput Biol*. 2012;8(6). doi:10.1371/JOURNAL.PCBI.1002358

322. Shao Y, Forster SC, Tsaliki E, et al. Stunted microbiota and opportunistic pathogen colonization in caesarean-section birth. *Nature*. 2019;574(7776):117-121. doi:10.1038/S41586-019-1560-1

323. Bäckhed F, Roswall J, Peng Y, et al. Dynamics and Stabilization of the Human Gut Microbiome during the First Year of Life. *Cell Host Microbe*. 2015;17(6):852. doi:10.1016/J.CHOM.2015.05.012

324. Fallani M, Young D, Scott J, et al. Intestinal microbiota of 6-week-old infants across Europe: geographic influence beyond delivery mode, breast-feeding, and antibiotics. *J Pediatr Gastroenterol Nutr*. 2010;51(1):77-84. doi:10.1097/MPG.0B013E3181D1B11E

325. Claesson MJ, Cusack S, O'Sullivan O, et al. Composition, variability, and temporal stability of the intestinal microbiota of the elderly. *Proc Natl Acad Sci U S A*. 2011;108 Suppl 1(Suppl 1):4586-4591. doi:10.1073/PNAS.1000097107

326. Chunduri A, Deepak · S, Reddy M, Jahanavi · M, Reddy · C Nagendranatha. Gut-Brain Axis, Neurodegeneration and Mental Health: A Personalized Medicine Perspective. 2088;62(4):505-515. doi:10.1007/s12088-022-01033-w

327. Doroszkiewicz J, Groblewska M, Mroczko B. The role of gut microbiota and gut–brain interplay in selected diseases of the central nervous system. *Int J Mol Sci*. 2021;22(18). doi:10.3390/ijms221810028

328. Gershon MD, Gross Margolis K. The gut, its microbiome, and the brain: connections and communications. *J Clin Invest*. 2021;131(18). doi:10.1172/JCI143768

329. Sommer F, Bäckhed F. The gut microbiota--masters of host development and physiology. *Nat Rev Microbiol*. 2013;11(4):227-238. doi:10.1038/NRMICRO2974

330. Xu J, Gordon JI. Honor thy symbionts. *Proc Natl Acad Sci U S A*. 2003;100(18):10452-10459. doi:10.1073/PNAS.1734063100

331. Topping DL, Clifton PM. Short-chain fatty acids and human colonic function: roles of resistant starch and nonstarch polysaccharides. *Physiol Rev*. 2001;81(3):1031-1064. doi:10.1152/PHYSREV.2001.81.3.1031

332. Millet S, van Oeckel MJ, Aluwé M, Delezie E, de Brabander DL. Prediction of in vivo short-chain fatty acid production in hindgut fermenting mammals: problems and pitfalls. *Crit Rev Food Sci Nutr*. 2010;50(7):605-619. doi:10.1080/10408390802565939

333. Semin I, Ninnemann J, Bondareva M, Gimaev I, Kruglov AA. Interplay Between Microbiota, Toll-Like Receptors and Cytokines for the Maintenance of Epithelial Barrier Integrity. *Front Med (Lausanne)*. 2021;8. doi:10.3389/FMED.2021.644333

334. Jandhyala SM, Talukdar R, Subramanyam C, Vuyyuru H, Sasikala M, Reddy DN. Role of the normal gut microbiota. *World J Gastroenterol*. 2015;21(29):8836-8847. doi:10.3748/WJG.V21.I29.8787

335.   Berger M, Gray JA, Roth BL. The expanded biology of serotonin. *Annu Rev Med*. 2009;60:355-366. doi:10.1146/ANNUREV.MED.60.042307.110802

336.   Luczynski P, Neufeld KAMV, Oriach CS, Clarke G, Dinan TG, Cryan JF. Growing up in a Bubble: Using Germ-Free Animals to Assess the Influence of the Gut Microbiota on Brain and Behavior. *Int J Neuropsychopharmacol*. 2016;19(8):1-17. doi:10.1093/IJNP/PYW020

337.   Cook SI, Sellin JH. Review article: short chain fatty acids in health and disease. *Aliment Pharmacol Ther*. 1998;12(6):499-507. doi:10.1046/J.1365-2036.1998.00337.X

338.   Wong JMW, de Souza R, Kendall CWC, Emam A, Jenkins DJA. Colonic health: Fermentation and short chain fatty acids. *J Clin Gastroenterol*. 2006;40(3):235-243. doi:10.1097/00004836-200603000-00015

339.   Binder HJ. Role of colonic short-chain fatty acid transport in diarrhea. *Annu Rev Physiol*. 2010;72:297-313. doi:10.1146/ANNUREV-PHYSIOL-021909-135817

340.   Cummings JH, Pomare EW, Branch HWJ, Naylor CPE, MacFarlane GT. Short chain fatty acids in human large intestine, portal, hepatic and venous blood. *Gut*. 1987;28(10):1221-1227. doi:10.1136/GUT.28.10.1221

341.   Flint HJ. Gut microbial metabolites in health and disease. *Gut Microbes*. 2016;7(3):187-188. doi:10.1080/19490976.2016.1182295

342.   Louis P, Hold GL, Flint HJ. The gut microbiota, bacterial metabolites and colorectal cancer. *Nat Rev Microbiol*. 2014;12(10):661-672. doi:10.1038/NRMICRO3344

343.   Louis P, Flint HJ. Diversity, metabolism and microbial ecology of butyrate-producing bacteria from the human large intestine. *FEMS Microbiol Lett*. 2009;294(1):1-8. doi:10.1111/J.1574-6968.2009.01514.X

344.   Belzer C, Chia LW, Aalvink S, et al. Microbial Metabolic Networks at the Mucus Layer Lead to Diet-Independent Butyrate and Vitamin B12 Production by Intestinal Symbionts. *mBio*. 2017;8(5). doi:10.1128/MBIO.00770-17

345.   van Hoek MJA, Merks RMH. Redox balance is key to explaining full vs. partial switching to low-yield metabolism. *BMC Syst Biol*. 2012;6:22-22. doi:10.1186/1752-0509-6-22

346.   Reigstad CS, Salmonson CE, Rainey JF, et al. Gut microbes promote colonic serotonin production through an effect of short-chain fatty acids on enterochromaffin cells. *FASEB J*. 2015;29(4):1395-1403. doi:10.1096/FJ.14-259598

347.   Yano JM, Yu K, Donaldson GP, et al. Indigenous bacteria from the gut microbiota regulate host serotonin biosynthesis. *Cell*. 2015;161(2):264-276. doi:10.1016/J.CELL.2015.02.047

348.   del Colle A, Israelyan N, Margolis KG. Novel aspects of enteric serotonergic signaling in health and brain-gut disease. *Am J Physiol Gastrointest Liver Physiol*. 2020;318(1):G130-G143. doi:10.1152/AJPGI.00173.2019

349.   Krautkramer KA, Kreznar JH, Romano KA, et al. Diet-Microbiota Interactions Mediate Global Epigenetic Programming in Multiple Host Tissues. *Mol Cell*. 2016;64(5):982-992. doi:10.1016/J.MOLCEL.2016.10.025

350. Stilling RM, van de Wouw M, Clarke G, Stanton C, Dinan TG, Cryan JF. The neuropharmacology of butyrate: The bread and butter of the microbiota-gut-brain axis? *Neurochem Int*. 2016;99:110-132. doi:10.1016/J.NEUINT.2016.06.011

351. Milligan G, Shimpukade B, Ulven T, Hudson BD. Complex Pharmacology of Free Fatty Acid Receptors. *Chem Rev*. 2017;117(1):67-110. doi:10.1021/ACS.CHEMREV.6B00056

352. Chambers ES, Viardot A, Psichas A, et al. Effects of targeted delivery of propionate to the human colon on appetite regulation, body weight maintenance and adiposity in overweight adults. *Gut*. 2015;64(11):1744-1754. doi:10.1136/GUTJNL-2014-307913

353. Reigstad CS, Salmonson CE, Rainey JF, et al. Gut microbes promote colonic serotonin production through an effect of short-chain fatty acids on enterochromaffin cells. *FASEB J*. 2015;29(4):1395-1403. doi:10.1096/FJ.14-259598

354. de Vadder F, Kovatcheva-Datchary P, Goncalves D, et al. Microbiota-generated metabolites promote metabolic benefits via gut-brain neural circuits. *Cell*. 2014;156(1-2):84-96. doi:10.1016/J.CELL.2013.12.016

355. Li Z, Yi CX, Katiraei S, et al. Butyrate reduces appetite and activates brown adipose tissue via the gut-brain neural circuit. *Gut*. 2018;67(7):1269-1279. doi:10.1136/GUTJNL-2017-314050

356. Egorin MJ, Yuan ZM, Sentz DL, Plaisance K, Eiseman JL. Plasma pharmacokinetics of butyrate after intravenous administration of sodium butyrate or oral administration of tributyrin or sodium butyrate to mice and rats. *Cancer Chemother Pharmacol*. 1999;43(6):445-453. doi:10.1007/S002800050922

357. Schönfeld P, Wojtczak L. Short- and medium-chain fatty acids in energy metabolism: the cellular perspective. *J Lipid Res*. 2016;57(6):943-954. doi:10.1194/JLR.R067629

358. Boets E, Gomand S v., Deroover L, et al. Systemic availability and metabolism of colonic-derived short-chain fatty acids in healthy subjects: a stable isotope study. *J Physiol*. 2017;595(2):541-555. doi:10.1113/JP272613

359. Collins SM, Piche T, Rampal P. The putative role of inflammation in the irritable bowel syndrome. *Gut*. 2001;49(6):743-745. doi:10.1136/GUT.49.6.743

360. Xu JR, Luo JY, Shang L, Kong WM. Effect of change in an inhibitory neurotransmitter of the myenteric plexus on the pathogenetic mechanism of irritable bowel syndrome subgroups in rat models. *Chin J Dig Dis*. 2006;7(2):89-96. doi:10.1111/J.1443-9573.2006.00248.X

361. Lee YJ, Park KS. Irritable bowel syndrome: emerging paradigm in pathophysiology. *World J Gastroenterol*. 2014;20(10):2456-2469. doi:10.3748/WJG.V20.I10.2456

362. Todesco T, Rao A v., Bosello O, Jenkins DJA. Propionate lowers blood glucose and alters lipid metabolism in healthy subjects. *Am J Clin Nutr*. 1991;54(5):860-865. doi:10.1093/AJCN/54.5.860

363. Fushimi T, Suruga K, Oshima Y, Fukiharu M, Tsukamoto Y, Goda T. Dietary acetic acid reduces serum cholesterol and triacylglycerols in rats fed a cholesterol-rich diet. *Br J Nutr*. 2006;95(5):916-924. doi:10.1079/BJN20061740

364. Gao Z, Yin J, Zhang J, et al. Butyrate Improves Insulin Sensitivity and Increases Energy Expenditure in Mice. *Diabetes*. 2009;58(7):1509-1517. doi:10.2337/DB08-1637

365. Koh A, de Vadder F, Kovatcheva-Datchary P, Bäckhed F. From Dietary Fiber to Host Physiology: Short-Chain Fatty Acids as Key Bacterial Metabolites. *Cell*. 2016;165(6):1332-1345. doi:10.1016/J.CELL.2016.05.041

366. Erny D, Hrabě de Angelis AL, Prinz M. Communicating systems in the body: how microbiota and microglia cooperate. *Immunology*. 2017;150(1):7-15. doi:10.1111/IMM.12645

367. Pluznick JL. Microbial Short-Chain Fatty Acids and Blood Pressure Regulation. *Curr Hypertens Rep*. 2017;19(4). doi:10.1007/S11906-017-0722-5

368. Tahara Y, Yamazaki M, Sukigara H, et al. Gut Microbiota-Derived Short Chain Fatty Acids Induce Circadian Clock Entrainment in Mouse Peripheral Tissue. *Scientific Reports 2018 8:1*. 2018;8(1):1-12. doi:10.1038/s41598-018-19836-7

369. Donohoe DR, Garge N, Zhang X, et al. The Microbiome and Butyrate Regulate Energy Metabolism and Autophagy in the Mammalian Colon. *Cell Metab*. 2011;13(5):517-526. doi:10.1016/J.CMET.2011.02.018

370. Blouin JM, Penot G, Collinet M, et al. Butyrate elicits a metabolic switch in human colon cancer cells by targeting the pyruvate dehydrogenase complex. *Int J Cancer*. 2011;128(11):2591-2601. doi:10.1002/IJC.25599

371. Binder HJ. Role of colonic short-chain fatty acid transport in diarrhea. *Annu Rev Physiol*. 2010;72:297-313. doi:10.1146/ANNUREV-PHYSIOL-021909-135817

372. Breuer RI, Buto SK, Christ ML, et al. Rectal irrigation with short-chain fatty acids for distal ulcerative colitis. Preliminary report. *Dig Dis Sci*. 1991;36(2):185-187. doi:10.1007/BF01300754

373. VERNIA P, MARCHEGGIANO A, CAPRILLI R, et al. Short-chain fatty acid topical treatment in distal ulcerative colitis. *Aliment Pharmacol Ther*. 1995;9(3):309-313. doi:10.1111/J.1365-2036.1995.TB00386.X

374. di Sabatino A, Morera R, Ciccocioppo R, et al. Oral butyrate for mildly to moderately active Crohn's disease. *Aliment Pharmacol Ther*. 2005;22(9):789-794. doi:10.1111/J.1365-2036.2005.02639.X

375. Strandwitz P, Kim KH, Terekhova D, et al. GABA-modulating bacteria of the human gut microbiota. *Nat Microbiol*. 2019;4(3):396-403. doi:10.1038/S41564-018-0307-3

376. Byrne CS, Chambers ES, Alhabeeb H, et al. Increased colonic propionate reduces anticipatory reward responses in the human striatum to high-energy foods. *Am J Clin Nutr*. 2016;104(1):5-14. doi:10.3945/AJCN.115.126706

377. Arnoldussen IAC, Wiesmann M, Pelgrim CE, et al. Butyrate restores HFD-induced adaptations in brain function and metabolism in mid-adult obese mice. *Int J Obes*. 2017;41(6):935-944. doi:10.1038/IJO.2017.52

378. Liu J, Sun J, Wang F, et al. Neuroprotective Effects of Clostridium butyricum against Vascular Dementia in Mice via Metabolic Butyrate. *Biomed Res Int*. 2015;2015. doi:10.1155/2015/412946

379. Woodruff R. Palliative Medicine: Evidence-Based Symptomatic and Supportive Care for Patients with Advanced Cancer. Published online 2004.

380. Burke KM, LeMone P, Mohn-Brown E, Eby L. Medical-surgical nursing care. Accessed December 17, 2022. https://www.perlego.com/book/812049/medical-surgical-nursing-care-pdf

381. Raja SN, Carr DB, Cohen M, et al. The revised International Association for the Study of Pain definition of pain: concepts, challenges, and compromises. *Pain*. 2020;161(9):1976-1982. doi:10.1097/J.PAIN.0000000000001939

382. Radwany SM, von Gruenigen VE. Palliative and end-of-life care for patients with ovarian cancer. *Clin Obstet Gynecol*. 2012;55(1):173-184. doi:10.1097/GRF.0B013E31824B1AF1

383. Cherny NI, Thaler HT, Friedlander-Klar H, et al. Opioid responsiveness of cancer pain syndromes caused by neuropathic or nociceptive mechanisms: a combined analysis of controlled, single-dose studies. *Neurology*. 1994;44(5):857-861. doi:10.1212/WNL.44.5.857

384. Kennedy R, Abd-Elsayed A. The International Association for the Study of Pain (IASP) Classification of Chronic Pain Syndromes. *Pain*. Published online 2019:1101-1103. doi:10.1007/978-3-319-99124-5_234

385. Longstreth GF, Thompson WG, Chey WD, Houghton LA, Mearin F, Spiller RC. Functional bowel disorders. *Gastroenterology*. 2006;130(5):1480-1491. doi:10.1053/J.GASTRO.2005.11.061

386. Mansfield KE, Sim J, Jordan JL, Jordan KP. A systematic review and meta-analysis of the prevalence of chronic widespread pain in the general population. *Pain*. 2016;157(1):55-64. doi:10.1097/J.PAIN.0000000000000314

387. Regueiro M, Greer JB, Szigethy E. Etiology and Treatment of Pain and Psychosocial Issues in Patients With Inflammatory Bowel Diseases. *Gastroenterology*. 2017;152(2):430-439.e4. doi:10.1053/J.GASTRO.2016.10.036

388. Aziz Q, Giamberardino MA, Barke A, et al. The IASP classification of chronic pain for ICD-11: chronic secondary visceral pain. *Pain*. 2019;160(1):69-76. doi:10.1097/J.PAIN.0000000000001362

389. Procacci P, Zoppi M, Maresca M. Clinical approach to visceral sensation. *Prog Brain Res*. 1986;67(C):21-28. doi:10.1016/S0079-6123(08)62753-3

390. Gebhart GF. Visceral pain-peripheral sensitisation. *Gut*. 2000;47 Suppl 4(Suppl 4). doi:10.1136/GUT.47.SUPPL_4.IV54

391. Bath M, Owens J. Physiology, Viscerosomatic Reflexes. *StatPearls*. Published online May 8, 2022. Accessed December 17, 2022. https://www.ncbi.nlm.nih.gov/books/NBK559218/

392. Foreman RD. Integration of viscerosomatic sensory input at the spinal level. *Prog Brain Res*. 2000;122(C):209-221. doi:10.1016/S0079-6123(08)62140-8

393. Sikandar S, Dickenson AH. Visceral pain: the ins and outs, the ups and downs. *Curr Opin Support Palliat Care*. 2012;6(1):17-26. doi:10.1097/SPC.0B013E32834F6EC9

394. Opportunities & Challenges in Digestive Diseases Research: Recommendations of the National Commission on Digestive Diseases | NIDDK. Accessed December 17, 2022. https://www.niddk.nih.gov/about-niddk/strategic-plans-reports/opportunities-challenges-digestive-diseases-research-recommendations-national-commission

395. Enck P, Aziz Q, Barbara G, et al. Irritable bowel syndrome. *Nat Rev Dis Primers*. 2016;2:1-24. doi:10.1038/NRDP.2016.14

396. Farrell KE, Callister RJ, Keely S. Understanding and targeting centrally mediated visceral pain in inflammatory bowel disease. *Front Pharmacol*. 2014;5. doi:10.3389/FPHAR.2014.00027

397. Santoni M, Miccini F, Battelli N. Gut microbiota, immunity and pain. *Immunol Lett*. 2021;229:44-47. doi:10.1016/J.IMLET.2020.11.010

398. Moloney RD, O'Mahony SM, Dinan TG, Cryan JF. Stress-induced visceral pain: toward animal models of irritable-bowel syndrome and associated comorbidities. *Front Psychiatry*. 2015;6(FEB). doi:10.3389/FPSYT.2015.00015

399. Garakani A, Win T, Virk S, Gupta S, Kaplan D, Masand PS. Comorbidity of irritable bowel syndrome in psychiatric patients: a review. *Am J Ther*. 2003;10(1):61-67. doi:10.1097/00045391-200301000-00014

400. Frissora CL, Koch KL. Symptom overlap and comorbidity of irritable bowel syndrome with other conditions. *Curr Gastroenterol Rep*. 2005;7(4):264-271. doi:10.1007/S11894-005-0018-9

401. Whitehead WE, Palsson O, Jones KR. Systematic review of the comorbidity of irritable bowel syndrome with other disorders: what are the causes and implications? *Gastroenterology*. 2002;122(4):1140-1156. doi:10.1053/GAST.2002.32392

402. Elsenbruch S, Rosenberger C, Bingel U, Forsting M, Schedlowski M, Gizewski ER. Patients with irritable bowel syndrome have altered emotional modulation of neural responses to visceral stimuli. *Gastroenterology*. 2010;139(4). doi:10.1053/J.GASTRO.2010.06.054

403. Harrington AM, Brierley SM, Isaacs N, Hughes PA, Castro J, Blackshaw LA. Sprouting of colonic afferent central terminals and increased spinal mitogen-activated protein kinase expression in a mouse model of chronic visceral hypersensitivity. *Journal of Comparative Neurology*. 2012;520(10):2241-2255. doi:10.1002/CNE.23042

404. Brierley SM, Linden DR. Neuroplasticity and dysfunction after gastrointestinal inflammation. *Nat Rev Gastroenterol Hepatol*. 2014;11(10):611-627. doi:10.1038/NRGASTRO.2014.103

405. Brierley SM, Linden DR. Neuroplasticity and dysfunction after gastrointestinal inflammation. *Nat Rev Gastroenterol Hepatol*. 2014;11(10):611-627. doi:10.1038/NRGASTRO.2014.103

406. Todd AJ. Neuronal circuitry for pain processing in the dorsal horn. *Nat Rev Neurosci*. 2010;11(12):823-836. doi:10.1038/NRN2947

407. Bushnell MC, Čeko M, Low LA. Cognitive and emotional control of pain and its disruption in chronic pain. *Nat Rev Neurosci*. 2013;14(7):502-511. doi:10.1038/NRN3516

408. Wilder-Smith CH. The balancing act: endogenous modulation of pain in functional gastrointestinal disorders. *Gut*. 2011;60(11):1589-1599. doi:10.1136/GUTJNL-2011-300253

409. Heinricher MM, Tavares I, Leith JL, Lumb BM. Descending control of nociception: Specificity, recruitment and plasticity. *Brain Res Rev*. 2009;60(1):214-225. doi:10.1016/J.BRAINRESREV.2008.12.009

410. Denk F, McMahon SB, Tracey I. Pain vulnerability: a neurobiological perspective. *Nat Neurosci*. 2014;17(2):192-200. doi:10.1038/NN.3628

411. Neugebauer V, Li W, Bird GC, Han JS. The amygdala and persistent pain. *Neuroscientist*. 2004;10(3):221-234. doi:10.1177/1073858403261077

412. Giamberardino MAdele. Visceral pain : clinical, pathophysiological, and therapeutic aspects. Published online 2009:108. Accessed December 18, 2022. https://books.google.com/books/about/Visceral_Pain.html?hl=it&id=JPdlaBxO-DAC

413. Cervero F, Laird JMA. Visceral pain. *Lancet*. 1999;353(9170):2145-2148. doi:10.1016/S0140-6736(99)01306-9

414. Bueno L, Fioramonti J, Delvaux M, Frexinos J. Mediators and pharmacology of visceral sensitivity: From basic to clinical investigations. *Gastroenterology*. 1997;112(5):1714-1743. doi:10.1016/S0016-5085(97)70056-8

415. Giamberardino MA. Recent and forgotten aspects of visceral pain. *Eur J Pain*. 1999;3(2):77-92. doi:10.1053/EUJP.1999.0117

416. Gold MS, Gebhart GF. Nociceptor sensitization in pain pathogenesis. *Nature Medicine 2010 16:11*. 2010;16(11):1248-1257. doi:10.1038/nm.2235

417. Gebhart GF, Bielefeldt K. Physiology of Visceral Pain. *Compr Physiol*. 2016;6(4):1609-1633. doi:10.1002/CPHY.C150049

418. van der Schaar PJ, Lamers CBHW, Masclee AAM. The Role of the Barostat in Human Research and Clinical Practice. *http://dx.doi.org/101080/003655299750025552*. 2009;33(34):52-63. doi:10.1080/003655299750025552

419. Posserud I, Syrous A, Lindström L, Tack J, Abrahamsson H, Simrén M. Altered rectal perception in irritable bowel syndrome is associated with symptom severity. *Gastroenterology*. 2007;133(4):1113-1123. doi:10.1053/J.GASTRO.2007.07.024

420. Camilleri M, Katzka DA. Irritable bowel syndrome: methods, mechanisms, and pathophysiology. Genetic epidemiology and pharmacogenetics in irritable bowel syndrome. *Am J Physiol Gastrointest Liver Physiol*. 2012;302(10). doi:10.1152/AJPGI.00537.2011

421. Delvaux M. Do we need to perform rectal distention tests to diagnose IBS in clinical practice? *Gastroenterology*. 2002;122(7):2075-2078. doi:10.1053/gast.2002.34098

422. Ludidi S, Conchillo JM, Keszthelyi D, et al. Rectal hypersensitivity as hallmark for irritable bowel syndrome: defining the optimal cutoff. *Neurogastroenterol Motil*. 2012;24(8). doi:10.1111/J.1365-2982.2012.01926.X

423. Piché M, Arsenault M, Poitras P, Rainville P, Bouin M. Widespread hypersensitivity is related to altered pain inhibition processes in irritable bowel syndrome. *Pain*. 2010;148(1):49-58. doi:10.1016/J.PAIN.2009.10.005

424. Ness TJ, Gebhart GF. Colorectal distension as a noxious visceral stimulus: physiologic and pharmacologic characterization of pseudaffective reflexes in the rat. *Brain Res*. 1988;450(1-2):153-169. doi:10.1016/0006-8993(88)91555-7

425. Kamp EH, Jones RCW, Tillman SR, Gebhart GF. Quantitative assessment and characterization of visceral nociception and hyperalgesia in mice. *Am J Physiol Gastrointest Liver Physiol*. 2003;284(3). doi:10.1152/AJPGI.00324.2002

426. Björkman R, Hedner J, Hedner T, Henning M. Central, naloxone-reversible antinociception by diclofenac in the rat. *Naunyn Schmiedebergs Arch Pharmacol*. 1990;342(2):171-176. doi:10.1007/BF00166960

427. Schwartz ES, Gebhart GF. Visceral pain. *Curr Top Behav Neurosci*. 2014;20:171-197. doi:10.1007/7854_2014_315

428. O'Mahony SM, Dinan TG, Cryan JF. The gut microbiota as a key regulator of visceral pain. *Pain*. 2017;158 Suppl 1(4):S19-S28. doi:10.1097/J.PAIN.0000000000000779

429. de Palma G, Collins SM, Bercik P, Verdu EF. The microbiota-gut-brain axis in gastrointestinal disorders: stressed bugs, stressed brain or both? *J Physiol*. 2014;592(14):2989-2997. doi:10.1113/JPHYSIOL.2014.273995

430. Bravo JA, Julio-Pieper M, Forsythe P, et al. Communication between gastrointestinal bacteria and the nervous system. *Curr Opin Pharmacol*. 2012;12(6):667-672. doi:10.1016/J.COPH.2012.09.010

431. Pusceddu MM, Gareau MG. Visceral pain: gut microbiota, a new hope? doi:10.1186/s12929-018-0476-7

432. Verdú EF, Bercik P, Verma-Gandhu M, et al. Specific probiotic therapy attenuates antibiotic induced visceral hypersensitivity in mice. *Gut*. 2006;55(2):182. doi:10.1136/GUT.2005.066100

433. Rousseaux C, Thuru X, Gelot A, et al. Lactobacillus acidophilus modulates intestinal pain and induces opioid and cannabinoid receptors B R I E F C O M M U N I C AT I O N S. *NATURE MEDICINE VOLUME*. 2007;13(1). doi:10.1038/nm1521

434. Miranda PM, de Palma G, Serkis V, et al. High salt diet exacerbates colitis in mice by decreasing Lactobacillus levels and butyrate production. *Microbiome*. 2018;6(1):57. doi:10.1186/S40168-018-0433-4/TABLES/2

435. Chiu IM, Heesters BA, Ghasemlou N, et al. Bacteria activate sensory neurons that modulate pain and inflammation. *Nature*. 2013;501(7465):52-57. doi:10.1038/NATURE12479

436. Lomax AE, Pradhananga S, Sessenwein JL, Dervla O'malley X. MINI-REVIEW Neurogastroenterology and Motility Bacterial modulation of visceral sensation: mediators and mechanisms. *Am J Physiol Gastrointest Liver Physiol*. 2019;317:363-372. doi:10.1152/ajpgi.00052.2019.-The

437. Al-Nedawi K, Mian MF, Hossain N, et al. Gut commensal microvesicles reproduce parent bacterial signals to host immune and enteric nervous systems. *FASEB J*. 2015;29(2):684-695. doi:10.1096/FJ.14-259721

438. Muller PA, Koscsó B, Rajani GM, et al. Crosstalk between Muscularis Macrophages and Enteric Neurons Regulates Gastrointestinal Motility. *Cell*. 2014;158(5):1210. doi:10.1016/J.CELL.2014.08.002

439. Crouzet L, Gaultier E, Del'Homme C, et al. The hypersensitivity to colonic distension of IBS patients can be transferred to rats through their fecal microbiota. *Neurogastroenterology & Motility*. 2013;25(4):e272-e282. doi:10.1111/NMO.12103

440. O'Mahony SM, Felice VD, Nally K, et al. Disturbance of the gut microbiota in early-life selectively affects visceral pain in adulthood without impacting cognitive or anxiety-related behaviors in male rats. *Neuroscience*. 2014;277:885-901. doi:10.1016/J.NEUROSCIENCE.2014.07.054

441. Song Z, Xie W, Chen S, et al. High-fat diet increases pain behaviors in rats with or without obesity. *Sci Rep*. 2017;7(1). doi:10.1038/S41598-017-10458-Z

442. Reijnders D, Goossens GH, Hermes GDA, et al. Effects of Gut Microbiota Manipulation by Antibiotics on Host Metabolism in Obese Humans: A Randomized Double-Blind Placebo-Controlled Trial. *Cell Metab*. 2016;24(2):341. doi:10.1016/J.CMET.2016.07.008

443. de Filippo C, Cavalieri D, di Paola M, et al. Impact of diet in shaping gut microbiota revealed by a comparative study in children from Europe and rural Africa. *Proc Natl Acad Sci U S A*. 2010;107(33):14691-14696. doi:10.1073/PNAS.1005963107/SUPPL_FILE/PNAS.201005963SI.PDF

444. Tarrerias AL, Millecamps M, Alloui A, et al. Short-chain fatty acid enemas fail to decrease colonic hypersensitivity and inflammation in TNBS-induced colonic inflammation in rats. *Pain*. 2002;100(1-2):91-97. doi:10.1016/S0304-3959(02)00234-8

445. Xu D, Wu X, Grabauskas G, Owyang C. Butyrate-induced colonic hypersensitivity is mediated by mitogen-activated protein kinase activation in rat dorsal root ganglia. *Gut*. 2012;62(10):1466-1474. doi:10.1136/GUTJNL-2012-302260

446. Vicario N, Turnaturi R, Spitale FM, et al. Intercellular communication and ion channels in neuropathic pain chronicization. *Inflammation Research*. 2020;69(9):841-850. doi:10.1007/S00011-020-01363-9

447. Weissmann C, Albanese AA, Contreras NE, Gobetto MN, Castellanos LCS, Uchitel OD. Ion channels and pain in Fabry disease. *Mol Pain*. 2021;17. doi:10.1177/17448069211033172

448. Balemans D, Boeckxstaens GE, Talavera K, Wouters MM. Transient receptor potential ion channel function in sensory transduction and cellular signaling cascades underlying visceral hypersensitivity. *Am J Physiol Gastrointest Liver Physiol*. 2017;312:635-648. doi:10.1152/ajpgi.00401.2016

449. Wu LJ, Sweet TB, Clapham DE. International Union of Basic and Clinical Pharmacology. LXXVI. Current progress in the mammalian TRP ion channel family. *Pharmacol Rev*. 2010;62(3):381-404. doi:10.1124/PR.110.002725

450. Bandell M, Macpherson LJ, Patapoutian A. From chills to chilis: mechanisms for thermosensation and chemesthesis via thermoTRPs. *Curr Opin Neurobiol*. 2007;17(4):490-497. doi:10.1016/J.CONB.2007.07.014

451. Dhaka A, Viswanath V, Patapoutian A. Trp ion channels and temperature sensation. *Annu Rev Neurosci*. 2006;29:135-161. doi:10.1146/ANNUREV.NEURO.29.051605.112958

452. Clapham DE, Julius D, Montell C, Schultz G. International Union of Pharmacology. XLIX. Nomenclature and structure-function relationships of transient receptor potential channels. *Pharmacol Rev*. 2005;57(4):427-450. doi:10.1124/PR.57.4.6

453. Nilius B, Owsianik G, Voets T, Peters JA. Transient receptor potential cation channels in disease. *Physiol Rev*. 2007;87(1):165-217. doi:10.1152/PHYSREV.00021.2006

454. Matta JA, Ahern GP. Voltage is a partial activator of rat thermosensitive TRP channels. *J Physiol*. 2007;585(Pt 2):469-482. doi:10.1113/JPHYSIOL.2007.144287

455. Holzer P. Local effector functions of capsaicin-sensitive sensory nerve endings: involvement of tachykinins, calcitonin gene-related peptide and other neuropeptides. *Neuroscience*. 1988;24(3):739-768. doi:10.1016/0306-4522(88)90064-4

456. Holzer P. Transient receptor potential (TRP) channels as drug targets for diseases of the digestive system. *Pharmacol Ther*. 2011;131(1):142-170. doi:10.1016/J.PHARMTHERA.2011.03.006

457. Blackshaw LA, Brierley SM, Hughes PA. TRP channels: New targets for visceral pain. *Gut*. 2010;59(1):126-135. doi:10.1136/gut.2009.179523

458. Alaimo A, Rubert J. The Pivotal Role of TRP Channels in Homeostasis and Diseases throughout the Gastrointestinal Tract. *Int J Mol Sci*. 2019;20(21). doi:10.3390/IJMS20215277

459. Christianson JA, Bielefeldt K, Malin SA, Davis BM. Neonatal colon insult alters growth factor expression and TRPA1 responses in adult mice. *Pain*. 2010;151(2):540-549. doi:10.1016/J.PAIN.2010.08.029

460. Vergnolle N, Cenac N, Altier C, et al. A role for transient receptor potential vanilloid 4 in tonicity-induced neurogenic inflammation. *Br J Pharmacol*. 2010;159(5):1161-1173. doi:10.1111/J.1476-5381.2009.00590.X

461. Veldhuis NA, Poole DP, Grace M, McIntyre P, Bunnett NW. The G protein-coupled receptor-transient receptor potential channel axis: molecular insights for targeting disorders of sensation and inflammation. *Pharmacol Rev*. 2015;67(1):36-73. doi:10.1124/PR.114.009555

462. Tominaga M, Caterina MJ, Malmberg AB, et al. The cloned capsaicin receptor integrates multiple pain-producing stimuli. *Neuron*. 1998;21(3):531-543. doi:10.1016/S0896-6273(00)80564-4

463. Caterina MJ, Schumacher MA, Tominaga M, Rosen TA, Levine JD, Julius D. The capsaicin receptor: a heat-activated ion channel in the pain pathway. *Nature*. 1997;389(6653):816-824. doi:10.1038/39807

464. Everaerts W, Gees M, Alpizar YA, et al. The capsaicin receptor TRPV1 is a crucial mediator of the noxious effects of mustard oil. *Curr Biol*. 2011;21(4):316-321. doi:10.1016/J.CUB.2011.01.031

465. Gavva NR, Treanor JJS, Garami A, et al. Pharmacological blockade of the vanilloid receptor TRPV1 elicits marked hyperthermia in humans. *Pain*. 2008;136(1-2):202-210. doi:10.1016/J.PAIN.2008.01.024

466. Hwang SW, Cho H, Kwak J, et al. Direct activation of capsaicin receptors by products of lipoxygenases: endogenous capsaicin-like substances. *Proc Natl Acad Sci U S A*. 2000;97(11):6155-6160. doi:10.1073/PNAS.97.11.6155

467. Toyoda H. Ion channels involved in spontaneous pain. Published online September 5, 2018. doi:10.31487/J.NNB.2018.02.001

468. Hofmann L, Hose D, Grießhammer A, et al. Characterization of small fiber pathology in a mouse model of Fabry disease. *Elife*. 2018;7. doi:10.7554/ELIFE.39300

469. Patterson LM, Zheng H, Ward SM, Berthoud HR. Vanilloid receptor (VR1) expression in vagal afferent neurons innervating the gastrointestinal tract. *Cell Tissue Res*. 2003;311(3):277-287. doi:10.1007/S00441-002-0682-0

470. Ward SM, Bayguinov J, Won KJ, Grundy D, Berthoud HR. Distribution of the vanilloid receptor (VR1) in the gastrointestinal tract. *J Comp Neurol*. 2003;465(1):121-135. doi:10.1002/CNE.10801

471. Kadowaki M, Kuramoto H, Takaki M. Combined determination with functional and morphological studies of origin of nerve fibers expressing transient receptor potential vanilloid 1 in the myenteric plexus of the rat jejunum. *Auton Neurosci*. 2004;116(1-2):11-18. doi:10.1016/J.AUTNEU.2004.08.005

472. Robinson DR, Mcnaughton PA, Evans ML, Hicks GA. Characterization of the primary spinal afferent innervation of the mouse colon using retrograde labelling. *Neurogastroenterol Motil*. 2004;16(1):113-124. doi:10.1046/J.1365-2982.2003.00456.X

473. Ryu V, Gallaher Z, Czaja K. Plasticity of nodose ganglion neurons after capsaicin- and vagotomy-induced nerve damage in adult rats. *Neuroscience*. 2010;167(4):1227-1238. doi:10.1016/J.NEUROSCIENCE.2010.02.049

474. Zhao H, Sprunger LK, Simasko SM. Expression of transient receptor potential channels and two-pore potassium channels in subtypes of vagal afferent neurons in rat. *Am J Physiol Gastrointest Liver Physiol*. 2010;298(2). doi:10.1152/AJPGI.00396.2009

475. Michael GJ, Priestley J v. Differential Expression of the mRNA for the Vanilloid Receptor Subtype 1 in Cells of the Adult Rat Dorsal Root and Nodose Ganglia and Its Downregulation by Axotomy. *Journal of Neuroscience*. 1999;19(5):1844-1854. doi:10.1523/JNEUROSCI.19-05-01844.1999

476. Banerjee B, Medda BK, Lazarova Z, Bansal N, Shaker R, Sengupta JN. Effect of reflux-induced inflammation on transient receptor potential vanilloid one (TRPV1) expression in primary sensory neurons innervating the oesophagus of rats. *Neurogastroenterology & Motility*. 2007;19(8):681-691. doi:10.1111/J.1365-2982.2007.00947.X

477. Tan LL, Bornstein JC, Anderson CR. Distinct chemical classes of medium-sized transient receptor potential channel vanilloid 1-immunoreactive dorsal root ganglion neurons innervate the adult mouse jejunum and colon. *Neuroscience*. 2008;156(2):334-343. doi:10.1016/J.NEUROSCIENCE.2008.06.071

478. Tan LL, Bornstein JC, Anderson CR. Neurochemical and morphological phenotypes of vagal afferent neurons innervating the adult mouse jejunum. *Neurogastroenterol Motil*. 2009;21(9):994-1001. doi:10.1111/J.1365-2982.2009.01322.X

479. Christianson JA, McIlwrath SL, Koerber HR, Davis BM. Transient receptor potential vanilloid 1-immunopositive neurons in the mouse are more prevalent within colon afferents compared to skin and muscle afferents. *Neuroscience*. 2006;140(1):247-257. doi:10.1016/J.NEUROSCIENCE.2006.02.015

480. Brierley SM, Carter R, Jones W, et al. Differential chemosensory function and receptor expression of splanchnic and pelvic colonic afferents in mice. *Journal of Physiology*. 2005;567(1):267-281. doi:10.1113/JPHYSIOL.2005.089714

481. van Wanrooij SJM, Wouters MM, van Oudenhove L, et al. Sensitivity testing in irritable bowel syndrome with rectal capsaicin stimulations: role of TRPV1 upregulation and sensitization in visceral hypersensitivity? *Am J Gastroenterol*. 2014;109(1):99-109. doi:10.1038/AJG.2013.371

482. Sugiura T, Bielefeldt K, Gebhart GF. TRPV1 function in mouse colon sensory neurons is enhanced by metabotropic 5-hydroxytryptamine receptor activation. *J Neurosci*. 2004;24(43):9521-9530. doi:10.1523/JNEUROSCI.2639-04.2004

483. Amadesi S, Nie J, Vergnolle N, et al. Protease-Activated Receptor 2 Sensitizes the Capsaicin Receptor Transient Receptor Potential Vanilloid Receptor 1 to Induce Hyperalgesia. *The Journal of Neuroscience*. 2004;24(18):4300. doi:10.1523/JNEUROSCI.5679-03.2004

484. Chuang HH, Prescott ED, Kong H, et al. Bradykinin and nerve growth factor release the capsaicin receptor from PtdIns(4,5)P2-mediated inhibition. *Nature*. 2001;411(6840):957-962. doi:10.1038/35082088

485. Wouters MM, Balemans D, van Wanrooy S, et al. Histamine Receptor H1-Mediated Sensitization of TRPV1 Mediates Visceral Hypersensitivity and Symptoms in Patients With Irritable Bowel Syndrome. *Gastroenterology*. 2016;150(4):875-887.e9. doi:10.1053/J.GASTRO.2015.12.034

486. Lapointe TK, Basso L, Iftinca MC, et al. TRPV1 sensitization mediates postinflammatory visceral pain following acute colitis. *Am J Physiol Gastrointest Liver Physiol*. 2015;309:87-99. doi:10.1152/ajpgi.00421.2014.-Quiescent

487. van den Wijngaard RM, Klooker TK, Welting O, et al. Essential role for TRPV1 in stress-induced (mast cell-dependent) colonic hypersensitivity in maternally separated rats. *Neurogastroenterol Motil*. 2009;21(10). doi:10.1111/J.1365-2982.2009.01339.X

488. Liedtke W, Choe Y, Martí-Renom MA, et al. Vanilloid Receptor–Related Osmotically Activated Channel (VR-OAC), a Candidate Vertebrate Osmoreceptor. *Cell*. 2000;103(3):525-535. doi:10.1016/S0092-8674(00)00143-4

489. Strotmann R, Harteneck C, Nunnenmacher K, Schultz G, Plant TD. OTRPC4, a nonselective cation channel that confers sensitivity to extracellular osmolarity. *Nat Cell Biol*. 2000;2(10):695-702. doi:10.1038/35036318

490. Wissenbach U, Bödding M, Freichel M, Flockerzi V. Trp12, a novel Trp related protein from kidney. *FEBS Lett*. 2000;485(2-3):127-134. doi:10.1016/S0014-5793(00)02212-2

491. Gao X, Wu L, O'Neil RG. Temperature-modulated diversity of TRPV4 channel gating: activation by physical stresses and phorbol ester derivatives through protein kinase C-dependent and - independent pathways. *J Biol Chem*. 2003;278(29):27129-27137. doi:10.1074/JBC.M302517200

492. Suzuki M, Mizuno A, Kodaira K, Imai M. Impaired pressure sensation in mice lacking TRPV4. *J Biol Chem*. 2003;278(25):22664-22668. doi:10.1074/JBC.M302561200

493. Cenac N, Bautzova T, le Faouder P, et al. Quantification and Potential Functions of Endogenous Agonists of Transient Receptor Potential Channels in Patients With Irritable Bowel Syndrome. *Gastroenterology*. 2015;149(2):433-444.e7. doi:10.1053/J.GASTRO.2015.04.011

494. Xu F, Satoh E, Iijima T. Protein kinase C-mediated Ca2+ entry in HEK 293 cells transiently expressing human TRPV4. *Br J Pharmacol*. 2003;140(2):413-421. doi:10.1038/SJ.BJP.0705443

495. Grant AD, Cottrell GS, Amadesi S, et al. Protease-activated receptor 2 sensitizes the transient receptor potential vanilloid 4 ion channel to cause mechanical hyperalgesia in mice. *J Physiol*. 2007;578(Pt 3):715-733. doi:10.1113/JPHYSIOL.2006.121111

496. Watanabe H, Vriens J, Prenen J, Droogmans G, Voets T, Nillus B. Anandamide and arachidonic acid use epoxyeicosatrienoic acids to activate TRPV4 channels. *Nature 2003 424:6947*. 2003;424(6947):434-438. doi:10.1038/nature01807

497. Watanabe H, Davis JB, Smart D, et al. Activation of TRPV4 Channels (hVRL-2/mTRP12) by Phorbol Derivatives. *Journal of Biological Chemistry*. 2002;277(16):13569-13577. doi:10.1074/JBC.M200062200

498. Brierley SM, Page AJ, Hughes PA, et al. Selective Role for TRPV4 Ion Channels in Visceral Sensory Pathways. *Gastroenterology*. 2008;134(7):2059-2069. doi:10.1053/j.gastro.2008.01.074

499. Fichna J, Poole DP, Veldhuis N, et al. Transient receptor potential vanilloid 4 inhibits mouse colonic motility by activating NO-dependent enteric neurotransmission. *J Mol Med (Berl)*. 2015;93(12):1297-1309. doi:10.1007/S00109-015-1336-5

500. Fichna J, Mokrowiecka A, Cygankiewicz AI, et al. Transient receptor potential vanilloid 4 blockade protects against experimental colitis in mice: a new strategy for inflammatory bowel diseases treatment? *Neurogastroenterol Motil*. 2012;24(11). doi:10.1111/J.1365-2982.2012.01999.X

501.   Buhner S, Li Q, Vignali S, et al. Activation of human enteric neurons by supernatants of colonic biopsy specimens from patients with irritable bowel syndrome. *Gastroenterology*. 2009;137(4):1425-1434. doi:10.1053/J.GASTRO.2009.07.005

502.   Cenac N, Andrews CN, Holzhausen M, et al. Role for protease activity in visceral pain in irritable bowel syndrome. *J Clin Invest*. 2007;117(3):636-647. doi:10.1172/JCI29255

503.   Cenac N, Altier C, Chapman K, Liedtke W, Zamponi G, Vergnolle N. Transient receptor potential vanilloid-4 has a major role in visceral hypersensitivity symptoms. *Gastroenterology*. 2008;135(3). doi:10.1053/J.GASTRO.2008.05.024

504.   Materazzi S, Nassini R, Andrè E, et al. Cox-dependent fatty acid metabolites cause pain through activation of the irritant receptor TRPA1. *Proc Natl Acad Sci U S A*. 2008;105(33):12045-12050. doi:10.1073/PNAS.0802354105

505.   Andersson DA, Gentry C, Moss S, Bevan S. Transient receptor potential A1 is a sensory receptor for multiple products of oxidative stress. *J Neurosci*. 2008;28(10):2485-2494. doi:10.1523/JNEUROSCI.5369-07.2008

506.   Bautista DM, Movahed P, Hinman A, et al. Pungent products from garlic activate the sensory ion channel TRPA1. *Proc Natl Acad Sci U S A*. 2005;102(34):12248-12252. doi:10.1073/PNAS.0505356102

507.   Jordt SE, Bautista DM, Chuang HH, et al. Mustard oils and cannabinoids excite sensory nerve fibres through the TRP channel ANKTM1. *Nature*. 2004;427(6971):260-265. doi:10.1038/NATURE02282

508.   Karashima Y, Damann N, Prenen J, et al. Bimodal action of menthol on the transient receptor potential channel TRPA1. *J Neurosci*. 2007;27(37):9874-9884. doi:10.1523/JNEUROSCI.2221-07.2007

509.   Bandell M, Story GM, Hwang SW, et al. Noxious cold ion channel TRPA1 is activated by pungent compounds and bradykinin. *Neuron*. 2004;41(6):849-857. doi:10.1016/S0896-6273(04)00150-3

510.   Nagata K, Duggan A, Kumar G, García-Añoveros J. Nociceptor and hair cell transducer properties of TRPA1, a channel for pain and hearing. *J Neurosci*. 2005;25(16):4052-4061. doi:10.1523/JNEUROSCI.0013-05.2005

511.   Miller JJ, Aoki K, Moehring F, et al. Neuropathic pain in a Fabry disease rat model. *JCI Insight*. 2018;3(6). doi:10.1172/JCI.INSIGHT.99171

512.   Lennertz RC, Kossyreva EA, Smith AK, Stucky CL. TRPA1 mediates mechanical sensitization in nociceptors during inflammation. *PLoS One*. 2012;7(8). doi:10.1371/JOURNAL.PONE.0043597

513.   Wei H, Hämäläinen MM, Saarnilehto M, Koivisto A, Pertovaara A. Attenuation of Mechanical Hypersensitivity by an Antagonist of the TRPA1 Ion Channel in Diabetic Animals. *Anesthesiology*. 2009;111(1):147-154. doi:10.1097/ALN.0B013E3181A1642B

514.   Eid SR, Crown ED, Moore EL, et al. HC-030031, a TRPA1 selective antagonist, attenuates inflammatory- and neuropathy-induced mechanical hypersensitivity. *Mol Pain*. 2008;4. doi:10.1186/1744-8069-4-48

515.   Miller JJ, Aoki K, Moehring F, et al. Neuropathic pain in a Fabry disease rat model. *JCI Insight*. 2018;3(6). doi:10.1172/jci.insight.99171

516.   Story GM, Peier AM, Reeve AJ, et al. ANKTM1, a TRP-like Channel Expressed in Nociceptive Neurons, Is Activated by Cold Temperatures. *Cell*. 2003;112(6):819-829. doi:10.1016/S0092-8674(03)00158-2

517. Brierley SM, Hughes PA, Page AJ, et al. The ion channel TRPA1 is required for normal mechanosensation and is modulated by algesic stimuli. *Gastroenterology*. 2009;137(6):2084-2095.e3. doi:10.1053/J.GASTRO.2009.07.048

518. Kono T, Kaneko A, Omiya Y, Ohbuchi K, Ohno N, Yamamoto M. Epithelial transient receptor potential ankyrin 1 (TRPA1)-dependent adrenomedullin upregulates blood flow in rat small intestine. *Am J Physiol Gastrointest Liver Physiol*. 2013;304(4). doi:10.1152/AJPGI.00356.2012

519. Yang J, Li Y, Zuo X, Zhen Y, Yu Y, Gao L. Transient receptor potential ankyrin-1 participates in visceral hyperalgesia following experimental colitis. *Neurosci Lett*. 2008;440(3):237-241. doi:10.1016/J.NEULET.2008.05.093

520. Yang Y, Wang S, Kobayashi K, et al. TRPA1-expressing lamina propria mesenchymal cells regulate colonic motility. *JCI Insight*. 2019;4(9). doi:10.1172/JCI.INSIGHT.122402

521. Cattaruzza F, Spreadbury I, Miranda-Morales M, Grady EF, Vanner S, Bunnett NW. Transient receptor potential ankyrin-1 has a major role in mediating visceral pain in mice. *Am J Physiol Gastrointest Liver Physiol*. 2010;298(1):G81-G91. doi:10.1152/AJPGI.00221.2009

522. Kun J, Szitter I, Kemény Á, et al. Upregulation of the transient receptor potential ankyrin 1 ion channel in the inflamed human and mouse colon and its protective roles. *PLoS One*. 2014;9(9). doi:10.1371/JOURNAL.PONE.0108164

523. Barrett KE, Keely SJ. *CHLORIDE SECRETION BY THE INTESTINAL EPITHELIUM: Molecular Basis and Regulatory Aspects*. Vol 62.; 2000. www.annualreviews.org

524. Murek M, Kopic S, Geibel J. Evidence for intestinal chloride secretion. *Exp Physiol*. 2010;95(4):471-478. doi:10.1113/EXPPHYSIOL.2009.049445

525. Seidler U, Lenzen H, Cinar A, Tessema T, Bleich A, Riederer B. Molecular Mechanisms of Disturbed Electrolyte Transport in Intestinal Inflammation. *Ann N Y Acad Sci*. 2006;1072(1):262-275. doi:10.1196/ANNALS.1326.024

526. Binder HJ. Mechanisms of diarrhea in inflammatory bowel diseases. *Ann N Y Acad Sci*. 2009;1165:285-293. doi:10.1111/J.1749-6632.2009.04039.X

527. Ooi CY, Durie PR. Cystic fibrosis from the gastroenterologist's perspective. *Nat Rev Gastroenterol Hepatol*. 2016;13(3):175-185. doi:10.1038/nrgastro.2015.226

528. Gawenis LR, Bradford EM, Alper SL, Prasad V, Shull GE. AE2 Cl-/HCO3- exchanger is required for normal cAMP-stimulated anion secretion in murine proximal colon. *Am J Physiol Gastrointest Liver Physiol*. 2010;298(4). doi:10.1152/AJPGI.00178.2009

529. Gawenis LR, Stien X, Shull GE, et al. Intestinal NaCl transport in NHE2 and NHE3 knockout mice. *Am J Physiol Gastrointest Liver Physiol*. 2002;282(5). doi:10.1152/AJPGI.00297.2001

530. Schultheis PJ, Clarke LL, Meneton P, et al. Targeted disruption of the murine Na+/H+ exchanger isoform 2 gene causes reduced viability of gastric parietal cells and loss of net acid secretion. *J Clin Invest*. 1998;101(6):1243-1253. doi:10.1172/JCI1249

531. Simpson JE, Schweinfest CW, Shull GE, et al. PAT-1 (Slc26a6) is the predominant apical membrane Cl-/HCO 3- exchanger in the upper villous epithelium of the murine duodenum. *Am J Physiol Gastrointest Liver Physiol*. 2007;292(4):1079-1088. doi:10.1152/AJPGI.00354.2006/ASSET/IMAGES/LARGE/ZH30040747130007.JPEG

532. Jacob P, Rossmann H, Lamprecht G, et al. Down-regulated in adenoma mediates apical Cl-/HCO3- exchange in rabbit, rat, and human duodenum. *Gastroenterology*. 2002;122(3):709-724. doi:10.1053/gast.2002.31875

533. Wang Z, Petrovic S, Mann E, Soleimani M. Identification of an apical Cl(-)/HCO3(-) exchanger in the small intestine. *Am J Physiol Gastrointest Liver Physiol*. 2002;282(3). doi:10.1152/AJPGI.00338.2001

534. Höglund P, Haila S, Socha J, et al. Mutations of the Down–regulated in adenoma (DRA) gene cause congenital chloride diarrhoea. *Nature Genetics 1996 14:3*. 1996;14(3):316-319. doi:10.1038/ng1196-316

535. Bachmann O, Seidler U. News from the end of the gut--how the highly segmental pattern of colonic HCO₃⁻ transport relates to absorptive function and mucosal integrity. *Biol Pharm Bull*. 2011;34(6):794-802. doi:10.1248/BPB.34.794

536. Kiela PR, Kuscuoglu N, Midura AJ, et al. Molecular mechanism of rat NHE3 gene promoter regulation by sodium butyrate. *Am J Physiol Cell Physiol*. 2007;293(1). doi:10.1152/AJPCELL.00277.2006

537. Zeissig S, Fromm A, Mankertz J, et al. Butyrate Induces Intestinal Sodium Absorption via Sp3-Mediated Transcriptional Up-Regulation of Epithelial Sodium Channels. *Gastroenterology*. 2007;132(1):236-248. doi:10.1053/J.GASTRO.2006.10.033

538. Vidyasagar S, Barmeyer C, Geibel J, Binder HJ, Rajendran VM. Role of short-chain fatty acids in colonic HCO(3) secretion. *Am J Physiol Gastrointest Liver Physiol*. 2005;288(6). doi:10.1152/AJPGI.00415.2004

539. Hogan DL, Crombie DL, Isenberg JI, Svendsen P, Schaffalitzky De Muckadell OB, Ainsworth MA. CFTR mediates cAMP- and Ca2+-activated duodenal epithelial HCO3- secretion. *https://doi.org/101152/ajpgi19972724G872*. 1997;272(4 35-4). doi:10.1152/AJPGI.1997.272.4.G872

540. Barrett KE, Keely SJ. Integrative Physiology and Pathophysiology of Intestinal Electrolyte Transport. *Physiology of the Gastrointestinal Tract*. 2006;2:1931-1951. doi:10.1016/B978-012088394-3/50079-9

541. Cuppoletti J, Malinowska DH. Ion Channels of the Epithelia of the Gastrointestinal Tract. *Physiology of the Gastrointestinal Tract, Two Volume Set*. Published online April 30, 2012:1863-1876. doi:10.1016/B978-0-12-382026-6.00069-5

542. Xue J, Askwith C, Javed NH, Cooke HJ. Autonomic Nervous System and Secretion across the Intestinal Mucosal Surface.

543. Pressley TA. Structure and function of the Na,K pump: ten years of molecular biology. *Miner Electrolyte Metab*. 1996;22(5-6):264-271. Accessed December 20, 2022. https://europepmc.org/article/MED/8933497

544. Maciej Serda, Becker FG, Cleary M, et al. Colonic sodium-potassium adenosine triphosphate subunit gene expression: Ontogeny and regulation by adrenocortical steroids. G. Balint, Antala B, Carty C, Mabieme JMA, Amar IB, Kaplanova A, eds. *Endocrinology*. 1990;127(1):32-38. doi:10.2/JQUERY.MIN.JS

545. Sugiura T, Dang K, Lamb K, Bielefeldt K, Gebhart GF. Acid-sensing properties in rat gastric sensory neurons from normal and ulcerated stomach. *J Neurosci*. 2005;25(10):2617-2627. doi:10.1523/JNEUROSCI.2894-04.2005

546. Rong W, Hillsley K, Davis JB, Hicks G, Winchester WJ, Grundy D. Jejunal afferent nerve sensitivity in wild-type and TRPV1 knockout mice. *J Physiol*. 2004;560(3):867-881. doi:10.1113/JPHYSIOL.2004.071746

547. Payne JA, Forbush B. Molecular characterization of the epithelial Na-K-Cl cotransporter isoforms. *Curr Opin Cell Biol*. 1995;7(4):493-503. doi:10.1016/0955-0674(95)80005-0

548. Torchia J, Lytle C, Pon DJ, Forbush B, Sen AK. The Na-K-Cl cotransporter of avian salt gland. Phosphorylation in response to cAMP-dependent and calcium-dependent secretogogues. *Journal of Biological Chemistry*. 1992;267(35):25444-25450. doi:10.1016/s0021-9258(19)74061-7

549. Darman RB, Forbush B. A regulatory locus of phosphorylation in the N terminus of the Na-K-Cl cotransporter, NKCC1. *J Biol Chem*. 2002;277(40):37542-37550. doi:10.1074/JBC.M206293200

550. Lytle C, Forbush B. Regulatory phosphorylation of the secretory Na-K-Cl cotransporter: modulation by cytoplasmic Cl. *https://doi.org/101152/ajpcell19962702C437*. 1996;270(2 39-2). doi:10.1152/AJPCELL.1996.270.2.C437

551. D'Andrea L, Lytle C, Matthews JB, Hofman P, Forbush B, Madara JL. Na:K:2Cl cotransporter (NKCC) of intestinal epithelial cells. Surface expression in response to cAMP. *J Biol Chem*. 1996;271(46):28969-28976. doi:10.1074/JBC.271.46.28969

552. McRoberts JA, Beuerlein G, Dharmsathaphorn K. Cyclic AMP and Ca2+-activated K+ transport in a human colonic epithelial cell line. *Journal of Biological Chemistry*. 1985;260(26):14163-14172. doi:10.1016/s0021-9258(17)38698-2

553. Lomax RB, Warhurst G, Sandle GI. Characteristics of two basolateral potassium channel populations in human colonic crypts. *Gut*. 1996;38(2):243-247. doi:10.1136/GUT.38.2.243

554. Greger R, Bleich M, Warth R. New types of K+ channels in the colon. *Wien Klin Wochenschr*. 1997;109(3):497-500. doi:10.1007/BF01986871

555. Devor DC, Frizzell RA. Modulation of K+ channels by arachidonic acid in T84 cells. I. Inhibition of the Ca(2+)-dependent K+ channel. *Am J Physiol*. 1998;274(1). doi:10.1152/AJPCELL.1998.274.1.C138

556. Riordan JR, Rommens JM, Kerem BS, et al. Identification of the cystic fibrosis gene: cloning and characterization of complementary DNA. *Science*. 1989;245(4922):1066-1073. doi:10.1126/SCIENCE.2475911

557. Fuller CM, Benos DJ. CFTR! *Am J Physiol*. 1992;263(2 Pt 1). doi:10.1152/AJPCELL.1992.263.2.C267

558. Sheppard DN, Welsh MJ. Structure and function of the CFTR chloride channel. *Physiol Rev*. 1999;79(1 Suppl). doi:10.1152/PHYSREV.1999.79.1.S23

559. Welsh MJ, Smith AE. Molecular mechanisms of CFTR chloride channel dysfunction in cystic fibrosis. *Cell*. 1993;73(7):1251-1254. doi:10.1016/0092-8674(93)90353-R

560. Singh AK, Taskén K, Walker W, et al. Characterization of PKA isoforms and kinase-dependent activation of chloride secretion in T84 cells. *Am J Physiol*. 1998;275(2). doi:10.1152/AJPCELL.1998.275.2.C562

561. Reddy MM, Quinton PM. Hydrolytic and nonhydrolytic interactions in the ATP regulation of CFTR Cl-conductance. *Am J Physiol*. 1996;271(1 Pt 1):C35-42. doi:10.1152/AJPCELL.1996.271.1.C35

562. Picciotto MR, Cohn JA, Bertuzzi G, Greengard P, Nairn AC. Phosphorylation of the cystic fibrosis transmembrane conductance regulator. *Journal of Biological Chemistry*. 1992;267(18):12742-12752. doi:10.1016/S0021-9258(18)42339-3

563. Howard M, Jilling T, Duvall M, Frizzell RA. cAMP-regulated trafficking of epitope-tagged CFTR. *Kidney Int*. 1996;49(6):1642-1648. doi:10.1038/KI.1996.239

564. Jilling T, Kirk KL. The Biogenesis, Traffic, and Function of the Cystic Fibrosis Transmembrane Conductance Regulator. *Int Rev Cytol*. 1997;172:193-241. doi:10.1016/S0074-7696(08)62361-X

565. Loffing J, Moyer BD, McCoy D, Stanton BA. Exocytosis is not involved in activation of Cl- secretion via CFTR in Calu-3 airway epithelial cells. *Am J Physiol*. 1998;275(4). doi:10.1152/AJPCELL.1998.275.4.C913

566. Liedtke CM, Cole TS. Antisense oligonucleotide to PKC-epsilon alters cAMP-dependent stimulation of CFTR in Calu-3 cells. *Am J Physiol*. 1998;275(5). doi:10.1152/AJPCELL.1998.275.5.C1357

567. Jia Y, Mathews CJ, Hanrahan JW. Phosphorylation by protein kinase C is required for acute activation of cystic fibrosis transmembrane conductance regulator by protein kinase A. *J Biol Chem*. 1997;272(8):4978-4984. doi:10.1074/JBC.272.8.4978

568. French PJ, Bijman J, Edixhoven M, et al. Isotype-specific activation of cystic fibrosis transmembrane conductance regulator-chloride channels by cGMP-dependent protein kinase II. *J Biol Chem*. 1995;270(44):26626-26631. doi:10.1074/JBC.270.44.26626

569. Vaandrager AB, Smolenski A, Tilly BC, et al. Membrane targeting of cGMP-dependent protein kinase is required for cystic fibrosis transmembrane conductance regulator Cl- channel activation. *Proc Natl Acad Sci U S A*. 1998;95(4):1466-1471. doi:10.1073/PNAS.95.4.1466

570. Forte LR, Thorne PK, Eber SL, et al. Stimulation of intestinal Cl- transport by heat-stable enterotoxin: activation of cAMP-dependent protein kinase by cGMP. *Am J Physiol*. 1992;263(3 Pt 1). doi:10.1152/AJPCELL.1992.263.3.C607

571. Grubb BR, Gabriel SE. Intestinal physiology and pathology in gene-targeted mouse models of cystic fibrosis. *Am J Physiol*. 1997;273(2 Pt 1). doi:10.1152/AJPGI.1997.273.2.G258

572. Anderson MP, Sheppard DN, Berger HA, Welsh MJ. Chloride channels in the apical membrane of normal and cystic fibrosis airway and intestinal epithelia. *Am J Physiol*. 1992;263(1 Pt 1). doi:10.1152/AJPLUNG.1992.263.1.L1

573. Morris AP, Cunningham SA, Benos DJ, Frizzell RA. Cellular differentiation is required for cAMP but not Ca(2+)-dependent Cl- secretion in colonic epithelial cells expressing high levels of cystic fibrosis transmembrane conductance regulator. *J Biol Chem*. 1992;267(8):5575-5583. doi:10.1016/S0021-9258(18)42804-9

574. Berschneider HM, Knowles MR, Azizkhan RG, et al. Altered intestinal chloride transport in cystic fibrosis. *FASEB Journal*. 1988;2(10):2625-2629. doi:10.1096/FASEBJ.2.10.2838365

575. McEwan GTA, Hirst BH, Simmons NL. Carbachol stimulates Cl- secretion via activation of two distinct apical Cl- pathways in cultured human T84 intestinal epithelial monolayers. *Biochim Biophys Acta*. 1994;1220(3):241-247. doi:10.1016/0167-4889(94)90144-9

576. Merlin D, Jiang L, Strohmeier GR, et al. Distinct Ca2+- and cAMP-dependent anion conductances in the apical membrane of polarized T84 cells. *Am J Physiol*. 1998;275(2):C484-95. doi:10.1152/AJPCELL.1998.275.2.C484

577. Rozmahel R, Wilschanski M, Matin A, et al. Modulation of disease severity in cystic fibrosis transmembrane conductance regulator deficient mice by a secondary genetic factor. *Nat Genet*. 1996;12(3):280-287. doi:10.1038/NG0396-280

578. Wagner JA, McDonald T v., Nghiem PT, et al. Antisense oligodeoxynucleotides to the cystic fibrosis transmembrane conductance regulator inhibit cAMP-activated but not calcium-activated chloride currents. *Proc Natl Acad Sci U S A*. 1992;89(15):6785-6789. doi:10.1073/PNAS.89.15.6785

579. Morris AP, Scott JK, Ball JM, Zeng CQY, O'Neal WK, Estes MK. NSP4 elicits age-dependent diarrhea and Ca2+-mediated I- influx into intestinal crypts of CF mice. *Am J Physiol Gastrointest Liver Physiol*. 1999;277(2 40-2). doi:10.1152/AJPGI.1999.277.2.G431

580. Takahashi A, Sato Y, Shiomi Y, et al. Mechanisms of chloride secretion induced by thermostable direct haemolysin of Vibrio parahaemolyticus in human colonic tissue and a human intestinal epithelial cell line. *J Med Microbiol*. 2000;49(9):801-810. doi:10.1099/0022-1317-49-9-801

581. Lorrot M, Vasseur M. How do the rotavirus NSP4 and bacterial enterotoxins lead differently to diarrhea? *Virol J*. 2007;4. doi:10.1186/1743-422X-4-31

582. de La Fuente R, Namkung W, Mills A, Verkman AS. Small-molecule screen identifies inhibitors of a human intestinal calcium-activated chloride channel. *Mol Pharmacol*. 2008;73(3):758-768. doi:10.1124/MOL.107.043208

583. Fink G. Secretagogue. *Encyclopedia of Stress*. Published online January 1, 2007:435-439. doi:10.1016/B978-012373947-6.00339-1

584. Williams DA. pKa Values for Some Drugs and Miscellaneous Organic Acids and Bases. pH Values for Tissue Fluids. Williams DA, Lemke TL, Foye WO, eds. *Foye's Principles of Medicinal Chemistry*. 2002;1:128 pages. Accessed December 20, 2022. https://books.google.com/books/about/Foye_s_Principles_of_Medicinal_Chemistry.html?hl=it&id=qLJ6Bs1Qml4C

585. Khan TM, Patel R, Siddiqui AH. Furosemide. *StatPearls*. Published online June 3, 2022. Accessed December 20, 2022. https://www.ncbi.nlm.nih.gov/books/NBK499921/

586. Plata C, Meade P, Vázquez N, Hebert SC, Gamba G. Functional properties of the apical Na+-K+-2Cl-cotransporter isoforms. *J Biol Chem*. 2002;277(13):11004-11012. doi:10.1074/JBC.M110442200

587. Haas M, Forbush B. The Na-K-Cl cotransporters. *J Bioenerg Biomembr*. 1998;30(2):161-172. doi:10.1023/A:1020521308985

588. Cotton R, Suarez S, Reese J. Unexpected extra-renal effects of loop diuretics in the preterm neonate. *Acta Paediatr*. 2012;101(8):835-845. doi:10.1111/J.1651-2227.2012.02699.X

589. Fosnes GS, Lydersen S, Farup PG. Constipation and diarrhoea - common adverse drug reactions? A cross sectional study in the general population. *BMC Clin Pharmacol*. 2011;11. doi:10.1186/1472-6904-11-2

590. Yang N, Lei Z, Li X, et al. Chloroquine Stimulates Cl– Secretion by Ca2+ Activated Cl– Channels in Rat Ileum. *PLoS One*. 2014;9(1):87627. doi:10.1371/JOURNAL.PONE.0087627

591. Kaewsaro K, Nualplub S, Bumrungsri S, Khuituan P. Furosemide suppresses ileal and colonic contractility via interactions with GABA-A receptor in mice. *Clin Exp Pharmacol Physiol*. 2017;44(11):1155-1165. doi:10.1111/1440-1681.12824

592. Thiagarajah JR, Broadbent T, Hsieh E, Verkman AS. Prevention of Toxin-Induced Intestinal Ion and Fluid Secretion by a Small-Molecule CFTR Inhibitor. *Gastroenterology*. 2004;126(2):511-519. doi:10.1053/j.gastro.2003.11.005

593. Sonawane ND, Zhao D, Zegarra-Moran O, Galietta LJV, Verkman AS. Lectin conjugates as potent, nonabsorbable CFTR inhibitors for reducing intestinal fluid secretion in cholera. *Gastroenterology*. 2007;132(4):1234-1244. doi:10.1053/J.GASTRO.2007.02.018

594. Hanaoka K, Guggino WB. cAMP regulates cell proliferation and cyst formation in autosomal polycystic kidney disease cells. *J Am Soc Nephrol*. 2000;11(7):1179-1187. doi:10.1681/ASN.V1171179

595. Li H, Findlay IA, Sheppard DN. The relationship between cell proliferation, Cl- secretion, and renal cyst growth: a study using CFTR inhibitors. *Kidney Int*. 2004;66(5):1926-1938. doi:10.1111/J.1523-1755.2004.00967.X

596. Tradtrantip L, Sonawane ND, Wan N, Verkman AS. Nanomolar Potency Pyrimido-pyrrolo-quinoxalinedione CFTR Inhibitor Reduces Cyst Size in a Polycystic Kidney Disease Model. *J Med Chem*. 2009;52(20):6447. doi:10.1021/JM9009873

597. Narahashi T. Tetrodotoxin: a brief history. *Proc Jpn Acad Ser B Phys Biol Sci*. 2008;84(5):147-154. doi:10.2183/PJAB.84.147

598. Cheng CA, Hwang DF, Tsai YH, et al. Microflora and tetrodotoxin-producing bacteria in a gastropod, Niotha clathrata. *Food and Chemical Toxicology*. 1995;33(11):929-934. doi:10.1016/0278-6915(95)00061-6

599. Miranda-Morales M, Ochoa-Cortes F, Stern E, Lomax AE, Vanner S. Axon reflexes evoked by transient receptor potential vanilloid 1 activation are mediated by tetrodotoxin-resistant voltage-gated Na+ channels in intestinal afferent nerves. *J Pharmacol Exp Ther*. 2010;334(2):566-575. doi:10.1124/JPET.110.165969

600. Nieto FR, Cobos EJ, Tejada MÁ, Sánchez-Fernández C, González-Cano R, Cendán CM. Tetrodotoxin (TTX) as a Therapeutic Agent for Pain. *Mar Drugs*. 2012;10(2):281-305. doi:10.3390/MD10020281

601. González-Cano R, Ruiz-Cantero MC, Santos-Caballero M, Gómez-Navas C, Tejada M, Nieto FR. Tetrodotoxin, a Potential Drug for Neuropathic and Cancer Pain Relief? *Toxins (Basel)*. 2021;13(7). doi:10.3390/TOXINS13070483

602. Beyak MJ, Ramji N, Krol KM, Kawaja MD, Vanner SJ. Two TTX-resistant Na+ currents in mouse colonic dorsal root ganglia neurons and their role in colitis-induced hyperexcitability. *Am J Physiol Gastrointest Liver Physiol*. 2004;287(4). doi:10.1152/AJPGI.00154.2004

603. Vanner S, Macnaughton WK. Submucosal secretomotor and vasodilator reflexes. *Neurogastroenterology & Motility*. 2004;16(SUPPL. 1):39-43. doi:10.1111/J.1743-3150.2004.00473.X

604. Wang B, An N, Shaikh AS, et al. Hyperosmolarity evokes histamine release from ileum mucosa by stimulating a cholinergic pathway. *Biochem Biophys Res Commun*. 2017;493(2):1037-1042. doi:10.1016/J.BBRC.2017.09.093

605. Carbachol. In: *Meyler's Side Effects of Drugs*. Elsevier; 2016:80. doi:10.1016/b978-0-444-53717-1.00448-0

606. O'Shaughnessy KM. Cholinergic and antimuscarinic (anticholinergic) mechanisms and drugs. In: *Clinical Pharmacology: Eleventh Edition*. Elsevier Inc.; 2012:372-381. doi:10.1016/B978-0-7020-4084-9.00061-6

607. Pouokam E, Diener M. Segmental differences in ion transport in rat cecum. *Pflugers Arch*. 2019;471(7):1007-1023. doi:10.1007/S00424-019-02276-1/FIGURES/12

608. Hirota CL, McKay DM. Cholinergic regulation of epithelial ion transport in the mammalian intestine. *Br J Pharmacol*. 2006;149(5):463-479. doi:10.1038/SJ.BJP.0706889

609. Lomasney KW, Houston A, Shanahan F, Dinan TG, Cryan JF, Hyland NP. Selective influence of host microbiota on cAMP-mediated ion transport in mouse colon. *Neurogastroenterology & Motility*. 2014;26(6):887-890. doi:10.1111/NMO.12328

610. Hyland NP, Cox HM. The regulation of veratridine-stimulated electrogenic ion transport in mouse colon by neuropeptide Y (NPY), Y1 and Y2 receptors. *Br J Pharmacol*. 2005;146(5):712-722. doi:10.1038/SJ.BJP.0706368

611. van Koppen CJ, Kaiser B. Regulation of muscarinic acetylcholine receptor signaling. *Pharmacol Ther*. 2003;98(2):197-220. doi:10.1016/S0163-7258(03)00032-9

612. Alasbahi RH, Melzig MF. Plectranthus barbatus: A review of phytochemistry, ethnobotanical uses and pharmacology part 1. *Planta Med*. 2010;76(7):653-661. doi:10.1055/s-0029-1240898

613. Alasbahi RH, Melzig MF. Forskolin and derivatives as tools for studying the role of cAMP. *Pharmazie*. 2012;67(1):5-13. doi:10.1691/ph.2012.1642

614. Sassone-Corsi P. The cyclic AMP pathway. *Cold Spring Harb Perspect Biol*. 2012;4(12). doi:10.1101/CSHPERSPECT.A011148

615. Yun CHC, Oh S, Zizak M, et al. cAMP-mediated inhibition of the epithelial brush border Na^+/H^+ exchanger, NHE3, requires an associated regulatory protein. *Proc Natl Acad Sci U S A*. 1997;94(7):3010-3015. doi:10.1073/PNAS.94.7.3010/ASSET/91360E15-1326-4A6E-9086-29E66DD696C4/ASSETS/GRAPHIC/PQ0773014004.JPEG

616. Catterall WA. Activation of the action potential Na^+ ionophore of cultured neuroblastoma cells by veratridine and batrachotoxin. *Journal of Biological Chemistry*. 1975;250(11):4053-4059. doi:10.1016/S0021-9258(19)41385-9

617. Maciej Serda, Becker FG, Cleary M, et al. Effects of nerve stimulation on ion transport in mouse jejunum: Responses to Veratrum alkaloids. G. Balint, Antala B, Carty C, Mabieme JMA, Amar IB, Kaplanova A, eds. *Journal of Pharmacology and Experimental Therapeutics*. 1990;252(2):636-642. doi:10.2/JQUERY.MIN.JS

618. Holzer P. Capsaicin: cellular targets, mechanisms of action, and selectivity for thin sensory neurons. *Pharmacol Rev*. 1991;43(2).

619. Haanpää M, Treede RD. Capsaicin for neuropathic pain: linking traditional medicine and molecular biology. *Eur Neurol*. 2012;68(5):264-275. doi:10.1159/000339944

620. Vanner S, Macnaughton WK. Submucosal secretomotor and vasodilator reflexes. *Neurogastroenterol Motil*. 2004;16 Suppl 1(SUPPL. 1):39-43. doi:10.1111/J.1743-3150.2004.00473.X

621. Larsen EH. Hans H. Ussing - Scientific work: Contemporary significance and perspectives. *Biochim Biophys Acta Biomembr*. 2002;1566(1-2):2-15. doi:10.1016/S0005-2736(02)00592-8

622. Palmer LG, Andersen OS. The two-membrane model of epithelial transport: Koefoed-Johnsen and Ussing (1958). *J Gen Physiol*. 2008;132(6):607-612. doi:10.1085/JGP.200810149

623. Clarke LL. A guide to Ussing chamber studies of mouse intestine. *Am J Physiol Gastrointest Liver Physiol*. 2009;296(6). doi:10.1152/ajpgi.90649.2008

624. USSING HH, ZERAHN K. Active transport of sodium as the source of electric current in the short-circuited isolated frog skin. *Acta Physiol Scand*. 1951;23(2-3):110-127. doi:10.1111/J.1748-1716.1951.TB00800.X

625. Larsen EH. Reconciling the Krogh and Ussing interpretations of epithelial chloride transport - presenting a novel hypothesis for the physiological significance of the passive cellular chloride uptake. *Acta Physiol (Oxf)*. 2011;202(3):435-464. doi:10.1111/J.1748-1716.2010.02239.X

626. Hardcastle J, Hardcastle PT. gamma-Aminobutyric acid and intestinal secretion. *Gastroenterology*. 1996;111(4):1163-1164. doi:10.1016/S0016-5085(96)70096-3

627. Schulzke JD, Gitter AH, Mankertz J, et al. Epithelial transport and barrier function in occludin-deficient mice. *Biochim Biophys Acta*. 2005;1669(1):34-42. doi:10.1016/J.BBAMEM.2005.01.008

628. Wu RY, Pasyk M, Wang B, et al. Spatiotemporal maps reveal regional differences in the effects on gut motility for Lactobacillus reuteri and rhamnosus strains. *Neurogastroenterol Motil*. 2013;25(3):e205-14. doi:10.1111/NMO.12072

629. Thomson A, Smart K, Somerville MS, et al. The Ussing chamber system for measuring intestinal permeability in health and disease. *BMC Gastroenterol*. 2019;19(1). doi:10.1186/S12876-019-1002-4

630. Abdulnour-Nakhoul SM, Nakhoul NL. Ussing Chamber Methods to Study the Esophageal Epithelial Barrier. *Methods Mol Biol*. 2021;2367:215-233. doi:10.1007/7651_2020_324

631. Westerhout J, Wortelboer H, Verhoeckx K. Ussing Chamber. *The Impact of Food Bioactives on Health: In Vitro and Ex Vivo Models*. Published online January 1, 2015:263-273. doi:10.1007/978-3-319-16104-4_24

632. Shamsuddin AKM, Quinton PM. Native small airways secrete bicarbonate. *Am J Respir Cell Mol Biol*. 2014;50(4):796-804. doi:10.1165/RCMB.2013-0418OC

633. Formaggio F, Rimondini R, Delprete C, et al. L-Acetylcarnitine causes analgesia in mice modeling Fabry disease by up-regulating type-2 metabotropic glutamate receptors. *Mol Pain*. 2022;18. doi:10.1177/17448069221087033

634. Shan Li Z, Schmauss C, Cuenca A, Ratcliffe E, Gershon MD. Behavioral/Systems/Cognitive Physiological Modulation of Intestinal Motility by Enteric Dopaminergic Neurons and the D 2 Receptor: Analysis of Dopamine Receptor Expression, Location, Development, and Function in Wild-Type and Knock-Out Mice. Published online 2006. doi:10.1523/JNEUROSCI.4720-05.2006

635. Christianson JA, Gebhart GF. Assessment of colon sensitivity by luminal distension in mice. Published online 2007. doi:10.1038/nprot.2007.392

636. Lucarini E, Parisio C, Branca JJV, et al. Deepening the Mechanisms of Visceral Pain Persistence: An Evaluation of the Gut-Spinal Cord Relationship. *Cells*. 2020;9(8). doi:10.3390/CELLS9081772

637. Chen Y, Lin C, Tang Y, Chen AQ, Liu CY, Lu DL. ZD 7288, an HCN channel blocker, attenuates chronic visceral pain in irritable bowel syndrome-like rats. *World J Gastroenterol*. 2014;20(8):2091-2097. doi:10.3748/WJG.V20.I8.2091

638. McCloy RA, Rogers S, Caldon CE, Lorca T, Castro A, Burgess A. Partial inhibition of Cdk1 in G2 phase overrides the SAC and decouples mitotic events. *Cell Cycle*. 2014;13(9):1400-1412. doi:10.4161/CC.28401/SUPPL_FILE/KCCY_A_10928401_SM0001.ZIP

639. Eeckhout E, Wullaert A. Extraction of DNA from Murine Fecal Pellets for Downstream Phylogenetic Microbiota Analysis by Next-generation Sequencing. *Bio Protoc*. 2018;8(3). doi:10.21769/BIOPROTOC.2707

640. Masella AP, Bartram AK, Truszkowski JM, Brown DG, Neufeld JD. PANDAseq: Paired-end assembler for illumina sequences. *BMC Bioinformatics*. 2012;13(1):1-7. doi:10.1186/1471-2105-13-31/FIGURES/4

641. Bolyen E, Rideout JR, Dillon MR, et al. Reproducible, interactive, scalable and extensible microbiome data science using QIIME 2. *Nat Biotechnol*. 2019;37(8):852-857. doi:10.1038/S41587-019-0209-9

642. Callahan BJ, McMurdie PJ, Rosen MJ, Han AW, Johnson AJA, Holmes SP. DADA2: High-resolution sample inference from Illumina amplicon data. *Nature Methods 2016 13:7*. 2016;13(7):581-583. doi:10.1038/nmeth.3869

643. McDonald D, Price MN, Goodrich J, et al. An improved Greengenes taxonomy with explicit ranks for ecological and evolutionary analyses of bacteria and archaea. *ISME J*. 2012;6(3):610-618. doi:10.1038/ISMEJ.2011.139

644. Rognes T, Flouri T, Nichols B, Quince C, Mahé F. VSEARCH: a versatile open source tool for metagenomics. *PeerJ*. 2016;4(10). doi:10.7717/PEERJ.2584

645. Lozupone C, Knight R. UniFrac: a new phylogenetic method for comparing microbial communities. *Appl Environ Microbiol*. 2005;71(12):8228-8235. doi:10.1128/AEM.71.12.8228-8235.2005

646. Wickham H. ggplot2. Published online 2016. doi:10.1007/978-3-319-24277-4

647. The R Journal: Plotrix. Accessed December 27, 2022. https://journal.r-project.org/articles/RN-2006-026/

648. Vegan: community ecology package | McGlinn lab. Accessed December 27, 2022. https://www.mcglinnlab.org/publication/2019-01-01_oksanen_vegan_2019/

649. Lynch CMK, Cowan CSM, Bastiaanssen TFS, et al. Critical windows of early-life microbiota disruption on behaviour, neuroimmune function, and neurodevelopment. *Brain Behav Immun*. 2023;108:309-327. doi:10.1016/J.BBI.2022.12.008

650. Hsieh TC, Ma KH, Chao A. iNEXT: an R package for rarefaction and extrapolation of species diversity (Hill numbers). *Methods Ecol Evol*. 2016;7(12):1451-1456. doi:10.1111/2041-210X.12613

651. Lubbe S, Filzmoser P, Templ M. Comparison of zero replacement strategies for compositional data with large numbers of zeros. *Chemometrics and Intelligent Laboratory Systems*. 2021;210:104248. doi:10.1016/J.CHEMOLAB.2021.104248

652. Aitchison J, Barceló-Vidal C, Martín-Fernández JA, Pawlowsky-Glahn V. Logratio analysis and compositional distance. *Math Geol*. 2000;32(3):271-275. doi:10.1023/A:1007529726302/METRICS

653. Benjamini Y, Hochberg Y. Controlling the False Discovery Rate: A Practical and Powerful Approach to Multiple Testing. *Journal of the Royal Statistical Society: Series B (Methodological)*. 1995;57(1):289-300. doi:10.1111/J.2517-6161.1995.TB02031.X

654. Bastiaanssen TFS, Quinn TP, Loughman A. Treating Bugs as Features: A compositional guide to the statistical analysis of the microbiome-gut-brain axis. Published online July 25, 2022. doi:10.48550/arxiv.2207.12475

655. Douglas GM, Maffei VJ, Zaneveld JR, et al. PICRUSt2 for prediction of metagenome functions. *Nature Biotechnology 2020 38:6*. 2020;38(6):685-688. doi:10.1038/s41587-020-0548-6

656. Valles-Colomer M, Falony G, Darzi Y, et al. The neuroactive potential of the human gut microbiota in quality of life and depression. *Nature Microbiology 2019 4:4*. 2019;4(4):623-632. doi:10.1038/s41564-018-0337-x

657. Lomasney KW, Hyland NP. The application of Ussing chambers for determining the impact of microbes and probiotics on intestinal ion transport. *Can J Physiol Pharmacol*. 2013;91(9):663-670. doi:10.1139/cjpp-2013-0027

658. Ramos A, Pereira E, Martins GC, Wehrmeister TD, Izídio GS. Integrating the open field, elevated plus maze and light/dark box to assess different types of emotional behaviors in one single trial. *Behavioural brain research*. 2008;193(2):277-288. doi:10.1016/J.BBR.2008.06.007

659. Pei J, Foong P, Tough IR, Cox HM, Bornstein JC, Foong JPP. Properties of cholinergic and non-cholinergic submucosal neurons along the mouse colon. *The Authors The Journal of Physiology C*. 2014;592:777-793. doi:10.1113/jphysiol.2013.265686

660. Cable WJL, Kolodny EH, Adams RD. Fabry disease. *Neurology*. 1982;32(5):498-498. doi:10.1212/WNL.32.5.498

661. Francini-Pesenti F, Ravarotto V, Bertoldi G, Spinella P, Calò LA. Could nutritional therapy take us further in our approaches to Fabry disease? *Nutrition*. 2020;72. doi:10.1016/J.NUT.2019.110664

662. Üçeyler N, Biko L, Hose D, Hofmann L, Sommer C. Comprehensive and differential long-term characterization of the alpha-galactosidase A deficient mouse model of Fabry disease focusing on the sensory system and pain development. *Mol Pain*. 2016;12. doi:10.1177/1744806916646379

663. Camilleri M, Sellin JH, Barrett KE. Pathophysiology, Evaluation, and Management of Chronic Watery Diarrhea. *Gastroenterology*. 2017;152(3):515-532.e2. doi:10.1053/j.gastro.2016.10.014

664. Julio-Pieper M, Hyland NP, Bravo JA, Dinan TG, Cryan JF. A novel role for the metabotropic glutamate receptor-7: modulation of faecal water content and colonic electrolyte transport in the mouseb ph_713 367..375. *Br J Pharmacol*. 2010;160:367-375. doi:10.1111/j.1476-5381.2010.00713.x

665. Krug SM, Schulzke JD, Fromm M. Tight junction, selective permeability, and related diseases. *Semin Cell Dev Biol*. 2014;36:166-176. doi:10.1016/J.SEMCDB.2014.09.002

666. Marchiando AM, Graham WV, Turner JR. Epithelial barriers in homeostasis and disease. *Annu Rev Pathol*. 2010;5:119-144. doi:10.1146/ANNUREV.PATHOL.4.110807.092135

667. Maciej Serda, Becker FG, Cleary M, et al. A pilot study of motility and tone of the left colon in patients with diarrhea due to functional disorders and dysautonomia. G. Balint, Antala B, Carty C, Mabieme JMA, Amar IB, Kaplanova A, eds. *American Journal of Gastroenterology*. 1997;92(2):297-302. doi:10.2/JQUERY.MIN.JS

668. Chey WY, Jin HO, Lee MH, Sun SW, Lee KY. Colonic motility abnormality in patients with irritable bowel syndrome exhibiting abdominal pain and diarrhea. *Am J Gastroenterol*. 2001;96(5):1499-1506. doi:10.1111/J.1572-0241.2001.03804.X

669. Tobin JM, Delbridge LMD, di Nicolantonio R, Bhathal P. Development of colorectal sensitization is associated with increased eosinophils and mast cells in dextran sulfate sodium-treated rats. *Dig Dis Sci*. 2004;49(7-8):1302-1310. doi:10.1023/B:DDAS.0000037827.07367.2D

670. Jones RCW, Otsuka E, Wagstrom E, Jensen CS, Price MP, Gebhart GF. Short-term sensitization of colon mechanoreceptors is associated with long-term hypersensitivity to colon distention in the mouse. *Gastroenterology*. 2007;133(1):184-194. doi:10.1053/J.GASTRO.2007.04.042

671. Jones RCW, Xu L, Gebhart GF. The mechanosensitivity of mouse colon afferent fibers and their sensitization by inflammatory mediators require transient receptor potential vanilloid 1 and acid-sensing ion channel 3. *J Neurosci*. 2005;25(47):10981-10989. doi:10.1523/JNEUROSCI.0703-05.2005

672. Elsenbruch S, Rosenberger C, Enck P, Forsting M, Schedlowski M, Gizewski ER. Affective disturbances modulate the neural processing of visceral pain stimuli in irritable bowel syndrome: an fMRI study. *Gut*. 2010;59(4):489-495. doi:10.1136/GUT.2008.175000

673. van Oudenhove L. Visceral sensory and cognitive-affective neuroscience: towards integration? *Gut*. 2010;59(4):431-432. doi:10.1136/GUT.2009.192658

674. Schmid J, Langhorst J, Gaß F, et al. Placebo analgesia in patients with functional and organic abdominal pain: a fMRI study in IBS, UC and healthy volunteers. *Gut*. 2015;64(3):418-427. doi:10.1136/GUTJNL-2013-306648

675. Cantarero-Prieto D, Moreno-Mencia P. The effects of gastrointestinal disturbances on the onset of depression and anxiety. *PLoS One*. 2022;17(1 1). doi:10.1371/JOURNAL.PONE.0262712

676. Somatization Symptoms and Hypochondriacal Features in the Ge... : Psychosomatic Medicine. Accessed January 7, 2023. https://journals.lww.com/psychosomaticmedicine/Abstract/2001/07000/Somatization_Symptoms_and_Hypochondriacal_Features.12.aspx

677. Toussaint A, Hüsing P, Kohlmann S, Brähler E, Löwe B. Excessiveness in Symptom-Related Thoughts, Feelings, and Behaviors: An Investigation of Somatic Symptom Disorders in the General Population. *Psychosom Med*. 2021;83(2):164-170. doi:10.1097/PSY.0000000000000903

678. Lydiard RB, Greenwald S, Weissman MM, Johnson J, Drossman DA, Ballenger JC. Panic disorder and gastrointestinal symptoms: findings from the NIMH Epidemiologic Catchment Area project. *https://doi.org/101176/ajp151164*. 2006;151(1):64-70. doi:10.1176/AJP.151.1.64

679. Ålander T, Svärdsudd K, Johansson SE, Agréus L. Psychological illness is commonly associated with functional gastrointestinal disorders and is important to consider during patient consultation: A population-based study. *BMC Med*. 2005;3(1):1-12. doi:10.1186/1741-7015-3-8/TABLES/5

680. Bener A, Al-Hamaq A, Dafeeah EE. High Prevalence of Depression, Anxiety and Stress Symptoms Among Diabetes Mellitus Patients. *Open Psychiatr J*. 2011;5(1):5-12. doi:10.2174/1874354401105010005

681. Goldsmith DR, Rapaport MH, Miller BJ. A meta-analysis of blood cytokine network alterations in psychiatric patients: comparisons between schizophrenia, bipolar disorder and depression. *Molecular Psychiatry 2016 21:12*. 2016;21(12):1696-1709. doi:10.1038/mp.2016.3

682. Ancona A, Petito C, Iavarone I, et al. The gut-brain axis in irritable bowel syndrome and inflammatory bowel disease. *Dig Liver Dis*. 2021;53(3):298-305. doi:10.1016/J.DLD.2020.11.026

683. Sarid O, Slonim-Nevo V, Pereg A, et al. Coping strategies, satisfaction with life, and quality of life in Crohn's disease: A gender perspective using structural equation modeling analysis. *PLoS One*. 2017;12(2):e0172779. doi:10.1371/JOURNAL.PONE.0172779

684. Graff LA, Walker JR, Bernstein CN. Depression and Anxiety in Inflammatory Bowel Disease:A Review of Comorbidity and Management. *Inflamm Bowel Dis*. 2009;15(7):1105-1118. doi:10.1002/IBD.20873

685. Ali N, Gillespie S, Laney D. Treatment of Depression in Adults with Fabry Disease. *JIMD Rep*. 2018;38:13-21. doi:10.1007/8904_2017_21

686. Bolsover FE, Murphy E, Cipolotti L, Werring DJ, Lachmann RH. Cognitive dysfunction and depression in Fabry disease: a systematic review. *J Inherit Metab Dis*. 2014;37(2):177-187. doi:10.1007/S10545-013-9643-X

687. Körver S, Geurtsen GJ, Hollak CEM, et al. Depressive symptoms in Fabry disease: the importance of coping, subjective health perception and pain. *Orphanet J Rare Dis*. 2020;15(1). doi:10.1186/S13023-020-1307-Y

688. Greenwood-Van Meerveld B, Johnson AC. Stress-Induced Chronic Visceral Pain of Gastrointestinal Origin. *Front Syst Neurosci*. 2017;11. doi:10.3389/FNSYS.2017.00086

689. Camilleri M, Boeckxstaens G. Dietary and pharmacological treatment of abdominal pain in IBS. *Gut*. 2017;66(5):966-974. doi:10.1136/GUTJNL-2016-313425

690. Attal N, Bouhassira D. Pharmacotherapy of neuropathic pain: which drugs, which treatment algorithms? *Pain*. 2015;156 Suppl 1(4):S104-S114. doi:10.1097/01.J.PAIN.0000460358.01998.15

691. Micheli L, Lucarini E, Nobili S, et al. Ultramicronized N-palmitoylethanolamine contributes to morphine efficacy against neuropathic pain: implication of mast cells and glia. *Curr Neuropharmacol*. 2022;21. doi:10.2174/1570159X21666221128091453

692. Cryan JF, Holmes A. The ascent of mouse: advances in modelling human depression and anxiety. *Nat Rev Drug Discov*. 2005;4(9):775-790. doi:10.1038/NRD1825

693. Integrating the open field, elevated plus maze and light/dark box to assess different types of emotional behaviors in one single trial. Behavioural Brain Research, 193(2), 277–288 | 10.1016/j.bbr.2008.06.007. Accessed January 7, 2023. https://sci-hub.st/https://doi.org/10.1016/j.bbr.2008.06.007

694. Prut L, Belzung C. The open field as a paradigm to measure the effects of drugs on anxiety-like behaviors: a review. *Eur J Pharmacol*. 2003;463(1-3):3-33. doi:10.1016/S0014-2999(03)01272-X

695. Crawley JN. Exploratory behavior models of anxiety in mice. *Neurosci Biobehav Rev*. 1985;9(1):37-44. doi:10.1016/0149-7634(85)90030-2

696. Bale TL, Contarino A, Smith GW, et al. Mice deficient for corticotropin-releasing hormone receptor-2 display anxiety-like behaviour and are hypersensitive to stress. *Nat Genet*. 2000;24(4):410-414. doi:10.1038/74263

697. Kraeuter AK, Guest PC, Sarnyai Z. The Open Field Test for Measuring Locomotor Activity and Anxiety-Like Behavior. In: *Methods in Molecular Biology*. Vol 1916. Humana Press Inc.; 2019:99-103. doi:10.1007/978-1-4939-8994-2_9

698. Kraeuter AK, Guest PC, Sarnyai Z. The Elevated Plus Maze Test for Measuring Anxiety-Like Behavior in Rodents. In: *Methods in Molecular Biology*. Vol 1916. Humana Press Inc.; 2019:69-74. doi:10.1007/978-1-4939-8994-2_4

699. File SE. The contribution of behavioural studies to the neuropharmacology of anxiety. *Neuropharmacology*. 1987;26(7B):877-886. doi:10.1016/0028-3908(87)90065-7

700. Trullas R, Skolnick P. Differences in fear motivated behaviors among inbred mouse strains. *Psychopharmacology (Berl)*. 1993;111(3):323-331. doi:10.1007/BF02244948

701. Ramos A, Mellerin Y, Mormède P, Chaouloff F. A genetic and multifactorial analysis of anxiety-related behaviours in Lewis and SHR intercrosses. *Behavioural brain research*. 1998;96(1-2):195-205. doi:10.1016/S0166-4328(98)00023-0

702. Ramos A, Pereira E, Martins GC, Wehrmeister TD, Izídio GS. Integrating the open field, elevated plus maze and light/dark box to assess different types of emotional behaviors in one single trial. *Behavioural Brain Research*. 2008;193(2):277-288. doi:10.1016/J.BBR.2008.06.007

703. Izídio GS, Lopes DM, Spricigo L, Ramos A. Common variations in the pretest environment influence genotypic comparisons in models of anxiety. *Genes Brain Behav*. 2005;4(7):412-419. doi:10.1111/J.1601-183X.2005.00121.X

704. Povedano M, Gascón J, Gálvez R, Ruiz M, Rejas J. Cognitive function impairment in patients with neuropathic pain under standard conditions of care. *J Pain Symptom Manage*. 2007;33(1):78-89. doi:10.1016/J.JPAINSYMMAN.2006.07.012

705. Glass JM. (suppl 2) Fibromyalgia and Cognition. *J Clin Psychiatry*. 2008;20.

706. Morais LH, Schreiber HL, Mazmanian SK. The gut microbiota–brain axis in behaviour and brain disorders. *Nat Rev Microbiol*. 2021;19(4):241-255. doi:10.1038/S41579-020-00460-0

707. Moloney RD, Johnson AC, O'Mahony SM, Dinan TG, Greenwood-Van Meerveld B, Cryan JF. Stress and the Microbiota-Gut-Brain Axis in Visceral PaRelevance to Irritable Bowel Syndrome. *CNS Neurosci Ther*. 2016;22(2):102-117. doi:10.1111/cns.12490

708. Barbara G, Barbaro MR, Fuschi D, et al. Inflammatory and Microbiota-Related Regulation of the Intestinal Epithelial Barrier. *Front Nutr*. 2021;8. doi:10.3389/fnut.2021.718356

709. Candela M, Rampelli S, Turroni S, et al. *Unbalance of Intestinal Microbiota in Atopic Children*.; 2012. http://www.biomedcentral.com/1471-2180/12/95

710. Margolis KG, Cryan JF, Mayer EA. The Microbiota-Gut-Brain Axis: From Motility to Mood. *Gastroenterology*. 2021;160(5):1486-1501. doi:10.1053/j.gastro.2020.10.066

711. Bastiaanssen TFS, Cowan CSM, Claesson MJ, Dinan TG, Cryan JF. Making Sense of … the Microbiome in Psychiatry. *International Journal of Neuropsychopharmacology*. 2019;22(1):37-52. doi:10.1093/ijnp/pyy067

712. Sudo N, Chida Y, Aiba Y, et al. Postnatal microbial colonization programs the hypothalamic-pituitary-adrenal system for stress response in mice. *Journal of Physiology*. 2004;558(1):263-275. doi:10.1113/jphysiol.2004.063388

713. Aresti Sanz J, el Aidy S. Microbiota and gut neuropeptides: a dual action of antimicrobial activity and neuroimmune response. *Psychopharmacology (Berl)*. 2019;236(5):1597-1609. doi:10.1007/s00213-019-05224-0

714. Barrett E, Ross RP, O'Toole PW, Fitzgerald GF, Stanton C. γ-Aminobutyric acid production by culturable bacteria from the human intestine. *J Appl Microbiol*. 2012;113(2):411-417. doi:10.1111/j.1365-2672.2012.05344.x

715. Yano JM, Yu K, Donaldson GP, et al. Indigenous bacteria from the gut microbiota regulate host serotonin biosynthesis. *Cell*. 2015;161(2):264-276. doi:10.1016/j.cell.2015.02.047

716. Eckburg PB, Bik EM, Bernstein CN, et al. *Diversity of the Human Intestinal Microbial Flora*. www.sciencemag.org/cgi/content/full/1110591/DC1

717. Robinson AM, Gondalia S v., Karpe A v., et al. Fecal microbiota and metabolome in a mouse model of spontaneous chronic colitis: Relevance to human inflammatory bowel disease. *Inflamm Bowel Dis*. 2016;22(12):2767-2787. doi:10.1097/MIB.0000000000000970

718. Comelli EM, Simmering R, Faure M, et al. Multifaceted transcriptional regulation of the murine intestinal mucus layer by endogenous microbiota. *Genomics*. 2008;91(1):70-77. doi:10.1016/j.ygeno.2007.09.006

719. Krogius-Kurikka L, Lyra A, Malinen E, et al. Microbial community analysis reveals high level phylogenetic alterations in the overall gastrointestinal microbiota of diarrhoea-predominant irritable bowel syndrome sufferers. *BMC Gastroenterol*. 2009;9. doi:10.1186/1471-230X-9-95

720. Chu M, Zhang X. Bacterial Atlas of Mouse Gut Microbiota. *Cell Microbiol*. 2022;2022:1-21. doi:10.1155/2022/5968814

721. Wang J, Lang T, Shen J, Dai J, Tian L, Wang X. Core gut bacteria analysis of healthy mice. *Front Microbiol*. 2019;10(APR). doi:10.3389/fmicb.2019.00887

722. Gu S, Chen D, Zhang JN, et al. Bacterial Community Mapping of the Mouse Gastrointestinal Tract. *PLoS One*. 2013;8(10). doi:10.1371/journal.pone.0074957

723. Lagkouvardos I, Lesker TR, Hitch TCA, et al. Sequence and cultivation study of Muribaculaceae reveals novel species, host preference, and functional potential of this yet undescribed family. *Microbiome*. 2019;7(1). doi:10.1186/s40168-019-0637-2

724. Tavella T, Rampelli S, Guidarelli G, et al. Elevated gut microbiome abundance of Christensenellaceae, Porphyromonadaceae and Rikenellaceae is associated with reduced visceral adipose tissue and healthier metabolic profile in Italian elderly. *Gut Microbes*. 2021;13(1):1-19. doi:10.1080/19490976.2021.1880221

725. Durbán A, Abellán JJ, Jiménez-Hernández N, et al. Structural alterations of faecal and mucosa-associated bacterial communities in irritable bowel syndrome. *Environ Microbiol Rep*. 2012;4(2):242-247. doi:10.1111/j.1758-2229.2012.00327.x

726. Huang K, Dong W, Liu W, et al. 2- O-β- d -Glucopyranosyl- l -ascorbic Acid, an Ascorbic Acid Derivative Isolated from the Fruits of Lycium Barbarum L., Modulates Gut Microbiota and Palliates Colitis in Dextran Sodium Sulfate-Induced Colitis in Mice. *J Agric Food Chem*. 2019;67(41):11408-11419. doi:10.1021/acs.jafc.9b04411

727. Parker BJ, Wearsch PA, Veloo ACM, Rodriguez-Palacios A. The Genus Alistipes: Gut Bacteria With Emerging Implications to Inflammation, Cancer, and Mental Health. *Front Immunol*. 2020;11. doi:10.3389/fimmu.2020.00906

728. Moschen AR, Gerner RR, Wang J, et al. Lipocalin 2 Protects from Inflammation and Tumorigenesis Associated with Gut Microbiota Alterations. *Cell Host Microbe*. 2016;19(4):455-469. doi:10.1016/j.chom.2016.03.007

729. Jiang H, Ling Z, Zhang Y, et al. Altered fecal microbiota composition in patients with major depressive disorder. *Brain Behav Immun*. 2015;48:186-194. doi:10.1016/j.bbi.2015.03.016

730. Polansky O, Sekelova Z, Faldynova M, Sebkova A, Sisak F, Rychlik I. Important metabolic pathways and biological processes expressed by chicken cecal microbiota. *Appl Environ Microbiol*. 2016;82(5):1569-1576. doi:10.1128/AEM.03473-15

731. Moschen AR, Gerner RR, Wang J, et al. Lipocalin 2 Protects from Inflammation and Tumorigenesis Associated with Gut Microbiota Alterations. *Cell Host Microbe*. 2016;19(4):455-469. doi:10.1016/j.chom.2016.03.007

732. Parker BJ, Wearsch PA, Veloo ACM, Rodriguez-Palacios A. The Genus Alistipes: Gut Bacteria With Emerging Implications to Inflammation, Cancer, and Mental Health. *Front Immunol*. 2020;11. doi:10.3389/fimmu.2020.00906

733. Reichardt N, Duncan SH, Young P, et al. Phylogenetic distribution of three pathways for propionate production within the human gut microbiota. *ISME Journal*. 2014;8(6):1323-1335. doi:10.1038/ismej.2014.14

734. Killingsworth J, Sawmiller D, Shytle RD. Propionate and Alzheimer's Disease. *Front Aging Neurosci*. 2021;12. doi:10.3389/fnagi.2020.580001

735. Gargari G, Taverniti V, Gardana C, et al. Fecal Clostridiales distribution and short-chain fatty acids reflect bowel habits in irritable bowel syndrome. *Environ Microbiol*. 2018;20(9):3201-3213. doi:10.1111/1462-2920.14271

736. Shaidullov IF, Sorokina DM, Sitdikov FG, Hermann A, Abdulkhakov SR, Sitdikova GF. Short chain fatty acids and colon motility in a mouse model of irritable bowel syndrome. *BMC Gastroenterol*. 2021;21(1). doi:10.1186/s12876-021-01613-y

737. Reigstad CS, Salmonson CE, Rainey JF, et al. Gut microbes promote colonic serotonin production through an effect of short-chain fatty acids on enterochromaffin cells. *FASEB Journal*. 2015;29(4):1395-1403. doi:10.1096/fj.14-259598

738. Esquerre N, Basso L, Defaye M, et al. Colitis-Induced Microbial Perturbation Promotes Postinflammatory Visceral Hypersensitivity. *CMGH*. 2020;10(2):225-244. doi:10.1016/j.jcmgh.2020.04.003

739. Dalile B, van Oudenhove L, Vervliet B, Verbeke K. The role of short-chain fatty acids in microbiota–gut–brain communication. *Nat Rev Gastroenterol Hepatol*. 2019;16(8):461-478. doi:10.1038/s41575-019-0157-3

740. Whittle N, Singewald N. HDAC inhibitors as cognitive enhancers in fear, anxiety and trauma therapy: Where do we stand? *Biochem Soc Trans*. 2014;42(2):569-581. doi:10.1042/BST20130233

741. Waldecker M, Kautenburger T, Daumann H, Busch C, Schrenk D. Inhibition of histone-deacetylase activity by short-chain fatty acids and some polyphenol metabolites formed in the colon. *Journal of Nutritional Biochemistry*. 2008;19(9):587-593. doi:10.1016/j.jnutbio.2007.08.002

742. Molinaro A, Bel Lassen P, Henricsson M, et al. Imidazole propionate is increased in diabetes and associated with dietary patterns and altered microbial ecology. *Nat Commun*. 2020;11(1). doi:10.1038/s41467-020-19589-w

743. Kushkevych I, Cejnar J, Treml J, Dordević D, Kollar P, Vítězová M. Recent Advances in Metabolic Pathways of Sulfate Reduction in Intestinal Bacteria. *Cells*. 2020;9(3). doi:10.3390/cells9030698

744. Singh SB, Lin HC. Hydrogen sulfide in physiology and diseases of the digestive tract. *Microorganisms*. 2015;3(4):866-889. doi:10.3390/microorganisms3040866

745. Bosi A, Banfi D, Bistoletti M, Giaroni C, Baj A. Tryptophan Metabolites Along the Microbiota-Gut-Brain Axis: An Interkingdom Communication System Influencing the Gut in Health and Disease. *International Journal of Tryptophan Research*. 2020;13. doi:10.1177/1178646920928984

746. Tedeschi L, Carai MAM, Frison G, et al. Endogenous γ-hydroxybutyric acid is in the rat, mouse and human gastrointestinal tract. *Life Sci*. 2003;72(22):2481-2488. doi:10.1016/S0024-3205(03)00143-7

747. Bermudez-Martin P, Becker JAJ, Caramello N, et al. The microbial metabolite p-Cresol induces autistic-like behaviors in mice by remodeling the gut microbiota. *Microbiome*. 2021;9(1). doi:10.1186/s40168-021-01103-z

748. Camilleri M. Physiological underpinnings of irritable bowel syndrome: Neurohormonal mechanisms. *Journal of Physiology*. 2014;592(14):2967-2980. doi:10.1113/jphysiol.2014.270892

749. Mickle AD, Shepherd AJ, Mohapatra DP. Nociceptive TRP channels: Sensory detectors and transducers in multiple pain pathologies. *Pharmaceuticals*. 2016;9(4). doi:10.3390/ph9040072

750. Hofmann L, Hose D, Grießhammer A, et al. Characterization of small fiber pathology in a mouse model of Fabry disease. Published online 2018. doi:10.7554/eLife.39300.001

751. Boesmans W, Owsianik G, Tack J, Voets T, vanden Berghe P. TRP channels in neurogastroenterology: Opportunities for therapeutic intervention. *Br J Pharmacol*. 2011;162(1):18-37. doi:10.1111/j.1476-5381.2010.01009.x

752. Holzer P, Izzo AA. Themed Section: The pharmacology of TRP channels The pharmacology of TRP channels LINKED ARTICLES. Published online 2014. doi:10.1111/bph.2014.171.issue-10

753. Bellono NW, Bayrer JR, Leitch DB, et al. Enterochromaffin Cells Are Gut Chemosensors that Couple to Sensory Neural Pathways. *Cell*. 2017;170(1):185-198.e16. doi:10.1016/j.cell.2017.05.034

754. Moran MM, Allen McAlexander M, Bíró T, Szallasi A. Transient receptor potential channels as therapeutic targets. *Nat Rev Drug Discov*. 2011;10. doi:10.1038/nrd3456

755. Kaneko Y, Szallasi A. Transient receptor potential (TRP) channels: a clinical perspective. *Br J Pharmacol*. 2014;171(10):2474-2507. doi:10.1111/BPH.12414

756. Farmer AD, Ruffle JK. STATE-OF-THE-ART REVIEW Irritable bowel syndrome. Published online 2015. doi:10.7707/hmj.459

757. Akbar A, Yiangou Y, Facer P, et al. Expression of the TRPV1 receptor differs in quiescent inflammatory bowel disease with or without abdominal pain. *Gut*. 2010;59(6):767-774. doi:10.1136/GUT.2009.194449

758. Winston J, Shenoy M, Medley D, Naniwadekar A, Pasricha PJ. The vanilloid receptor initiates and maintains colonic hypersensitivity induced by neonatal colon irritation in rats. *Gastroenterology*. 2007;132(2):615-627. doi:10.1053/J.GASTRO.2006.11.014

759. Engel MA, Khalil M, Mueller-Tribbensee SM, et al. The proximodistal aggravation of colitis depends on substance P released from TRPV1-expressing sensory neurons. *J Gastroenterol*. 2012;47(3):256-265. doi:10.1007/S00535-011-0495-6

760. Nagpal R, Mishra SK, Deep G, Yadav H. Role of TRP channels in shaping the gut microbiome. *Pathogens*. 2020;9(9):1-16. doi:10.3390/pathogens9090753

761. Vergnolle N. TRPV4: New therapeutic target for inflammatory bowel diseases. *Biochem Pharmacol*. 2014;89(2):157-161. doi:10.1016/j.bcp.2014.01.005

762. Nilius B, Voets T. The puzzle of TRPV4 channelopathies. *EMBO Rep*. 2013;14(2):152-163. doi:10.1038/EMBOR.2012.219

763. Poole DP, Amadesi S, Veldhuis NA, et al. Protease-activated Receptor 2 (PAR2) Protein and Transient Receptor Potential Vanilloid 4 (TRPV4) Protein Coupling Is Required for Sustained Inflammatory Signaling. *J Biol Chem*. 2013;288(8):5790. doi:10.1074/JBC.M112.438184

764. Fichna J, Mokrowiecka A, Cygankiewicz AI, et al. Transient receptor potential vanilloid 4 blockade protects against experimental colitis in mice: a new strategy for inflammatory bowel diseases treatment? *Neurogastroenterol Motil*. 2012;24(11). doi:10.1111/J.1365-2982.2012.01999.X

765. Ueda T, Shikano M, Kamiya T, Joh T, Ugawa S. The TRPV4 channel is a novel regulator of intracellular Ca2+ in human esophageal epithelial cells. *Am J Physiol Gastrointest Liver Physiol*. 2011;301(1). doi:10.1152/AJPGI.00511.2010

766. Patil MJ, Salas M, Bialuhin S, Boyd JT, Jeske NA, Akopian AN. Sensitization of small-diameter sensory neurons is controlled by TRPV1 and TRPA1 association. *FASEB J*. 2020;34(1):287-302. doi:10.1096/FJ.201902026R

767. Lapointe TK, Altier C. Channels The role of TRPA1 in visceral inflammation and pain. Published online 2011. doi:10.4161/chan.5.6.18016

768. Engel MA, Leffler A, Niedermirtl F, et al. TRPA1 and substance P mediate colitis in mice. *Gastroenterology*. 2011;141(4):1346-1358. doi:10.1053/J.GASTRO.2011.07.002

769. Meseguer V, Alpizar YA, Luis E, et al. TRPA1 channels mediate acute neurogenic inflammation and pain produced by bacterial endotoxins. *Nat Commun*. 2014;5. doi:10.1038/NCOMMS4125

770. Kun J, Szitter I, Kemény Á, et al. Upregulation of the transient receptor potential ankyrin 1 ion channel in the inflamed human and mouse colon and its protective roles. *PLoS One*. 2014;9(9). doi:10.1371/JOURNAL.PONE.0108164

771. Li Q, Guo CH, Chowdhury MA, Dai TL, Han W. TRPA1 in the spinal dorsal horn is involved in post-inflammatory visceral hypersensitivity: in vivo study using TNBS-treated rat model. *J Pain Res*. 2016;9:1153-1160. doi:10.2147/JPR.S118581

772. Erickson A, Deiteren A, Harrington AM, et al. Voltage-gated sodium channels: (NaV)igating the field to determine their contribution to visceral nociception. *J Physiol*. 2018;596(5):785. doi:10.1113/JP273461

773. Namer B, Ørstavik K, Schmidt R, et al. Changes in ionic conductance signature of nociceptive neurons underlying fabry disease phenotype. *Front Neurol*. 2017;8(JUL):335. doi:10.3389/FNEUR.2017.00335/FULL

774. Sanchez-Niño MD, Aguilera-Correa JJ, Politei J, Esteban J, Requena T, Ortiz A. Unraveling the drivers and consequences of gut microbiota disruption in Fabry disease: The lyso-Gb3 link. *Future Microbiol*. 2020;15(4):227-231. doi:10.2217/fmb-2019-0249

775. van Eijk M, Ferra MJ, Boot RG, Aerts JMFG. Lyso-glycosphingolipids: Presence and consequences. *Essays Biochem*. 2020;64(3):565-578. doi:10.1042/EBC20190090

776. Williams JM, Duckworth CA, Burkitt MD, Watson AJM, Campbell BJ, Pritchard DM. Epithelial Cell Shedding and Barrier Function: A Matter of Life and Death at the Small Intestinal Villus Tip. *Vet Pathol*. 2015;52(3):445-455. doi:10.1177/0300985814559404

777. Nowak A, Mechtler T, Kasper DC, Desnick RJ. Correlation of Lyso-Gb3 levels in dried blood spots and sera from patients with classic and Later-Onset Fabry disease. *Mol Genet Metab*. 2017;121(4):320-324. doi:10.1016/J.YMGME.2017.06.006

778. Grubb BR, Lee E, Pace AJ, Koller BH, Boucher RC. Intestinal ion transport in NKCC1-deficient mice. *Am J Physiol Gastrointest Liver Physiol*. 2000;279(4 42-4). doi:10.1152/AJPGI.2000.279.4.G707/ASSET/IMAGES/LARGE/H31000117009.JPEG

779. Tang L, Fang X, Winesett SP, et al. Bumetanide increases Cl--dependent short-circuit current in late distal colon: Evidence for the presence of active electrogenic Cl- absorption. Published online 2017. doi:10.1371/journal.pone.0171045

780. Ballout J, Diener M. The role of HCO3– in propionate-induced anion secretion across rat caecal epithelium. *Pflugers Arch*. 2021;473(6):937-951. doi:10.1007/s00424-021-02565-8

781. Rao M. An increasingly complex view of intestinal motility. *Nat Rev Gastroenterol Hepatol*. 2020;17(2):72-73. doi:10.1038/s41575-019-0249-0

782. Rao MC. Physiology of electrolyte transport in the gut: Implications for disease. *Compr Physiol*. 2019;9(3):947-1023. doi:10.1002/cphy.c180011

783. Geibel JP, Singh S, Rajendran VM, Binder HJ. *HCO 3 Secretion in the Rat Colonic Crypt Is Closely Linked to Cl Secretion*.

784. Bienrdorf FA, Gorden P, Fordtran JS. *Pathogenesis of Congenital Alkalosis with Diarrhea IMPLICATIONS FOR THE PHYSIOLOGY OF NORMAL ILEAL ELECTROLYTE ABSORPTION AND SECRETION*.

785. Powell DW, Solberg LI, Plotkin GR, Catlin DH, Maenza RM, Formal SB. Experimental Diarrhea: III. Bicarbonate transport in rat salmonella enterocolitis. *Gastroenterology*. 1971;60(6):1076-1086. doi:10.1016/S0016-5085(71)80035-5

786. Wang J, Zahra A, Wang YF, Wu J. Understanding the Physiological Role of Electroneutral Na+-Coupled HCO3– Cotransporter and Its Therapeutic Implications. *Pharmaceuticals*. 2022;15(9). doi:10.3390/ph15091082

787. Isenberg JI, Ljungstrijm M, Safsten B, Flemstrom G. *Proximal Duodenal Enterocyte Transport: Evidence for Na+-H+ and Cl-HCO; Exchange and NaHC03 Cotransport*.

788. Binder HJ, Rajendran V, Sadasivan V, Geibel JP. *Bicarbonate Secretion A Neglected Aspect of Colonic Ion Transport*.

789. Talbot C, Lytle C. Segregation of Na/H exchanger-3 and Cl/HCO 3 exchanger SLC26A3 (DRA) in rodent cecum and colon. *Am J Physiol Gastrointest Liver Physiol*. 2010;299:358-367. doi:10.1152/ajpgi.00151.2010.-The

790. Sheldon RJ, Malarchik ME, Burks TF, Porreca F. ABBREVIATIONS: VIP, vasoactive intestinal polypeptide; PD,transmural potential difference; I@, short-circuit current; G@, tissue conductance; TTX, Effectsof NerveStimulation on IonTransport in MouseJejunum: Responses to Veratrum Alkaloids1. Published online 1990.

791. Foong JPP, Bornstein JC. MGluR1 receptors contribute to non-purinergic slow excitatory transmission to submucosal VIP neurons of guinea-pig ileum. *Front Neurosci*. 2009;3(MAY). doi:10.3389/neuro.21.001.2009

ACKNOWLEDGMENTS